IMPERIAL

MIM Lab
Mechatronics in Medicine

Forbidden Region Dynamic Active Constraints for Tele-Operative Surgery

Author Zejian Cui
Supervisors Prof. Ferdinando Rodriguez y Baena[1]
Prof. Brian Davies[1]

Submitted 27th December 2024

[1]Department of Mechanical Engineering, Imperial College London, UK.

A thesis submitted in fulfilment of the requirements for the degree of *Philosophiae Doctor*

Mechatronics in Medicine Laboratory, Department of Mechanical Engineering,
Imperial College London

Mechatronics in Medicine Laboratory,
Hamlyn Centre of Robotic Surgery,
Department of Mechanical Engineering,
Bessemer Building,
Imperial College London,
South Kensington,
SW7 2AZ

Zejian Cui © 2024

But the higher we climb, feels like we're both none the wiser

---

Adele - *I Drink Wine*

Statement of Originality

I, Zejian Cui, hereby declare that this document contains my own, original work. In cases where other people's work has been utilised, such as figures, illustrations, and results, appropriate acknowledgements, copyright laws, and references have been provided, as per departmental requirements.

The thesis contained in this document has exclusively ever been submitted for the purpose of my PhD degree.

The template and formatting for this document was kindly provided by Dr. Spyridon Souipas.

Copyright

The copyright of this thesis rests with the author. Unless otherwise indicated, its contents are licensed under a Creative Commons Attribution-Non Commercial 4.0 International Licence (CC BY-NC).

Under this licence, you may copy and redistribute the material in any medium or format for both commercial and non-commercial purposes. You may also create and distribute modified versions of the work. This is on the condition that you credit the author.

When reusing or sharing this work, ensure you make the licence terms clear to others by naming the licence and linking to the licence text. Where a work has been adapted, you should indicate that the work has been changed and describe those changes.

Please seek permission from the copyright holder for uses of this work that are not included in this licence or permitted under UK Copyright Law.

Acknowledgements

First and foremost, I would like to express my immense gratitude to my family, who have been supporting me in every way possible throughout this journey.

Secondly, I would like to sincerely thank my PhD supervisor, Prof. Ferdinando Rodriguez y Baena, who has been both a visionary leader and an approachable mentor, guiding me in both my work and personal life. Words cannot express enough my indebtedness to you for your unwavering confidence in me through both good and bad results. Reflecting on the journey from the first time I made your acquaintance, while proposing my individual master's project, to now as I approach the sunset of my PhD, there was never a moment when I felt abandoned to face adversities alone, whether professionally or personally, thanks to your presence. I always feel it is a great privilege to be a member of MIM, a loving research community where we are all showered with the sunshine of your humour, care, and support. It is the camaraderie and enthusiasm for work spread in the office that drive me forward every day, and it is a blessing to witness the welcoming changes that have taken place at the Hamlyn centre over the years.

Additionally, I would like to thank Dr. Ulrich Hansen, a trustworthy and beloved mentor whom I have known since I was a master's student here. Without your help, this memorable academic voyage in London would never have commenced.

Specifically, I would like to thank Dr. Ana Cruz Ruiz, a great friend and congenial colleague with whom I often "exchange pleasantries" over afternoon tea breaks. It amazes me to realise how much time has passed since we first met during an online social meeting in the COVID period. I always appreciate the opportunity you offered me to be part of the Robotics Forum Postgraduate Network committee, where I met more like-minded people across Imperial working in various aspects of robotics.

Finally, I want to thank all those who have lent kind help to me, both professionally and personally, during my Ph.D. Without your support and companionship, this journey would have been a bland, solitary pilgrimage.

Ps. Special thanks to Dr. Taylor Swift for being a prolific singer & song writer, releasing the soul-touching albums "Folklore", "Evermore", "Midnight" and "The tortured poets department", which soothed my nerves during my countless sleepless nights when I was facing periods of emotional upheavals during the COVID period and beyond.

Abstract

Robotic-assisted minimally invasive surgery has gained greater popularity compared to conventional surgery. However, one of the biggest technical limitations of most commercial tele-operative surgical robots is the lack of haptic feedback, which increases surgeons' mental workload and reduces task safety. This thesis explores potential approaches for addressing this issue.

To identify potential avenues for providing haptic guidance to users during tele-operation, a comprehensive review was conducted, narrowing down Active Constraints (AC) as the predominant technical approach in this study. To facilitate algorithm verification in a tele-operation scenario, the first-generation da Vinci Research Kit (dVRK) was employed. Through an extensive review process and a user questionnaire study, major technical constraints of the dVRK were exposed.

To address the positioning inaccuracy caused by multiple time-variant factors in the dVRK robot, an on-the-fly calibration framework was then proposed. Both quantitative and qualitative experiments were conducted to verify the effectiveness of the proposed framework, which was then compared with other state-of-the-art methods.

To develop an AC pipeline that accounts for eventualities in a real clinical setting, a Forbidden Region Dynamic Active Constraints (FRDAC) framework was then proposed. In vitro trajectory tracking experiments were designed to aid quantitative assessment of the method, including its effectiveness in maintaining task safety, which was confirmed by successfully maintaining a pre-defined safety distance across all trials.

Finally, to further examine the proposed FRDAC pipeline in a user-present tele-operation scenario, a pilot user study was conducted. The tracking results demonstrate the effectiveness of the proposed FRDAC pipeline in maintaining a safety distance in a dynamic scenario compared to when no AC was provided to the user. Although the pipeline has proven effectiveness through in vitro experiments, it is acknowledged that certain limitations exist and should be addressed in future studies.

Contents

1 Introduction **18**

1.1 Overview . . . 19
1.2 Thesis Aim & Objectives . . . 22
1.3 Contributions . . . 23
1.4 Thesis Structure . . . 25

2 Literature Review **27**

2.1 Introduction . . . 28
2.2 Surgical robots . . . 29
2.2.1 The development of surgical robots . . . 29
2.2.2 Surgical robots for tele-operative surgery . . . 30
2.2.3 Research in tele-operative surgery . . . 33
2.3 Overview of Active Constraints . . . 36
2.3.1 Active Constraints implementation stages . . . 36
2.3.2 Guidance Active Constraints versus Forbidden Region Active Constraints 37
2.3.3 Static Active Constraints versus Dynamic Active Constraints . . . 37
2.3.4 Active Constraints generation . . . 38
2.3.5 Active Constraints evaluation . . . 39
2.3.6 Active Constraints enforcement . . . 40
2.3.6.1 Simple functions of constraint proximity . . . 40
2.3.6.2 Proxy and linkage simulation . . . 40
2.3.6.3 Non-energy storing constraints . . . 41
2.3.6.4 Potential fields . . . 42
2.3.6.5 Constrained joint optimisation . . . 43
2.3.7 Dynamic Active Constraints . . . 43
2.3.7.1 Guidance Dynamic Active Constraints . . . 44
2.3.7.2 Forbidden Region Dynamic Active Constraints . . . 45
2.3.8 Summary . . . 46
2.4 Overview of the first-generation dVRK . . . 48
2.4.1 Backgrounds . . . 48
2.4.2 Searching Methodology . . . 50
2.4.2.1 Literature review . . . 50

2.4.2.2 Consultation with researchers . . . 50
2.4.3 Kinematics Calibration . . . 50
2.4.3.1 Need for kinematics calibration . . . 51
2.4.3.2 Challenges in accurate positioning . . . 51
2.4.3.3 Methods for kinematics calibration . . . 53
2.4.4 Hand-eye Calibration . . . 55
2.4.4.1 Need for hand-eye calibration . . . 56
2.4.4.2 Challenges in dVRK hand-eye calibration . . . 56
2.4.4.3 dVRK hand-eye calibration methods . . . 56
2.5 Conclusion . . . 58

3 On-the-fly hand-eye calibration for the da Vinci surgical robot 60
3.1 Introduction . . . 61
3.1.1 Hand-eye calibration . . . 61
3.1.2 $\mathbf{AX} = \mathbf{XB}$ problems . . . 61
3.1.3 $\mathbf{AX} = \mathbf{YB}$ problems . . . 64
3.1.4 Evaluation metrics . . . 65
3.1.5 Hand-eye calibration for cable-driven robots . . . 67
3.2 Methods . . . 70
3.2.1 Cylindrical tool shaft central axis reconstruction . . . 70
3.2.2 Estimation of hand-eye calibration parameters using the PF . . . 74
3.2.2.1 Particle Initialization . . . 74
3.2.2.2 Particle prediction . . . 74
3.2.2.3 Particle weights update . . . 75
3.2.2.4 Resampling . . . 76
3.2.3 Joint 4 reading calibration . . . 77
3.3 Experiments . . . 78
3.3.1 Quantitative Analysis - Experiment 1 . . . 78
3.3.2 Qualitative Analysis - Experiment 2 . . . 79
3.4 Results and discussions . . . 82
3.4.1 Results - Experiment 1 . . . 82
3.4.2 Results - Experiment 2 . . . 82
3.5 Conclusion . . . 85

4 Proof of concept study on FRDAC in tele-operative surgery 86
4.1 Introduction . . . 87
4.2 Methods . . . 89
4.2.1 AC Generation . . . 89
4.2.2 AC Evaluation . . . 91

4.2.3 AC Enforcement . . . 92
4.3 Experiments . . . 94
4.3.1 Overview . . . 94
4.3.2 Hardware Setup . . . 95
4.3.3 Hybrid Force-Position Controller . . . 95
4.3.4 Algorithm Implementation . . . 95
4.3.4.1 Preparation tasks . . . 95
4.3.4.2 Workflow . . . 96
4.3.5 Deformation measurements . . . 97
4.3.6 Parameters selection . . . 97
4.4 Results and discussions . . . 100
4.4.1 Static trajectory tracking results . . . 100
4.4.2 Dynamic trajectory tracking results . . . 102
4.5 Conclusion . . . 108

5 Pilot user study on FRDAC in tele-operative surgery 109
5.1 Introduction . . . 110
5.2 Methods . . . 112
5.2.1 AC generation . . . 112
5.2.2 AC evaluation . . . 112
5.2.3 AC enforcement . . . 114
5.2.3.1 Energy redirection approach . . . 114
5.2.3.2 Mapping between SSMs and PSMs . . . 116
5.2.3.3 Impedance controller in the first-generation dVRK . . . 117
5.3 Experiments . . . 118
5.3.1 Experiments design . . . 118
5.3.2 Experimental setup . . . 120
5.4 Results and discussions . . . 121
5.4.1 Static trajectory tracking results . . . 121
5.4.2 Dynamic trajectory tracking results . . . 121
5.4.3 Discussion . . . 123
5.5 Conclusion . . . 127

6 Conclusion 128
6.1 Main Conclusions . . . 129
6.1.1 Chapter 2 Conclusions: Related Work . . . 131
6.1.2 Chapter 3 Conclusions: On-the-fly hand-eye calibration for the da Vinci surgical robot . . . 131

6.1.3 Chapter 4 Conclusions: Proof-of-concept study on FRDAC in tele-operative surgery . . . 132
6.1.4 Chapter 5 Conclusions: Pilot user study on FRDAC in tele-operative surgery 132
6.1.5 Main Conclusion . . . 133
6.2 Limitations . . . 134
6.2.1 Chapter 3 Limitations: On-the-fly hand-eye calibration for the da Vinci surgical robot . . . 135
6.2.2 Chapter 4 Limitations: Proof-of-concept study on FRDAC in tele-operative surgery . . . 135
6.2.3 Chapter 5 Limitations: Pilot user study on FRDAC in tele-operative surgery 136
6.3 Future Work . . . 138

References **141**

Appendices **151**
A Questionnaire study among dVRK users . . . 151
A.1 Kinematics and dynamics data . . . 151
A.2 Imaging data . . . 151
A.3 System state data . . . 151
A.4 Questionnaire Analysis . . . 152
B Figure Licenses . . . 154

List of Figures

2.1 Illustration of the Zeus robot (Computer Motion Inc.) . . . 31
2.2 The evolution of the da Vinci robot (Intuitive Surgical Inc.) . . . 32
2.3 Illustration of the VERSIUS robot (Cambridge Medical Robot Inc.) . . . 33
2.4 Illustration of the HUGO robot (Medtronics Inc.). . . . 34
2.5 Illustration GAC and FRAC. . . . 38
2.6 Illustration of the proxy and linkage representation in AC enforcement. . . . 41
2.7 Illustration of potential fields approaches in AC enforcement. . . . 42
2.8 The first-generation dVRK. . . . 49
2.9 Backlash of the da Vinci surgical instrument. . . . 52
2.10 Compliance of the da Vinci instrument. . . . 52

3.1 Illustration of $\mathtt{AX} = \mathtt{XB}$ problems. . . . 62
3.2 Illustration of $\mathtt{AX} = \mathtt{YB}$ problems. . . . 65
3.3 Cylinder edge projection . . . 70
3.4 Illustration of cylinder projection model . . . 71
3.5 Illustration of hand-eye transformation . . . 74
3.6 Flowchart for the on-the-fly hand-eye calibration framework . . . 75
3.7 Illustration of joint coordinate frames of the da Vinci instrument. . . . 76
3.8 Illustration of calibration on joint 4 angle reading. . . . 77
3.9 Cylindrical tool central axis reconstruction in experiment 1. . . . 78
3.10 Rectification of the initial hand-eye transformation matrix in experiment 2. . . . 80
3.11 Cylindrical tool central axis reconstruction in experiment 2. . . . 80
3.12 Comparison of particle filter observation models between our framework and [106]. . . . 81
3.13 A visual illustration of the effectiveness of the calibration framework in experiment 1. . . . 82
3.14 Comparison of tool tip positioning errors with a limited size of training dataset. . . . 83
3.15 Comparison of projection errors. . . . 84

4.1 Mesh-represented FRDAC generation. . . . 89
4.2 Comparison of average point registration errors. . . . 91
4.3 Illustration of AC evaluation and AC enforcement. . . . 93
4.4 Hardware setup in the user-free experiments. . . . 94

4.5 FRDAC algorithm workflow . . . 98
4.6 Illustration of the magnitude of "super fast" deformation. . . . 99
4.7 Comparison of static trajectory tracking between $\boldsymbol{Exp}_{\text{ours}}$ and $\boldsymbol{Exp}_{\text{Rydén}}$ in Chapter 4. 100
4.8 Static trajectory tracking results in Chapter 4. . . . 101
4.9 Comparison of d_{phantom} between $\boldsymbol{Exp}_{\text{ours}}$ and $\boldsymbol{Exp}_{\text{Rydén}}$ during dynamic tracking in Chapter 4. . . . 102
4.10 Comparison of d_{traj} between $\boldsymbol{Exp}_{\text{ours}}$ and $\boldsymbol{Exp}_{\text{Rydén}}$ during dynamic tracking in Chapter 4. . . . 103
4.11 Illustration of when Ryden's method generates false guidance due to noisy point cloud in $\boldsymbol{Exp}_{\text{Rydén}}$. . . . 105
4.12 Illustration of dynamic tracking (Mixed run 4). . . . 106
4.13 Comparison of AC evaluation time costs between $\boldsymbol{Exp}_{\text{ours}}$ and $\boldsymbol{Exp}_{\text{Rydén}}$ in several runs. . . . 106
4.14 AC evaluation in $\boldsymbol{Exp}_{\text{Rydén}}$. . . . 107

5.1 Expiration and inspiration aorta model created in Blender[170] . . . 113
5.2 Illustration of AC evaluation using DIBS . . . 114
5.3 Illustration of the dissipative AC controller . . . 116
5.4 Mapping between the SSMs and PSMs in tele-operation mode . . . 117
5.5 Illustration of when FRDAC is triggered on during trajectory tracking. . . . 119
5.6 Experimental setup in the user-present experiments in Chapter 5. . . . 120
5.7 Static trajectory tracking results in Chapter 5. . . . 122
5.8 Dynamic trajectory tracking results in Chapter 5. . . . 122
5.9 Dynamic reference trajectory overlay, frame 42. . . . 125
5.10 Dynamic reference trajectory overlay, frame 61. . . . 126

A.1 Questionnaire study among dVRK users. . . . 153

List of Tables

3.1 Comparison studies in pixel discrepancies. 84

4.1 Dynamic trajectory tracking time in $\boldsymbol{Exp}_{\text{ours}}$ 104
4.2 Dynamic trajectory tracking time in $\boldsymbol{Exp}_{\text{Rydén}}$ 104
4.3 Comparison of the computational cost incurred by different FRDAC approaches in $\boldsymbol{Exp}_{\text{ours}}$ and $\boldsymbol{Exp}_{\text{Rydén}}$. 104

5.1 P value of one-way ANOVA tests for tracking experiments in Chapter 5. 123

Acronyms

2D Two-Dimensional. 25, 44, 51, 54, 65, 66, 68, 79, 136
3D Three-Dimensional. 19, 25, 31, 44, 45, 51, 54, 65, 66, 70, 89, 96, 114, 118, 123, 134, 135, 139

AC Active Constraints. 7, 10, 11, 13, 14, 18, 20–23, 25–28, 36–44, 46, 47, 51, 58, 59, 86–89, 91–97, 100, 103, 104, 106–112, 114–119, 121, 123, 124, 127, 129–139
AFib atrial fibrillation. 44
ANOVA Analysis of Variance. 15, 123
API Application Programming Interface. 96
AR Augmented Reality. 34

BV Boundary Volume. 112
BVs Boundary Volumes. 91

CAD Computer Aided Design. 54, 67, 68, 90
CPD Coherent Point Drift. 46, 88, 90
CT Computerized Tomography. 19, 29, 38, 45, 87, 89, 138
CTG Constraints Tool Geometries. 36, 37, 39, 40, 44, 59, 91, 92, 97, 112

DAC Dynamic Active Constraints. 37, 38, 43, 44, 46, 47, 59
DH Denavit-Hartenberg. 51, 55, 67, 76
DIBS Deformation Invariant Boundary Spheres. 91, 92, 96, 97, 100, 102, 103, 112
DL Deep Learning. 35
DOFs Degrees of Freedom. 20, 30–32, 53, 111, 114, 116, 134, 137, 139
dVRK da Vinci Research Kit. 7, 11–14, 18, 21–23, 25, 27, 28, 49, 59, 60, 74, 76–79, 85, 94–96, 109, 111, 116–118, 123, 124, 127, 129–132, 136, 137, 139, 151–153

ECM Endoscopic Camera Manipulator. 20, 151
EKF Extended Kalman Filter. 45, 54, 67

FPFH Fast Point Feature Histograms. 90, 97, 112
FRAC Forbidden Region Active Constraints. 13, 37–39, 44, 46, 58, 86, 87, 110, 132
FRDAC Forbidden Region Dynamic Active Constraints. 7, 10–15, 22, 25–27, 37, 45, 46, 48, 59, 85–127, 130, 132–140

GAC Guidance Active Constraints. 13, 37–40, 44, 46, 58, 87, 110
GDAC Guidance Dynamic Active Constraints. 37, 38, 44, 45, 59
GPU Graphics Processing Unit. 91, 95, 103

HD High-Definition. 152
HIP Haptic Interface Point. 40, 96, 97, 100, 115

IM Interactive Manipulation-based. 57
IoU Intersection over Union. 68

LM Levenberg-Marquardt. 65, 73

LPs laparoscopic radical prostatectomies. 20

MIS Minimally Invasive Surgery. 19, 29, 33, 58
MRI Magnetic Resonance Imaging. 38, 45, 87, 89

PF Particle Filter. 10, 54, 68, 74, 85
PSM1 Patient Side Manipulator 1. 78, 94–97, 118, 120
PSMs Patient Side Manipulators. 11, 14, 20, 53, 73, 116, 117, 151

RAS Robotic Assisted Surgery. 18, 19, 29, 58, 86, 87
RCM Remote Centre of Motion. 56, 68, 73–76
RGBD Red, Green, Blue, Depth. 78, 95, 118, 123, 136
RMIS Robotic Assisted Minimally Invasive Surgery. 21, 43, 50, 56, 58, 59, 87, 94, 131
RNN Recurrent Neural Network. 78
ROS Robot Operating System. 95, 96, 117

SAM Segment Anything Model. 79, 135, 138
SD Standard-Definition. 152
SSMR Surgeon Side Manipulator Right. 120
SSMs Surgeon Side Manipulators. 11, 14, 20, 53, 116, 117, 151
SUJs Set-up Joints. 56
SVD Singular Value Decomposition. 63, 64

US Ultrasound. 38, 45

VF Virtual Fixtures. 20, 21, 25, 27, 36, 38, 58, 87

Chapter 1

Introduction

This chapter reviews the development of Robotic Assisted Surgery (RAS) and introduces some of the state-of-the-art commercially available surgical platforms that are designed for conducting RAS. The most commercially successful surgical robot, the da Vinci robot, a tele-operative surgical platform, was reported to exhibit a major technical drawback: the lack of haptic feedback for surgeons, which increases the mental workload of surgeons, and consequently, jeopardises patients' safety. To address this issue, this thesis has been formulated to develop a strategy to provide haptic guidance for surgeons to reduce their mental workload as well as to ensure task safety. The focus of this thesis is the development of a dynamic Active Constraints (AC) pipeline that can be integrated into a tele-operative surgical testing platform, which is the first-generation da Vinci Research Kit (dVRK). To realise these goals, essential research tasks of this thesis have been defined. Firstly, a detailed review of the state-of-the-art studies on the implementation of AC in tele-operative surgery is required. Secondly, technical details and latent caveats in the integration of AC and the hardware platform should be recognised. Thirdly, methods for addressing pertinent technical constraints of the robot should be developed to pave the way for the integration of the AC pipeline. Fourthly, a bespoke dynamic AC pipeline for tele-operative surgery, allowing for tissue deformation at interactive speeds, should be developed. Ultimately, the effectiveness of the proposed dynamic AC pipeline should be verified in a realistic experimental scenario with user-in-the-loop.

1.1 Overview

Minimally Invasive Surgery (MIS) has gained more popularity over traditional open surgery because it introduces a less invasive approach to conducting surgery, thus leading to a smaller size of wound and reduced hospitalization time for patients [1]. However, it demands more skills from surgeons to conduct surgeries under a limited vision, with less dexterity in a restricted environment, which results in a steeper learning curve and heavier mental workload [2]. To address these drawback, the concept of RAS emerged, with the aim of enhancing surgeons' ability to perform surgical tasks to a high accuracy even under challenging conditions. The introduction of robots to the operating theatre results in magnified Three-Dimensional (3D) vision, enhanced dexterity, and increased repeatability in performing tasks, such as cutting and suturing, to a high accuracy [3].

The first RAS took place in 1985. An industrial robot PUMA 200 holding a probe at its end-effector was deployed together with a Computerized Tomography (CT) scanner for brain biopsy [4]. Once a target point is identified on the CT image, the end-effector is positioned close to an entry point next to the head of the patient, guiding the path through which surgeons could insert biopsy needles. Although the robot was used unpowered, and there was no intra-operative interaction between the robot and the surgeon, this clinical trial demonstrated a higher accuracy achieved by a calibrated robot over using a manually adjustable frame, and it laid the foundation for the future uptake of RAS. In contrast to the cases where surgical robots are used as "passive" tool holders, such as in [4], there also exists robots that are allowed to have more complex motions during operation, hence are classified as "active". Examples of first-generation "active" surgical robots include laparoscopic camera robots that can advance and move the camera to provide better visions for surgeons; "Robodoc", an orthopaedic surgical robot that can perform cutting tasks based on pre-operative plans, and "Probot", a prostatectomy robot that can execute a fixed series of motions. However, the major drawback of active surgical robots is a rising concern for safety and potential liability issues. Additionally, the inability to react to dynamic surgical situations restricted its application scenarios to rigid surgery and tasks that do not require high accuracy. To address these limitations, the idea of establishing synergy between surgeons and robots phased in, hence the concept of "cooperative" surgical robots. Instead of devolving surgical tasks to robots, surgeons take full charge of the surgery whilst receiving assistance from robots, in the form of haptic guidance. Examples of first-generation "cooperative" surgical robots include ACROBOT [5], a platform for knee replacement surgery, which provides various magnitudes of force feedback for surgeons during cutting different regions of knee bones, and the Zeus system, a tele-manipulator system which improves surgical task precision through filtering the hand tremor of users.

Over the course of almost 30 years' development, today's state-of-the-art mainstream medical robots that are commercially available include: CORI surgical system (Smith & Nephew) for orthopaedics surgery; ROSA robot (Zimmer Biomet) designed to assist with spine surgeries; MAKO

(Stryker) for joint replacement surgery; Versius robot (CMR) featuring a small and modular design for laparoscopic surgery; MONARCH platform (Johnson & Johnson) tailored for bronchoscopic surgery; HUGO robot (Medtronics), a telesurgery platform that features one open console and four independent arm carts, and the da Vinci robot (Intuitive Surgical Inc). Among all the surgical robots mentioned above, the da Vinci robot is undoubtedly the most successful surgical system, with over 14 million procedures having been performed [6] and over 7,500 da Vinci robots installed around the world [7]. A full da Vinci robot consists of two Surgeon Side Manipulators (SSMs), three Patient Side Manipulators (PSMs) and one Endoscopic Camera Manipulator (ECM). The system provides better visual feedback for surgeons as they put their heads on the headrest whist observing surgical instruments attached on PSMs following their hand movements with a scaled magnitude. Clinical trials have demonstrated the effectiveness of using the da Vinci robot in treating laparoscopic radical prostatectomies (LPs), supported by significantly better surgical outcomes compared to open surgery [8]. However, a major technical limitation of the system is the lack of haptic feedback [9], forcing surgeons to develop understandings of the current surgical scenario through pure visual information, which increases the learning curve for inexperienced users. Admittedly, there has been constant controversy over the role of haptic feedback and its necessity in tele-operative surgery [10]; however, this thesis assumes that haptics provides additional beneficial effects to surgery. It was not until March 2024, when da Vinci 5 was released, that the first-of-its-kind tele-operative surgical robot with force feedback appeared. Nevertheless, a da Vinci 5 system is estimated to cost between 2 and 2.5 million dollars [11], which is 15 % more expensive than a da Vinci Xi system, a previous version of the robot without haptic modules equipped, and nearly double the price of a HUGO robot (Medtronics), which costs between 0.9 and 1.2 million dollars [12]. Therefore, it remains valuable to develop a cost-effective strategy that facilitates the telesurgery process for surgeons and is generalisable across different platforms.

A direct approach to addressing the limitation above is to incorporate a multi Degrees of Freedom (DOFs) force sensor attached onto the instrument so that the measured interaction force between the instrument and tissue can be relayed to the surgeon. This approach, however, requires the incorporation of an external device that measures dynamic force interactions into the closed-loop system, which may jeopardise system stability. Additionally, accurate force measurement requires placing the sensor to the tip of the instrument, which generates more constraints on the size and mechanical properties of the sensor. Moreover, the need for safety and usability adds to the cost of designing a haptic sensing device that can withstand extreme sterilisation conditions [13]. An alternative approach is to generate haptic guidance that informs surgeons of the current status without relying on external devices other than the built-in setup. This virtually generated haptic guidance is referred to as Virtual Fixtures (VF), also named AC.

AC/VF are high-level control algorithms that aim to enhance surgical performance by providing haptic guidance whereby movements that conform to pre-operative plans and safety requirements are allowed and enhanced, whereas those that violate these requirements are prohibited. [14]. The

concept of VF was first conceived by Rosenberg, who made an analogy that VF are to surgical tasks what a ruler is to drawing a straight line [15, 16]. VF, a generalised "ruler", can be interpreted as a perceptual overlay to enhance user performance by generating sensory cues to reduce users' mental workload. Compared to a "real" fixture that is physically touchable, VF are algorithmic generations and do not introduce mechanical constraints to hardware design and thus are transferable across different platforms. The efficacy of AC in enhancing surgical task performance was validated through clinical trials [17], where an AC enabled robot, Acrobot, was tested on hands-on knee replacement surgery. The results showed that a better accuracy in joint alignment was achieved and that a significant enhancement in postoperative improvement was recorded with the assistance of AC compared to conventional surgery. However, up until now, there is still a lack of studies in verifying the efficacy of AC within a tele-operative clinical setup. There are several reasons for this. First, compared to hands-on knee replacement surgery, there are more dynamic factors to allow for in telesurgery, such as the interaction between the instrument and tissue surface. Second, there requires a better integration of the developed AC strategy with the tele-surgery platform. Third, unlike hands-on surgery where surgeons feel directly the haptic guidance, in telesurgery, the haptic cues need to be transferred from the patient side to the surgeon side, which incurs a time delay, hence resulting in a more demanding set of requirements. To help push the frontier of the field, it is valuable to develop a bespoke AC pipeline for telesurgery whilst addressing these challenges.

While a manually-designed hardware platform to test algorithms developed for teleoperation is usually required, in this study, we employ a readily available testing platform built out of the first-generation da Vinci robots, named as the dVRK. Thanks to an initiative launched in 2012, a set of retired first-generation da Vinci robots was repurposed and converted into dVRKs, which consist of both a software package and hardware controllers, to further propel Robotic Assisted Minimally Invasive Surgery (RMIS) research on the da Vinci surgical platform. These dVRKs have been distributed to research institutions around the world. Until now, more than 40 research groups across 10 countries have benefited from the initiative, forming a thriving dVRK research community, with more than 250 peer-reviewed research papers on the dVRK having been published [18]. Although research conducted on the dVRK branches into different topics, almost all of these works deal with data directly provided by the dVRK, containing kinematics, image and system information. These data are arguably the best source of information available to users who wish to keep abreast of the latest state of the robot as they develop novel research on the dVRK. However, blind reliance on the fidelity of these data can be risky. The inaccuracy of dVRK data partly arises from the intrinsic design of the tele-surgical platform, and partly from limitations of the factory calibration of the hardware. Therefore, it is essential to identify and address these technical constraints before a bespoke AC pipeline can be effectively integrated into the system.

1.2 Thesis Aim & Objectives

The aim of this thesis is to explore Forbidden Region Dynamic Active Constraints (FRDAC) for tele-operative surgery, addressing the requirements and limitations of the current AC designs for tele-operative surgery, as well as the technical constraints of the dVRK, the testing platform into which the developed AC pipeline is integrated.

Research Task 1
Explore relevant literature on the topic of AC applied to tele-operative surgery to recognise the design requirements and identify limitations of current approaches.

Research Task 2
Explore relevant literature on the dVRK to identify technical constraints of the system and essential calibrations to compensate for these constraints when conducting various aspects of research involving the robot.

Research Task 3
Develop a calibration framework to address the end-effector positioning error induced by the cable-driven property of first-generation dVRKs, to provide more accurate inputs for the AC pipeline.

Research Task 4
Establish a bespoke AC pipeline for tele-operative surgery, allowing for factors such as dynamic movements of tissue surfaces and the speed requirement for effective haptic guidance to be met.

Research Task 5
Verify the effectiveness of the established AC pipeline within a realistic experimental setup with user-in-the-loop.

1.3 Contributions

The contributions of this thesis are listed below:

Detailed Literature Review of the technical constraints of the first-generation dVRK
The first notable contribution of this thesis is a comprehensive review of technical constraints and essential calibrations of first-generation dVRKs. In this review, common technical problems encountered by dVRK users are recorded and analysed, which include kinematics calibration, hand-eye calibration *etc.* Potential avenues to address these problems are also provided.

Develop an on-the-fly hand-eye calibration pipeline to improve positioning accuracy
The second contribution of this thesis involves the development of an on-the-fly hand-eye calibration framework that aims to address the technical constraints of the first-generation dVRK. The proposed calibration framework leverages real-time image information and provides a means to improving the end-effector positioning accuracy. The experimental results demonstrated an average decrease in positioning error and a more consistent calibration outcome compared to state-of-the-art offline calibration approach.

A new AC formulation for tele-operative surgery
The third contribution of this thesis involves the establishment of a dynamic AC pipeline for tele-operative surgery to prevent violations of safety regions, allowing for tissue movements. In vitro experiments were conducted using a pulsating aorta phantom to verify the efficacy of the developed pipeline. Comparative studies demonstrate the robustness and time-efficiency of this new pipeline compared to a state-of-the-art AC pipeline employing different AC representations.

Proof of concept validation of the developed dynamic AC strategy in a tele-operative scenario with user-in-the-loop
The final contribution of this thesis is the validation of the dynamic AC pipeline in a dynamic user-present scenario on the first-generation dVRK.

The relevant contributions listed below provide further evidence of these contributions:

- *Cui, Z., Cartucho, J., Giannarou, S. and Rodriguez y Baena, F., 2023. Caveats on the first-generation da Vinci research kit: Latent technical constraints and essential calibrations. IEEE Robotics & Automation Magazine.*
- *Cui, Z. and Rodriguez y Baena, F., 2023. Proof of Concept Implementation of Forbidden Region Dynamic Active Constraints in Minimally Invasive Surgery. Proceedings of The 15th Hamlyn*

Symposium on Medical Robotics 2023.

- *Cui, Z. and Rodriguez y Baena, F., 2024. Calibration Framework for Positioning Accuracy Improvement of da Vinci Surgical Instruments. Proceedings of The 16th Hamlyn Symposium on Medical Robotics 2024.*
- *Cui, Z. and Rodriguez y Baena, F., Forbidden Region Dynamic Active Constraints in Robot-Assisted Minimally Invasive Surgery. IEEE Robotics & Automation Letters. (Accepted in January 2025)*
- *Cui, Z. and Rodriguez y Baena, F., On-the-fly hand-eye calibration framework for the da Vinci surgical robot. IEEE Transactions on Medical Robotics and Bionics. (Currently under review for the special issue entitled "The Hamlyn Symposium on Medical Robotics 2024".)*

These five contributions are derived from the work undertaken and presented throughout the technical chapters 3, 4, and 5.

1.4 Thesis Structure

In Chapter 2, a literature review is presented, which aims to equip readers with knowledge of technical concepts that recur in this thesis and to help form a high-level understanding of how the subsequent technical chapters are connected. The review is divided into three parts: the first part begins with an overview of surgical robots, tracing the history of the development of these robots, with a focus on tele-operated surgery. After identifying the advantages and disadvantages of tele-operated surgical platforms, the concept of AC, also known as VF is introduced, along with its clinical application scenarios and technical implementation details. Following this, the first-generation dVRK, the robot upon which all the experimental studies in the following chapters are conducted, is introduced in detail. Additionally, several technical constraints of the da Vinci robot are analysed, and potential avenues to resolve these constraints are presented. This technical analysis indicates obstacles that need to cleared towards developing an effective FRDAC strategy for tele-operative surgery. At the end of Chapter 2, a conclusion is presented, summarising the requirements in FRDAC design that need to be fulfilled and pertinent constraints of the hardware platform that need to be overcome, in support of the subsequent technical chapters.

Chapter 3 introduces the design of an on-the-fly hand-eye calibration framework for improving instrument positioning accuracy of the first-generation dVRK. After a brief introduction to hand-eye calibration, the mathematical backbone of the calibration framework which leverages the cylindrical geometry of surgical instruments is described in detail. Experiments to verify and compare the effectiveness of the proposed calibration framework against other methods mentioned in the literature are outlined. The calibration performance is characterised by both 3D end effector positioning errors and Two-Dimensional (2D) projection errors on the image. The formation of the calibration pipeline enables a more accurate estimation of end-effector position obtained from dVRK kinematics data. In theory, the end-effector position is then to be used as input to a bespoke FRDAC framework outlined in Chapter 4.

Chapter 4 presents the conception of a bespoke FRDAC pipeline for tele-operative surgery, taking into account dynamic tissue deformation caused by respiration. The literature review section focuses on the technical aspects of the three interrelated stages that consist of the implementation of AC, namely AC generation, AC evaluation and AC enforcement. The establishment of the overall FRDAC pipeline is elaborated. To verify the effectiveness of the pipeline, the design of *in vitro* experiments, where a surgical instrument tracks predefined trajectories above the surface of a pulsating aorta phantom, emulating the presence of a human, are outlined. The trajectory tracking performance is compared with that of another FRDAC method, where FRDAC are represented using simple geometric shapes, specifically spheres. To evaluate different FRDAC methods, both tracking accuracy and the safety distance maintained between the instrument and tissue surface are used as metrics. The implications of different FRDAC methods in a more realistic scenario

where there is human presence, are discussed.

Chapter 5 presents a further validation of the previously proposed FRDAC pipeline in a user-present tele-operation scenario. Initially, a literature review on AC user studies are undertaken, demonstrating the criteria needed to evaluate AC performance in a user-present scenario. Following that, a detailed description of the experimental setup and surgical tasks designed for user experiments is provided. Results obtained from different FRDAC methods are recorded and analysed. Limitations of the pilot user study and future work are discussed.

The thesis concludes with Chapter 6, where the narrow limitations indicated in the previous technical chapters are reiterated, and more general limitations are also considered. In addition, potential approaches that could improve the results of the studies are elaborated. Furthermore, future avenues to push forward the work presented in this thesis are summarised.

Chapter 2

Literature Review

This chapter introduces the background theory and key concepts that help facilitate a better understanding of the subsequent chapters, while also presenting some highly relevant research. This chapter begins with an overview of surgical robots, tracing the history of the development of these robots, with a focus on tele-operated surgery. After identifying the advantages and disadvantages of tele-operated surgical platforms, the concept of AC, also known as VF is introduced, along with its clinical application scenarios and technical implementation details. Following this, the first-generation dVRK, the robot upon which all the experimental studies in the following chapters are conducted, is introduced in great detail. Additionally, several technical constraints entrenched in the robot are analysed, and potential avenues to resolve these constraints are presented. This technical analysis indicates obstacles that need to cleared towards developing an effective FRDAC strategy for tele-operative surgery.

2.1 Introduction

The overarching goal of this thesis is to develop a control framework that assists surgeons in performing tele-operated surgery in a clinical setting, aiming to reduce their mental workload during complex procedures and thereby enhance task safety. To achieve this goal, there are two essential elements that need to be considered: algorithm development and algorithm validation. The development of a bespoke algorithm to be implemented in tele-operated surgery presents different challenges compared to hands-on surgery. Therefore, an analysis of robots for tele-operated surgery and their specific requirements need to be presented. In addition, the design of the control framework needs to be justified through evaluating similar strategies in the current literature, and the high-level design goals, as well as implementation modules, need to be clarified. Eventually, to validate the designed control framework, an integration of the algorithm and the hardware platform is needed. However, prior to the final integration, there are several obstacles that need to be addressed to ensure an unbiased validation outcome. Therefore, identifying these challenges and being aware of the procedures to overcome these challenges are needed. To this end, the structure of this chapter is arranged as follows.

The first section presents an overview of the development of surgical robots from their inception to their current status, with an emphasis on tele-operated surgical robots. Landmark events in the history of surgical robots development are highlighted. Specifically, some of the trending commercially available tele-operated surgical platforms are introduced. The advantages and disadvantages of these platforms, as well as prevalent research aimed to address these disadvantages, are also discussed, which justifies the adoption of AC as the avenue of research in this thesis.

The second section presents an overview of AC including its concept, classifications, and implementation details. The current literature on AC is evaluated, with a focus on the implementation of AC on tele-operated surgery. Existing challenges and potential solutions to address these gaps are discussed, forming the basis for the algorithm development.

The final section presents an overview of the first-generation dVRK, the hardware platform upon which the developed algorithm is tested. In addition to an introduction of its technical components and operational details, its inherent technical limitations and potential solutions to address these limitations are discussed in depth. The analysis forms the basis for the calibration framework designed to ensure the fidelity of the algorithm validation outcome. This section has been published in IEEE Robotics & Automation Magazine [19].

The synthesis of these three sections aims to provide readers with a clearer understanding of the research objectives of this thesis. As a prelude to rest of the thesis, this chapter justifies the organisation of the following technical chapters and aims to equip readers with the basic knowledge needed to understand them better.

2.2 Surgical robots

Since the first RAS was conducted in the 1980s, the practice of introducing robots to the clinical theatre has steadily increased. In recent years, there has been a rising number of research on medical robotics. The potential benefits of deploying robots within the operating theatre, such as an improvement in task performance and a reduction in operating time, not only promise a bright future that motivates researchers to strive for these advancements, but also have attracted more people from industry to join the competitive business landscape. The advantages provided by the assistance of robots are most evident in MIS, where traditional approaches pose great challenges to surgeons in manipulating instruments within a confined workspace, leading to an increased mental workload. Over the past three decades, there have emerged both commercially available surgical robot products in the market and prototypes that are still in an early research stage, targeting a vast range of surgical applications. Therefore, it is valuable to first review literature to identify the benefits and limitations of the current surgical robots, which will help guide the direction for future research.

2.2.1 The development of surgical robots

The first publication [4], released in 1988, documented the practice of using a robot inside the clinical theatre, where an industrial robot PUMA 200 (Unimation Inc.) was deployed to guide a probe attached at its end-effector along a straight trajectory during insertion for CT-guided brain tumour biopsies. Although the robot was not purposely built for medical surgery applications and functioned merely as a tool holder, the significance of this feat was remarkable in that it widened the application field of robots and demonstrated their ability to provide a higher level of positioning accuracy compared to human manual operation. Motivated by the success of the initial clinical trial, several robotic platforms that are customised for surgical applications emerged shortly thereafter. These robots played a more active role in the overall surgical workflow.

In 1989, the first surgical robot tailored for prostatecotomy (PROBOT) was developed at Imperial College London [20]. In contrast to the passive role played by the PUMA robot in the first clinical trial, PROBOT was able to execute the tasks of removing prostate gland tissue, following a pre-operative cutting procedure without further interference from surgeons. Compared to a fully-manual approach to performing prostatectomy in a confined working environment, a robot was shown to be adept at achieving a high cutting precision without damaging adjacent tissue or encountering fatigue issues. The advantage of employing a robot to achieve high accuracy and high repeatability was also favoured in orthopaedic surgery. Later in 1992, surgical robot ROBODOC (Integrated Surgical Systems) was developed for assisting total hip arthroplasty surgery [21]. After receiving information on location and orientation to be reached from a patient's CT scan, the robot was able to independently machine a bespoke implant cavity on the femur with high accu-

racy. Although both PROBOT and ROBODOC freed the hands of surgeons during surgical operation, their application scenarios were restricted to semi-rigid and rigid operations, respectively, where tissue movements and tool-tissue interactions were either not considered or negligible. More importantly, surgeons were dissatisfied with being out of the loop, raising concerns over safety and liability issues [22].

The developments in surgical robots were also reflected in laparoscopic surgery. In 1994, AESOP (Automated Endoscopic System for Optical Positioning, Computer Motion Inc.) robot systems became commercially available [23]. The robot allowed surgeons to control the orientation and advancements of endoscopes either manually, through foot pedals, or even by voice commands during navigation [24], instead of relying on another human assistant to manipulate the endoscope camera. This provides surgeons with a more stable visual field. Another revolutionary breakthrough was recorded in 1998, when ZEUS (Computer Motion Inc.), a tele-operative surgical platform, was commercially released. The entire surgical platform consists of one AESOP arm and two surgical arms, each with 4 DOFs, mimicking the hand movements of surgeons sitting at the console and manipulating joysticks. Figure.2.1 presents the design of the ZEUS robot. The advantages of ZEUS were demonstrated through a variety of complex surgical tasks in cardiovascular surgery [25], owing to its mechanical designs that can filter out hand tremor and enhance dexterity through scaling down the hand movements of surgeons. More remarkably, the first transcontinental tele-operative laparoscopic cholecystectomy was performed on ZEUS [26], validating the feasibility of tele-surgery across a long distance. From a safety perspective, ZEUS robot ensures that instruments on the patient side remain static when there is no command sent across from the surgeon side, thus ensuring that surgeons always are in charge. Compared to hands-on surgery, tele-operative surgical platform improves ergonomics for surgeons when operating within a distance from patients. Moreover, the prospect of allowing surgeons to perform surgery across a long distance with tele-presence can alleviate inequalities in the distribution of healthcare resources and reduce the cost of healthcare per patient in the long run. Shortly after the launch of Zeus, in 1999, another tele-surgical platform, the first-generation da Vinci surgical robot was released [27], consisting of a surgeon console, a vision cart and three robotic arms holding an endoscopic camera and instruments. In 2003, Intuitive Surgical Inc. acquired Computer Motion Inc., establishing itself as a pioneer in the surgical robots market for more than two decades [27].

2.2.2 Surgical robots for tele-operative surgery

The conception of tele-operative surgical robots has largely resolved the challenges faced in conventional laparoscopic surgery, and its efficacy was first verified through clinical trials involving urologic and cardiac surgeries using the da Vinci robot [29]. It was also shown that the advantages of using a tele-operative system, compared to conventional procedures, are most evident in radical prostatectomy, with evidence showing reduced pain levels and better post-operative recovery outcomes in patients [30]. The first-generation da Vinci robot system consists of a surgeon console,



Figure 2.1: Illustration of the Zeus robot (Computer Motion Inc.) This picture is from [28] (Licensed by the author of the referenced document. Written proof in the appendix)

three robotic arms attached to the patient trolley and a vision cart. Surgeons can place their eyes on a binocular stereoscopic vision system that enables them to form a 3D view as seen by the endoscopic camera while their hands are manipulating 7 DOFs joysticks that transmit scaled hand movements to the instruments operated on a patient. Surgical instruments are attached to two of the patient-side robotic arms, while an endoscopic camera is attached to the third. Video information streamed from the endoscopic camera is projected on to the vision cart screen, providing assistants with real-time visualisation of the surgical scenario. To make the da Vinci robot system better adapted to a wider range of surgical applications, its design has gone through rounds of iterations. Stemming from the original design where there were only three robotic arms, in 2002, the design that incorporates a fourth arm holding an extra instrument came out, with an aim to assisting surgeons in exposing anatomical structures more easily [31]. However, one drawback in the original design was that the instruments lack a wide range of motion, requiring more techni-

cal efforts when positioning multiple entry ports during operation. This forced surgeons to adopt a more complicated hybrid approach when accessing multi-quadrants of the abdomen with the robot, which restricted its applications in gastrointestinal surgery. To compensate for this problem, the da Vinci Si system, with longer instruments and a wider range of motion, was released in 2009. Studies validated the advantage of this new design in facilitating colorectal procedures [32]. To further enhance ergonomics and reduce user learning curve, a more sleek design, the da Vinci Xi, equipped with lightweight robotic arms and an endoscopic camera with a reduced size, was launched in 2014. Multiple studies revealed that the average operation time was comparable with da Vinci Si, but the price is more costly [33]. The most recent breakthrough in the robot design was in 2024, when the latest version da Vinci V was released, marking the first version of the da Vinci robot that allows haptic feedback to be received by surgeons. The latest version of the robot has resolved the long-standing problem of a lack of haptic feedback, which has been considered as one big area for improvement in tele-surgical platforms [34]. The evolution in the design of the da Vinci robot is shown in Figure.2.2.

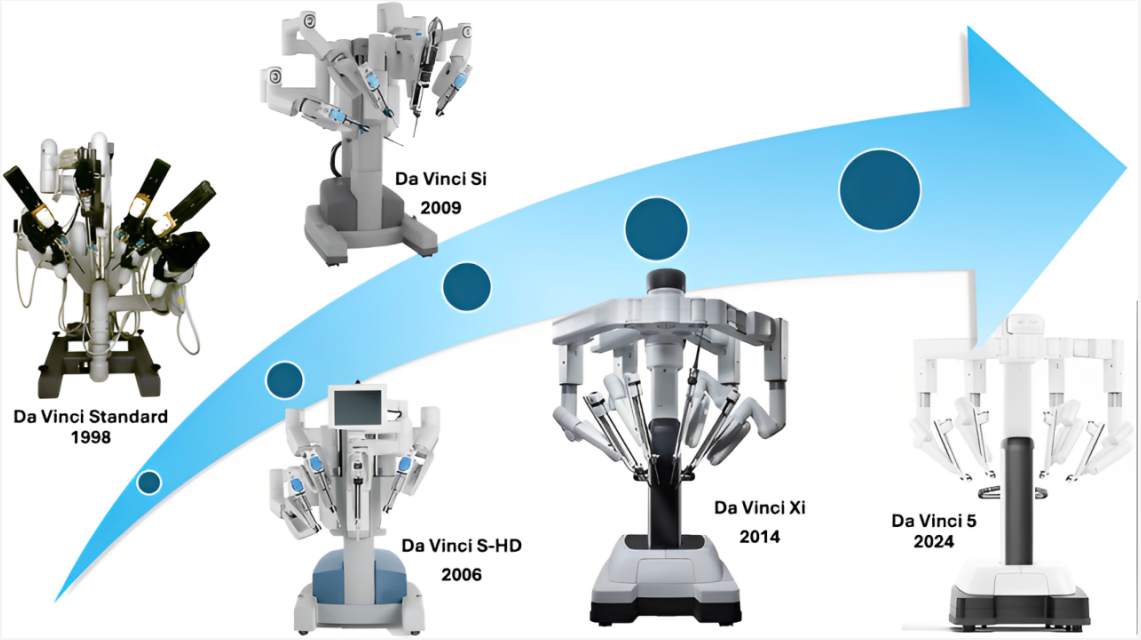


Figure 2.2: The evolution of the da Vinci robot (Intuitive Surgical Inc.) This picture is from [35]. (Licensed by the author of the referenced document. Written proof in the appendix)

Undoubtedly, the da Vinci robot is by far the most successful surgical robot available in the market, with over 7,500 platforms currently deployed in the clinical theatre and more than 10 million surgical procedures having been conducted [7]. However, in recent years, there has seen a rapid growth in the development of new tele-operated surgical robots, which are gradually expanding in the market. In 2019, the VERSIUS robot (Cambrdige Medical Robot Inc.), a 7DOFs tele-operated robot with up to four robotic arms, was first introduced into the market for assisting surgeons with general surgeries. Featuring a small and modular design and an open console, the VERSIUS robot

(Figure.2.3) was marketed to have the advantages of a small footprint and an enhanced portability. Different from the da Vinci robot, VERSIUS adopts a "decentralised" design where all the robotic arms are attached to their individual surgical carts. The feasibility of using a VERSIUS robot during human operation was verified across a range of MIS, including prostate surgery [36], thoractic surgery [37] and colorectal surgery [38]. Bearing a similar "decentralised" design, in 2021, the HUGO robot (Medtronics Inc.) was released, including a surgeon console, three robotic arms holding instruments and one arm holding an endoscopic camera. Since 2023, the HUGO robot (Figure.2.4) has been deployed in hospitals in the UK, and more than 1,500 operations are performed each year [39]. The cost of a HUGO robot is estimated between 0.9 and 1.2 million dollars, which is 20-40% cheaper than a da Vinci Xi system (between 1.5 and 2.5 million dollars) [12], and there is clinical evidence showing that there is no statistical significance in the surgical outcomes achieved using both platforms, including operative time, blood loss and post-operative complications [40], which foreshadows its potential in the market. The burgeoning of new tele-operated surgical robots in recent years is also suspected to be related to the fact that the patent that Intuitive bought from ZEUS has expired [41], and hence more competitions in this field are expected in the future.

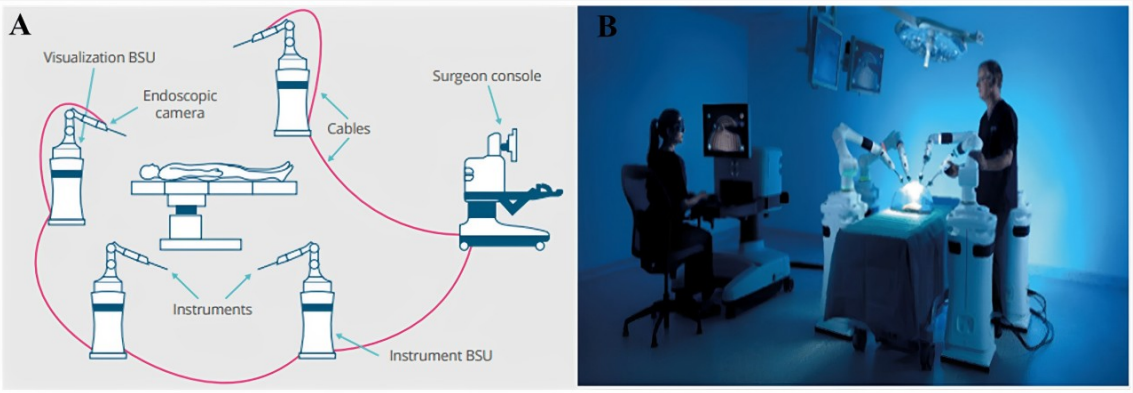


Figure 2.3: Illustration of the VERSIUS robot (Cambridge Medical Robot Inc.) The entire system consists of one surgeon console, three instruments and one visualisation Bed Side Unit (BSU). The system features a decentralised design. This picture is from [42] (Licensed under CC BY-NC 4.0)

2.2.3 Research in tele-operative surgery

A rising popularity in tele-operative surgery was also reflected in the research area. Even as early as 2000, researchers started to envision the future of general tele-operated robots, including a higher-level of intelligence which can free users from being distracted by low-level trivial tasks, and a more miniaturised design that can be of assistance to applications in more inaccessible spaces [44]. The same objective is also applied to tele-operated surgical robots. After the beginning of introducing the da Vinci robots to the operating theatre, Corcione *et al.*[2] mentioned that the designs of the robot could be improved by increasing the number of robotic arms to better manage intra-operative emergencies such as bleeding, and by miniaturising the size of surgical instruments to reduce in-

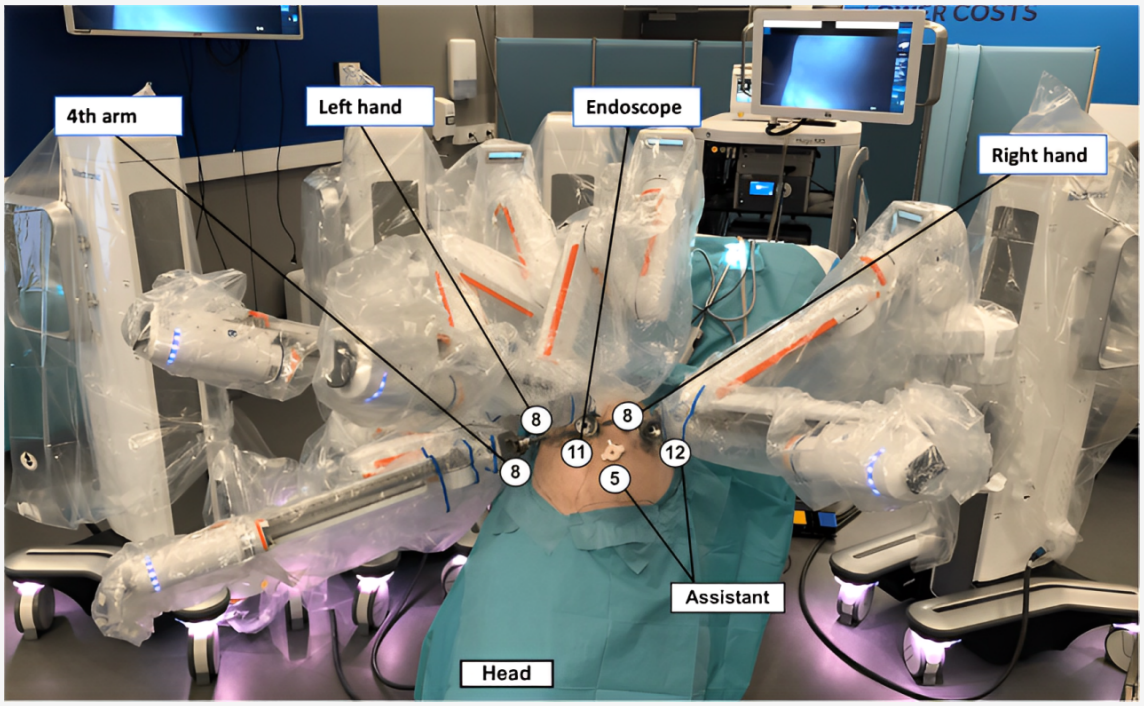


Figure 2.4: Illustration of the HUGO robot (Medtronics Inc.). Like the VERSIUS robot, the HUGO robot also features a "decentralised" design. This picture is from [43] (Licensed by the author of the referenced document. Written proof in the appendix)

vasiveness. In 2013, Freschi *et al.*[9] also proposed that one major limitation of tele-manipulators, even the da Vinci robots, is the lack of haptic feedback for surgeons, which leads to higher forces being applied to tissues and increases surgeons' mental workload during complex surgical procedures. The lack of haptic feedback was also considered as a key factor that contributed to a steeper learning curve for surgeons, as reflected by an increase in the number of cases required to achieve a standardised technical expertise and a higher likelihood of encountering untoward peri-operative situations, such as deviation from the path and damages to healthy tissues [45].

To compensate for these issues and help reduce the cognitive burden of surgeons, research has been conducted in various directions. One of the mainstream school of thoughts is to provide more effective intraoperative image guidance. Accurate registration of pre-operative images to intraoperative images captured by the endoscopic camera can facilitate the process of identifying regions of interests on the tissue surface. By overlaying preoperative plans to the field of view of surgeons using Augmented Reality (AR), surgeons receive additional visual guidance during task implementation. The other prevalent school of thought is to provide haptic guidance for surgeons to reduce their mental workload, especially when conducting complex and delicate procedures [46]. The most straightforward solution is to integrate into the robotic system an external force/torque sensor attached on the instrument tip so that surgeons can perceive the force/torque measured by the sensor in the form of stimulation on their fingers and hands generated from motors. However, this approach poses more challenges in instrument design in terms of size and material selection

to accommodate for extreme sterilisation conditions per se. Although with the advancement of Deep Learning (DL), there emerged studies on estimating the interaction force through sensor-free approaches [47], the consistency of the force estimation accuracy across various surgical procedures still needs to be investigated, and the prerequisite data collection procedure, which involves the installation of a sensing device on the instrument in a clinical theatre, remains demanding. More importantly, the incorporation of haptic devices that reproduce forces/torques usually introduces time-varying destablising factors, such as sudden grip and release, hard contacts, *etc.*, which jeopardise the stability and transparency of the surgical system and thereby affect task safety [48]. An alternative way is to incorporate a tactile device instead of a haptic device, as tactile feedback is sent via direct stimuli on the fingertip of users, rather than generating another active force/torque. However, the mapping from the side of measurement to the side of perception is more challenging because it involves processing measurements at an array of collection points, and the assistance provided by pure tactile feedback was shown to be less effective than full haptic feedback, as expected [48]. An alternative way is to provide virtually generated force/torque guidance, without impairing the stability of the system, which is the research focus of this thesis. An overview of this alternative strategy is presented in Section.2.3

2.3 Overview of Active Constraints

AC also named as VF are high-level control strategies to assist in human-robot collaborations by providing anisotropic guidance for users so that motions that comply with safety requirements and pre-operative plans are allowed whereas those that violate these requirements are annulled. Bowyer *et al.*[14] in 2013 conducted a thorough survey and proposed a systematic framework for AC implementation, which includes three interrelated stages, namely, AC generation, AC evaluation, and AC enforcement. This review clarifies essential concepts within this research topic and categorises literature based on the implementation stages that comprise the proposed framework, which is widely adopted by subsequent research. However, there lacks a survey on more recent research articles on AC. Therefore, to help readers better understand the technical details and contributions of the research undertaken in this thesis, it is important to present an up-to-date review of related research conducted in recent years, evaluating both the contributions and limitations. To this end, in this subchapter, key concepts of AC that frequently appear in this thesis will be explained, and the contributions and limitations of current research studies on AC will be evaluated. Although this review focuses more on recent publications, several seminal studies covered in the previous review [14] will also be referenced. Readers who require detailed explanations of more comprehensive concepts of AC can refer to [14]. Relevant papers are searched by entering the keywords "Active Constraint" and "surgical robot", or "Victual Fixture" and "surgical robot", on Google Scholar and PubMed.

2.3.1 Active Constraints implementation stages

Being control algorithms that assist in human-robot collaborations, AC aim to provide users with additional virtual guidance during the implementation of complicated surgical procedures. To better understand the role that AC plays during surgery, the analogy proposed by Rosenberg [15] can be recalled, which states that "VF are to humans what rulers are to drawing a straight line." Following this analogy, when the drawn line is detected to deviate from the target straight line, the resistance between the pen and ruler serves as a cue sent to the person, informing them of the current situation and signalling that corrective actions are needed. Similarly, during surgery, when the current situation is detected to be precarious or off-track, an effective signal should be generated by AC and transmitted to the surgeon, informing them to take evasive action. Such signals are usually in the form of forces/torques. Despite a wide range of applications in which AC can be helpful and various robotic platforms with which AC can be incorporated, the implementation of AC follows a standardised procedure, consisting of three interrelated stages, namely, AC generation, AC evaluation, and AC enforcement [14]. Briefly speaking, AC generation is the process where tissue anatomies and surgical instruments, which are termed as Constraints Tool Geometries (CTG), are both represented using geometric shapes, such as points, lines, meshes *etc.*. The next step is AC evaluation, which determines whether corrective actions need to be taken for the current

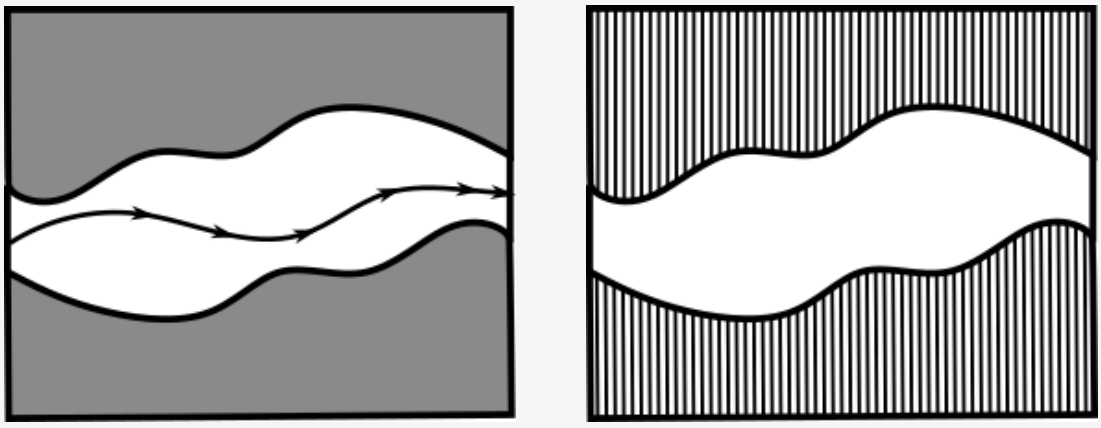
situation, through evaluating, for example, the minimum distance between the tissue surface and the CTG. When it is determined that further actions are needed, the final stage AC enforcement will be triggered into action, generating a force/torque to be transmitted to the user. The selection of different methods for these stages depends on the application scenarios, which will be further discussed below.

2.3.2 Guidance Active Constraints versus Forbidden Region Active Constraints

Depending on the objectives in surgical applications, AC can be largely divided into Forbidden Region Active Constraints (FRAC), also known as "Regional Constraints", which aim to prevent robots from violating specific anatomical areas [49], and Guidance Active Constraints (GAC), which aim to assist robots to follow pre-defined pathways during navigation in a constrained workspace, for example, in endonasal surgery [50] and neurosurgery [51]. A graphical illustration is shown in Figure.2.5. It was demonstrated that with the assistance of FRAC, occurrences of tissue damage were reduced [52] and kinematics singularities could be avoided [53], and that, with the assistance of GAC, precision in tracking reference trajectory was significantly improved [54]. Moreover, it was shown through user studies that with the extra guidance of FRAC and GAC, task implementation time was reduced [55] and there was a reduction in mental workload reflected by less operation pressure in both hands-on manipulation [56] and tele-operation [55]. Although the distinction between FRAC and GAC springs from different purposes of application, the adoption of FRAC and GAC are not mutually exclusive, even for a single surgical task. More often than not, the synergy of both AC strategies is preferred. In surgical tasks where more than one instrument are used, there are requirements of both tool collision avoidance and precise trajectory tracking, hence requiring both FRAC and GAC. The synergy of multiple AC also applies to single type of AC when multiple task objectives need to be satisfied. In situations where both tool collisions and tissue damage need to be avoided, a global FRAC can be applied to protect both the instrument and tissue anatomy, by monitoring the distance between multiple collidable objects [50].

2.3.3 Static Active Constraints versus Dynamic Active Constraints

Static AC refer to AC that remain unchanged throughout a surgical procedure. Dynamic Active Constraints (DAC) refer to AC that need to be constantly updated to accommodate dynamic scenarios in the task space, as a result of changes in the physical environment of patients or task objectives determined by surgeons. The adoption of static AC or DAC depends on the type of surgery and accuracy requirements. In orthopaedic surgery where movements of bone structures are negligible, static AC would suffice, whereas in beating heart surgery where vessel surfaces constantly deform due to the pulsation of the heart, it is necessary to adopt DAC. The concepts of static AC and DAC are in relation to whether AC change intra-operatively, regardless of application purposes, and hence GAC and FRAC can evolve into Guidance Dynamic Active Constraints (GDAC) and FR-



(a) Illustration of GAC **(b) Illustration of FRAC**

Figure 2.5: Illustration GAC and FRAC. In Figure.2.5a, the central curvilinear line with arrows refers to the reference trajectory on which the surgical instrument should stay. In Figure.2.5b, the shaded areas refer to forbidden regions which the instrument should avoid.

DAC, respectively, whenever needed. The update of DAC usually relies on the integration of another sensing device that monitors the movement of the dynamic surgical scenario. Ren *et al.*[57] first developed a dynamic VF framework that protects the surface of a beating heart, and the dynamic update was achieved through registering a pre-scanned CT image to the real-time Ultrasound (US) image of the heart. To enhance tool maneuverability in beating heart surgery, GDAC can also be constantly generated from real-time Magnetic Resonance Imaging (MRI) images through extraction of boundary points identified in these images followed by generation of guidance curves using spline interpolation [58]. The implementation of DAC, however, is restricted by the speed at which dynamic information is captured by the sensing device and the accuracy of data processing. It was stated in [58] that the speed at which intra-opeartive MRI images are collected is capped at 20Hz. In [57], only a rigid-body registration algorithm was adopted, neglecting deformation of the beating heart surface.

2.3.4 Active Constraints generation

AC generation is the first step of AC implementation, where geometric primitives are used to represent areas of interest. Usually, geometric primitives such as points, planes, cylinders *etc.*are used to represent FRAC, and lines, curves *etc.*are used to represent GAC. Point representation is the most common practice because it is easier to construct directly from an external sensing device, for example, depth sensing cameras. Usually, each point on the tissue surface is assigned with a safety distance, forming the radius of a protective sphere around itself. To prevent violations of the overall tissue surface, a protective layer can be constructed as the mutual areas of the protective spheres surrounding a group of points on the tissue surface. When an instrument is detected to have penetrated the protective layer, a repulsive force will be generated by FRAC, as in [59, 60]. The choice of geometric representations also depends on task objectives and application scenar-

ios. In arthroscopy surgery, instruments are required to scan across the articular cartilage surface without inserting pressing on it. In this case, plane representations can be adopted to construct an offset plane from the cartilage surface that needs protection. When motions along the inward-pointing normal direction of the surface are detected, repulsive forces will be generated. During navigation, the target trajectory can be directly applied as GAC. When the discrepancy between the actual and reference trajectory is greater than a threshold, a corrective force will be generated. It is worth mentioning that the selection of AC representation determines the computational cost incurred during the AC evaluation stage. A fine geometric representation allows instruments to approach closer to areas of interest, which can potentially improve task accuracy but may jeopardise safety.

2.3.5 Active Constraints evaluation

AC evaluation is the stage where an enquiry is conducted to determine whether AC forces/torques need to be generated. For FRAC,a proximity query is conducted between the CTG and the areas to be protected, and when the minimum detected distance is smaller than a safety threshold, AC will be triggered into action. For simple geometric representations and a small number of geometric primitives, the proximity query process can be quickly conducted using basic linear algebra. However, when fine geometric representations, such as meshes, are used, or when the number of query points is too large, the computational cost becomes more significant. Possible ways to speed up this process include downsampling query points and developing more efficient proximity query algorithms. The FRAC implementation pipeline developed in [59] states that points on the constrained vessel surface are first downsampled before being constructed into a k-d tree [61] to speed up the proximity query process, managing to reach a control frequency of 250 Hz. For mesh-represented tissue surface, the number of mesh vertices usually amounts to hundreds of thousands [62], and in this case, spatial partitioning and bounding volume hierarchies are efficient ways to speed up the query process [63]. These algorithms help facilitate the process by rearranging query points in an optimised tree structure such that during traversals, a large portion of these points can be partitioned out without the need for exhaustive coverage. However, initial construction of these structures can be time consuming and hence must be done pre-operatively. The time for the proximity query between a cylindrical instrument and a finely represented brain mesh containing 500,000 polygons can be shortened from 86 ms to 0.9 ms when using the bounding volume hierarchies structure compared to exhaustive searching [62]. For GAC, there are less evident mentions of AC evaluation, potentially because of the more prevalent use of simple geometric representations, such as lines and curves, making it redundant to elaborate on this process. Overall, there is little research solely focused on AC evaluation, and the selection of AC methods largely depends on the AC generation stage.

2.3.6 Active Constraints enforcement

Following AC evaluation, when AC is actually triggered, AC forces/torques will be generated. Following the naming conventions proposed in [14], prevalent approaches to generating AC forces in recent literature include a) Simple functions of constraint proximity, b) Proxy and linkage simulation, c) Non-energy storing constraints, d) Potential fields, and e) Constrained joint optimisation. A brief introduction of these AC enforcement approaches will be presented below.

2.3.6.1 Simple functions of constraint proximity

Simple functions of constraint proximity method leverages the results obtained from the AC evaluation stage, the minimum distance between the CTG and areas of interest, and the closest point pair. The most straightforward way to generate AC forces is to introduce a spring system with a fixed stiffness, and the AC force can be modelled as a linear function of the minimum distance between the closest point pair. This force can be either repulsive or attractive, depending on application scenarios. Although this approach was originally widely adopted, Abbott and Okamura found that in a tele-manipulation system, directly applying linear constraints can potentially cause system instability [64], and that the selection of the stiffness value should be deliberated. More importantly, a simple spring system fails to consider the situation where a robot moves quickly past close to areas of interest, and ideally, a larger force should be generated to inform users. To address this issue, the simple spring model was extended to a spring-damper model, where the viscous term takes robot movements into consideration. The additional damping term enables the generation of anisotropic AC forces so that movements towards target positions are favoured compared to other directions. It lends special help in GAC where target points constantly progress, and hence the robot will be constrained to follow the reference trajectory dynamically.

2.3.6.2 Proxy and linkage simulation

Proxy and linkage simulation is also a commonly used method that builds upon a spring-damper model between the robot end-effector and a virtual proxy point, which represents the target position. A graphic illustration is presented in Figure.2.6. In [60], the point at the robot end-effector is denoted as Haptic Interface Point (HIP), and a virtual proxy point follows around the HIP in safe regions. However, when the robot accidentally moves inside the forbidden region, the proxy point will remain on the forbidden region surface, and therefore, there will be a separation between the proxy point and HIP. In this case, an AC will be generated as a spring force, which is a function of the distance between the proxy point and HIP, guiding the HIP to back out of the forbidden region, as implemented in [65]. The drawback is that the force was generated using a pure spring model, which induces jittery movements, and the introduction of a damping term could have resolved this issue. Additionally, the biggest problem with a controller that built from either a pure elastic or viscoelastic model is that energy passivity is not guaranteed, which can potentially jeopardise task safety.

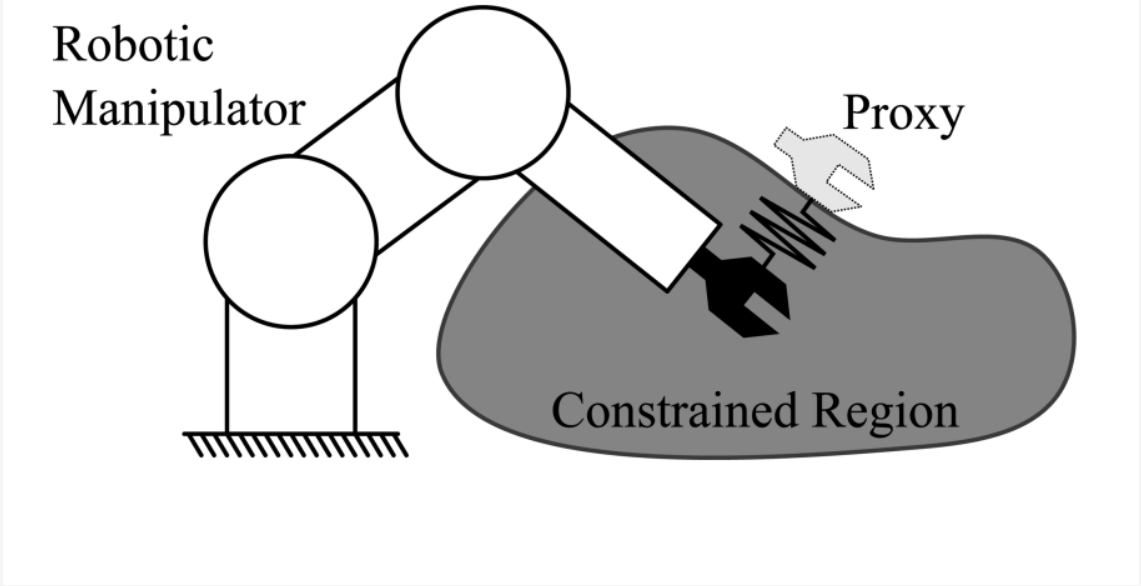


Figure 2.6: Illustration of the proxy and linkage representation in AC enforcement. This picture is from [14] (Licensed by the author of the referenced document. Written proof in the appendix)

2.3.6.3 Non-energy storing constraints

Non-energy storing constraints were initially developed out of the concern that AC controllers should exhibit the property of being energy dissipative. An energy dissipative robot system does not actively generate energy itself, but instead only harnesses the energy input provided by users. This ensures that robots do not move independently without users' instructions during operation and remain static whenever users cut off energy inputs. This is important, especially in hands-on surgeries, because it guarantees that surgeons are always in control of the operation, thereby ensuring task safety and avoiding liability issues. Friction forces are intrinsically dissipative mechanics and have inspired researchers to incorporate plasticity models into the design of non-energy storing constraints. Kikuuwe *et al.*[66] proposed a simulated plasticity model to generate dissipative AC forces as penetration proceeds in the plastic region. Their method claimed to have resolved the discontinuity issue by enabling users to sense the boundary between the elastic and plastic regions without crossing it. The feasibility of adopting such a simulated plastic model on haptic devices was demonstrated, but there was a lack of a quantitative comparison against other existing models, and it was reported to lack fidelity in certain scenarios [67]. To address these problems, Bowyer *et al.*in [68] leveraged an elasto-plastic model and developed an energy redirection approach where directive friction forces are applied obliquely to the desired direction of movement. In this case, even if the current direction of movement is orthogonal to the desired direction, users can still sense

components of the generated AC force and then take prompt actions. The energy redirection was initially only achievable within the same force dimension. A subsequent study [69] extended this energy redirection approach to isotropic dimensions, including both forces and torques. Although friction forces have the advantages of improving task safety, Enayati *et al.*pointed out in [70] that plastic forces are less intuitive for humans to sense compared to elastic and viscous forces because they are not proportional to the movements exerted by users. Therefore, apart from task implementation efficacy, the level of comfort experienced by users when receiving AC forces should also be considered.

2.3.6.4 Potential fields

Potential fields methods offer a different approach to computing AC forces without relying on a mechanical model. Originally, potential fields methods were developed to generate force guidance to avoid obstacles. All points of interest in the task space are assigned potential values determined by a global potential function. The potential function ensures that points that are close to obstacles and far from target trajectories have high potential values, while those in the opposite conditions have low potential values. The gradient of the potential value at each point represents the desired moving direction in that region, and the summation of these regional forces forms the global AC force which guides users to avoid obstacles and move towards target points. A graphic illustration is presented in Figure.2.7. Although potential fields methods were classified as non-energy-passive approaches in [14], in more recent studies, researchers started to develop passive potential fields implementations by selecting appropriate potential functions [71] and imposing restrictions on motion parameters [72] to ensure task safety in tele-operation scenarios. To accommodate for scenarios where multiple task objectives must be satisfied simultaneously, the superposition of potential field functions can be adopted.

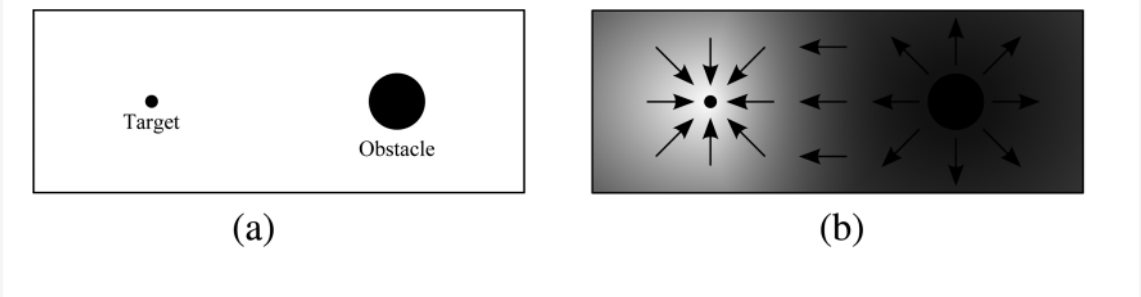


Figure 2.7: Illustration of potential fields approaches in AC enforcement. In the generated potential field, instruments are guided to move away from the obstacle and towards the target point. This picture is from [14] (Licensed by the author of the referenced document. Written proof in the appendix)

2.3.6.5 Constrained joint optimisation

Constrained joint optimisation methods enforce AC forces/torques directly to robot joints by performing computations in the joint space instead of the Cartesian space. Equality and inequality constraints in both the robot end-effector and robot joints can be merged into an overall objective function, over which optimisation is conducted. The results from the optimisation include desired joint displacements and velocities that can be directly used as commands. Kwok *et al.*in [73] adopted such method to assist an articulated snake robot in navigating along a constraint pathway during endoscopic surgery. A close fitting between the robot and the pathway is required, and the flexibility of the robot within the anatomic structure should be maximised to enable the gathering of a panoramic endoscopic view without raising safety concerns. All these constraints are represented mathematically, and after performing optimisations, desirable joint displacements are returned. The advantage of constrained joint optimisation methods is their ability to select the most suitable joint configuration that achieve the same outcome movement at the end-effector. However, searching for the optimised configuration using iterative algorithms can be computationally expensive [14]. Originally, Funda *et al.*tackled the optimisation problem with inequality constraints using quadratic programming methods [74]. In later studies [75], as more nonlinear constraints were incorporated into the framework, researchers realised the hefty computational cost and gradually shifted towards approaches such as constraints linearisation. Another important factor in adopting constrained joint optimisation methods is the concern about the stability of the closed-loop system. Gonçalves *et al.*in [76] developed a kinematic controller that finds control actions in the robot joint space using linear programming, allowing for both equality and inequality constraints whilst maintaining Lyapunov stability. Marinho *et al.*in [77] built upon this controller and developed the Vector Field Inequality approach, which provides preventative guidance by regulating joint speeds when the instrument is detected approaching a forbidden region. Their method relies on mathematically describing the distance between two collidable objects and finding the Jacobian matrix relating the time derivative of this distance with joint speeds. They further extended their research by allowing for multiple collidable objects in a dynamic environment and developing rich descriptions of constraints, as presented in [50].

2.3.7 Dynamic Active Constraints

The motivation for conducting research on DAC is to address a broader range of clinical applications and more realistic surgical scenarios. Implementations of static AC are based on assumptions such as AC representations remaining unchanged on tissue surfaces, which limits their applicability to a small number of realistic situations, as in orthopaedic surgery. Additionally, adjustments to pre-operative surgical plans according to intra-operative data are necessary in certain scenarios. Therefore, considering dynamic scenarios would broaden the scope of assistance provided by AC to soft-tissue surgery, which is an essential step before AC can be effectively used in tele-operative RMIS. However, the transition from AC to DAC involves additional challenges that

must be addressed.

To begin with, the definition of "dynamic" is task-dependent, and the levels of difficulty in adapting static AC methods to these dynamic situations are different. For instance, in the treatment of atrial fibrillation (AFib), circumnavigating the surface of a beating heart along a pre-defined trajectory is essential during the separation of pulmonary veins, a key part of the maze procedure [78]. The adoption of GAC can effectively facilitate this navigation process, but it is required to continuously adjust the pre-defined trajectory, generated from pre-operative images, according to the dynamic movement of the beating heart. During partial nephrectomy procedures, cautery devices are manipulated to maintain a distance from the moving kidney surface, and instrument coupling must be avoided during operations to prevent surgical complications. In this case, FRAC can lend great help in preventing both violations of tissue surface and instrument coupling by constructing forbidden regions around both the anatomical structures and the instruments. To provide effective and timely protection, FRAC must adapt to the dynamic movements of the kidney tissue and the changing positions of the instruments. From these surgical applications, it is evident that "dynamic" generally refers to situations where both the CTG and the constraints need to be updated on-the-fly. Due to different levels of complexity in capturing and quantifying these dynamic movements, the difficulty of DAC implementations also varies.

2.3.7.1 Guidance Dynamic Active Constraints

For GDAC, "dynamic" scenarios often refer to situations where a pre-planned trajectory needs to be updated or where a reference trajectory is generated based on intra-operative data. The major challenge in this process lies in GDAC generation: accurately describing the reference trajectory. In cases where a pre-operative trajectory has already been obtained, the problem of GDAC generation simplifies to a registration problem, where the trajectory plan constructed from off-line medical images is intra-operatively registered to the robot frame, with the help of fiducial markers *per se*. Such practices are most commonly adopted in surgeries where anatomic structures surrounding the path can be assumed as rigid, such as in endoscopic sinus surgery [75], in which case rigid registrations would suffice. However, registration accuracy remains a significant source of uncertainty and can potentially lead to detrimental outcomes when tissue movements are significant or when obstacle avoidance is required during trajectory tracking. Even in cases where a reference trajectory is generated intra-operatively, the accuracy issue remains. Dagnino *et al.*in [79] developed a tele-operated catheter robot, where the tip of the catheter is tele-manipulated to follow the centreline of a pulsating vessel volume. When the distance between the catheter tip and the vessel wall falls below the radius of the cross-section, a viscous force is generated. Their method relies on identifying the catheter tip and vessel contours from a real-time 2D video stream using simple computer vision algorithms. However, the limitations are that the reconstructed 3D positions of the catheter tip and reference trajectory may not be accurate because of a lack of stereo information. With the incorporation of a stereo camera system, another common approach to generating GDAC

is manually sampling control points from intra-operative stereo images, followed by parametric curve fitting. Selvaggio *et al.* in [80] generated reference trajectories as cubic splines, which require only four inputs to define path parameters. These four inputs include the starting point, the starting tangent, the end point, and the end tangent on the path. The first two inputs usually represent the position and velocity direction of the robot end effector and can be directly obtained from robot kinematics, whereas the last two inputs are not as obvious and must be calculated from images, which are prone to inaccuracies. Without relying on visual feedback to sample control points, Selvaggio *et al.* later proposed in [81] an approach to adapting GDAC online by recording interaction points with the help of external force sensors. These recorded interaction points are then used to generate a reference trajectory through cubic spline fitting via optimisation.

2.3.7.2 Forbidden Region Dynamic Active Constraints

For FRDAC, the challenges differ in whether the objective is to avoid tool collisions or tissue violations. Moccia *et al.* in [82] used the term "dynamic active constraints" to refer to virtually constructed cylinders around instruments to avoid tool collisions during task operation. They pointed out that although tool positions can be obtained from robot encoder readings and forward kinematics, the accuracy is low because of the intrinsic cable-driven robot design. Therefore, the challenge in this case is how to calibrate the positions of instruments on-the-fly. They developed an Extended Kalman Filter (EKF) framework, where 3D tool positions are reconstructed through triangulation over segmented stereo images, and these positions are used as observations in the EKF framework to calibrate tool positions. Another approach to avoid dynamic tool collisions was described in [77], where a combined distance representation is used to determine whether potential collisions exist between instruments or between instruments and the surrounding environment. Through mathematical calculations, Marinho *et al.* discovered the relationship between the derivatives of these distance representations and joint velocities, and when the distance is detected to fall below/above a threshold, action commands are sent to the robot joints. Therefore, one important factor, or potential challenge, in implementing FRDAC to avoid tool collisions is obtaining accurate tool positions, either directly from kinematics or through other means.

For applications where FRDAC are adopted to prevent surgical instruments from violating tissue surfaces, all the challenges associated with preventing tool collisions still exist. In addition, the biggest technical difficulty is accurately describing the deforming tissue surface. Predominantly, there are two schools of thoughts: updating pre-planned forbidden regions and generating forbidden regions on-the-fly. Ren *et al.* in [57] first proposed an approach to continuously registering a beating heart model obtained from pre-operative MRI/CT scans to intra-operative US images using rigid-body registration algorithms. Although their method relies on assumptions of periodic heart beating movements and ignores temporal surgical deformations, it laid the paradigm for future studies that rely on both pre-operative and intra-operative data to update FRDAC, despite the different types of data involved. To accommodate for more complex tissue deformations, non rigid

registration algorithms can be adopted. Wang *et al.*in [83] adopted the Coherent Point Drift (CPD) algorithm to conduct non-rigid registration from a pre-scanned phantom model to an intra-operative point cloud generated from a surface scanner to allow for local deformation caused by tool-surface interaction. The challenge here, however, is how to perform accurate registrations without delaying the workflow of operation. Although in [83], a tele-operated force-controlled probe was used to provide surface geometric data, a more common practice is using cameras to stream real-time information. Rydén *et al.*in [60] incorporated a depth-sensing camera that provides point cloud of a beating heart surface, from which FRDAC are generated on-the-fly without relying on pre-operative information. Although their method bypasses the time-consuming process of registration, it still involves preprocessing raw point clouds to create a protective surface with fidelity for accurate algorithm implementation. More importantly, it is usually challenging to differentiate forbidden regions from safe regions during operation. Therefore, the biggest challenge of adopting FRDAC to avoid tissue violation is how to leverage a sensing device that can provide both timely and accurate descriptions of tissue movements, assisted by advanced computer vision algorithms.

Apart from these mainstream studies, there also exists research studies that tackle FRDAC and DAC under the same framework. Bischof *et al.*in [84] developed a unified approach to generating AC in both static and dynamic scenarios. Their approach is built upon previous studies on the development of a path following controller and a surface following controller that considers the implementation of AC as a control problem. The path following controller ensures that the tip of an instrument closely follows a reference trajectory, which is the objective of GAC. The surface following controller ensures that the instrument tip moves freely only along the tangential direction of a surface that is within a safety distance from anatomical structures, and any further penetration movements are prohibited, which is the objective of FRAC. To account for dynamic situations, the magnitude of deformation is pre-modelled and sent into the controller as desired path deviation so that the control law permits deviations from the reference trajectory/surface by a certain amount. However, this approach is only applicable to situations where only periodic movements are involved. Additionally, it was noted that continuously searching for the closest reference surface from the moving instrument tip is computationally expensive, which hinders real-time application.

2.3.8 Summary

In this subsection, the concept of AC was explained, and essential information on AC implementation was presented. Although AC, as a high-level control strategy, have the potential to enhance task performance by providing virtual haptic guidance, challenges still exist to be overcome before they can be adopted in a real clinical setup. Depending on the surgical procedure and task objectives, different AC strategies should be adopted and tailored, resulting in varying levels of complexity. Specifically, depending on whether the primary concern is to ensure task accuracy or task safety, GAC and FRAC should be adopted accordingly. Additionally, when dynamic factors are

prevalent in a certain surgical procedure, DAC should be adopted. The complexity in AC implementation is also determined by the hardware system into which they are incorporated. For example, when an AC is actively generated and transmitted to the user side during instrument manipulation, the energy dissipativity of the system is of crucial importance to ensure safety. In contrast, when the generated AC force is passively perceived by users, for example, via impedance, the requirement for generating a dissipative AC force becomes less stringent. Therefore, it is important to consider hardware components prior to the development of a bespoke AC pipeline, as described in the following subsection.

2.4 Overview of the first-generation dVRK

Tele-surgical robotic systems provide a well-established form of assistance in the operating theatre, with evidence of growing uptake in recent years. Until now, the da Vinci surgical system (Intuitive Surgical Inc, Sunnyvale, California) has been the most widely adopted robot of this kind, with more than 7,500 systems in current clinical use worldwide [7]. To accelerate research on robotic-assisted surgery, the retired first-generation da Vinci robots have been redeployed for research use as dVRK, which have been distributed to research institutions around the world to support both training and research in the sector. In the past ten years, a great amount of research on the dVRK has been carried out across a vast range of research topics. Therefore, the first-generation dVRK can also serve as a convenient testing platform for the development of FRDAC strategy. However, before directly implementing algorithms on the dVRK, there are several caveats in the robot that researchers should be aware of. These caveats arise from the technical constraints embedded within the robot system, which have been gradually identified as common issues by dVRK users throughout the distribution of these robots. In this subchapter, an overview of the first-generation dVRK will be presented, along with a detailed description of the technical constraints embedded within the system that affect the implementation of FRDAC. Studies conducted to address these technical constraints will also be reviewed.

2.4.1 Backgrounds

Robotic-Assisted Minimally Invasive Surgery (RMIS) has gained significant popularity in recent years due to its advantage of causing less tissue trauma and reducing hospitalization time for patients. Of all surgical robotic platforms available in the market, the da Vinci robot (Intuitive Surgical Inc, Sunnyvale, California) has dominated RMIS, with more than 10M operations having been performed on this platform in the past twenty years [18]. To further propel RMIS research on the da Vinci surgical platform, in 2012, an initiative was launched to repurpose retired first-generation da Vinci robots by converting them into dVRKs [85], which consist of both a software package and hardware controllers. A graphic illustration of the first-generation dVRK is presented in Figure.2.8. These dVRKs have been distributed to research institutions around the world. Until now, more than 40 research groups across 10 countries have benefited from the initiative, forming a thriving dVRK research community, with more than 250 peer-reviewed research papers on the dVRK having been published.

Although research conducted on the dVRK branches into different topics, almost all of these works deal with data directly provided by the dVRK, containing kinematics, image and system information, as described in [18]. These data are arguably the best source of information available to users who wish to keep abreast of the latest state of the robot as they develop novel research on the dVRK. However, blind reliance on the fidelity of these data can be risky. The inaccuracy of dVRK data

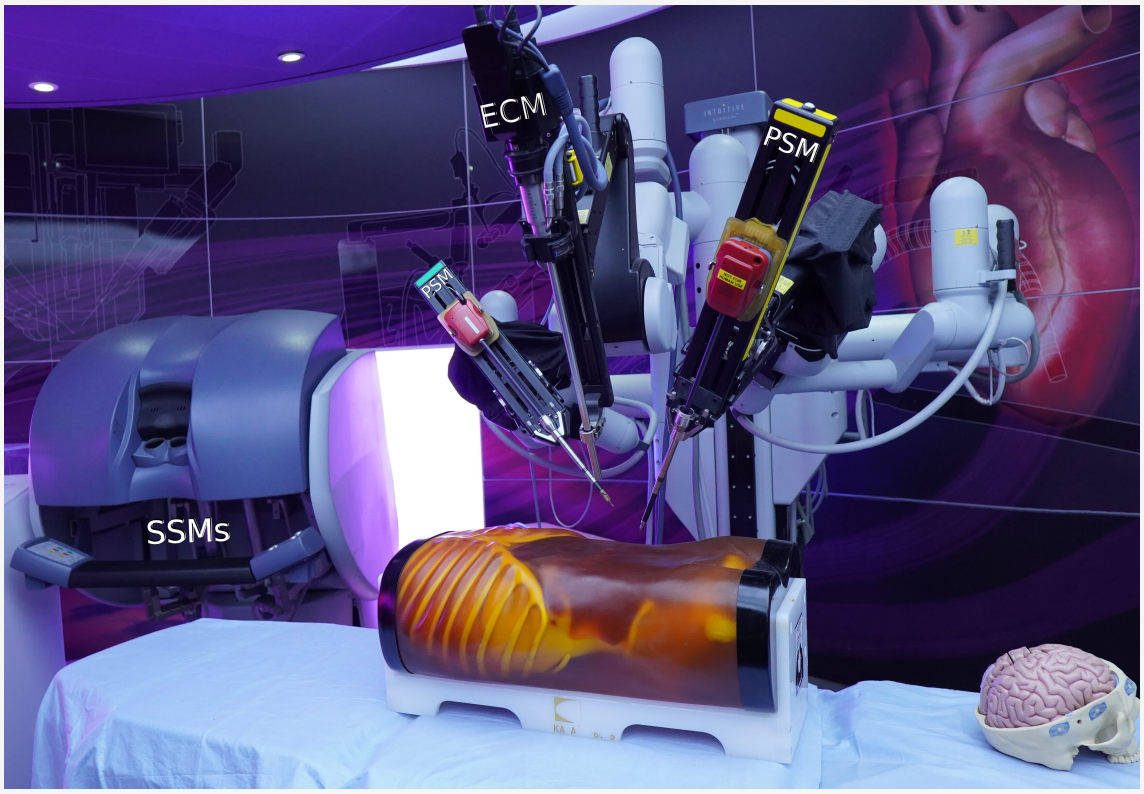


Figure 2.8: The first-generation dVRK.

partly arises from the intrinsic design of the tele-surgical platform, and partly from limitations of the factory calibration of the hardware, which has only been improved upon in recent years thanks to a growing interest in the field and the many contributions of researchers working with the dVRK. Awareness of these seminal works should be heightened within the dVRK community. However, thus far, there only exists one review paper about the dVRK [18], which focuses on categorizing research in terms of relevant high-level application areas.

To fill this gap, the author *et al.*in [19] conducted a study to analyse the technical constraints identified within the first-generation dVRK so that users can be aware of these shortcomings and take corrective actions to overcome these, in pursuit of better research outcomes. This review study is based on existing literature and the feedback from researchers of the dVRK community.

According to initial research, there is a general consensus among dVRK users about the inaccuracies within the dVRK kinematics and image data, which necessitates studies on essential kinematics and camera calibration. Allowing for the fact that hand-eye calibration is an indispensable part of teleoperation, the accuracy of which can have a profound impact on subsequent task implementations, significant attention should also be dedicated to hand-eye calibration. Considering the relevance of these calibrations with the research objective of this thesis, only kinematics calibration and hand-eye calibration are presented in detail in this subchapter.

2.4.2 Searching Methodology

2.4.2.1 Literature review

To identify the most significant technical constraints that have hampered research progress with the dVRK, the author *et al.*first looked into all papers on the dVRK across different research application areas and gathered common issues that researchers claimed to have affected task performance, taking advantage of the latest review paper on the subject, which encompasses papers on the dVRK from year 2014 to 2021 [18]. Other relevant papers covered in the survey were searched through typing the keywords "dVRK" paired with "error", "calibration" and "task performance" individually on Google Scholar, ScienceDirect and RefWorks .

2.4.2.2 Consultation with researchers

Having gathered a list of technical issues reported by dVRK users in the literature, the author *et al.*consulted with leading researchers of the dVRK community (Mr. Anton Deguet and Dr. Simon DiMaio) about whether these issues have been discovered under the first-generation dVRK and thus can be regarded as universal.

After that consultation, the author *et al.*designed a questionnaire featuring selected technical issues, which we deemed to be "universal", and had it distributed within the dVRK community[1]. The questionnaire study conducted among dVRK users is presented in Appendix.A. Based on their inputs, the author *et al.*summarised that there exist four essential calibrations that must be undertaken. It should be noted that, due to their technical relevance to the rest of the thesis, only "Kinematics Calibration" and "Hand-eye Calibration" are presented in this subsection.

2.4.3 Kinematics Calibration

A well-acknowledged technical issue within the dVRK is its time-variant inaccurate forward kinematics, which induces a poor surgical tool tip pose estimation, reflected by a discrepancy in readings of up to 1.02mm [86, 87] between the alleged tip pose streamed from the dVRK and the ground truth observed by an external means. This discrepancy, termed positioning error in this paper, has exceeded the sub-millimetre positioning accuracy required by RMIS[88], having repercussions on diverse research projects implemented on the dVRK. Note that kinematics errors exist in all individual joints of the dVRK. However, it is in the end effector position that the discrepancy caused by the kinematics errors is most evident, because of the accumulation of errors across all the joints.

[1]More info at: https://jhudvrk.slack.com

2.4.3.1 Need for kinematics calibration

For research on surgical subtask automation, accurate positioning is required, such as in debridement [89], suturing [90, 91], needle extraction [92], and peg transfer [93–95], where a surgical instrument is required to move to the target grasping point. For research on the development of AC via the dVRK, positioning accuracy will affect the proximity query result, and therefore the entire enforcement stage of the AC implementation [49, 55, 82, 96]. Even for research on image-based hand-eye calibration [97], inaccurate surgical tool kinematic data leads to an inaccurate 3D pose estimation and thereby affects the accuracy of its back-projected 2D pixel position, which serves as a criterion for evaluating different hand-eye calibration strategies.

2.4.3.2 Challenges in accurate positioning

I. Cable-driven effects: The dVRK surgical platform, which is a cable-driven robotic system [98], has an inherent issue in obtaining accurate joint readings from the built-in encoders. This is because all encoders are mounted adjacent to actuators but distant from joints, where the actual joint angles are estimated through transmission kinematics [99]. However, unknown parameters such as pulley-cable friction and nonlinearities [100] contribute to inaccuracies in joint angle estimation, which result in dVRK joint encoder readings not reflecting actual joint positions. These errors in joint space subsequently affect the estimated end effector tip pose through Denavit-Hartenberg (DH) parameters and forward kinematics. The DH parameters here only concern active joints.

II. Inaccurate kinematic parameters: The wear and tear of the dVRK not only induces cable slack [101], which affects the parameters in the transmission kinematics, resulting inaccurate joint encoder readings, but also entails instrument damage which leads to additional inaccuracies in the DH parameters of the forward kinematics, causing the estimated tool-tip pose to stray from the actual one. Another significant source of error is due to the potentiometers, which is explained in detail in [19].

III. Other non-kinematic error sources: Other than kinematic factors, non-kinematic factors such as external forces exerted onto the tool shaft and backlash between the tool shaft and cannula, illustrated in Figure.2.9 ,would also contribute to an overall erroneous end-tip pose estimation [102, 103]. These external forces will affect the tension of cables associated to tool tips, leading to an error in transmission kinematics. In addition, they will also cause a displacement of the tool shaft because of compliance, as illustrated in Figure.2.10; this displacement is not detectable by the encoders [102], and thus positioning error accumulates.

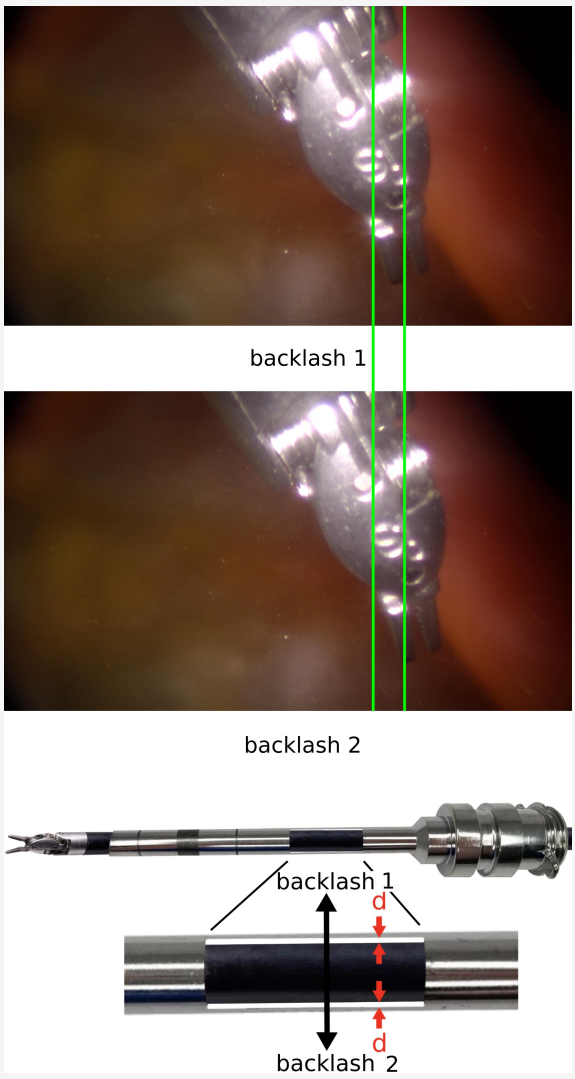


Figure 2.9: Backlash of the da Vinci surgical instrument. As illustrated in red (d), there is a gap between the surgical instrument's shaft and the cannulae. Therefore, the point of contact between this shaft and the cannulae can change. This phenomenon is known as backlash. Backlash causes the tool to move without being reflected by the encoder readings. Backlash is evident in the figure, illustrated in green, where the "S" character of Intuitive's logo has moved to a different location, given that the camera is static.



Figure 2.10: Compliance of the da Vinci instrument. Similarly to backlash, this compliance is not reflected on encoder readings, and hence not reflected in the joint position estimation.

2.4.3.3 Methods for kinematics calibration

Methods that are available in the current literature to compensate for dVRK positioning errors can be classified in term of the specific error source they are aiming to address, namely encoder readings, kinematics parameters and other non-kinematic factors.

I. Compensation for encoder readings: Methods that aim to compensate encoder reading inaccuracies can be divided into two classes: encoder reading calibration and tool-tip pose estimation. Both classes recognize the nature of the erroneous encoder readings. However, the former focuses on finding actual joint positions in joint space, while the latter places an emphasis on finding the actual tool-tip pose.

I.I. Encoder reading calibration: Methods for calibrating encoder readings follow a standardized pipeline that involves modelling, measurement and parameter fitting [104]. To start with, a model parameterized by η, which maps encoder readings obtained from transducers to actual joint positions, is conceived. In the subsequent measurement stage, robot joints are commanded to move to designated positions while ground truth values of joint positions are gathered via an external measurement system. Finally, different fitting models, which can be either linear or nonlinear, are adopted to estimate the η that best fits designated joint positions to ground truth measurements.

Major differences between methods in this class are the selection of calibration models and approaches to measuring the ground truth. Following the calibration paradigm, Huang *et al.* [103] started off using a linear model to map encoder readings to ground truth values gathered by tracking infrared markers mounted on the end effector with an optical camera system, namely the NDI Polaris [105]. To better estimate and account for the nonlinear nature of cable stretch and friction, Hwang *et al.* adopted a data-driven approach to training deep learning models that map collected readings to actual joint positions gathered in a similar way [93].

With access to the forward kinematics of a system, which maps encoder readings to actual joint positions, one can find an inverse calibration model that generates encoder commands that drive a robot to reach desired joint positions. Such methods lend themselves to implementing automatic surgical tasks [89, 93, 95], where a surgical tool is requested to accurately move to a given pose. However, there are several drawbacks in model-based calibration methods. First, as pointed out in [106], model-based calibration methods are hard to implement outside of a lab setting because of the need for additional sensors, calibration objects, and tedious data collection procedures. Second, an invariant calibration model fails to accurately reflect a dynamic mapping relationship as, e.g., the cable wears and tears over time. Third, adopting model-based approaches requires greater efforts to find the ground truth values of the joint positions for the 7-DOFs da Vinci robot. Although there exists numerical inverse kinematics solvers for the SSMs and the PSMs, running

at 1.5 KHz [2] Furthermore, the accuracy of the ground truth measurement provided by an external sensor, a depth-sensing camera for example, is also inevitably affected by the inaccuracy in camera parameters and the hand-eye transformation matrix.

I.II. Tool-tip pose estimation: In addition to generating joint commands that drive a robot to reach the desired state, there are times when the actual tool-tip pose in the Cartesian space is more important, not least in situations where the minimum distance between a surgical tool and its surrounding geometry needs to be precisely returned. Typically, pose estimation methods utilize both kinematic and image data. First, a tool-tip pose inferred from encoder readings and the forward kinematics of the system serves as an initial guess, then another tip-pose is obtained out of 2D image data, serving as an observation. By combining the initial guess with the observed result, a more accurate tip-pose can be estimated.

Literature on dVRK-based tip-pose estimation varies mainly in terms of the choice of computer vision-based strategy for 3D tool-tip pose reconstruction and the selection of 3D pose estimators. Moccia *et al.*[82] proposed a binary segmentation-based 3D pose reconstruction strategy, where the 3D pose is reconstructed by first finding the tool-tip on both binary-masked images captured by a stereoscopic endoscopic camera, followed by triangulation. Without relying on a pre-trained tool segmentation model, Richter *et al.*[106] simply attached markers on tool joints and used these to correct the discrepancy between detected markers and back-projected joint positions on the image plane. Ye *et al.*[107] leveraged the Computer Aided Design (CAD) model of surgical instruments and conducted keypoints matching between online generated part-based templates and 2D images to measure the accuracy of the tool pose estimated from the dVRK. For 3D pose estimators, EKF and Particle Filter (PF) have also been proposed [82, 106–108].

Given that most pose estimation methods exploit image data, the accuracy of 3D tool tip pose reconstruction is highly reliant on the quality of gathered images and the robustness of the pose reconstruction strategies. Therefore, image-dependent pose estimation methods are likely to deliver subpar performances in situations when the camera fails to capture surgical tools in full view or when blood-stained surgical tools fail to be detected and segmented, which are likely to occur within a surgical setting.

In theory, estimator-based pose estimation methods can also be utilized for estimating joint positions j_1-j_6. However, as suggested by the findings in [106], an increase in the number of unknown variables increases the system nonlinearity and yields less accurate estimation results. It is also worth mentioning that spurious feature detection and false feature correspondences could also impair the estimation accuracy. Finally, the computational efforts for feature detection in some pose estimation methods are not negligible, such as edge detection in [106], tool segmentation in

[2] One numerical solver is provided at https://github.com/jhu-cisst/cisst, there is a lack of kinematics parameters identification procedures. Hence the fidelity of the nominal kinematics parameters for the disposable surgical instruments relies on the quality of manufacture, which, however, can be imprecise.

[82], which may render these methods less suitable to be incorporated in a modern clinical setting.

II. Compensation of kinematics parameters: The dVRK returns the surgical tool-tip pose based on both joint readings and the system's forward kinematics, which means that calibrated encoder readings are a necessary but not sufficient condition for accurate tool tracking. The nominal dVRK DH kinematics parameters assume that adjacent joint axes are orthogonal and without intersections [109]. However, these assumptions fail to hold up in a real clinical setting. In [103], authors have shown that there are intersections between adjacent tool axes and additional calibration needs to be conducted on the dVRK kinematics parameters to account for these. A standardized approach to calibrating these kinematics parameters relies on external sensors attached onto the joints, which are used to track complex movements as the robot is driven along random trajectories. This process enables joint axes vectors to be estimated, from which corresponding kinematics parameters can be extracted using linear algebra.

III. Compensation of external force factors Research on this topic stems from the observation that the dVRK surgical tools are intrinsically mildly compliant and can deflect under external environmental forces. However, such deflection is undetectable by joint encoder readings, and hence the end tip pose estimation can suffer further. One way to compensate for the external force factors is through estimation of the external forces/torques. In [102], it is assumed that the deflection on the slender dVRK tool shaft is the most salient one, and a compliance model is established by connecting the deflection of the surgical tool in the lateral direction with encoder readings for the first two joints. Alternatively, Yilmaz *et al.*[110] proposed a neural network-based method for estimating inverse dynamic torques such that the external forces/torques can be obtained by subtracting the inverse dynamic torques from the joint torque readings. In both cases, the estimation of the external force factors builds upon the knowledge of system dynamic equations, which are supported by studies on dVRK dynamics modelling, such as [111]. Another way to address the external force factors is to directly monitor the forces/torques by attaching force sensing devices without further modifications of the original instruments, as proposed in [112], although there is still great room for improvement in sensing accuracy.

2.4.4 Hand-eye Calibration

Hand-eye calibration has been widely researched in robotics. It aims to find the transformation from the camera frame to the robot frame. There exists some ambiguity in the definition of a hand-eye calibration problem in the dVRK community, with some researchers defining it as finding the transformation from the camera frame to the frame of the robot arm to which the camera is attached [113, 114], while most other researchers place their focus on finding the transformation from the camera frame to the base frame of another robot arm to which a surgical tool is attached. Although for a generalized hand-eye calibration problem, the robot frame is unspecified, in the

remaining part of this subsection, the dVRK hand-eye calibration problem is defined as per the latter school of thought.

2.4.4.1 Need for hand-eye calibration

The importance of developing an accurate and time-efficient hand-eye calibration strategy is twofold. In a teleoperation scenario, an accurate hand-eye transformation matrix enables a better alignment between the surgeon's view and the endoscopic camera view so that surgeons can see the surgical tools move in sync with their hand movements, making the teleoperation more intuitive. Through an operation, there are times when the robot arms need to be repositioned to adjust to different surgical tasks, and whenever its Set-up Joints (SUJs) are relocated, the hand-eye calibration needs to be recomputed. Even though it is desirable to develop a hand-eye calibration method that is both accurate and time-efficient, in a teleoperation scenario, time-efficiency takes priority over accuracy because humans can compensate for a slight misalignment between the movements of their hands and the surgical tools. However, for automatic surgical tasks, the accuracy of hand-eye calibration is of paramount importance because all robot motion commands are generated out of visual information captured by the endoscopic camera, and these visual cues cannot be correctly perceived by the robot arm unless an accurate transformation matrix is provided.

2.4.4.2 Challenges in dVRK hand-eye calibration

Although there is a rich literature on hand-eye calibration problems in a generalized robotic framework, the development of calibration strategies for the da Vinci robot, which is customized for RMIS, is still challenging due to several intrinsic constraints of the system. As observed in [115–118], most widely-adopted hand-eye calibration methods require an external calibration object such as a planar chequerboard and external hardware. However, these methods are not applicable in a RMIS environment where the working space is narrow and introducing external calibration objects is impractical. In addition, the Remote Centre of Motion (RCM) constraint [119] of the patient-side robots limit the number of possible joint configurations available, which renders general calibration methods yet more challenging to implement in this context.

2.4.4.3 dVRK hand-eye calibration methods

Most hand-eye calibration problems pivot on solving $\mathtt{AX} = \mathtt{XB}$ [120] or its derivative $\mathtt{AX} = \mathtt{YB}$ [121], where $\mathtt{X}$ represents the transformation matrix of interest, and $\mathtt{A}$ and $\mathtt{B}$ are matrices that can be deduced from kinematic readings and extrinsic calibration, such as the chequerboard calibration method [122]. To allow for the specific constraints of the da Vinci robot, researchers in the dVRK community build upon traditional hand-eye calibration methods to produce bespoke approaches that are better suited for the task. Although there are a handful of research works that rely on classical calibration objects (*e.g.*[123, 124]), most recent approaches have opted for more nuanced implementations. Pachtrachai *et al.* [114] proposed an approach which utilizes a tool-tracking al-

gorithm so that the surgical tool itself functions as a calibration object *per se*. Cartucho *et al.* [125, 126] designed a cylindrical marker that can be attached around the shaft of a surgical tool, serving as a compatible calibration object. And Wang *et al.* [119] developed an algorithm which purely depends on the dVRK kinematic readings and image information captured by the endoscopic camera. Much as great progress has been made, the benefit of avoiding the use of external calibration objects has come at the price of worse calibration accuracy.

To improve the calibration accuracy and the robustness of calibration algorithms against noise, research also focuses on designing advanced $\mathtt{AX} = \mathtt{XB}$ solvers [113, 114, 127]. In cases where the hand-eye calibration needs to be performed in real-time to compensate for the dVRK kinematic positioning error, computational efficiency must also be considered [127]. Zhong *et al.* [97] proposed an Interactive Manipulation-based (IM) computation method that enables fast extraction of the position and orientation term of hand-eye calibration, although they did not regard hand-eye calibration as $\mathtt{AX} = \mathtt{XB}$ or $\mathtt{AX} = \mathtt{YB}$ problem in their work.

2.5 Conclusion

RAS has gained increasing popularity in the clinical setting because robots provide more consistent assistance and greater accuracy compared to human operation, leading to improved surgical outcomes and reduced operation time. The efficacy of RAS has been demonstrated through a wide range of operations, including neurosurgery, orthopaedic surgery, urological surgery, *etc.*. With rising awareness of the advantages of RAS among both clinicians and researchers, there has been an increasing amount of research on related topics. Commercially available surgical robots have emerged and been deployed in real clinical settings. Although RAS can be adopted for various types of surgeries, its benefits are most remarkable in MIS because it enables surgeons to operate more dexterously with better visual guidance within a confined workspace. Among all commercially available surgical robot platforms, the da Vinci robot is the most widely adopted, holding the largest market share and the largest number of clinical uses. The da Vinci robot, a tele-operated surgical platform, consists of a surgeon side console, centralised patient side robotic arms, and a vision cart. Although the advantages of the da Vinci robot have been validated through clinical trials involving urologic and cardiac surgeries, its intrinsic design is not flawless. Specifically, one of the major limitations in the design of tele-operated surgical robots is the lack of haptic feedback for surgeons, which forces surgeons to interpret surgical scenarios purely through visual information, hence increasing surgeons' mental workload, especially for novices. Although in 2024 the da Vinci V was released, marking the first version of the da Vinci robot which is equipped with haptic feedback, most other tele-operated surgical robots still lack this feature, which requires more production cost. To compensate for this limitation, research has been conducted to provide haptic guidance for surgeons to reduce their mental workload. Although the integration of an external force sensing device is the most straightforward approach, it leads to more restrictions on instruments design and can potentially cause system instability. An alternative approach is to generate virtual haptic guidance using information captured by existing system devices, without introducing additional sensing modules. Even in the future, when robots are equipped with haptic feedback in a more cost-effective manner, the virtual guidance would ensure additional task safety. This leads to the research focus of this thesis, AC, which are also named as VF.

AC are high-level control strategies to assist in human-robot collaborations by providing anisotropic guidance for users so that motions that comply with safety requirements and pre-operative plans are allowed whereas those that violate these requirements are annulled. The efficacy of AC in reducing surgeons' mental workload and improving alignment accuracy has been validated through clinical studies on hands-on knee replacement surgeries, and it also displays great potential to be adopted in RMIS. Based on the task objectives AC aim to achieve, AC can be divided into FRAC, which prevents collisions and violations of tissue anatomies, and GAC, which assists instruments in following a pre-defined surgical plan. The implementation of AC can be divided into three interrelated stages, namely AC generation, AC evaluation, and AC enforcement. The generation stage

aims to represent constraints using geometric primitive, and when the enquiry result obtained from the evaluation stage indicates that further actions are needed, an AC force will be generated from the enforcement stage. Challenges during AC development include how to accommodate for a more realistic surgical scenario where dynamic tissue movements need to be considered, requiring geometric representations of AC to be updated on-the-fly. To further facilitate RMIS surgeries in a real clinical scenario, the transition from AC to DAC is required. Although both GDAC and FRDAC can help facilitate surgeries, this thesis specifically focuses on the development of FRDAC because it is applicable in a wider range of scenarios, even when GDAC is also adopted. To provide effective haptic guidance from FRDAC, the fidelity of the force generated must be maintained. To achieve this goal, first, accurate descriptions of both the CTG and constraints are required so that AC can be adapted accordingly. Second, the haptic guidance provided by FRDAC should provide timely and effective assistance for users without causing further distractions. Third, the generated force should be certified as safe and that it will not cause instabilities to the system. Therefore, an essential research task of this thesis is to develop an effective bespoke FRDAC pipeline which can be integrated with a generalised tele-operative robotic system.

In this study, the bespoke FRDAC pipeline was verified on the first-generation dVRK, a repurposed version of the first-generation da Vinci robot developed for research and training purposes. However, this robot system contains several technical constraints, and without proper calibration, it may affect the accuracy of the validation results for the developed FRDAC strategy. Specifically, kinematics calibration and hand-eye calibration are essential procedures in this study because of their direct impact on the FRDAC development. Kinematics calibration aims to reduce the dVRK positioning error, which directly affects the description of CTG around surgical instruments. Hand-eye calibration affects the accuracy of transforming the instrument position from the robot frame to the camera frame, where the final calculation is conducted. Considering the time-variant nature of kinematics errors and that hand-eye calibration can resolve the inaccuracy in encoder readings, an efficient approach would be to conduct on-the-fly hand-eye calibration. Therefore, another essential research task of this thesis to develop a clinically adaptable calibration approach that unifies kinematic calibration and hand-eye calibration so that the FRDAC algorithm validation can be smoothly performed. The development of an on-the-fly hand-eye calibration framework is presented in the following chapter.

Chapter 3

On-the-fly hand-eye calibration for the da Vinci surgical robot

The previous chapter highlighted several intrinsic technical constraints in the first-generation dVRK that affect the positioning accuracy of surgical instruments. To maintain task safety during tele-surgery, it is important to accurately monitor the proximity between the instrument and the tissue surface as the instrument moves. Therefore, it is essential to develop a method for calibrating the instrument's position.

As explained in the previous chapter, this positioning inaccuracy is caused by multiple time-variant factors including wear and tear, inaccurate forward transmission kinematics, etc.. Research has been conducted to address this issue by tackling different sources of error. One approach is training an offline model that calibrates erroneous joint encoder readings, thereby improving the accuracy of the end-effector position estimation. However, such methods fail to account for the time-variant nature of the error sources. An offline model trained on data collected during a limited time span is prone to errors during operations occurring after the training period. To avoid this drawback, an alternative approach is to perform calibrations intra-operatively, based on information captured on-the-fly.

This chapter introduces an on-the-fly calibration framework that builds on a particle filter, leveraging the cylindrical geometry of surgical instruments without relying on key points detection. Both quantitative and qualitative experiments were conducted to verify the effectiveness of the proposed framework, which was then compared with other state-of-the-art methods. The experimental results demonstrate an average decrease in positioning error from 3.30 mm to 1.38 mm. Compared to another particle filter framework that uses key point features as observations, the new method yielded a similar result in terms of mean back projection errors, albeit with a wider range of error distribution. This study suggests that for future studies aiming to achieve sub-millimetre positioning accuracy, calibration on individual robot joint angles, whilst incorporating real-time feedback, is required.

3.1 Introduction

3.1.1 Hand-eye calibration

The da Vinci surgical system (Intuitive Inc®, Sunnyvale, California) is the most widely-adopted tele-operative surgical platform in the world, with more than 7,500 systems deployed in clinical theatres thus far [7]. The system allows surgeons to observe the surgical scene captured by the da Vinci endoscopic camera and to manipulate surgical instruments despite a physical separation from patients. To align the view of surgeons with the view of the endoscopic camera, hand-eye calibration is always needed.

Hand-eye calibration is a well-studied research topic in the field of robotics, for applications involving the use of cameras. The primary purpose of hand-eye calibration is to calculate the transformation matrix between the robot frame and the camera frame. In most scenarios, hand-eye calibration is performed only once before operation, and it is typically addressed by solving an $\mathtt{AX} = \mathtt{XB}$ [120] or $\mathtt{AX} = \mathtt{YB}$ [121] problem. By convention, $\mathtt{X}$ represents the unknown 4×4 homogeneous transformation matrix between the robot base frame and camera frame. This process always involves the use of markers to determine $\mathtt{A}$ and $\mathtt{B}$ matrices. In the eye-on-hand configuration, where a camera is fixed relative to the robot end effector and moves in sync with the robot arm, an $\mathtt{AX} = \mathtt{XB}$ model is usually constructed. Specifically, $\mathtt{A}$ represents the transformation of the robot end effector relative to the robot base frame between consecutive time intervals, and $\mathtt{B}$ represents the transformation of the marker in relation to the camera frame over the same intervals. In another configuration where the camera remains static while the robot arm moves, an $\mathtt{AX} = \mathtt{YB}$ model is usually constructed. In this case, a marker is attached to the moving robot arm, and $\mathtt{Y}$ represents the unknown transformation between the marker and the robot end effector. Both $\mathtt{AX} = \mathtt{XB}$ and $\mathtt{AX} = \mathtt{YB}$ problems are usually solved through optimisation after collecting a series of $\mathtt{A}$ and $\mathtt{B}$ matrices.

3.1.2 $\mathtt{AX} = \mathtt{XB}$ problems

A graphic illustration of $\mathtt{AX} = \mathtt{XB}$ problems is presented in Figure.3.1. Methods for solving $\mathtt{AX} = \mathtt{XB}$ problems can be generally classified into separation methods, where the rotation and translation components in $\mathtt{X}$ are calculated separately, and simultaneous methods, where the two components are calculated simultaneously. Mathematically, $\mathtt{AX} = \mathtt{XB}$ problems can be decomposed into the following two equations that must be satisfied simultaneously.

$$\mathtt{R_A R_X} = \mathtt{R_X R_B} \tag{3.1}$$

$$\mathtt{R_A t_X} + \mathtt{t_A} = \mathtt{R_X t_B} + \mathtt{t_X} \tag{3.2}$$

$\mathtt{X}$ represents the unknown 4×4 homogeneous transformation matrix from the robot end-effector

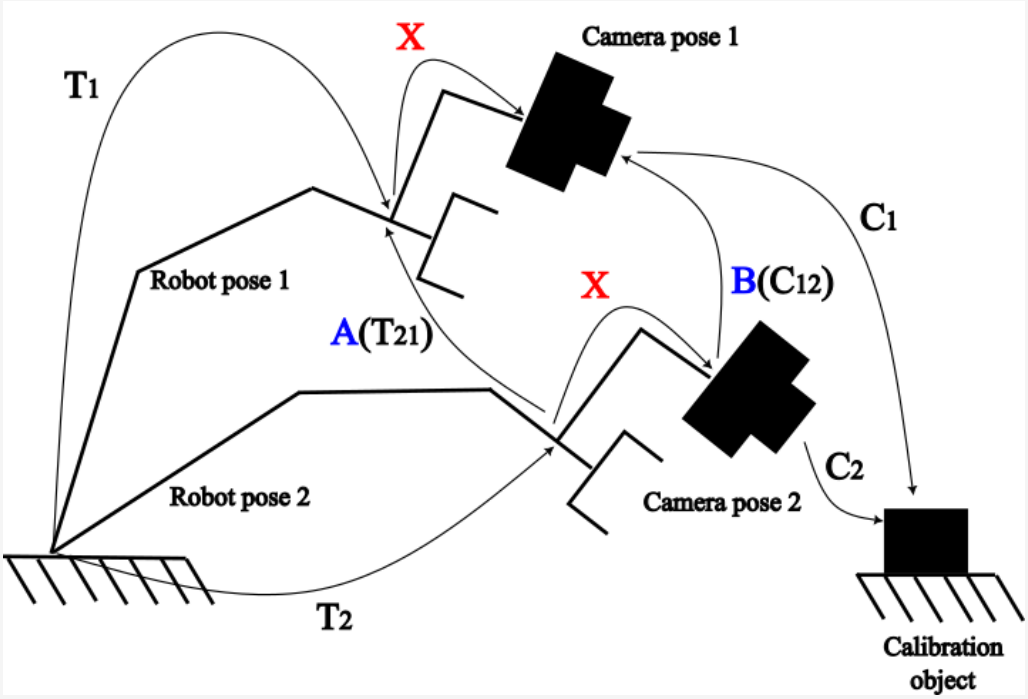


Figure 3.1: Illustration of $\mathtt{AX} = \mathtt{XB}$ problems.

coordinate frame to the camera frame, consisting of a 3×3 rotational matrix $\mathtt{R_x}$and a 3×1 vector $\mathbf{t_x}$. $\mathtt{A}$ represents the transformation for the robot end-effector frame between sequential instances, consisting of $\mathtt{R_A}$ and $\mathbf{t_A}$. $\mathtt{B}$ represents the transformation for the camera frame, consisting of $\mathtt{R_B}$ and $\mathbf{t_B}$. Both $\mathtt{A}$ and $\mathtt{B}$ are known matrices: $\mathtt{A}$ can be calculated from robot kinematics, and $\mathtt{B}$ can be obtained from the calibration object, as illustrated in Figure.3.1.

One of the most widely adopted separation methods is Tsai's method [128]. In their study, the rotation matrix is represented by a unit axis and angle of rotation using Rodrigues' rotation formula [129]. Eq.3.1 is then converted from matrix form into vector form, which facilitates the calculation of the vector form of $\mathtt{R_x}$ using the least square method. The calculated $\mathtt{R_x}$ is then substituted into Eq.3.2 to find the translation component $\mathbf{t_x}$. Tsai's method is the most representative separation method for solving $\mathtt{AX} = \mathtt{XB}$ problems, but one of its drawbacks is that errors in $\mathtt{R_x}$ tend to be carried over to $\mathbf{t_x}$ due to the separative calculation procedure. Shiu *et al.*adopted a different approach when solving Eq.3.1 in [130]. They first tried to find a set of special solutions for the rotation vector and leveraged these special solutions to find the general solution to the equation. Following that, a least square method was adopted to find $\mathbf{t_x}$, with a given $\mathtt{R_x}$. Because trigonometry is introduced during the process of finding the general solution, the pose angle of the robot needs to avoid 0 and π. Wang in [131] proposed a multi-class calibration approach that provides closed-form solutions. The selection of different classes depends on the availability of pre-calibrated reference objects. Class A requires positioning the reference object at a pre-calibrated position, which is too demanding to be applied in a realistic scenario. Class B leverages the mobility of robots and frees the need

of pre-calibration. Class C only requires a visible point as calibration object and fully utilises the mobility and dexterity of robots. By commanding the robot end-effector to move along a structured trajectory with pose restrictions, the rotation component $\mathbf{R_x}$ and translation component $\mathbf{t_x}$ can be solved separately. However, the experimental results showed that the accuracy of the multi-class calibration approach is lower than Tsai's method despite at a higher algorithm complexity. Additionally, this method requires at least 5 samples to obtain solutions. To find the closed-form solution in the Euclidean space, Park and Martin in [132] converted parameters from the Cartesian space into Lie algebra. After the mapping, a unique solution to Eq.3.1 becomes easier to obtain. Then the translation component is found through formulating a least square problem, where inaccuracies in $\mathbf{A}$ and $\mathbf{B}$ matrices during data collections are accounted for.

Different from separation methods, simultaneous methods aim to solve $\mathbf{R_x}$ and $\mathbf{t_x}$ at the same time. Horaud *et al.* in [133] proposed a method where the perspective matrix is applied on both sides of the original equation. After representing the rotation matrix using a unit quaternion and decomposing rotation and translation components from the matrix $\mathbf{X}$, the solutions to original equation can be found through minimising two objective functions which regulate $\mathbf{R_x}$ and $\mathbf{t_x}$, respectively. Because the two objective functions are independent from each other, the error in $\mathbf{R_x}$ will not be carried over to $\mathbf{t_x}$, which resolves the major drawback of separation methods. Daniilidis in [134] proposed a new formulation of hand-eye calibration using dual quaternions to generate a linear system, and the solution for $\mathbf{R_x}$ and $\mathbf{t_x}$ are obtained through Singular Value Decomposition (SVD). The study in [134] suggests that simultaneous methods that conduct linear optimisation achieve higher reconstruction accuracy in a monocular setup compared to simultaneous methods that tackle nonlinear optimisation and separation methods.

All these algorithms mentioned above rely on an external marker, which restricts their applications in a real clinical setup. To address this limitation, there also emerged studies featuring the development of marker-free hand-eye calibration methods. Marker-free calibration methods came out as modifications on both separation and simultaneous methods. Ma in [135] proposed a self-calibration method without relying on extra reference objects. This method requires the robot end-effector to follow a sequence of non-coplanar translational motions to obtain the rotation component of the camera pose relative to the robot frame. Following that, the translation component of the camera pose is recovered through linear algebra. Although this method reduces algorithm complexity, its robustness against noisy observations is low, and the calibration results are prone to errors, as reflected in other marker-free calibration methods [136, 137]. Apart from a reduced calibration accuracy, removing markers also results in extra difficulties when conducting optimisations. To avoid obtaining local minima results, Zhao in [138] converted the original optimisation problem into a convex optimisation problem after applying Kronecker product to the original parameters. Heller *et al.* in [137] leveraged epipolar constraints and proposed a branch-and-bound approach to address the original optimisation problem using linear programming. Although a global optimum result is guaranteed from their algorithm, the accuracy highly relies on the fidelity of cam-

era intrinsic parameters.

3.1.3 $\mathtt{AX} = \mathtt{YB}$ problems

A graphic illustration of $\mathtt{AX} = \mathtt{YB}$ problems is presented in Figure.3.2. Compared to $\mathtt{AX} = \mathtt{XB}$ problems, $\mathtt{AX} = \mathtt{YB}$ solvers aim to address situations where the camera is not directly mounted onto the moving robot arm. A mathematical formulation is provided as below.

$$\mathtt{R_A R_X} = \mathtt{R_Y R_B} \tag{3.3}$$

$$\mathtt{R_A t_X} + \mathtt{t_A} = \mathtt{R_Y t_B} + \mathtt{t_Y} \tag{3.4}$$

Different from subsection.3.1.2, $\mathtt{X}$ here represents the unknown transformation between the robot base frame and the camera frame. As illustrated in Figure.3.2, a marker is attached to the robot, remaining static relative to the robot end-effector. $\mathtt{Y}$ represents the unknown transformation from the robot end-effector frame to the marker frame. $\mathtt{A_i}$ represents the transformation from the robot end-effector frame to its base frame as the robot moves, and $\mathtt{B_i}$ represents the transformation from the fixed camera to the marker frame. $\mathtt{A_i}$ can be directly obtained robot kinematics, and $\mathtt{B_i}$ can be calculated using computer vision techniques.

Similar to $\mathtt{AX} = \mathtt{XB}$ solvers, $\mathtt{AX} = \mathtt{YB}$ solvers can also be classified into separation methods and simultaneous methods. Separation methods address Eq.3.3 and Eq.3.4 separately. One prevalent separation approach to addressing $\mathtt{AX} = \mathtt{YB}$ problems is transforming the original equations and finding closed-form solutions for rotation components $\mathtt{R_x}$,$\mathtt{R_y}$before calculating translation components $\mathbf{t_x}$,$\mathbf{t_y}$. Methods under this category largely differ in parameter transformations. Shah in [139] applied Kronecker products on Eq.3.3 and derived closed-form solutions to $\mathtt{R_x}$and $\mathtt{R_y}$using SVD. $\mathbf{t_x}$and $\mathbf{t_y}$were then found through solving a linear equation, with at least three measurements needed to guarantee unique solutions. Instead of using Kronecker products, Zhuang *et al.*in [140] used quaternion representations and rewrote Eq.3.3 as a linear equation between measurement variables and quaternion representations of $\mathtt{R_x}$and $\mathtt{R_y}$. SVD was then applied on the transformed relationship to find $\mathtt{R_x}$and $\mathtt{R_y}$. Eventually, $\mathtt{R_x}$and $\mathtt{R_y}$were substituted into Eq.3.4 to obtain $\mathbf{t_x}$and $\mathbf{t_y}$. One caveat of this method is that the rotation angle must avoid 0 and π because of quaternion representations. Another prevalent separation approach is solving $\mathtt{AX} = \mathtt{YB}$ through iterative approaches. Hirsh *et al.*in [141] developed an iterative method for estimating $\mathtt{X}$ and $\mathtt{Y}$ matrices. Initially, three closed-loop equations satisfying the transformation relationship in the hand-eye calibration setup were proposed. An identity matrix as used for the initial guess, and the values of $\mathtt{X}$ and $\mathtt{Y}$ were adjusted alternately until the convergence criteria were satisfied.

Simultaneous methods can be categorised into optimisation-based approach and closed-form approach. Optimisation methods solve the following minimisation problem in the homogeneous

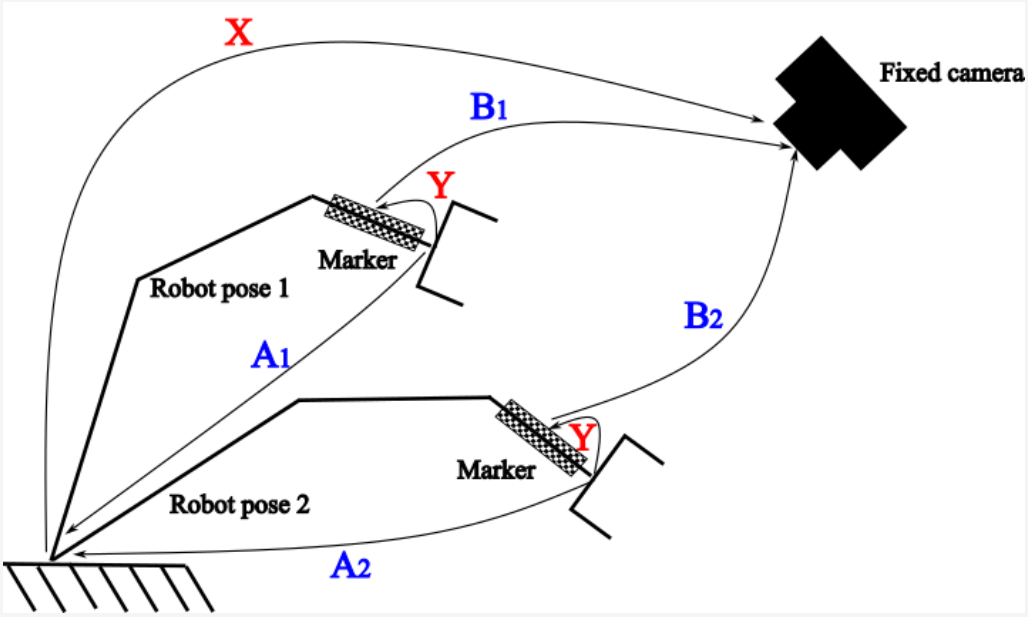


Figure 3.2: Illustration of $\mathtt{AX} = \mathtt{YB}$ problems.

space or its parameterisation in another space.

$$\min_{\mathtt{X},\mathtt{Y}\in SE(3)} ||\mathtt{AX} - \mathtt{YB}|| \tag{3.5}$$

Dornaika and Horaud in [142] proposed an optimisation framework where a global error function of both rotation and translation elements was used for nonlinear optimisation. The final results were obtained using the Levenberg-Marquardt (LM) method. One important factor in optimisation-based approaches is the establishment of a proper objective function, which affects convergence conditions. To allow for a natural weighting between the rotation and translation components, Strobl and Hirzinger in [143] proposed a new error metric which satisfies zero-mean Gaussian distributions. And the solutions for $\mathtt{X}$ and $\mathtt{Y}$ were obtained through numerical optimisations. To guarantee optimal results after conducting optimisation, Zhao in [144] formulated the $\mathtt{AX} = \mathtt{YB}$ problem into a semi-convex optimisation problem using dual quaternion representations. An iterative solver that alternates between linear programming and semi-definite programming was adopted. For the closed-form approach, Li *et al.* in [145] adopted Kronecker product to simply original equations and derived the closed-form solutions for $\mathtt{X}$ and $\mathtt{Y}$ using the least square method.

3.1.4 Evaluation metrics

To evaluate the performance of hand-eye calibration algorithms, quantitative evaluation metrics are needed. When ground truth values for $\mathtt{X}$ and $\mathtt{Y}$ are available, standardised quantitative metrics include average rotation error e_R and average translation error e_t. When ground truth values are not available, metrics include average 2D projection error e_{PR} and average 3D reconstruction error

e_{3D}.

e_R and e_t gauge the inaccuracy of the estimated rotation component and translation component of matrix $\mathtt{X}$, respectively. Mathematically, for $\mathtt{AX} = \mathtt{XB}$ problems, e_R and e_T are expressed as

$$e_R = \frac{1}{n}\sum_{i=1}^{n} ||\Theta((\mathtt{R_{Ai}R_X})^{-1}\mathtt{R_XR_{Bi}})|| \tag{3.6}$$

$$e_t = \frac{1}{n}\sum_{i=1}^{n} ||\mathtt{R_{Ai}}\mathbf{t_X} + \mathbf{t_{Ai}} - \mathtt{R_X}\mathbf{t_{Bi}} - \mathbf{t_X}|| \tag{3.7}$$

for $\mathtt{AX} = \mathtt{YB}$ problems, e_R and e_t can be expressed as

$$e_R = \frac{1}{n}\sum_{i=1}^{n} ||\Theta((\mathtt{R_{Ai}R_X})^{-1}\mathtt{R_YR_{Bi}})|| \tag{3.8}$$

$$e_t = \frac{1}{n}\sum_{i=1}^{n} ||\mathtt{R_{Ai}}\mathbf{t_X} + \mathbf{t_{Ai}} - \mathtt{R_Y}\mathbf{t_{Bi}} - \mathbf{t_Y}|| \tag{3.9}$$

In Eq.3.6 and 3.8, Θ represents the operation that converts a rotation matrix to an axis angle; the footnote i indicates the ith measurement, and $||$ represents the $\mathcal{L}^2$ norm. When ground truth values are not available, these metrics are used to compare the relative calibration performance between different methods.

An indirect way to measure calibration performances when ground truth values are not available is to use e_{PR} and e_{3D}, which are interchangeable between one another. e_{PR} measures the pixel discrepancy between the back projection of a 3D point and its observation on the image plane. e_{3D} measures the discrepancy in the 3D Cartesian space between a reconstructed 3D point from a pixel point. Mathematically, e_{PR} and e_{3D} are expressed as follows.

$$e_{PR} = \sqrt{\frac{1}{n}\sum_{i=1}^{n} ||p_{ij} - \Pi(\mathtt{K}, \mathtt{X}, \mathtt{Y}, \mathtt{B_i}, P_j^w)||} \tag{3.10}$$

$$e_{RC} = \sqrt{\frac{1}{n}\sum_{i=1}^{n} ||P_j^w - \Pi^{-1}(\mathtt{K}, \mathtt{X}, \mathtt{Y}, \mathtt{B_i}, p_{ij})||} \tag{3.11}$$

In Eq.3.10 and 3.11, n represents the total number of observations; P_j^w represents a feature point in the 3D world coordinate; p_{ij} represents the ith observation on the image plane for P_j^w; $\mathtt{K}$ represents the camera intrinsic matrix; Π represents the back projection operation that transforms a 3D point in the world coordinate to the image plane, and Π^{-1} represents the inverse operation that reconstructs 2D pixel points to their 3D mappings in the world coordinate. Because both the back projection and reconstruction process involve the hand-eye calibration result as well as camera intrinsic parameters, e_{PR} and e_{3D} are affected by the inaccuracy of $\mathtt{K}$.

3.1.5 Hand-eye calibration for cable-driven robots

Regardless of the use of markers in the hand-eye calibration methods mentioned above, hand-eye calibration is usually conducted once before operation, and the $\mathbf{X}$ matrix is used throughout the rest of the operation without modification. However, for cable-driven robots, hand-eye calibration serves an additional purpose of improving positioning accuracy beyond aligning the coordinate frame between the robot and the camera.

Cable-driven robots, such as the first generation da Vinci robot, suffer from positioning inaccuracy at its end-effector because encoder readings for robot joints do not accurately reflect their positions. This discrepancy arises because the joint positions returned from encoders are typically estimated through transmission kinematics. However, the presumed transmission kinematics model is not always accurate due to factors such as nonlinear cable-pulley friction, backlash etc. Errors in robot joints accumulate through forward kinematics via DH matrices, leading to pose estimation inaccuracies for the end effector [19]. While humans can automatically compensate for this error during tele-operation, it becomes non-trivial for surgical task automation, where precise tool positioning is required. With a growing interest in surgical robot automation, it is equally important to address the challenge of improving the positioning accuracy of surgical instruments.

Research that focuses on improving end effector positioning accuracy for the da Vinci robot can be broadly classified into two categories: the model-based calibration approach and the direct pose estimation approach. The model-based calibration approach aims to calibrate encoder readings for joint angle positions. These methods typically rely on a pre-trained model that maps raw encoder readings to their ground truths values [93]. Consequently, accurate end effector positions can be obtained through forward kinematics. These methods are effective in various surgical situations, as they are independent of using feedback from real-time surgical scenarios. However, Cui *et al.* [19] pointed out that model-based approaches are often not practical outside a lab setting due to the requirement of a tedious data collection process, often involving markers. Moreover, a pre-trained model may not allow for the wear-and-tear that surgical instruments sustain over time.

On the contrary, the direct pose estimation approach often relies on real-time feedback obtained from external sensors, such as cameras, to calibrate the estimation of tool pose from kinematic data. Although pose estimation can be derived from pure visual information, Allan *et al.* [146] noted in their study that their fully vision-based pose estimation approach was outperformed by the hybrid approach presented in [107], which utilises both kinematics and visual data. A standardized pipeline for implementing hybrid pose estimation methods involves first establishing a state estimator and then incorporating visual feedback as observations to evaluate state estimations. Major differences among hybrid pose estimation methods are the selection of state estimators and the extraction of visual information. Ye *et al.* [107] initially proposed an EKF framework, where 6 unknown parameters that comprise a supplementary hand-eye transformation matrix were estimated. Template matching is performed between an online-generated tool model from tool CAD

files and the observed one from 2D images. Hao *et al.* [147] also leveraged tool CAD files to render instrument silhouettes and compared them with instrument masks to evaluate state estimations within a PF framework. Although Intersection over Union (IoU) between a rendered tool silhouette and an observed tool mask serves as an indicator of prediction accuracy, silhouette generation per frame takes around 3.3 second, which precludes its adoption for applications with higher speed requirements. Alternatively, some researchers have turned to incorporating key point feature detection in their calibration frameworks. Richter *et al.* [106] officially provided mathematical proof to support the practice of performing hand-eye calibration for compensating errors in joint angle readings for cable-driven robots. Furthermore, they proposed a PF framework where particles are updated based on the distance between individual particle predictions and detected key points on surgical instruments. The effectiveness of their approach was verified on the da Vinci robot in a virtual surgical scenario through simulation. Subsequently, Lu *et al.* [148] developed a more effective key point detection method for the da Vinci robot through transfer learning. All these studies build upon the assumption that surgical instruments remain within the field of view of the camera and that accurate key point matching is available. However, as indicated in [149], high-speed movement of surgical instruments, occlusions, and blurry images lead to spurious feature detection, hence resulting in tracking failures. Moreover, challenging conditions such as poor illumination conditions and situations where surgical instruments are stained in blood, are not uncommon in a surgical scenario, which poses an even larger challenge for accurate key point detection and matching.

To address these challenges, in this chapter, a calibration framework is proposed, which supports on-the-fly hand-eye calibration for the da Vinci robot without relying on key point feature detection on surgical instruments. The framework centres on a PF instead of a Kalman filter, thereby eliminating the assumption of model linearization and Gaussian noise [150]. Instead of utilising key point features as observations, the framework leverages the cylindrical geometry of surgical instruments and the RCM constraint of all da Vinci end effectors. It establishes an observation model based on information extracted from detected cylinder edges. These edges also facilitate direct calibrations on the joint 4 position. Both quantitative and qualitative studies were conducted to verify the effectiveness of the framework. In the quantitative study, the framework was compared with a model-based calibration approach by evaluating calibrated tool poses against ground truth measurements obtained from a bespoke marker. In the qualitative study, the framework was compared with another particle-filter framework that relies on key point detection and matching.

Primary work conducted in this chapter has been presented at the 2024 Hamlyn Symposium on Medical Robotics, with the proceeding published as: ***Cui, Z. and Rodriguez y Baena, F., 2024. Calibration Framework for Positioning Accuracy Improvement of da Vinci Surgical Instruments. Proceedings of The 16th Hamlyn Symposium on Medical Robotics 2024.*** A more comprehensive version of this study has been submitted as a regular journal paper to IEEE Transactions on Medical Robotics and Bionics, entitled ***"On-the-fly hand-eye calibration framework for the da Vinci surgical***

robot", and is currently under review for the special issue entitled "The Hamlyn Symposium on Medical Robotics 2024".

3.2 Methods

To accommodate situations such as occlusion and surgical instruments moving out of the camera view, a calibration framework has been developed, which does not involve detecting key point features on surgical instruments. Instead, it relies solely on segmented tool shaft information from images captured by stereoscopic cameras. In this study, it is assumed that edge information about cylindrical instruments is readily available, either via marker-based conventional computer vision approaches or deep learning-based approaches. The entire calibration framework is comprised of three stages, described in the following subsections.

3.2.1 Cylindrical tool shaft central axis reconstruction

The algorithm begins by constructing the geometric model of a cylindrical tool shaft $\mathcal{C}$ with radius r_c in the homogeneous camera coordinate frame. The origin of the homogeneous camera coordinate frame is denoted as $\mathbf{O} = [0, 0, 0, 1]^{\mathrm{T}}$; the axis vector of $\mathcal{C}$ is denoted as $\mathbf{r}$; $\tilde{\mathbf{M}}_o$, or its homogeneous form $\mathbf{M}_o = [\tilde{\mathbf{M}}_o^{\mathrm{T}}, 1]^{\mathrm{T}}$, represents a 3D point on the central axis of $\mathcal{C}$; vector $\mathbf{w}$ is defined as $\mathbf{w} = \mathbf{r} \times \mathbf{M}_o$. The plücker coordinate of the central axis is $(\mathbf{r}, \mathbf{w})$. Doignon *et al.* in [151] proposed that any 3D point $\mathbf{M}$ on the surface of $\mathcal{C}$ satisfies the equation

$$\mathbf{M}^{\mathrm{T}} \begin{bmatrix} [\mathbf{r}]_\times [\mathbf{r}]_\times^{\mathrm{T}} & [\mathbf{r}]_\times \mathbf{w} \\ \mathbf{w}^{\mathrm{T}} [\mathbf{r}]_\times^{\mathrm{T}} & ||\mathbf{w}||^2 - r_c^2 \end{bmatrix} \mathbf{M} = 0 \tag{3.12}$$

where $[\mathbf{r}]_\times$ represents the skew symmetric matrix constructed from vector $\mathbf{r}$, and $||\mathbf{w}||$ is the $\mathcal{L}^2$ norm of vector $\mathbf{w}$. The coordinate definition for a 3D cylindrical object is shown in Figure.3.3.

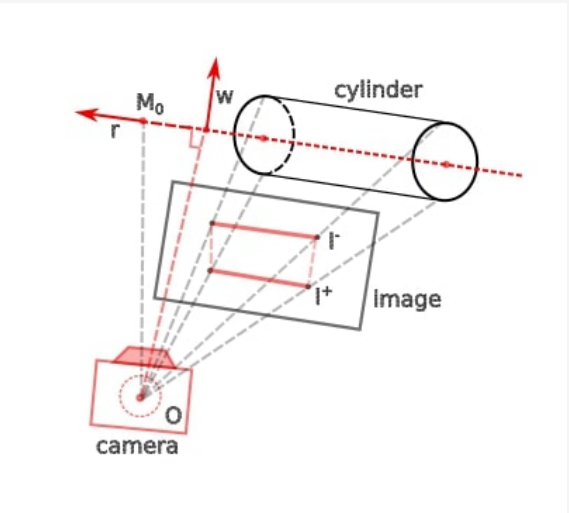


Figure 3.3: Cylinder edge projection

According to perspective projection theory, 3D point $\mathbf{M} = [x, y, z, 1]$ and its projection on the image plane $\mathbf{m} = (u, v, 1)$ is related by projection matrix $\mathtt{P}_{3\times4} = [\mathtt{K}_{3\times3}|\mathtt{0}_{3\times1}]$, where $\mathtt{K}_{3\times3}$ represents the intrinsic matrix of a camera. This relationship can be explicitly expressed as

$$z\mathbf{m} = z\begin{bmatrix} u \\ v \\ 1 \end{bmatrix} = \mathtt{K}\begin{bmatrix} x \\ y \\ z \end{bmatrix} = \mathtt{P}\mathbf{M} \tag{3.13}$$

By substituting $\mathbf{M}$ with $\mathbf{m}$ in Eq.3.12 using the relationship in Eq.3.13, we obtain the following equation in terms of z, given by $Az^2 + 2Bz + C = 0$, where $A = \mathbf{m}^\mathtt{T}(\mathtt{K}^{-\mathtt{T}})[\mathbf{r}]_\times[\mathbf{r}]_\times^\mathtt{T}\mathbf{m}$, $B = \mathbf{m}^\mathtt{T}(\mathtt{K}^{-\mathtt{T}})[\mathbf{r}]_\times\mathbf{w}$, and $C = ||\mathbf{w}||^2 - r_c^2$. This quadratic equation indicates that for any $\mathbf{m}$ on the image plane, there exists two corresponding 3D points on the surface of the cylinder $\mathcal{C}$. Image points on the edges of the projection of $\mathcal{C}$ correspond to a single z value in the 3D coordinate frame, leading to the discriminant of the quadratic function $B^2 - AC = 0$, which can be simplified as

$$(\frac{r_cB}{\sqrt{C}} + \mathbf{w}^\mathtt{T}\mathtt{K}^{-1}\mathbf{m})^\mathtt{T}(\frac{r_cB}{\sqrt{C}} - \mathbf{w}^\mathtt{T}\mathtt{K}^{-1}\mathbf{m}) = 0 \tag{3.14}$$

After further mathematical simplifications, the image point $\mathbf{m}$ on the two edges of the projection of $\mathcal{C}$ satisfies the following relationships, allowing us to subsequently find the mathematical expression for the two edges $\mathbf{I}^-$ and $\mathbf{I}^+$

$$\begin{cases} (\mathtt{K}^{-\mathtt{T}}(\mathtt{I} - \alpha[\mathbf{r}]_\times)\mathbf{w})^\mathtt{T}\mathbf{m} = 0 \equiv \mathbf{I}^{-\mathtt{T}}\mathbf{m} = 0 \\ (\mathtt{K}^{-\mathtt{T}}(\mathtt{I} + \alpha[\mathbf{r}]_\times)\mathbf{w})^\mathtt{T}\mathbf{m} = 0 \equiv \mathbf{I}^{+\mathtt{T}}\mathbf{m} = 0 \end{cases} \tag{3.15}$$

with $\alpha = \frac{r_c}{\sqrt{||\mathbf{w}||^2 - r_c^2}}$. The relationship between edge projections and plane normal vectors is shown in Figure.3.4.

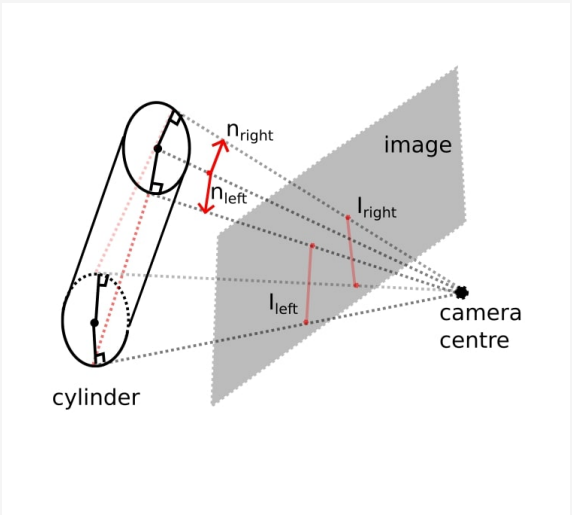


Figure 3.4: Illustration of cylinder projection model

We then define a real 3×3 matrix $\mathtt{C} = \mathbf{I}^{-\mathtt{T}}\mathbf{I}^{+} + \mathbf{I}^{+\mathtt{T}}\mathbf{I}^{-}$, which is a rank 2 symmetrical matrix. It is also found that all image points $\mathbf{m}$ on the edges satisfy $\mathbf{m}^{\mathtt{T}}\mathtt{C}\mathbf{m} = 0$.

Lu *et al.* in [152] showed that $\mathtt{C}$ encodes 3D pose information of cylinder $\mathcal{C}$. Expanding $\mathtt{K}^{\mathtt{T}}\mathtt{C}\mathtt{K}$ from Eq.3.14, the following relationship is obtained.

$$\begin{aligned}
\mathtt{K}^{\mathtt{T}}\mathtt{C}\mathtt{K} =& \mathtt{K}^{\mathtt{T}}(\mathbf{I}^{-}\mathbf{I}^{+\mathtt{T}} + \mathbf{I}^{+}\mathbf{I}^{-\mathtt{T}})\mathtt{K} \\
=& -2(\alpha^2[\mathbf{r}]_\times \mathbf{w}\mathbf{w}^{\mathtt{T}}[\mathbf{r}]_\times - \mathbf{w}\mathbf{w}^{\mathtt{T}}) \\
=& -2||\mathbf{w}||^2[\mathbf{r}]_\times(\alpha^2\frac{\mathbf{w}\mathbf{w}^{\mathtt{T}}}{||\mathbf{w}||^2} + \frac{[\mathbf{w}]_\times[\mathbf{w}]_\times^{\mathtt{T}}}{||\mathbf{w}||^2})[\mathbf{r}]_\times^{\mathtt{T}} \\
=& -2||\mathbf{w}||^2[\mathbf{r}]_\times(\mathtt{I} - (1-\alpha^2)\frac{\mathbf{w}\mathbf{w}^{\mathtt{T}}}{||\mathbf{w}||^2})[\mathbf{r}]_\times^{\mathtt{T}} \\
=& -2||\mathbf{w}||^2(\mathtt{I} - \mathbf{r}\mathbf{r}^{\mathtt{T}} - \mathbf{z}\mathbf{z}^{\mathtt{T}}) \\
=& -2||\mathbf{w}||^2 \begin{bmatrix} \mathbf{a} & \mathbf{z}_u & \mathbf{r} \end{bmatrix} \begin{bmatrix} 1 & 0 & 0 \\ 0 & 1-\sigma^2 & 0 \\ 0 & 0 & 0 \end{bmatrix} \begin{bmatrix} \mathbf{a}^{\mathtt{T}} \\ \mathbf{z}_u^{\mathtt{T}} \\ \mathbf{r}^{\mathtt{T}} \end{bmatrix}
\end{aligned} \tag{3.16}$$

where $\mathbf{z} = \frac{1-\alpha^2}{||\mathbf{w}||}[\mathbf{r}]_\times \mathbf{w}$, $\mathbf{a} = \mathbf{z}_u \times \mathbf{r} \equiv \mathbf{w}$ and $\mathbf{z}_u = \mathbf{z}/\sigma$. After applying singular vector decomposition, $\mathtt{K}^{\mathtt{T}}\mathtt{C}\mathtt{K} = \mathtt{U}\mathtt{D}\mathtt{U}^{\mathtt{T}} = \mathtt{U}\mathrm{diag}(\lambda_1, \lambda_2, 0)\mathtt{U}^{\mathtt{T}}$, and hence $\mathtt{U} = [\mathbf{a}, \mathbf{z}_u, \mathbf{r}]$. We also have $\sigma = ||\mathbf{z}|| = \sqrt{1-\alpha^2} = \sqrt{1-\frac{\lambda_2}{\lambda_1}} \Rightarrow \alpha = \sqrt{\frac{\lambda_2}{\lambda_1}} \Rightarrow \frac{r_c}{\sqrt{||\mathbf{w}||^2 - r_c^2}} = \sqrt{\frac{\lambda_2}{\lambda_1}} \Rightarrow ||\mathbf{w}|| = r_c\sqrt{1+\frac{\lambda_2}{\lambda_1}}$. With $(\mathbf{r}, \mathbf{w})$, we can recover the pose of cylinder $\mathcal{C}$ in the camera frame, and the distance d from camera origin O to the cylinder central axis is equal to $||\mathbf{w}||$. In [153], it was shown that, when d is recovered from a monocular setup, it is always inaccurate, and hence, in this study, only information about the reconstructed central axis is utilised.

The left and right edges of the cylindrical tool shaft in the image can be detected using traditional computer vision algorithms, such as Canny Edge Detector [154]. The left and right edges detected in the left lens are denoted as $\mathbf{I}_1^l$ and $\mathbf{I}_2^l$, respectively, and those in the right frame as $\mathbf{I}_1^r$ and $\mathbf{I}_2^r$. Instead of directly obtaining $\mathtt{C}$ from $\mathbf{I}_1$ and $\mathbf{I}_2$, numerical optimization approaches are used because the edges detected from images can be noisy and erroneous. n pixel points on both the left and right edges in both frames are randomly sampled. Sampled points in the left frame are denoted as $\mathbf{m}_i^l = (u_i^l, v_i^l)$, and those in the right frame as $\mathbf{m}_i^r = (u_i^r, v_i^r)$, with $i = 1, 2, ...n$.

The estimation of $\mathtt{C}$ from a set of observed edge points is similar to the estimation of a fundamental matrix. From $\mathbf{m}^{\mathtt{T}}\mathtt{C}\mathbf{m} = 0$, the following relationship is obtained

$$u_i^2C_{11} + 2u_iv_iC_{12} + 2u_iC_{13} + v_i^2C_{22} + 2v_iC_{23} + C_{33} = 0 \tag{3.17}$$

with C_{ij} representing the element on the ith row and jth column of $\mathtt{C}$. A column vector is then

constructed

$$\mathbf{c} = (C_{11}, C_{12}, C_{13}, C_{22}, C_{23}, C_{33})^{\mathtt{T}} \tag{3.18}$$

and observation matrix $\mathtt{U_n}$

$$\mathtt{U_n} = \begin{bmatrix} u_1^2 & 2u_1v_1 & 2u_1 & v_1^2 & 2v_1 & 1 \\ . & . & . & . & . & . \\ . & . & . & . & . & . \\ u_n^2 & 2u_nv_n & 2u_n & v_n^2 & 2v_n & 1 \end{bmatrix}_{n\times 6} \tag{3.19}$$

The following relationship is satisfied

$$\mathtt{U_n}\mathbf{c} = \mathbf{0} \tag{3.20}$$

Since the matrix $\mathtt{C}$, as a fundamental matrix, is defined up to a scale, we can add the constraint $||\mathbf{c}|| = 1$ to the vector $\mathbf{c}$. Typically, with $n \geq 6$, there are infinite solutions to equation (3.20), which is an overdetermined system. The solution to equation (3.20) is $\mathbf{c} = \rho\mathbf{c}_1 + \mu\mathbf{c}_2$, where $\mathbf{c}_1$ and $\mathbf{c}_2$ are the two singular vectors associated with the two smallest singular values of $\mathtt{U_n}$, and ρ and μ are constants constrained by $\rho^2 + \mu^2 = 1$, to satisfy the constraint $||\mathbf{c}|| = 1$. To find ρ and μ, $\lambda = -\rho/\mu$ is introduced. λ is equal to one of the three eigenvalues of matrix $\mathtt{C_2C_1^{-1}}$ that leads to the smallest $||\mathtt{U_n}\mathbf{c}||$, where $\mathtt{C_1}$, $\mathtt{C_2}$ are 3×3 matrices constructed from vectors $\mathbf{c}_1$,$\mathbf{c}_2$. Afterward, the LM algorithm [155] is applied to optimise the estimation of $\mathtt{C}$, satisfying $\sum_{i=1}^{n}(\mathbf{m}_i^{\mathtt{T}}\mathtt{C}\mathbf{m}_i)^2 = 0$.

The estimations of $\mathtt{C}$ for the left and the right camera frame are denoted as $\mathtt{C}_l$ and $\mathtt{C}_r$, respectively. $\mathtt{K}_l$ and $\mathtt{K}_r$ represent the intrinsic matrices for the left and right lens, respectively. By applying Eq.3.16, $\mathbf{w}_l, \mathbf{r}_l$ and $\mathbf{w}_r, \mathbf{r}_r$ can be recovered, for both frames. The central axis projection on the left and right frames $\mathbf{I}_c^l$ and $\mathbf{I}_c^r$ can be expressed as $\mathbf{I}_c^l \equiv \mathtt{K}_l^{-\mathtt{T}}\mathbf{w}_l$ and $\mathbf{I}_c^r \equiv \mathtt{K}_r^{-\mathtt{T}}\mathbf{w}_r$ [156]. Leveraging the extrinsic matrix between the left and right lenses $[\mathtt{R_{12}}|\mathbf{t}_{12}]$, we can reconstruct the 3D cylinder central line $\mathtt{L}$ through triangulation using the method proposed in [157]. The central axis is represented by two non-coincident points $P_{3\times 1}$ and $Q_{3\times 1}$ on the line as $\mathtt{W} = [[P^{\mathtt{T}}, 1]^{\mathtt{T}}, [Q^{\mathtt{T}}, 1]^{\mathtt{T}}]^{\mathtt{T}}$.

Since cylindrical instruments are mounted to the PSMs of the da Vinci robots, which move around a RCM, the RCM position in the camera frame can be recovered from a collection of central lines $\{\mathtt{W}_i, i = 1, 2...n\}$. The position of the RCM on the da Vinci instrument in a hand-eye calibration setup is illustrated in Figure.3.5. Our goal is to find point P_{rcm} that is of the closest distance to all the central lines in $\{\mathtt{W}_i\}$, by solving the following equations

$$n_i = (P_i - Q_i)/||P_i - Q_i|| \tag{3.21}$$

$$\sum_{i=1}^{n}[n_in_i^{\mathtt{T}} - \mathtt{I_{3\times 3}}]P_{rcm} = \sum_{i=1}^{n}[n_in_i^{\mathtt{T}} - \mathtt{I_{3\times 3}}]P_i \tag{3.22}$$

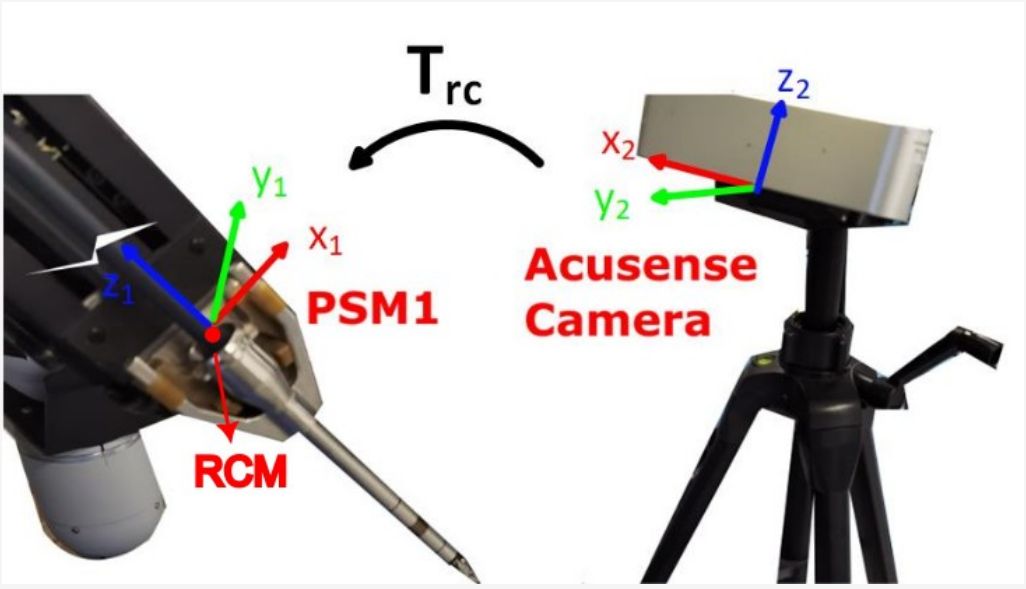


Figure 3.5: Illustration of hand-eye transformation The unknown matrix $\mathtt{T}_{\mathtt{rc}}$ describes the transformation from the camera frame to the robot base frame, the frame where the RCM is centred.

3.2.2 Estimation of hand-eye calibration parameters using the PF

The entire procedure for estimating hand-eye transformation matrix using a particle filter is illustrated in Figure.3.6. A PF was chosen instead of a Kalman filter because it eliminates the assumption of model linearization and Gaussian noise and hence is more generalisable [150].

The 4×4 initial hand-eye calibration matrix $\mathtt{T}_{\mathtt{cr}}^{\mathtt{init}}$ can be represented by a 3×1 rotation vector $\mathbf{R}_{\mathtt{vec}}^{\mathtt{init}}$ and a 3×1 translation vector $\mathbf{t}_{\mathtt{vec}}^{\mathtt{init}}$. To estimate the hand-eye transformation matrix on-the-fly, a particle filter framework is established, consisting of 4 stages, as described below.

3.2.2.1 Particle Initialization

N_{p} particles are selected for initialization, as $\{\mathcal{P}_1, \mathcal{P}_2, ..., \mathcal{P}_{N_{\mathrm{p}}}\}$. Initially, each particle is assigned with the same weight $w_i = 1/N_{\mathrm{p}}$. Covariance matrices for $\mathbf{R}_{\mathtt{vec}}$ and $\mathbf{t}_{\mathtt{vec}}$ are denoted as $\Sigma_{\mathtt{R}} = diag([\sigma_{1_R}, \sigma_{2_R}, \sigma_{3_R}]^{\mathtt{T}})$ and $\Sigma_{\mathtt{t}} = diag([\sigma_{1_t}, \sigma_{2_t}, \sigma_{3_t}]^{\mathtt{T}})$, respectively. In the initialization stage, for all N_{p} particles, the estimated states for $\mathbf{R}_{\mathtt{vec}}$ and $\mathbf{t}_{\mathtt{vec}}$ are assigned to be $\hat{\mathbf{R}}_{\mathtt{vec}} = \mathbf{R}_{\mathtt{vec}}^{\mathtt{init}}$ and $\hat{\mathbf{t}}_{\mathtt{vec}} = \mathbf{t}_{\mathtt{vec}}^{\mathtt{init}}$, respectively. The initial average estimations for $\mathbf{R}_{\mathtt{vec}}$ and $\mathbf{t}_{\mathtt{vec}}$ across all particles are $\overline{\mathbf{R}}_{\mathtt{vec}} = \mathbf{R}_{\mathtt{vec}}^{\mathtt{init}}$ and $\overline{\mathbf{t}}_{\mathtt{vec}} = \mathbf{t}_{\mathtt{vec}}^{\mathtt{init}}$, respectively.

3.2.2.2 Particle prediction

For particle $\mathcal{P}_i$, its state estimation vectors $\hat{\mathbf{R}}_{\mathtt{vec}}^i$ and $\hat{\mathbf{t}}_{\mathtt{vec}}^i$ are updated as $\hat{\mathbf{R}}_{\mathtt{vec}}^i = \mathcal{N}(\hat{\mathbf{R}}_{\mathtt{vec}}^i, \Sigma_{\mathtt{R}})$ and $\hat{\mathbf{t}}_{\mathtt{vec}}^i = \mathcal{N}(\hat{\mathbf{t}}_{\mathtt{vec}}^i, \Sigma_{\mathtt{t}})$, with $\mathcal{N}$ representing multi-dimensional Gaussian distribution. From the dVRK [158], we can obtain the unit axial direction vector for the cylindrical tool shaft $\vec{\mathbf{v}}_{04}$, distance

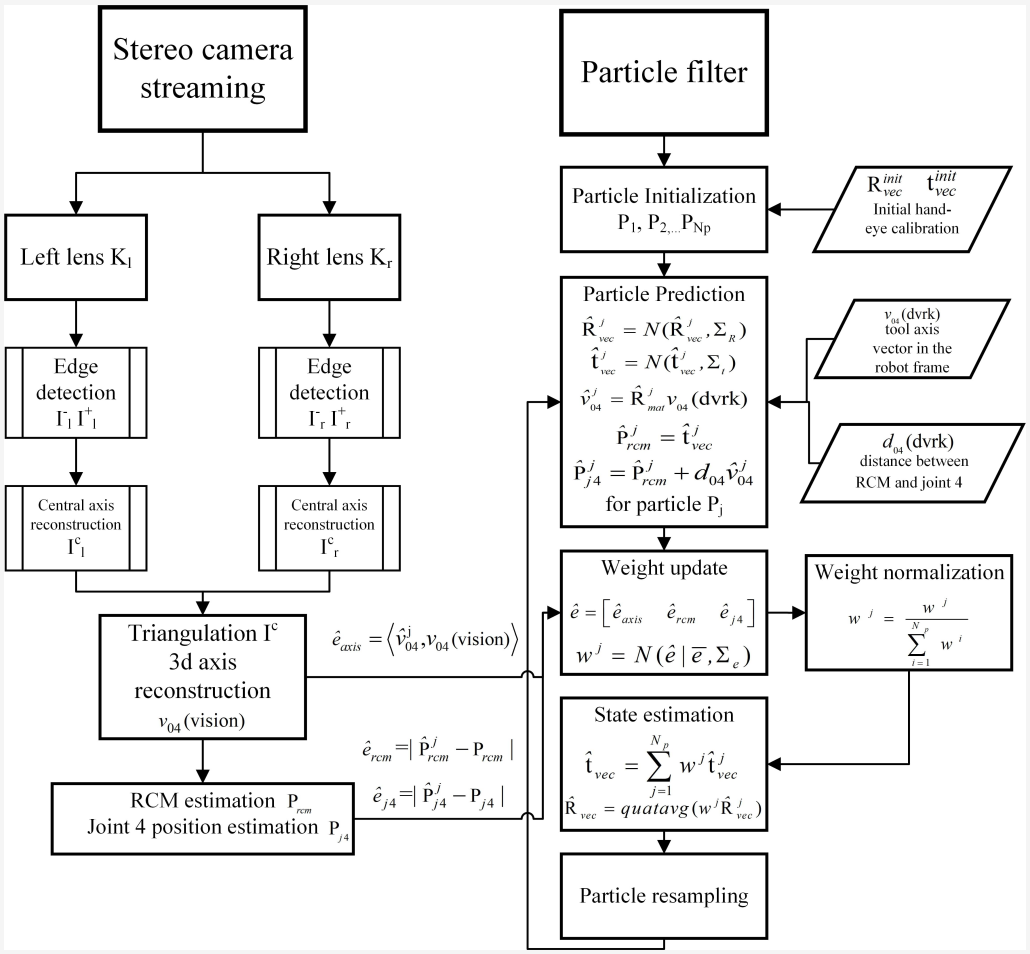


Figure 3.6: Flowchart for the on-the-fly hand-eye calibration framework

d_{04} between the RCM and joint 4, and joint 4 position P_{j4}. Figure.3.7 illustrates joint positions and coordinate frames of the da Vinci instrument. Then particle predictions for axial direction and joint 4 position in the camera frame are updated as $\hat{\vec{\mathbf{v}}}^i_{04}$ and $\hat{P}^i_{j4}$, respectively.

3.2.2.3 Particle weights update

Particle weight w_i is updated based on by the discrepancy between its predictions and observations. Error $\hat{e}_{axis} = \langle \vec{\mathbf{v}}_{04}, \hat{\vec{\mathbf{v}}}^i_{04} \rangle$ is defined as the angle between the observed central tool axis and particle prediction; $\hat{e}_{rcm} = ||P_{rcm} - \hat{P}^i_{rcm}||$, is defined as the distance between the observed RCM position in the camera frame and particle prediction, and $\hat{e}_{j_4} = ||P_{j4} - \hat{P}^i_{j4}||$, is defined as the distance between the observed joint 4 position in the camera frame and particle prediction. Then discrepancy vector is defined as $\hat{\mathbf{e}} = [\hat{e}_{axis}, \hat{e}_{rcm}, \hat{e}_{j_4}]^\mathsf{T}$, mean discrepancy vector $\bar{\mathbf{e}} = [\bar{e}_{axis}, \bar{e}_{rcm}, \bar{e}_{j_4}]$, and discrepancy covariance matrix $\Sigma_\mathbf{e} = diag([\sigma_{e_{axis}}, \sigma_{e_{rcm}}, \sigma_{e_{j_4}}]^\mathsf{T})$. w_i is updated as follows

$$w_i = \mathcal{N}(\hat{\mathbf{e}} | \bar{\mathbf{e}}, \Sigma_\mathbf{e}) \tag{3.23}$$

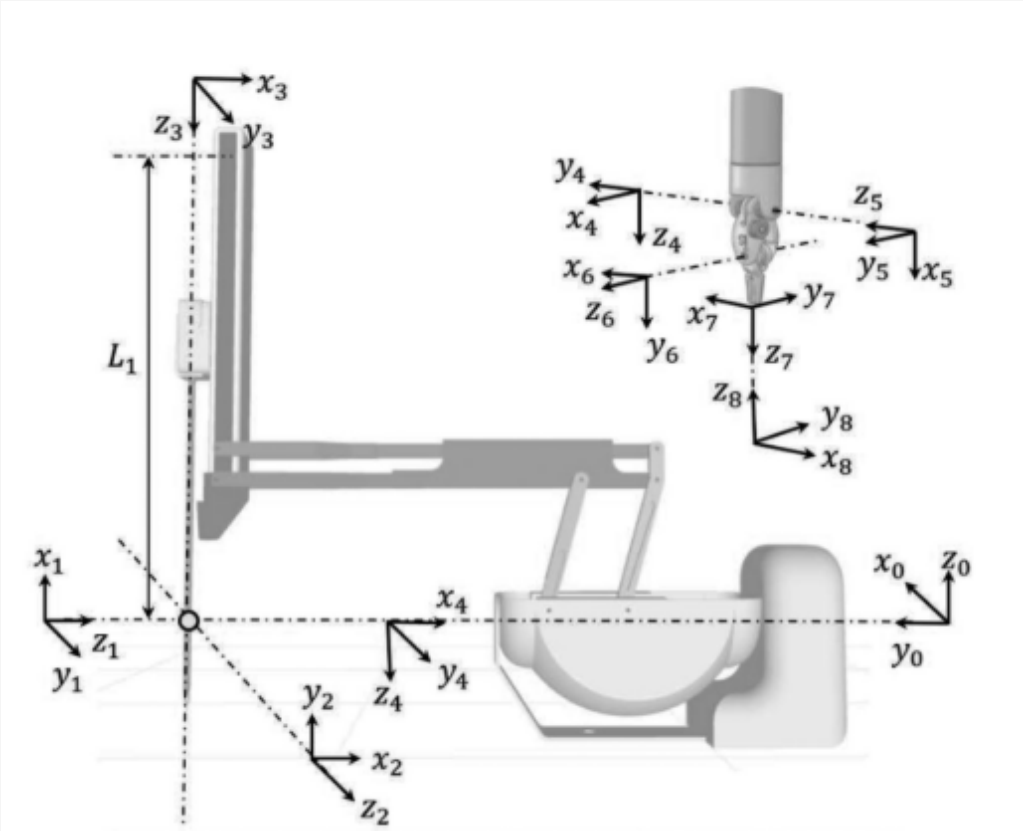


Figure 3.7: Illustration of joint coordinate frames of the da Vinci instrument. This picture is from [93] (Licensed by the author of the referenced document. Written proof in the appendix.) The RCM is a fixed position, around which joint frame 0,1,2,4 are centred. L_1 is a constant value, used in calculating DH matrices. The centres of joint 3 and 4 frame move along with the instrument. The distance between joint 4 and the RCM is also the value that describes the sliding distance of the instrument along $\mathbf{z_3}$ axis, which can be obtained from the dVRK.

Finally, the particle weight is normalised such that

$$w_i = \frac{w_i}{\sum_{i=1}^{N_\mathrm{p}} w_i} \tag{3.24}$$

Although Figure.3.6 illustrates that particle predictions in the 3D space are used to update particle weights, it should be noted that particle predictions on the image plane can also be used to update particle weights, as demonstrated in subsection 3.3.2.

3.2.2.4 Resampling

When the number of effective particles falls below a certain threshold, stratified resampling will be performed.

3.2.3 Joint 4 reading calibration

It was shown in [93] that encoder reading errors from the dVRK are most prominent in $\{q_4, q_5, q_6\}$. To better improve end effector positioning accuracy, we propose an approach that calibrates the joint 4 angle based on image information. As illustrated in Figure.3.8, edge projections of cylindrical tool shafts correspond to the normal vectors of planes formed by cylinder edges and the camera centre. The angle α between the normal vectors at consecutive time instances is equal to the rotation angle of the cylinder. Therefore, with an accurate initial value for joint 4 angle, joint 4 angle reading can be calibrated on-the-fly. Calibration on joint 4 encoder reading is described in Eq.3.25.

$$j_4^k = j_4^0 + \sum_{i=0}^{k-1} \alpha^i \tag{3.25}$$

where j_4^k represents the calibrated joint 4 angle at the kth instance, j_4^0 represents the initial joint 4 angle, and α^i represents the angle between normal vectors at the ith and the $i+1$th instance.

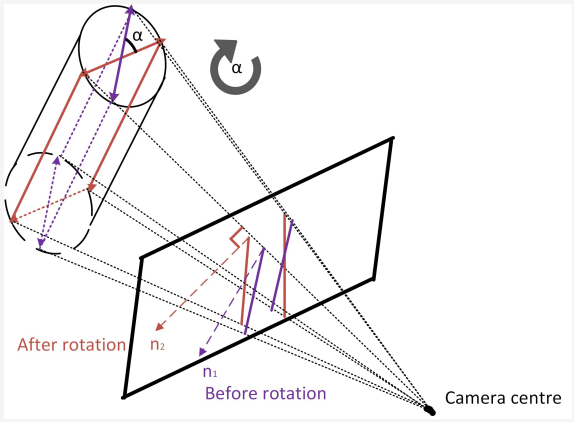


Figure 3.8: Illustration of calibration on joint 4 angle reading. The angle between vector n_1 and n_2 is equal to the rotation angle α

3.3 Experiments

3.3.1 Quantitative Analysis - Experiment 1

A quantitative experiment was designed to assess the effectiveness of the proposed calibration framework in reducing end-effector positioning errors. The purpose of this experiment is to compare the model-based calibration approach with the on-the-fly calibration approach. To obtain a quantitative measurement of tool positions, an asymmetrical marker was designed using NDI passive marker spheres (Northern Digital Inc®). Surgical instrument Forceps (400036E, Intuitive Inc®) was affixed to Patient Side Manipulator 1 (PSM1), which was moved to random poses during the experiment. To identify the marker spheres, we used a Red, Green, Blue, Depth (RGBD) camera, the Acusense 3D (Revopoint 3D Inc®), with a resolution of 0.5 mm at a working distance of 500 mm, and a depth capturing rate of 10 Hz. To facilitate tool shaft segmentation, reflective tape was wrapped around the tool shaft. Tool edges were detected using Canny edge detection algorithm [154] in OpenCV [159], and Hough transformation [160] was then applied. Figure.3.9 shows the procedures for central axis reconstruction in experiment 1.

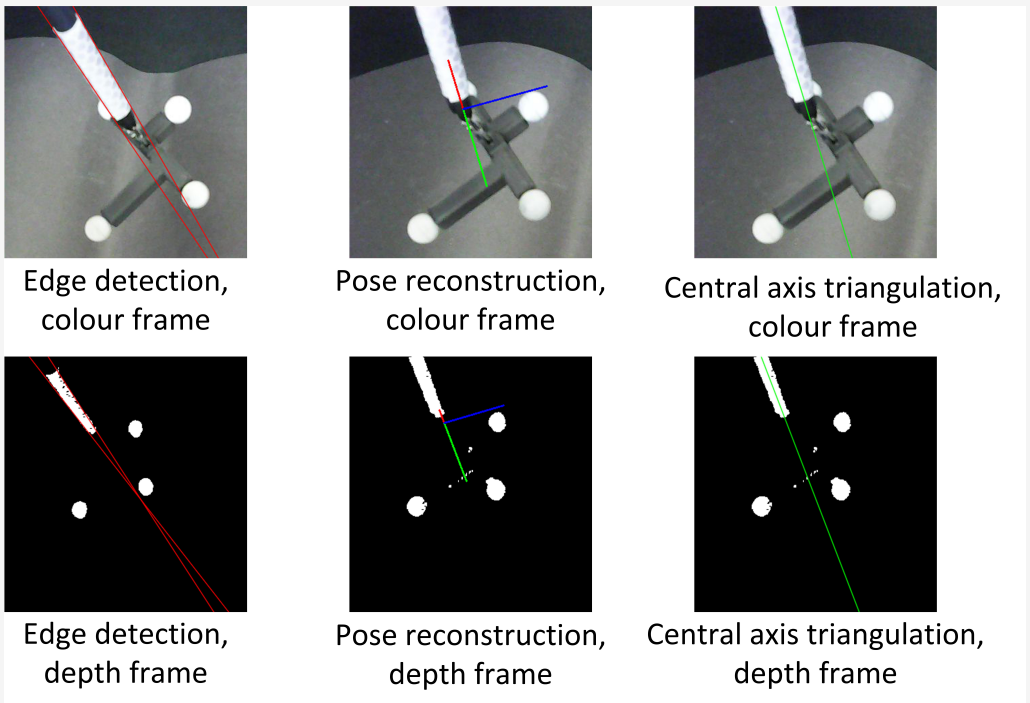


Figure 3.9: Cylindrical tool central axis reconstruction in experiment 1.

The proposed approach was compared with the model-based calibration approach in [93]. Before the comparison study, 200 pairs of data were collected in 39 mins, including both joint angle readings from the dVRK and their ground truth measurements obtained from the designed infrared marker. A Recurrent Neural Network (RNN) calibration model was trained as per the methodology

outlined in their study [1]. During the comparison study, another 200 pairs of data were gathered by randomly moving the surgical instrument to different poses within the field of view of the camera. Initial hand-eye calibration was conducted using the same method as in [93]. The result was then used to initialise 1,500 particles in the proposed framework. Subsequently, both calibration approaches were adopted to calibrate the dVRK joint angle readings.

3.3.2 Qualitative Analysis - Experiment 2

A qualitative experiment was conducted to compare the proposed calibration framework in this study with the approach proposed in [106], where key points on a surgical instrument were detected and used as observations for a particle filter. The purpose of this experiment is to evaluate the impact of different observed features received by a particle filter on the overall calibration performance. Both calibration approaches were tested on a publicly available dataset[2], which includes videos of a da Vinci surgical instrument operating upon a tissue phantom, along with kinematic data of the robot. Manually labelled key points on the instrument are marked in blue, and the pixel discrepancy between their 2D projections on the image plane via the hand-eye transformation matrix and their visual observations can be used to qualitatively gauge the accuracy of hand-eye calibration. Although initial hand-eye calibration was performed, the accuracy was low. To address this, before conducting experiments, kinematic recordings were first synchronised with image frames and then rectified the initial hand-eye transformation matrix. Figure.3.10 shows the improvement on the accuracy of the initial hand-eye calibration after rectification.

Without the use of reflective markers, Segment Anything Model (SAM) was used [161] to obtain tool masks, from which tool shaft edge information can be further extracted. The procedure for central line reconstruction in experiment 2 is illustrated in Figure.3.11.

Comparison studies were then conducted on the video dataset. The observation model in [106] relies on key point detection, whereas the observation model in the proposed framework is based on the difference between the observed central line and the predicted central lines by particles, as illustrated in Figure.3.12.

[1] https://github.com/BerkeleyAutomation/dvrkCalibration
[2] https://sites.google.com/ucsd.edu/super-framework

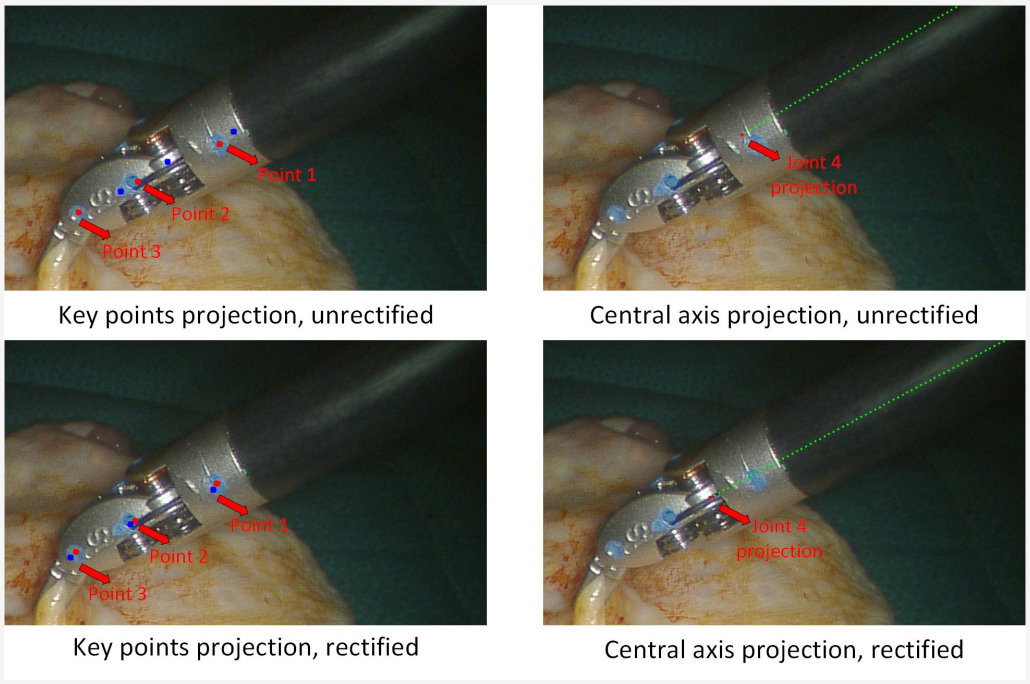


Figure 3.10: Rectification of the initial hand-eye transformation matrix in experiment 2.

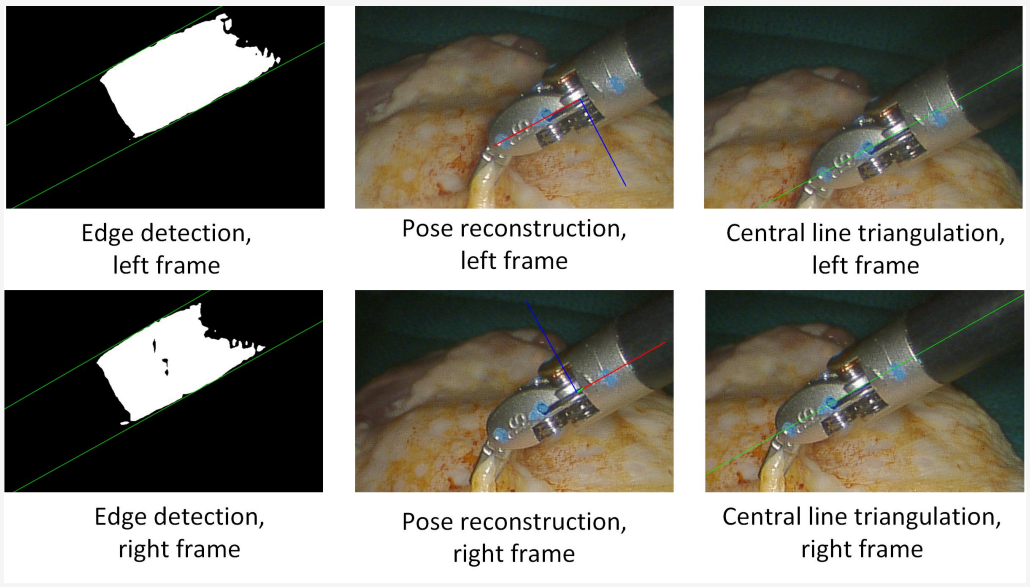
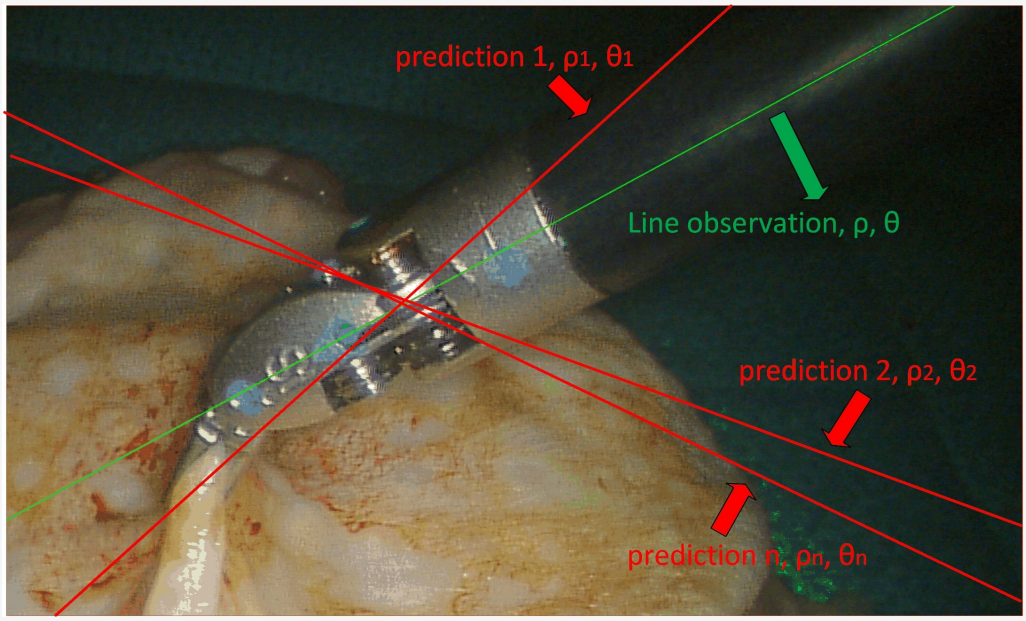
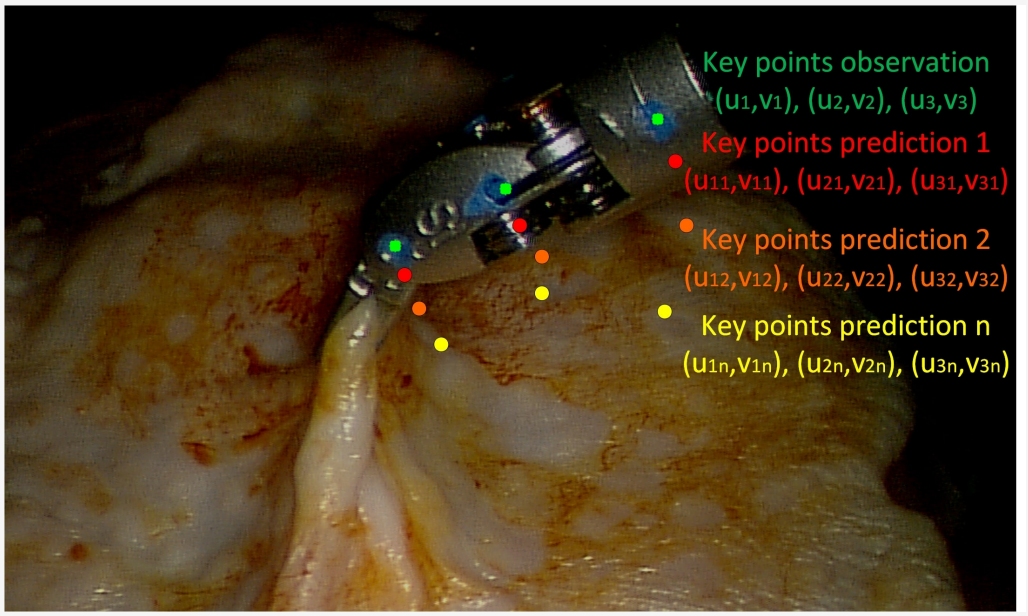


Figure 3.11: Cylindrical tool central axis reconstruction in experiment 2.



(a) Particle filter observation model in our framework



(b) Particle filter observation model in [106]

Figure 3.12: Comparison of particle filter observation models between our framework and [106]. In our framework, particle weights are updated based on the accuracy of central line projection: $w_i \propto \alpha_1 e^{|\rho-\rho_i|} + \beta_1 e^{|\theta-\theta_i|}$. In [106], particle weights are updated based on the accuracy of key points projection: $w_i \propto \alpha_2 e^{-\sum_{j=1}^{3}|u_j-u_{ji}|+|v_j-v_{ji}|}$. $\alpha_1, \alpha_2, \beta$ are positive scaling factors. In (a), the central axis in green represents the projection of the reconstructed tool axis, and red lines represent axis projections from different particle predictions. In (b), green points represent observed key points, and points of other colours represent projections of key points from different particle estimations.

3.4 Results and discussions

3.4.1 Results - Experiment 1

Figure.3.13 illustrates the calibration performance through the overlay of the instrument. The calibrated end effector positions under different calibration approaches were also compared with their ground truth values, as illustrated in Figure.3.14.

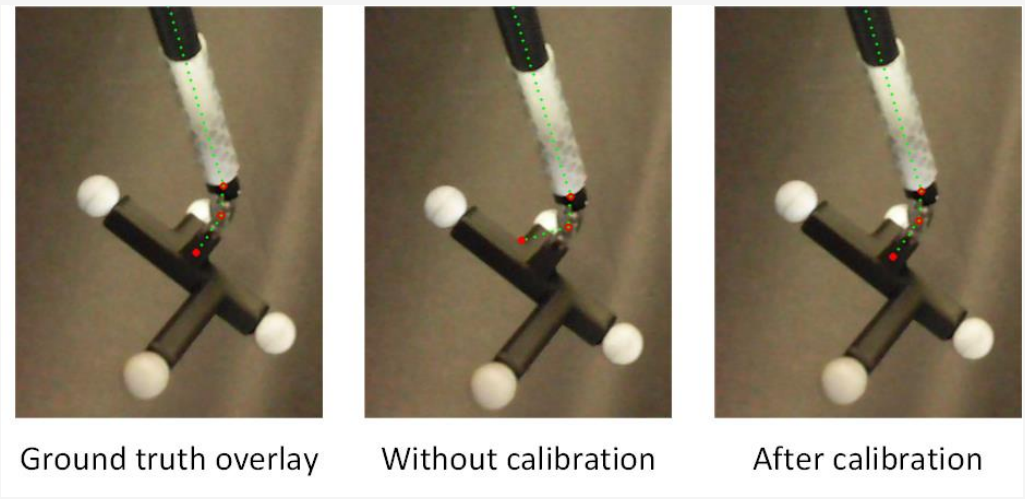


Figure 3.13: A visual illustration of the effectiveness of the calibration framework in experiment 1. The calibration result is indicated by the overlay of tool skeleton.

It is shown in Figure.3.14 that, with the calibration proposed in this study, the average positioning error reduces from 3.30mm to 1.38mm, with a more concentrated error distribution. Additionally, results show that, with particle filter calibration alone, the average positioning error reduces to 2.81mm, which highlights the importance of additional calibrations on joint 4 angle readings. When compared to the model-based calibration approach in [93], the proposed method delivered better calibration performance. While it is acknowledged that model-based calibration approaches effectively increase task success rate, as reported in their study, it is suspected that their results, which are better compared to those reported here, may be attributed to the larger training dataset (4,000). The experiment presented here suggests that model-based calibration approaches may be unreliable when there is a limited number of training data.

3.4.2 Results - Experiment 2

The back projections of marker points 1, 2 and 3 under different calibration approaches were gathered and compared with their corresponding observations on the image plane, obtained through colour filtering. The results are presented in Table 3.1 and Figure.3.15.

Table.3.1 shows that the two particle-filter based calibration frameworks delivered similar results in terms of average projection errors for key points 1 and 3. However, Figure.3.15 shows that key

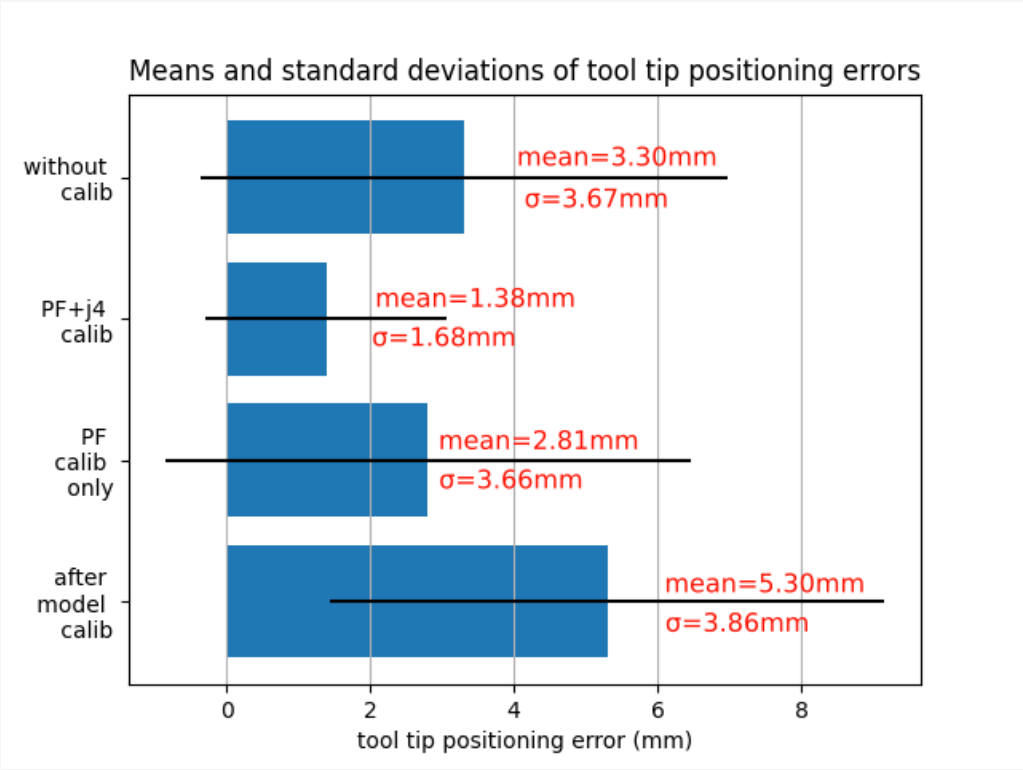


Figure 3.14: Comparison of tool tip positioning errors with a limited size of training dataset. Our quantitative study compares the pose estimation results obtained from our calibration framework and [93]. "**PF**" denotes particle filter calibration only; "**PF+j4 calib**" denotes both particle filter and joint 4 calibrations.

point-based calibration framework results in a more consistent error distribution. With only edge information utilised in the proposed framework, it suggests that calibrations on the hand-eye transformation matrix may not rely on feature detection on the end effector. Although the results in Table.3.1 indicate that additional calibrations on joint 4 did not significantly improve the overall positioning accuracy, it is suspected because joint 4 only rotated by 0.097 rad during the entire recording. It is also noted that the average back projection error for key point 3 is the largest of the three. Accurate pixel alignment for point 3 relies on both an accurate hand-eye transformation matrix and accurate joint angle values. Therefore, it is suggested that, to achieve a better positioning accuracy, additional calibrations on individual joint angle readings are necessary.

points	Approach in this study				Approach in [106]			
	j4 calibration (y/n)				j4 calibration (y/n)			
	no		yes		no		yes	
	mean	std	mean	std	mean	std	mean	std
point1	10.1	2.9	10.7	2.9	11.6	3.6	11.2	3.4
point2	7.6	3.5	8.8	4.0	4.5	4.0	5.0	3.9
point3	20.2	6.1	20.4	6.2	23.0	3.1	22.8	3.1

Table 3.1: Comparison studies in pixel discrepancies. Pixel discrepancies between back projected blue markers and their observations under different calibration approaches.

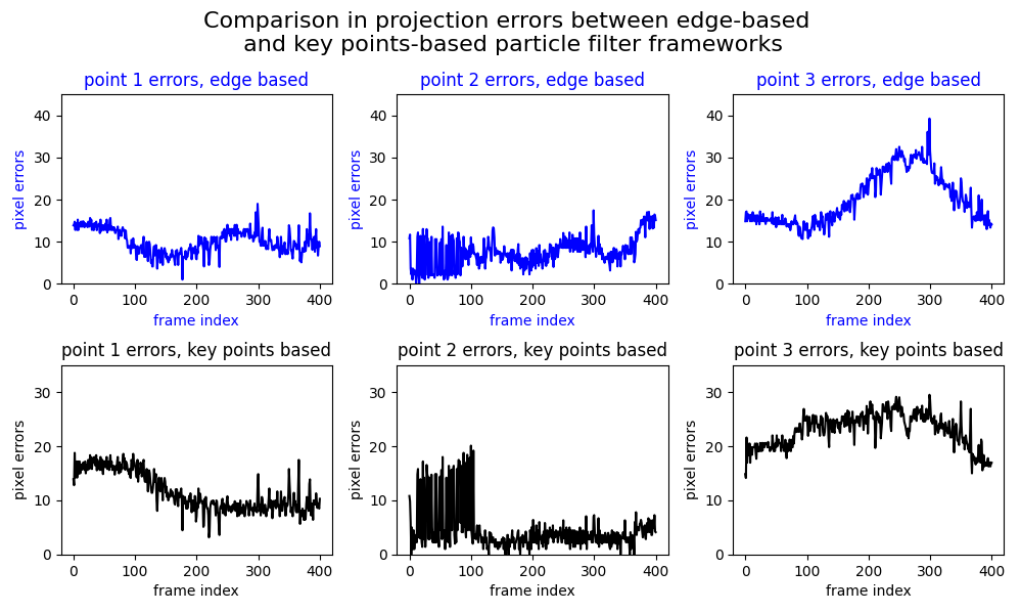


Figure 3.15: Comparison of projection errors. Comparison of projection errors for manually labelled marker point 1,2,3 between our particle filter framework and [106].

3.5 Conclusion

In this study, an on-the-fly hand-eye calibration framework was proposed to improve end-effector positioning accuracy for da Vinci surgical instruments. The entire calibration framework comprises a particle filter for estimating the hand-eye transformation matrix and an individual calibration module for dVRK joint 4 angle readings. The proposed method solely relies on edge information from cylindrical tool shafts, avoiding dependence on feature detection on the end effector, which makes it more robust to challenging surgical scenarios, such as occlusion.

Both quantitative and qualitative studies were conducted to verify the effectiveness of the proposed framework in improving end-effector positioning accuracy. Comparison studies were also conducted between the proposed approach and other calibration approaches. The experimental results show that an on-the-fly calibration approach that incorporates real-time feedback about the surgical scenario outperforms model-based approaches when there is a limited size of training data. Additionally, compared to another PF framework where key points on surgical instruments are utilised to construct the observation model, the proposed framework delivers similar average calibration accuracy, albeit with a wider range of error distribution.

After calibrating instrument tip position, which serves as input for proximity queries between the instrument and the dynamic tissue surface, the next step is to develop a tailored FRDAC pipeline that utilises the calibrated instrument position. The design of the FRDAC pipeline is presented in the following chapter.

Chapter 4

Proof of concept study on FRDAC in tele-operative surgery

Following from Chapter 3, where an on-the-fly hand-eye calibration framework was proposed to provide more accurate instrument positions, this chapter focuses on developing the FRDAC framework that accommodates for dynamic tissue deformation. In RAS, FRAC represent a control strategy that helps maintain task safety by generating anisotropic haptic guidance to surgeons. However, several challenges need to be overcome before FRAC can benefit tele-operative surgery in a clinical setting. These challenges include the ability to allow for dynamic tissue deformation, maintain energetic passivity, and speed of implementation, among others. In this study, a pipeline design for an energy dissipative FRAC strategy is proposed, which accommodates the dynamic tissue deformation caused by respiratory movements, by utilising a depth sensing camera. The proposed FRAC strategy adopts a fine mesh representation, with a total number of 122,806 polygons, while running at 43.48Hz. In vitro trajectory tracking experiments were designed, which were conducted by a "virtual" surgeon to aid quantitative assessment of the method, including its effectiveness in maintaining task safety, which was confirmed by successfully maintaining a pre-defined safety distance across all trials. Comparative studies were also conducted to investigate the robustness and time-efficiency of our method against other FRAC methods that rely on simple geometry AC representations. It is demonstrated that the proposed method provides a more robust and effective guidance overall, while maintaining comparable, if not lower, time costs.

4.1 Introduction

In the field of RAS, AC, also known as VF, were first proposed by Rosenberg [15, 16], as strategies to ensure surgical task safety by providing surgeons with anisotropic haptic guidance. AC allow motions that comply with safety requirements, while negating those that violate safety requirements. Clinical practice has confirmed the effectiveness of AC in reducing the mental workload of surgeons and enhancing task performance [5], where AC were employed to assist a hands-on knee replacement operation. Additionally, AC can be helpful in tele-operative surgical scenarios, where the physical separation between the patient side and the surgeon side prevents surgeons from forming haptic awareness of a surgical instrument during operation, as they would in hands-on surgery. The lack of haptic information forces surgeons into evaluating task safety purely through visual feedback, which poses a cognitive challenge to inexperienced surgeons [13].

AC can be divided into two categories based on their application: FRAC, which help prevent potential violations of the safety region and tool collision, and GAC, which help keep surgical instruments on a pre-planned trajectory or move them towards a target. In RMIS, the primary focus is on task safety, and this study is specifically concerned with FRAC. There are several challenges that need to be overcome before FRAC can be incorporated into a modern clinical setting. First, to provide surgeons with smooth haptic guidance, the speed at which haptic cues are sent needs to reach at least 1,000 Hz [162]. Second, during operation, soft tissues undergo deformation caused by respiration and tool-tissue interactions, requiring FRAC to be updated in real-time to adjust to a dynamic situation. Third, the accuracy requirement in RMIS is more stringent, posing a greater challenge for the implementation of FRAC. For example, the cauterization task in kidney cancer surgery requires maintaining a safety distance of 5 mm between the laser fibre held by a robot end effector and the kidney surface [163].

To address these challenges, prior work has focused on developing FRDAC, which provides more advantages in incorporating real-time tissue changes compared to FRAC. Although there exists studies such as [50], where collision avoidance between dynamic objects is achieved through monitoring distance functions and distance Jacobians, which encode dynamic factors, relying purely on the robot data, a more common practice is to incorporate an external sensing modality. Ren *et al.* [57] first proposed a FRDAC pipeline for beating heart surgery, where preoperative CT/MRI images are continuously registered to the real-time ultrasound images, enabling the update of FRDAC on the surface of a beating heart. Using a different imaging modality as a stero camera, Yamamoto *et al.* [164] incorporated in their haptic interfaces reconstruction of surface point cloud, upon which FRAC is constructed. More directly, Rydén *et al.* [60, 65] used a depth-sensing camera, Xbox Kinect (Microsoft Corp.), in their FRDAC design to protect a beating heart. The camera streams a point cloud representing the surface of a beating heart at 30Hz, so that the AC constructed around each point on the tissue surface could be constantly updated.

One existing issue among the FRDAC methods mentioned above is that the accuracy requirement can conflict with the objective of targeting real-time applications in FRDAC design. Rydén *et al.* [65] chose simple geometries, specifically spheres, to represent AC. This reduces the time required for each round of AC implementation, making it more suitable for clinical application. However, simple geometries are unable to represent complex tissue surface features [14], which can reduce the accuracy of AC implementation. On the other hand, representing FRDAC using complex geometries always involves conducting non-rigid registration from a finely described non-deformed tissue surface to a dynamically moving tissue surface. Non-rigid registration methods, such as the CPD method, can be computationally demanding *per se*, which may be challenging when capturing the deformation caused by respiration at a rate of 2Hz. Another issue is that most of the existing FRDAC pipelines do not consider energy dissipativity. This is important because it ensures that there is no energy stored from user input, and hence precludes surgical tools being actively driven to move without the active involvement of surgeons, thus maintaining task safety and avoiding liability issues. Existing non-energy storing methods include controllers based on a plasticity model [66], an energy redirection approach based on an elasto-plastic friction model [69], and controllers based on a viscosity model [70].

To address these challenges, in this chapter, a bespoke FRDAC pipeline is designed to prevent soft tissue violations in a dynamic situation, while ensuring the entire system remains energetically dissipative. The proposed pipeline embodies these following contributions. First, an approach is proposed to generating FRDAC that are capable of describing complex geometric features of a deforming tissue surface whilst satisfying the requirement for real time application. Second, a dissipative controller is incorporated into the design of FRDAC, which helps to guarantee overall safety during operation. *in vitro* experiments were conducted to verify the effectiveness of the proposed FRDAC implementation pipeline and quantify the impact of the complexity of AC representation on task performance in a dynamic scenario. The structure of this chapter is defined as follows. In section 4.2, a detailed description of the proposed FRDAC implementation pipeline is provided. In section 4.3, the experimental design of this study is described. The result and discussion are presented in section 4.4, followed by the conclusion in section 4.5.

Preliminary work in this chapter was presented at the 2023 Hamlyn Symposium on Medical Robotics, with the proceeding published as ***Cui, Z. and Rodriguez y Baena, F., 2023. Proof of Concept Implementation of Forbidden Region Dynamic Active Constraints in Minimally Invasive Surgery. Proceedings of The 15th Hamlyn Symposium on Medical Robotics 2023.***. A more comprehensive version of this study has been accepted by IEEE Robotics & Automation Letters, entitled ***"Forbidden Region Dynamic Active Constraints in Robot-Assisted Minimally Invasive Surgery"***.

4.2 Methods

According to [14], a standardised pipeline for AC implementation consists of three interrelated stages, namely AC generation, AC evaluation and AC enforcement. In the remainder of this section, the description of the proposed FRDAC design will be divided into three subsections, following the order of AC implementation.

4.2.1 AC Generation

AC generation is crucial to represent the tissue surface to be protected using constraints. The complexity of these geometrical representations affects the difficulty of checking for safety region violations, which occurs in the AC evaluation phase. To enable a more detailed representation of deforming tissue surface features, triangle meshes are used for AC generation instead of surface primitives, such as spheres and planes. To monitor tissue deformation and to enable online updates of AC, a depth sensing camera is incorporated into the pipeline design. The registration process is illustrated in Figure.4.1.

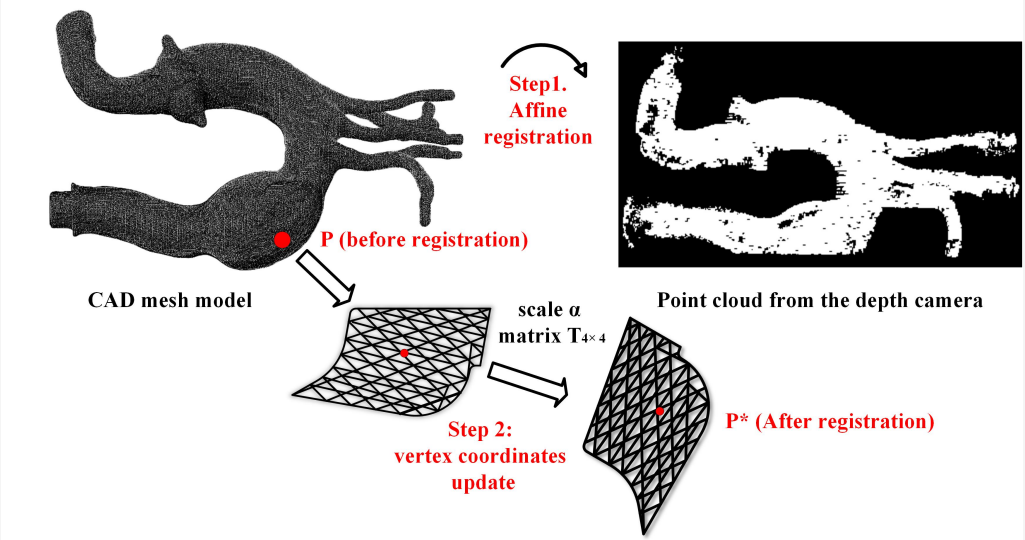


Figure 4.1: Mesh-represented FRDAC generation.

With the point cloud describing the current state of the tissue surface available, there are two ways to update the mesh-represented FRDAC. One way is to conduct 3D reconstruction using the point cloud without relying on any *a priori* knowledge of the tissue geometry. The other is to register a pre-scanned tissue model with the point cloud. The first approach typically involves surface normals estimation, which is time-consuming when point cloud density is high, making it unsuitable for real-time applications. Although the second approach relies on a pre-scanned tissue model, it is usually available through post-processes CT or MRI scans.

To register the pre-scanned tissue model to the point cloud representing the deforming tissue sur-

face, non-rigid point cloud registration can be used. Although the classic CPD method [165] has been greatly improved to accelerate the speed of non-rigid registration, as shown in examples such as [166, 167], these model-free registration methods still fail to complete each round of registration within 0.5s, for a registration task that involves the registration of 10,000 source points to as many target points, which is typical in these applications. As an alternative, it is assumed that the deformation caused by respiration can be modelled as an affine transformation to address the challenge of real-time application. Under this assumption, the TEASER++ method [168] is incorporated into the pipeline design, which enables rapid and robust global affine registration. To further enhance the robustness of the registration, the Fast Point Feature Histograms (FPFH) features[169] are first extracted from both the tissue model and the target point cloud to establish the initial correspondences, which are then leveraged by the TEASER++ method.

To verify the assumption above, two deformed aorta phantom models were first created in Blender [170], reflecting the status of inspiration and expiration, by applying inhomogeneous displacement along the surface normal direction to vertices in different anatomical regions. The amount of the applied displacement is based on the study in [171]. Then the registration performance between TEASER++ and the non-rigid registration algorithm BCPD++ [167] were compared for cases of both inspiration and expiration. The average registration error is defined as $\frac{1}{\mathrm{N}}\sum_{i=1}^{\mathrm{N}}||P_i^{gt}-P_i^{reg}||$, where N represents the total number of vertices on the phantom model, P_i^{gt} represents the ground truth position of the i^{th} vertex in the deformed model, and P_i^{reg} represents the position of the i^{th} vertex after registration. In the case of expiration, the average registration error using TEASER++ is 2.52 mm with a registration size of (8,000,8,000), and the error using BCPD++ is 2.55 mm, with a registration size of (2,000,2,000). In the case of inspiration, the average error is 2.40 mm using TEASER++, and 2.34 mm using BCPD++.

The extraction of the FPFH features relies on surface normal estimation, which delays the speed of the overall registration. To further speed up the registration process, FPFH feature extraction is performed only once in the first round of the FRDAC implementation, and it is assumed that the feature correspondences are preserved in the following rounds of implementation as long as the normal features of the tissue surface do not change drastically during operation. After registration, points on the CAD can be updated to the camera frame, shown in Eq.4.1.

$$\{P_{model}\} \xrightarrow[\mathrm{T}_{4\times4},scale]{\text{Affine registration}} \{P^*_{model}\} \tag{4.1}$$

This assumption is supported by the simulation results presented in Figure.4.2. To verify the assumption, FPFH feature correspondences were first extracted between the non-deformed and inspiration model, and then these correspondences were used for the registration to the expiration model. The registration test was compared against when FPFH feature correspondences are freshly established, across different sizes of point cloud. The t-tests results show that there is no statistical difference between the two approaches when the size of registration is less than

8,000.

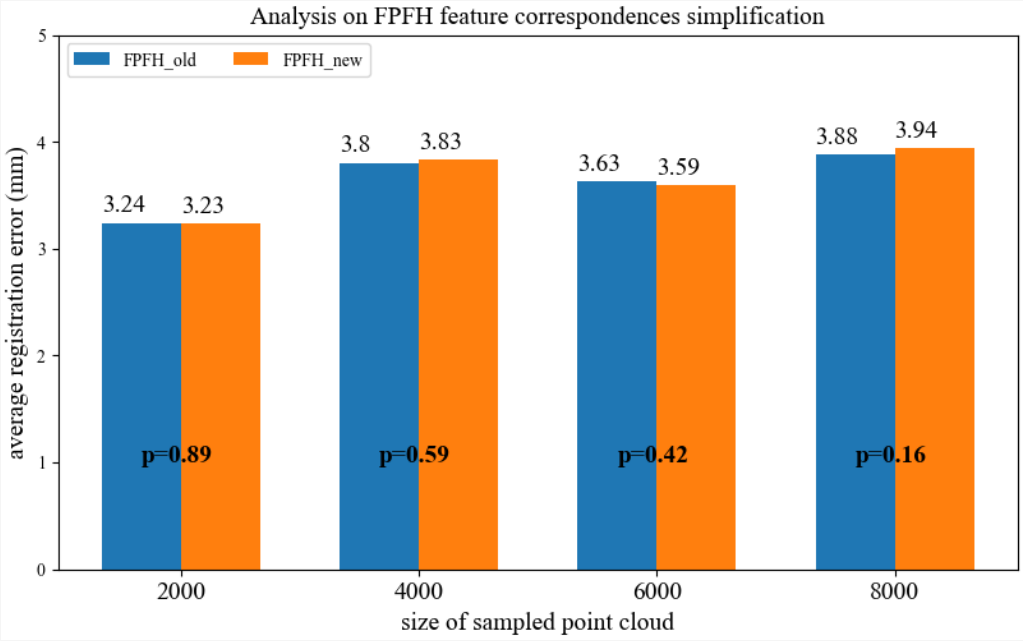


Figure 4.2: Comparison of average point registration errors. "FPFH_new" refers to when correspondences are freshly established; "FPFH_old" refers to when correspondences are assumed unchanged. The p value of t tests are also presented.

4.2.2 AC Evaluation

For FRDAC, AC evaluation means detecting whether there exists any violation of the safety region. During violation, the specific area on a surgical instrument that must be prevented from damaging tissue surfaces is defined as CTG, and a violation of the safety region occurs when d_{min}, the minimum distance between the CTG and the tissue surface, falls within a pre-defined safety distance d_{safe}. d_{min} is also the distance between the closest point pair, which is formed by P^*_{tool} on the CTG, and P^*_{tissue} on the tissue surface.

The difficulty of conducting AC evaluation largely depends on the representation of AC. For AC represented by simple geometries, such as lines, spheres and cylinders, the minimum distance between the CTG and the AC can be quickly calculated through simple linear algebra. However, for AC represented by hundreds of thousands of triangles in a mesh, the computational cost incurred by the proximity query is not negligible.

To accelerate the proximity query process, in this study, the Deformation Invariant Boundary Spheres (DIBS) method is adopted [62], which enables the proximity query between a cylindrical CTG and a dynamically moving brain mesh model with a resolution of 500,000 polygons to run at 1,587 Hz without Graphics Processing Unit (GPU) acceleration. The method's rapid performance is due to its ability to avoid reconstructing Boundary Volumes (BVs) when the tissue surface undergoes deformation. After the tissue model is registered to the target point cloud, the BVs constructed on

the tissue surface will also be updated, followed by a rapid proximity query facilitated by the DIBS method. The AC evaluation procedure is summarised in Eq.4.2.

$$\min \text{distance}(\text{CTG}, P^*_{model}) \xrightarrow[\text{d}_{\text{min}}]{\text{DIBS query}} \langle P^*_{tool}, P^*_{tissue} \rangle \tag{4.2}$$

4.2.3 AC Enforcement

The final stage of AC implementation is to compute the magnitude and the direction of the AC force to be sensed by a surgeon such that, when a violation of the safety region is detected, the surgeon can promptly retract the surgical instrument away from the moving tissue. While a widely used approach to generating an AC force is to apply a simple elastic-plastic model [66], which generates frictional forces that are antiparallel to the elastic displacement, one drawback of this model is that it becomes ineffective in generating a force that guides the CTG out of the safety region when a violation has already occurred [69]. Furthermore, using a simple elastic-plastic model does not ensure that the entire system is energetically dissipative, which can compromise task safety. To address these concerns, in this study, the dissipative controller developed in [68] is adopted. The dissipativity of the controller is maintained through an energy redirection approach. From the previous AC evaluation stage, the position of the closest point pairs on the CTG and the tissue surface can be obtained. The unit vector that connects the closest point pair is defined as penetration vector $\mathbf{v_{pen}}$, and the unit vector that aligns with the direction of the current needle tip movement is defined as motion vector $\mathbf{v_{mov}}$, pointing from the current instrument tip point P_{tip} towards the current target point P_{tgt}. After sending $\mathbf{v_{pen}}$ and $\mathbf{v_{mov}}$ into the dissipative controller, which works in $\mathbb{R}^3$, the friction component $\mathbf{v_{act}}$ will be calculated, which is then utilised to generate an AC force $\mathbf{f_{AC}}$. A graphical illustration is shown in Figure.4.3. Eq 4.3 summarizes the AC evaluation process, where Σ_0, Σ_1 represents a 3×3 friction stiffness matrix and viscous coefficient matrix, respectively.

$$\begin{aligned} \mathbf{v_{pen}} &= \frac{P^*_{tool} - P^*_{tissue}}{\text{d}_{\text{min}}} \\ \mathbf{v_{mov}} &= \frac{P_{tgt} - P_{tip}}{||(P_{tgt} - P_{tool}||} \\ \mathbf{f_{AC}} &= \Sigma_0 \mathbf{v_{act}} + \Sigma_1 \dot{\mathbf{v}}_{\mathbf{act}} \end{aligned} \tag{4.3}$$

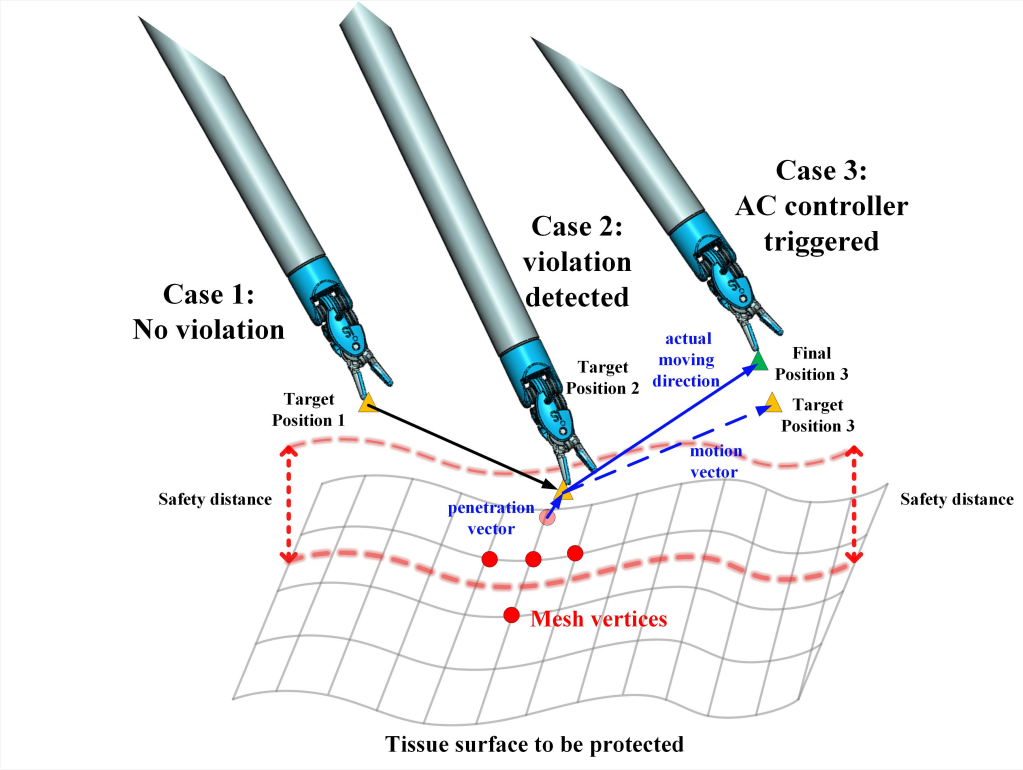


Figure 4.3: Illustration of AC evaluation and AC enforcement.

4.3 Experiments

4.3.1 Overview

To investigate the effectiveness of the proposed FRDAC pipeline in maintaining task safety in RMIS, experiments were conducted, where the proposed FRDAC assisted a surgical instrument in performing a trajectory tracking task whilst maintaining a preset safety distance d_{safe}. A trajectory tracking task was chosen because it was more feasible to evaluate its performance by computing the average distance between the instrument and the reference trajectory, which was updated online to reflect changes to the tissue surface. As a proof-of-concept implementation, the trajectory tracking experiments were conducted *in vitro*. To remove the human element from this study, a hybrid force-position controller was incorporated to emulate the ideal situation where a "virtual" surgeon could perfectly act upon the haptic force generated by the AC controller. Additionally, the proposed FRDAC strategy was compared against the FRDAC developed in [60] in assisting the same trajectory tracking task to quantify the effect of AC representation on the efficiency of AC implementation. Experiments were designed where both methods were used for assisting with trajectory tracking tasks in static and dynamic scenarios, across various levels of deformation. The remainder of this section describes the hardware setup, the design of the hybrid force-position controller, and the algorithm designed for the comparative experiments.

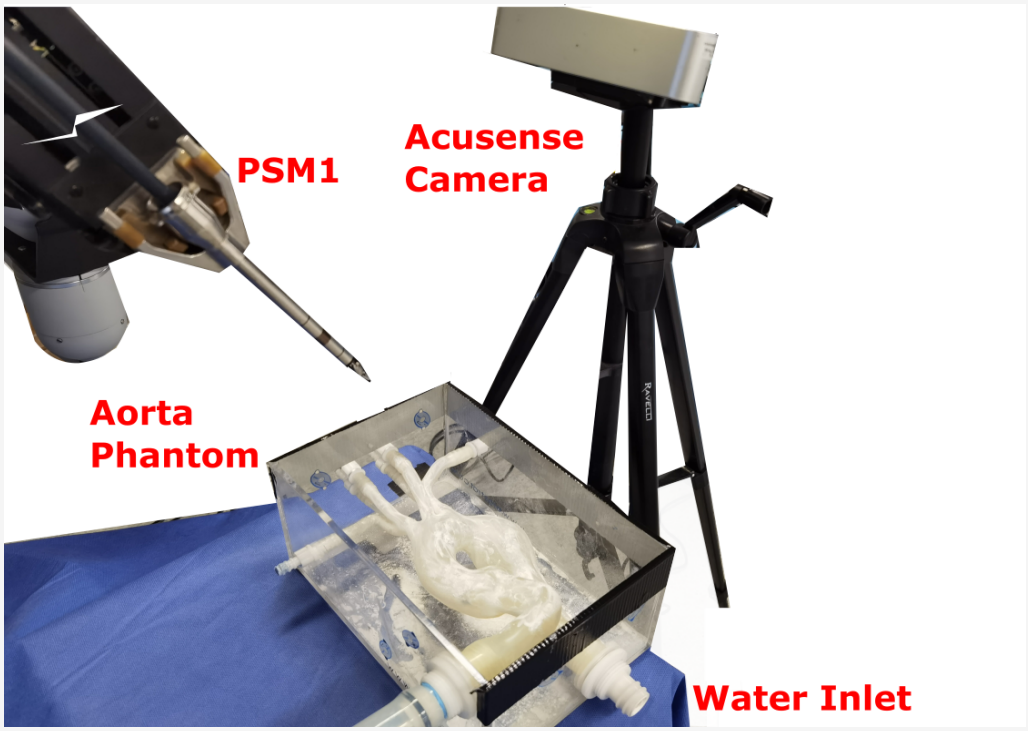


Figure 4.4: Hardware setup in the user-free experiments. The hardware setup consists of an Acusense 3D camera, an aorta silicone phantom and a pair of forceps held by dVRK PSM1

4.3.2 Hardware Setup

The experiments in this study were conducted using the first-generation dVRK [158]. A surgical instrument (Forceps 400036E, Intuitive Inc®) attached to PSM1 tracked a dynamic trajectory on the surface of a deforming aorta silicone phantom that was controlled by a water pump. A RGBD camera, the Acusense 3D (Revopoint 3D Inc®), with a resolution of 0.5 mm at a working distance of 500 mm, and a depth capturing rate of 10 Hz, was used. The algorithm for FRDAC implementation was written in C++ and executed as a Robot Operating System (ROS) node on Ubuntu 20.04 installed on a desktop (EliteDesk 800 G5, HP corp.) without GPU acceleration. The hardware setup is shown in Figure.4.4

4.3.3 Hybrid Force-Position Controller

It is postulated that, when an AC force is generated, it can effectively slide the surgical tool in the direction of the AC force as if a "virtual" surgeon was controlling it. The "virtual" surgeon here is assumed as a user who would move the instrument outside forbidden regions along the direction of the AC force. To facilitate such movement, a hybrid force-position controller is introduced, which is based on the approach presented in [172]. It computes the displacement of the end effector of the surgical tool in Cartesian space as:

$$\mathbf{\Delta x} = \mathbf{S f_{AC}}$$

where $\mathbf{\Delta x}$ is a 6×1 vector denoting the displacement of the end effector of the surgical tool in Cartesian space; $\mathbf{S} = diag\{s_1, s_2, s_3, s_4, s_5, s_6\}$ denotes a 6×6 compliance matrix, and $\mathbf{f_{AC}}$ denotes a 6×1 vector of the generated AC force. When a violation is detected and $\mathbf{f_{AC}}$ is generated, the "virtual" surgeon is expected to move the instrument along $\mathbf{\Delta x}$ until it is outside the forbidden region.

4.3.4 Algorithm Implementation

4.3.4.1 Preparation tasks

A reference trajectory was predefined on the non-deformed phantom surface. Prior to the experiments, the Acusense camera was required to be positioned at a distance between 500 mm and 600 mm from the phantom surface, and the transformation matrix from the camera frame to the PSM1 base frame was required.

I. Reference Trajectory Generation

Two circular reference trajectories $\{Ref_1\}$ and $\{Ref_2\}$ were designed for static and dynamic experiments, respectively. Both trajectories were generated by first manually selecting N_{raw} vertex points located on different anatomical regions of the phantom mesh model, and then finding the

best-fit circle that contains N_{full} points using the circle-fitting-3d library [1]. The best-fit circle was then translated along the normal direction of the circular plane by d_n to generate reference trajectories within varying distances from the phantom surface. These trajectories travel through different regions of the aorta while providing easy access to testing both FRDAC strategies in situations where safety regions are violated. It was chosen that $d_n = 1$ cm, $N_{full} = 72$ for $\{Ref_1\}$, and $d_n = 2$ cm, $N_{full} = 72$ for $\{Ref_2\}$.

II. Hand-eye Calibration

The transformation matrix ($\mathtt{T_{cr}}$) from the camera base frame to the PSM1 base frame was obtained from preoperative hand-eye calibration using two 3D-printed spheres, following the process described in [93]. Altogether, 50 point pairs were gathered to calculate the transformation matrix.

4.3.4.2 Workflow

In the comparison study, experimental trials that adopted the FRDAC developed in this study are denoted as $\boldsymbol{Exp}_{ours}$, and the ones that adopted the FRDAC proposed in [60] are denoted as $\boldsymbol{Exp}_{Rydén}$. The differences in the two implementations lie in how the FRDAC is updated, and how to determine the desired tool position when a violation of the safety region is detected. In $\boldsymbol{Exp}_{Rydén}$, the FRDAC is constructed as spheres around the points on the tissue surface, and the desired tool tip position (proxy position) keeps being updated from the current position, which is also called HIP, until the proxy state is free.

The workflows using different FRDAC methods are described as follows and summarized in Figure.4.5. After launching the ROS node, the camera first streams the point cloud on the tissue surface $\{\hat{Cloud}_{tissue}\}$, to which the point cloud on the non-deformed tissue model $\{Cloud_{tissue}\}$ is registered, returning the affine transformation matrix $\mathtt{A_{mc}}$ from the model frame to the camera frame. To accelerate the registration process, $\{\hat{Cloud}_{tissue}\}$ is uniformly downsampled to N_m points, and $\{Cloud_{tissue}\}$ is uniformly downsampled to N_s points. With $\mathtt{A_{mc}}$, the reference trajectory in the model frame $\{Ref\}$ is then updated to the camera frame as $\{\hat{Ref}\}$. Subsequently, $\{\hat{Ref}\}$ and $\{Cloud_{tissue}\}$ are transformed to the PSM1 base frame as $\{\tilde{Ref}\}$ and $\{\tilde{Cloud}_{tissue}\}$, respectively, through the hand-eye transformation matrix $\mathtt{T_{cr}}$. The joint values of PSM1 are then read from the dVRK Application Programming Interface (API), which are then fed into the forward kinematics to obtain the tip position $\tilde{P}_{tip}$. The tool tip is required to cover all the points on $\tilde{Ref}$ progressively from the first one, and when $||\tilde{P}_{tgt} - \tilde{P}_{tip}|| < \epsilon$, the target point is updated by one.

The AC generation and evaluation procedures differ in $\boldsymbol{Exp}_{ours}$ and $\boldsymbol{Exp}_{Rydén}$. In $\boldsymbol{Exp}_{ours}$, the vertex coordinates of the phantom model are updated via $\mathtt{A_{mc}}$, and the minimum distance between the tool tip and the tissue surface is evaluated via the DIBS method. In $\boldsymbol{Exp}_{Rydén}$, N_{bar} points are selected,

[1] https://pypi.org/project/circle-fitting-3d/

which are closest to the tool tip for proxy state update. If either the minimum distance returned by the DIBS query is smaller than d_{safe}, or the updated proxy position drifts away from the current HIP, an AC force will be generated. Otherwise, the tool tip will continue to move towards $\tilde{P}_{tgt}$.

To ensure fairness of the comparison, the same dissipative controller is adopted in ***Exp***$_{ours}$ and ***Exp***$_{Rydén}$, but with different definitions in $\mathbf{v_{pen}}$. In ***Exp***$_{ours}$, $\mathbf{v_{pen}}$ is defined as in subsection.4.2, whereas in ***Exp***$_{Rydén}$,$\mathbf{v_{pen}}$ is defined by the unit vector connecting the HIP (instrument tip) to the updated proxy point (desired tip position on the forbidden region surface). In both cases, $\mathbf{v_{mov}}$ is defined as the unit vector pointing from $\tilde{P}_{tip}$ to $\tilde{P}_{tgt}$. Both $\mathbf{v_{pen}}$ and $\mathbf{v_{mov}}$ are then sent to the AC controller to generate a frictional force $\mathbf{f_{AC}}$. Eventually, $\mathbf{f_{AC}}$ is sent to the hybrid force-position controller to generate a positional command $\mathbf{\Delta x_{AC}}$ to be received by PSM1.

4.3.5 Deformation measurements

To generate varying levels of deformation, the valve of the water pump connected to the phantom was adjusted. To quantify the magnitude of deformation, the Acusense camera was used to capture a series of point clouds of the pulsating phantom surface within a given amount of time. The magnitude of deformation is calculated in Open3D [173] as the range of distances between phantom surfaces in Open3D. The levels of deformation were classified into "slow", "fast" and "super fast", where the magnitudes of deformation are 2.43 mm, 3.64 mm and 4.80 mm, respectively. From visual observations, respiratory rate was set at around 1-2 Hz. Figure.4.6 illustrates the maximum levels of surface deformation during "super fast" deformation.

4.3.6 Parameters selection

In both ***Exp***$_{ours}$ and ***Exp***$_{Rydén}$, it was selected that $N_m = 8000; N_s = 8000$; FPFH search radius (source, target)=0.02 m; FPFH normal radius (source, target)=0.06 m; radius of cylindrical CTG=0.005 m; $d_{safe} = 0.010$ m; $\mathbf{s} = diag\{1000, 1000, 1000, 0, 0, 0\}$

Algorithm Workflow for Dynamic AC

Require: $Cloud_{\text{tissue}}$, T_{cr}
  int $i \leftarrow 1$ ▷ index for the current target point
  bool $violation \leftarrow false$
  while $i \leq N_{full}$ **do**
    $\hat{Cloud}_{\text{tissue}} \leftarrow \hat{Cloud}_{\text{tissue}}$ ▷ Acusense streaming
    $A_{mc} \leftarrow A_{mc}$ ▷ TEASER++
    update $\hat{Ref}$ to $\hat{Ref}$, $\tilde{Ref}$
    $\tilde{P}_{\text{tar}} \leftarrow \tilde{Ref}[i]$
    if $||\tilde{P}_{\text{tar}} - \tilde{P}_{\text{tip}}|| < \epsilon$ **then**
      $i \leftarrow min\langle i+1, N_{full}\rangle$
      $\tilde{P}_{\text{tar}} \leftarrow \tilde{Ref}[i]$
    end if
    if Exp_{ours} is on **then** ▷ mesh-represented FRDAC
      update $\{point_{\text{tissue}}, point_{\text{tool}}, d_{\text{min}}\}$
      if $d_{min} \leq d_{safe}$ **then**
        $violation \leftarrow true$
        $\vec{v}_{pen} \leftarrow \frac{point_{\text{tissue}} - point_{\text{tool}}}{||point_{\text{tissue}} - point_{\text{tool}}||}$
        $\vec{v}_{mov} \leftarrow \frac{\tilde{P}_{\text{tar}} - \tilde{P}_{\text{tip}}}{||\tilde{P}_{\text{tar}} - \tilde{P}_{\text{tip}}||}$
      end if
    else if $Exp_{\text{Rydén}}$ is on **then**
      ▷ sphere-represented FRDAC
      $HIP \leftarrow \tilde{P}_{\text{tip}}$
      $proxy \leftarrow proxy_{\text{updated}}$
      if $HIP \neq proxy$ **then**
        $violation \leftarrow true$
        $\vec{v}_{pen} \leftarrow \frac{proxy - HIP}{||proxy - HIP||}$
        $\vec{v}_{mov} \leftarrow \frac{\tilde{P}_{\text{tar}} - \tilde{P}_{\text{tip}}}{||\tilde{P}_{\text{tar}} - \tilde{P}_{\text{tip}}||}$
      end if
    end if
    if $violation = true$ **then**
      $\vec{f}_{AC} \leftarrow AC_{Enforce}(\vec{v}_{pen}, \vec{v}_{mov}, \tilde{P}_{\text{tip}})$
      $\vec{\Delta x}_{AC} \leftarrow Hybrid(\vec{f}_{AC})$
      $\vec{\Delta x} \leftarrow \frac{\vec{\Delta x}_{AC}}{||\vec{\Delta x}_{AC}||}$
    else
      $\vec{\Delta x} \leftarrow \frac{\tilde{P}_{\text{tar}} - \tilde{P}_{\text{tip}}}{||\tilde{P}_{\text{tar}} - \tilde{P}_{\text{tip}}||} min\langle||\tilde{P}_{\text{tar}} - \tilde{P}_{\text{tip}}||, stride_{max}\rangle$
    end if
    send $\vec{\Delta x}$ to PSM_1
  end while

Figure 4.5: FRDAC algorithm workflow

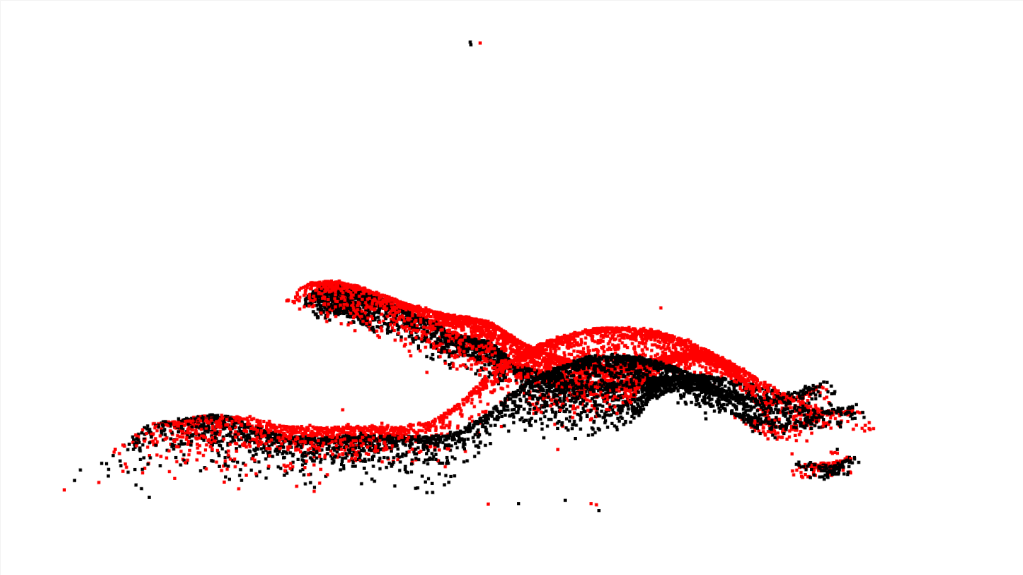


Figure 4.6: Illustration of the magnitude of "super fast" deformation. To illustrate the magnitude of deformation, tissue surface point clouds were continuously captured by a depth-sensing camera during periodic movements. These point clouds were analysed and plotted using Open3D [173]. The red and black points indicate the maximum levels of deformation during "super fast" deformation.

4.4 Results and discussions

4.4.1 Static trajectory tracking results

For static trajectory tracking, only one trial was conducted using both FRDAC strategies for tracking $\{Ref_1\}$. The static trajectory tracking performance is illustrated in Figure.4.7, and quantitative results are presented in Figure. 4.8. In $\boldsymbol{Exp}_{\text{ours}}$, a total of 149 points were gathered on the actual tool tip trajectory. Altogether, there were 62 cases where $\text{d}_{\text{min}} < \text{d}_{\text{safe}}$, indicating that the AC controller was in action. The average distance between the tool tip and updated target point on the reference trajectory $\text{d}_{\text{traj}} = \frac{1}{\text{N}} \sum_{i=1}^{\text{N}} ||P_i - Q_i|| = 8.91$ mm. where P_i and Q_i denote the i^{th} point on the actual tool tip trajectory and its corresponding target point on the updated reference trajectory, respectively. The average minimum distance from the phantom surface $\text{d}_{\text{phantom}} = \frac{1}{\text{N}} \sum_{i=1}^{\text{N}} \text{d}_{\text{min,i}} = 10.44$ mm, where $\text{d}_{\text{min,i}}$ denotes the minimum distance returned by the the DIBS query at the i^{th} instance.

In $\boldsymbol{Exp}_{\text{Rydén}}$, a total of 170 points were collected, and d_{traj} was 10.01 mm. Altogether, there were 51 cases where the proxy point moved away from the HIP, indicating that the AC controller was in action. $\text{d}_{\text{phantom}} = \frac{1}{\text{N}} \sum_{i=1}^{\text{N}} \min\langle P_i, \{Cloud_{tissue,\text{i}}\} \rangle$, where $\{Cloud_{tissue,\text{i}}\}$ represents the down-sampled tissue point cloud at the i^{th} instance. $\text{d}_{\text{phantom}}$ in both $\boldsymbol{Exp}_{\text{ours}}$ and $\boldsymbol{Exp}_{\text{Rydén}}$ being greater than $\text{d}_{\text{safe}} = 10$ mm indicates that both FRDAC methods can maintain task safety. Additionally, both d_{traj} and $\text{d}_{\text{phantom}}$ in $\boldsymbol{Exp}_{\text{ours}}$ being smaller than those in $\boldsymbol{Exp}_{\text{Rydén}}$ suggests that the DIBS method favours accuracy over a larger safety margin.

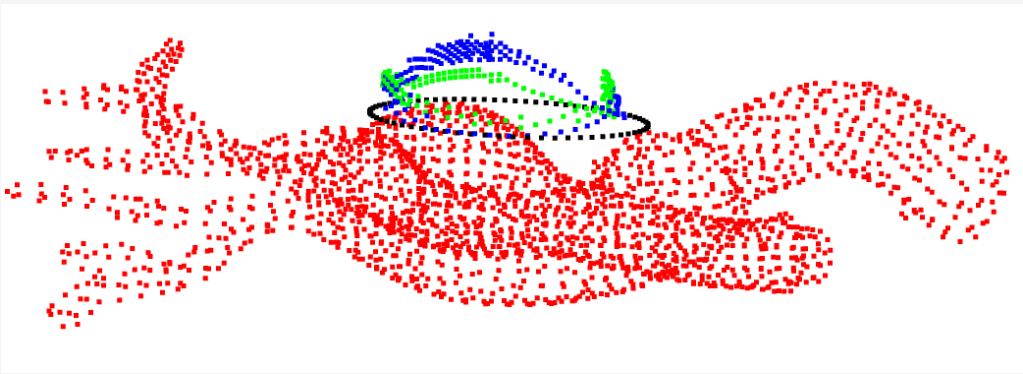


Figure 4.7: Comparison of static trajectory tracking between $\boldsymbol{Exp}_{\text{ours}}$ and $\boldsymbol{Exp}_{\text{Rydén}}$ in Chapter 4. $\boldsymbol{Ref}_1$ was used. Red represents the phantom model; black represents the reference circular trajectory $\boldsymbol{Ref}_1$; green represents the actual trajectory in $\boldsymbol{Exp}_{\text{ours}}$, and blue represents the actual trajectory in $\boldsymbol{Exp}_{\text{Rydén}}$. In an ideal static tracking scenario, the instrument tip should move away from the tissue surface when violations are detected. Otherwise, it should keep staying on the reference trajectory.

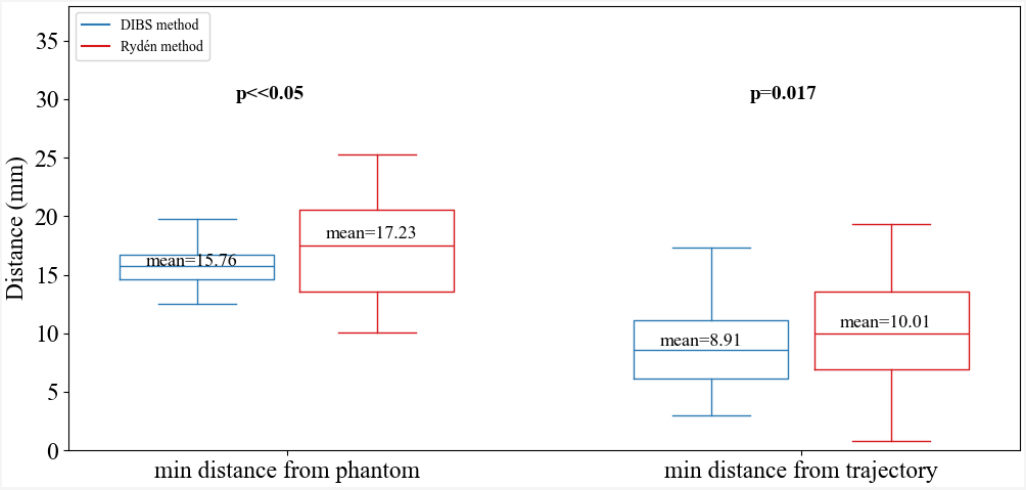


Figure 4.8: Static trajectory tracking results in Chapter 4. The minimum distance between the instrument and the moving phantom surface, as well as the constantly updated reference trajectory during $\boldsymbol{Exp}_{\text{ours}}$ and $\boldsymbol{Exp}_{\text{Rydén}}$ are presented. t tests were conducted, and it is denoted that $p << 0.05$ when $p < 0.005$. Outliers are not shown in the figure, as in Figure. 4.9 and Figure. 4.10.

4.4.2 Dynamic trajectory tracking results

For dynamic trajectory tracking experiments, experiments were conducted across different levels of deformation, namely, "slow", "fast" and "mixed" (where the level of deformation was changed from "slow" to "fast" to "super fast"). For each level of deformation, tracking experiments were conducted four times. The same metrics in subsection 4.4.1 were applied to evaluate their tracking performance. Tracking results using both FRDAC methods are presented in Figure.4.9 and Figure.4.10, and the time costs for all the experimental trials are recorded in TABLE 4.1 and 4.2.

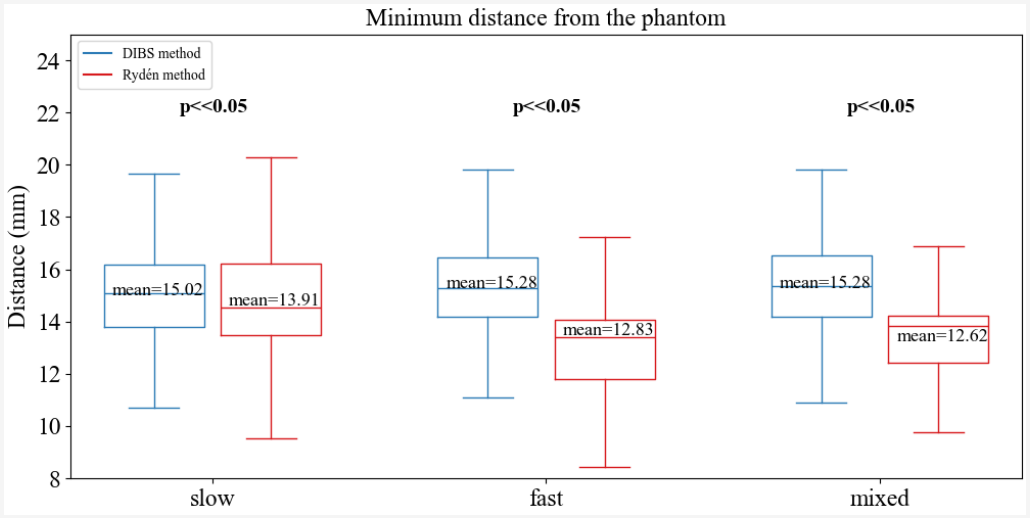


Figure 4.9: Comparison of $d_{phantom}$ between Exp_{ours} and $Exp_{Rydén}$ during dynamic tracking in Chapter 4. $d_{phantom}$ represents the minimum distance between the instrument and the moving phantom surface across all the trials. The range of $d_{phantom}$ goes below d_{safe}, indicating instances where the instrument tip penetrated the safety region after following movement commands generated by the hybrid force-position controller.

From Figure.4.9, it is noticed that in $\boldsymbol{Exp}_{ours}$ $d_{phantom} \geq d_{safe} = 15$ mm for all the experimental runs, which indicates that the DIBS method can maintain task safety across a range of deformation levels. It has been noticed that there are some unsuccessful runs in $\boldsymbol{Exp}_{Rydén}$, where the instrument got stuck in certain regions after receiving false guidance because of noisy surface point clouds, as illustrated in Figure.4.11. Although in $\boldsymbol{Exp}_{Rydén}$ $d_{phantom} \leq d_{safe} = 15$ mm, suggesting that violations of safety regions are not acted upon, this is also suspected to have been caused by noisy point clouds, leading to a smaller distance enquiry result between the instrument tip and its surrounding point cloud. From Figure.4.10, the DIBS method demonstrates a higher tracking accuracy with statistical significance as the level of deformation increases, which matches the previous finding in 4.4.1. The overall dynamic trajectory tracking performance is illustrated in Figure.4.12, where Mixed run 4 is used as an exemplar.

The overall tracking time recorded from Table 4.1 and 4.2 shows that the DIBS method is more time-efficient although it involves point cloud registration. It was also found that although some runs in $\boldsymbol{Exp}_{Rydén}$, for example, "Slow run4", "Fast run4" and "Mixed run2", contain less points on the needle

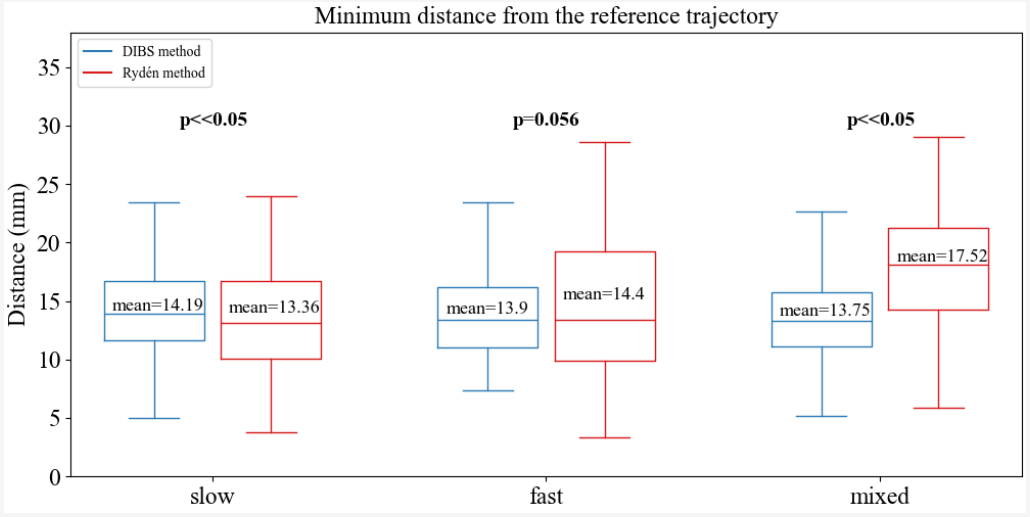


Figure 4.10: Comparison of d_{traj} between Exp_{ours} and $Exp_{Rydén}$ during dynamic tracking in Chapter 4. d_{traj} represents the minimum distance between the instrument and the constantly updated reference trajectory.

tip trajectory than their counterpart in Exp_{ours}, it took more time to complete a full tracking run. The time spent on AC evaluation using both FRDAC methods for these trials were analysed, and the results are presented in Figure. 4.13. The results show that the time cost for AC evaluation using the DIBS method is more consistent, whereas Ryden's method can be more time consuming, requiring more iterations before the proxy status reaches convergence, as shown in Figure. 4.14.

To evaluate the potential of the proposed FRDAC method for use in a modern clinical setting, the computational costs incurred for the two methods are summarised in Table.4.3.

The proposed FRDAC strategy, even though it involves point cloud registration, is still capable of running consistently at 43.48 Hz without external GPU acceleration, which is faster than the depth capturing rate of the camera and the tissue deformation rate achieved in these experiments. This confirms that the proposed method is fast enough to respond to tissue deformation changes appropriately, within the context of these experiments. On average, the proposed pipeline runs even faster than Rydén's method, which sometimes requires more time for AC evaluation.

Although the accuracy of the DIBS method is not directly affected by a local noisy point cloud, it relies on the global affine registration performance. Therefore, refining surface point may lead to better performance not only for the DIBS method but also for Rydén's method, which fails to extract point clouds surrounding the instrument in situations where, for instance, occlusions are present. Furthermore, to accommodate different types of deformation, for example, sudden tool-tissue interactions, non-rigid registration algorithms should be considered.

Run No.	1st	2nd	3rd	4th
Slow run time	7min 22s	7min 52s	7min 57s	7min 56s
Slow n_{points}	198	213	211	215
Slow n_{action}	94	105	102	107
Fast run time	4min 19s	4min 19s	4min 36s	4min 47s
Fast n_{points}	117	119	125	130
Fast n_{action}	51	52	54	57
Mixed run time	4min 31s	4min 30s	5min 8s	4min 29s
Mixed n_{points}	120	120	137	120
Mixed n_{action}	50	51	55	53

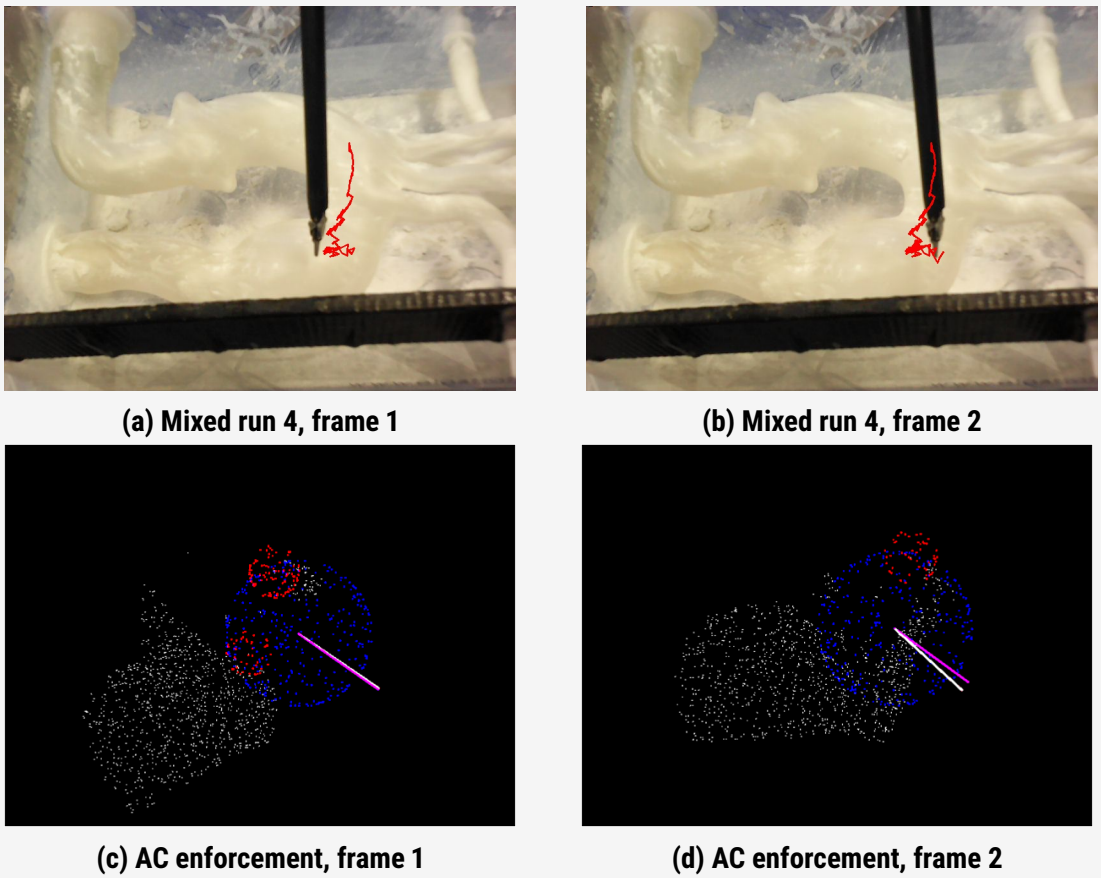
Table 4.1: Dynamic trajectory tracking time in Exp_{ours} Trajectory tracking experiments were conducted across various levels of deformation. "Mixed" represents that the level of deformation was changed from "slow" to "fast" to "super fast". n_{action} refers to the number of cases where AC was in action. The same definition applies in Table.4.2

Run No.	1st	2nd	3rd	4th
Slow run time	9min 59s	8min 16s	7min 25s	9min 40s
Slow n_{points}	218	176	160	211
Slow n_{action}	86	72	64	77
Fast run time	6min 25s	7min 28s	5min 16s	8min 17s
Fast n_{points}	141	165	116	183
Fast n_{action}	39	51	30	53
Mixed run time	5min 29s	5min	9min 59s	5min
Mixed n_{points}	118	113	219	115
Mixed n_{action}	40	57	77	58

Table 4.2: Dynamic trajectory tracking time in $Exp_{Rydén}$ The same levels of deformation were applied here as in TABLE.4.1

Methods	Ours	Rydén's
FPFH extraction time	0.028s (initial round only)	None
Registration time	0.016s	None
Registration size	(8,000, 8,000)	None
AC evaluation size	122,806 polygons	1,000 points
mean AC evaluation time	0.007s	0.028s
Total time cost	0.023s	0.028s
Frequency	43.48Hz	35.71Hz

Table 4.3: Comparison of the computational cost incurred by different FRDAC approaches in Exp_{ours} and $Exp_{Rydén}$. The computational costs listed here are in relation to a single round of AC generation/evaluation.



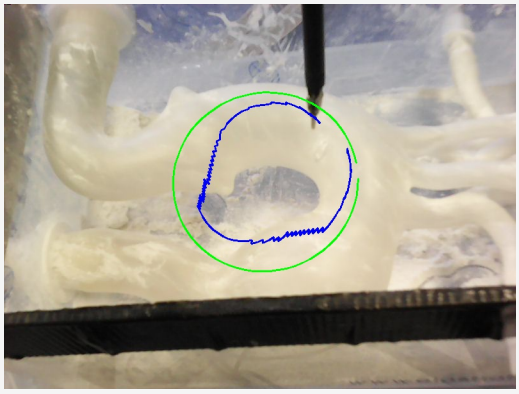
(a) Mixed run 4, frame 1

(b) Mixed run 4, frame 2

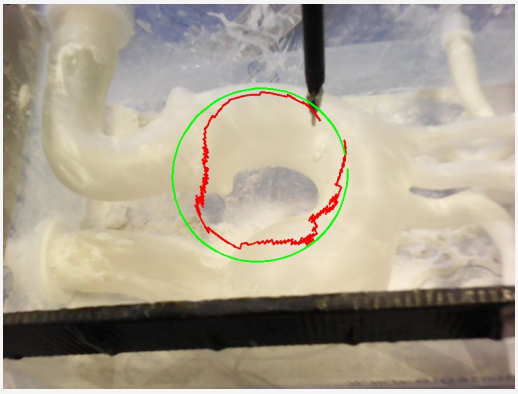
(c) AC enforcement, frame 1

(d) AC enforcement, frame 2

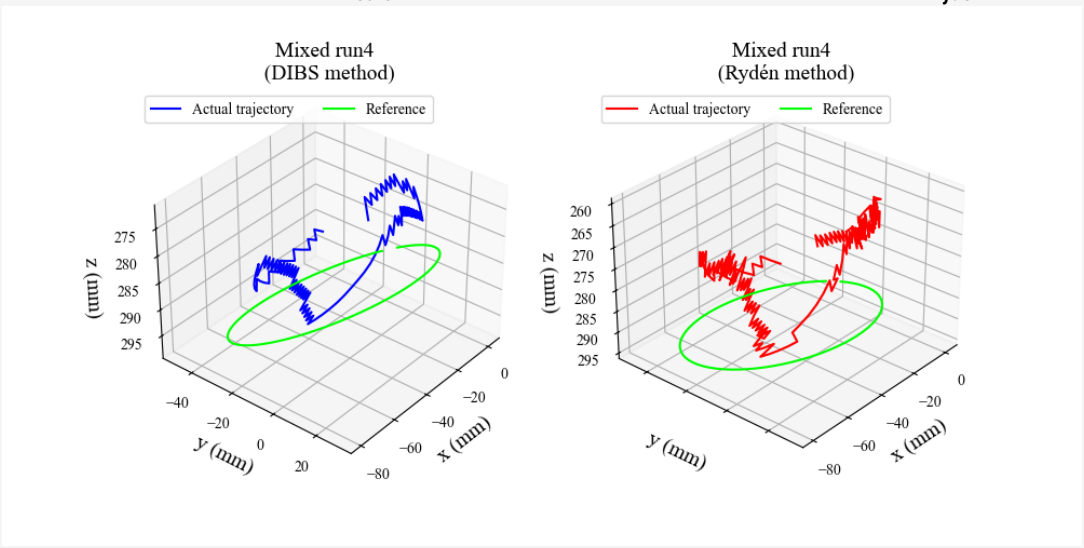
Figure 4.11: Illustration of when Ryden's method generates false guidance due to noisy point cloud in $Exp_{\text{Rydén}}$. Red spherical point clouds represent points in entrenched state. The white vector represents $\mathbf{v}_{\mathbf{pen}}$, and the violet vector represents $\mathbf{v}_{\mathbf{mov}}$. In frame 1 and 2, $\mathbf{v}_{\mathbf{pen}}$ does not reflect the actual surface normal direction, which leads to $\mathbf{v}_{\mathbf{mov}}$ drifting away from the reference trajectory.



(a) Trajectory in Exp_{ours}



(b) Trajectory in $Exp_{Rydén}$



(c) Comparison of the actual tracking trajectory in 3D

Figure 4.12: Illustration of dynamic tracking (Mixed run 4). Green, blue and red represent the reference trajectory, the actual trajectory in Exp_{ours} and in $Exp_{Rydén}$, respectively.

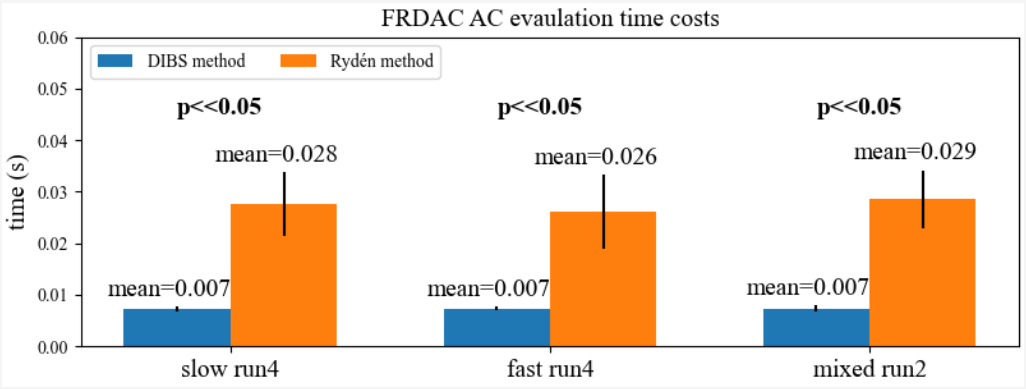
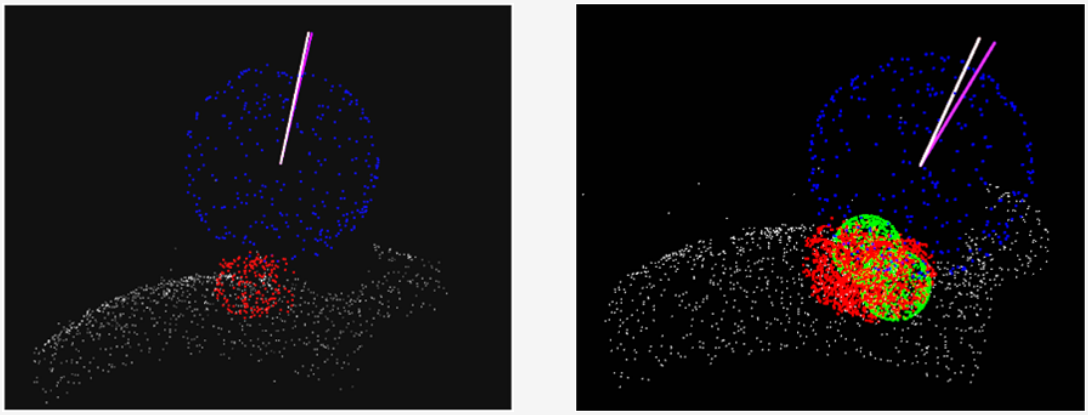


Figure 4.13: Comparison of AC evaluation time costs between Exp_{ours} and $Exp_{Rydén}$ in several runs.



(a) Case 1, AC evaluation time=0.0004s. **(b) Case 2, AC evaluation time=0.0644s.**

Figure 4.14: AC evaluation in $Exp_{\text{Rydén}}$. AC evaluation in $Exp_{\text{Rydén}}$ between the tool and the downsampled surface point cloud, with a size of 1,000. No surface points are within the detection range of the current HIP. Red and green point clouds represent surface points that are within the detection range of the current HIP.

4.5 Conclusion

In this study, the pipeline design for a dissipative FRDAC controller that utilises a depth-sensing camera to accommodate dynamic tissue deformation was proposed. An *a priori* phantom model is leveraged to register with a streamed point cloud on the deforming tissue surface, updating at interactive rates, thereby enabling an always current mesh-represented AC at a speed that allows interactive guidance within a clinical environment. *In vitro* experiments were conducted to verify the effectiveness of the proposed FRDAC pipeline in assisting a tele-operative trajectory tracking task implemented by a "virtual surgeon". The experimental results have indicated the capability of the proposed FRDAC controller to fulfil the task safety requirement at a millimetre level. Quantitative analysis of the advantage of the proposed mesh-represented FRDAC over the state-of-the-art, a sphere-represented FRDAC strategy was provided.

To facilitate pipeline implementation, certain assumptions were made when registering the pre-scanned aorta phantom model to the point cloud representing its pulsating surface during experiments. Although simulation results validate that affine registration suffices in the experimental setup, where only respiration movements are considered, it is still desirable to incorporate non-rigid registration into the pipeline in future studies to account for various scenarios of tissue deformation, such as local tool-tissue interactions. The increased computational costs incurred by non-rigid registration will hopefully be mitigated by the advent of more efficient computer vision algorithms and hardware support for accelerating computation.

During trajectory tracking tasks, it was prescribed that when the distance detected between the instrument and tissue surface falls within a safety threshold, an AC force will be generated. This builds upon the assumption that all areas of the tissue surface must be protected. However, in a more realistic surgical scenario, it is always at the discretion of surgeons to determine whether an area is forbidden or permissible. Therefore, to further reduce the mental workload of surgeons, an additional segmentation block should be incorporated into the pipeline design so that surgeons can be informed of the current forbidden regions and that the FRDAC implementation can be updated intra-operatively.

Lastly, as a proof of concept implementation, the human element was removed in this study. Future work will involve conducting user studies to examine the effectiveness of the proposed method in a real tele-operative surgical scenario, which will be presented in the following chapter.

Chapter 5

Pilot user study on FRDAC in tele-operative surgery

Following from the previous chapter, where the proposed mesh-represented FRDAC pipeline was evaluated in an automated manner assuming the presence of a "virtual" surgeon, this chapter focuses on evaluating the effectiveness of the FRDAC in a user-present tele-operation scenario. As a pilot user study, only the author, who has prior experience in the dVRK is involved. In the experiments, a tissue incision task was conducted in vitro by the user on a dynamically moving silicone aorta phantom, simulating periodic movements caused by respiration. The user was provided with visual cues and tasked with tele-operating an instrument to follow a pre-defined circular trajectory with the assistance of different FRDAC approaches. When the instrument was detected outside the circular region and within a predefined safety distance from the tissue surface, an AC force was generated and enforced via the built-in impedance controller. The tracking results demonstrate the effectiveness of the proposed FRDAC approach in maintaining a safety distance in a dynamic scenario compared to when no AC was provided to the user. The results also align with the previous findings in Chapter 4, showing that the mesh-represented FRDAC approach prioritises accuracy over a larger safety margin and can be implemented at a speed that supports interactive updates of tissue deformation. Limitations of the current study are discussed, and future studies are envisioned to evaluate the FRDAC pipeline in a more clinically relevant scenario.

5.1 Introduction

To verify the effectiveness of AC in a more clinically relevant scenario, user studies are essential. From the current literature, it is observed that both quantitative and qualitative approaches are commonly adopted to evaluate the effectiveness of AC. For instance, to assess the effectiveness of a tele-operated catheter robot equipped with haptic feedback for endovascular surgery, Dagniono *et al.*in [79] conducted an *in vitro* study. In this study, users were tasked with tele-operating the catheter robot inside a dynamic moving aortic arch phantom, without collisions with the inner wall of the phantom. Quantitative evaluation metrics included the distance maintained between the catheter tip and the endothelial wall, as well as task completion time. These metrics reflect the effectiveness of AC in ensuring task safety and implementation efficiency. Qualitative metrics were gathered through user questionnaires, where aspects such as the learning curve, level of comfort, ergonomic factors *etc.*were subjectively rated by users. This feedback provides developers with directions for future algorithm refinement. The necessity of both quantitative and qualitative metrics is universal for the development of both FRAC and GAC. Enayati *et al.*in [174] stated that the necessity stems from the ultimate goal of AC developments, which is to enhance task performance in the presence of a human operator. The inclusion of human elements introduces subjective variability in addition to implementation efficiency, which is typically evaluated in isolation within a simulated scenario. They mentioned that quantitative metrics, including the maximum force generated, speed, angular velocity *etc.*, depend on the specific application scenario. Similarly, the design subjective qualitative metrics, such as questionnaires and measures of cognitive load. also needs to vary depending on the users' experience levels.

The design of user studies can be classified based on the environment in which the experiments are conducted. There exist few studies where *ex vivo* experiments were conducted to evaluate AC performances. Rydén *et al.*in [60] validated that their FRDAC could protect penetration into the surface of a dynamic beating pig heart while maintaining a safety distance of 0.02m. However, due to the challenge of obtaining ethical approval to conduct animal trials, most studies evaluate AC methods through *in vitro* experiments, where a phantom is usually incorporated, and the experiments are designed to simulate a clinical procedure. Moccia *et al.*[82] designed experiments to evaluate the effectiveness of their AC in preventing tool collisions during a potential cauterisation task. In their experiments, users were tasked with tele-operating two da Vinci surgical instruments: one was held still at the centre of predefined circle, while the other one tracked the periphery of the circle across 270 degrees. To replicate a realistic surgical scenario, it is important to account for eventualities, such as dynamic tissue movements, image artifacts, occlusions etc., which are common in the operating theatre. To further facilitate algorithm validation, there also exists literature where user studies were conducted in a simulation environment. For instance, Leibrandt *et al.*in [51] validated their online AC generation algorithm through user experiments where users were required to manipulate a compliant robot that controls the movement of a virtual instrument

in a simulator that renders arthroscopy and neurosurgery. The adoption of a simulator enables researchers to conduct proof-of-concept studies more efficiently across various surgical procedures, while bypassing challenges that are ubiquitous in a real clinical context.

Another aspect that differentiates AC user studies is the hardware setup. Even when the same AC approach is adopted, the difficulty in having users perceive the guidance varies depending on the hardware setup. For an experimental setup where a haptic device is incorporated, such as the PHANToM™ Omni or Omega.x (Force Dimension Inc.), the generated AC force can be directly applied to the surgeon side and perceived by users. This usually applies to cases where the tele-operation setup is manually assembled, an example being [175], where a PHANToM™ Omni with 3 DOFs is paired to tele-operate a Kuka youBot with 5 DOFs. Although the haptic device provides active force feedback to users when an AC force is generated, addressing motion mapping between the two robots on each side can be challenging. This difficulty arises from the mismatch in the DOFs of each robot, which increases the mental workload of users during tele-operation. The challenge becomes even greater when users are required to perform teleoperation whilst observing the current scene through a camera view. Since hand-eye calibration is performed between the camera and the robot on the patient side, when the motion mapping between the robot on the surgeon and patient side is inaccurate, the movements that users observe from the camera are misaligned with their actual hand movements, leading to increased cognitive workload for users. On the other hand, commercially available tele-operative surgical robots offer the advantage of accurate motion mapping and downscaling between the surgeon and patient side. However, one of the biggest technical constraints of these robots is the lack of haptic feedback. As a result, when an AC force is generated, users on the surgeon side cannot directly sense the desired moving direction. Instead, the force can be passively perceived by uses through the built-in impedance controller, which increases the impedance along the direction opposite to the AC force.

Lastly, it is worth mentioning that most AC user studies focus on validating the efficacy of AC by comparing task performance with and without the adoption of AC in either static or dynamic situations. However, there is a lack of comparisons across different AC approaches. For example, although Marinho *et al.*in [77] mentioned that comparison studies were conducted between two sets of AC, they referred to testing two proximity query approaches under the same AC framework. It would be beneficial for researchers to conduct evaluations across different AC frameworks within the same application scenario. To this end, this pilot user study focuses on evaluating the effectiveness of the proposed FRDAC approach in a user-present dynamic tele-operation scenario on the first-generation dVRK. Comparative studies are conducted to validate the efficacy of the FRDAC and to compare it against other approaches.

5.2 Methods

5.2.1 AC generation

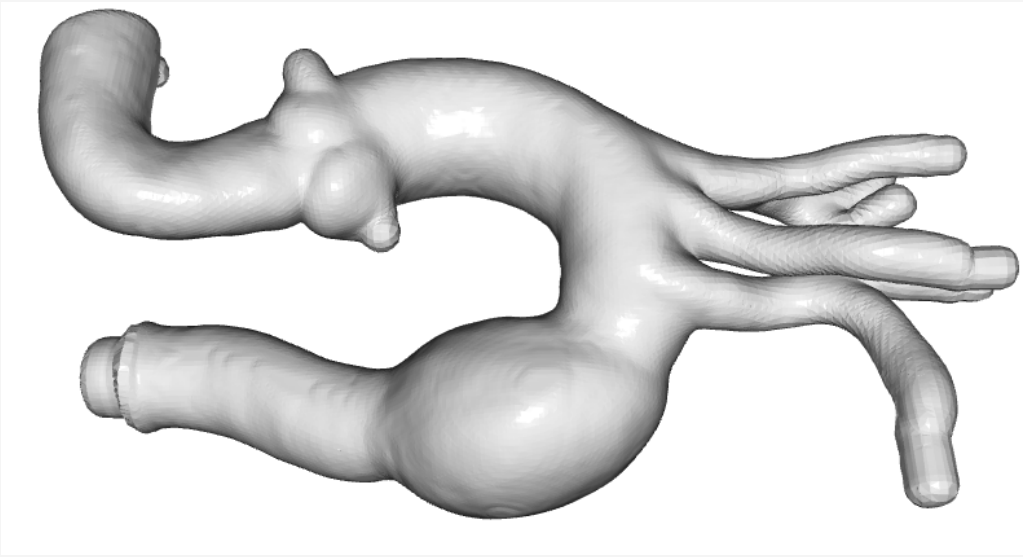
Following the standardised AC implementation pipeline, the first stage is to represent tissue surface that needs to be protected using geometry. Although simple geometries such as lines and points are the most common approaches, these representations fail to capture fine details of surface features. On the other hand, more complex geometry primitives, such as triangle meshes, can describe surface features in greater detail, but whenever deformation occurs, these meshes need to be updated, which demands high computational costs when fine mesh representations are adopted, and thereby affects the level of computational complexity of the following implementation procedures.

To better describe surface features, triangular meshes were adopted in this chapter, and the same AC generation strategy was adopted as described in Chapter.4. To facilitate the registration process, two assumptions were made. First, it was assumed that an affine transformation matrix suffices to describe deformation caused by respiration, leading to the selection the TEASER++ algorithm [168]. Second, to accelerate TEASER++ registration, it was assumed that finding FPFH features and establishing correspondences only need to be conducted once at the initial round, and then the feature correspondences remain unchanged during respiratory movements. Both assumptions were justified through simulation, as presented in Subsection.4.2.1. The expiration and inspiration aorta model are shown in Figure.5.1.

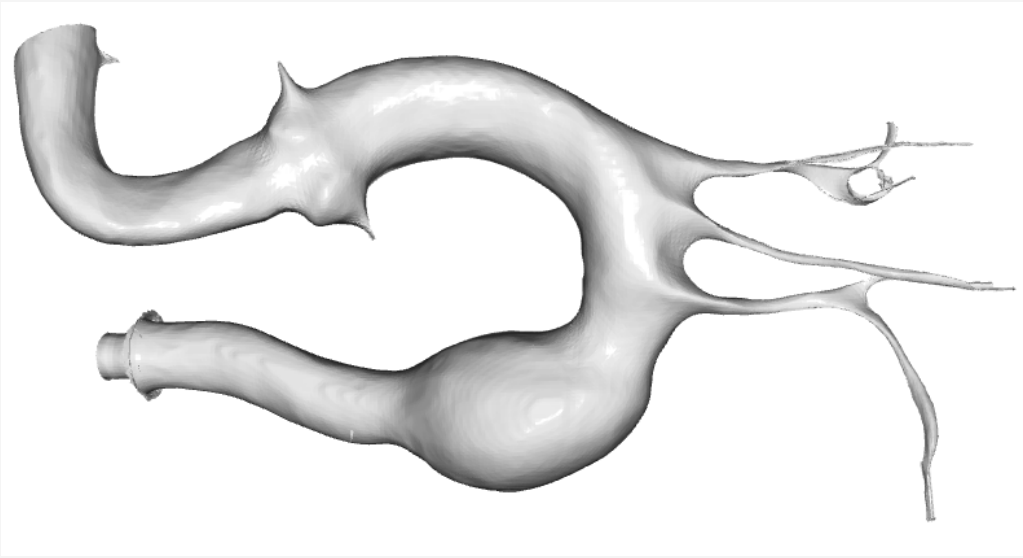
5.2.2 AC evaluation

Following the AC generation, AC evaluation is required to determine whether violations of safety regions have already occurred. This process usually involves proximity query between the instrument and tissue surface to be protected. For complex geometry representations, the time cost for AC evaluation is significant. In this study, the DIBS algorithm was adopted for AC evaluation between the surgical instrument and a finely represented phantom surface in a dynamic scenario. Details of the algorithm implementation can be found in [62], and a summary of the DIBS algorithm is presented below.

In Figure.5.2, it is shown that Boundary Volume (BV), represented as spheres, are created around the phantom surface. The instrument is depicted as a cylinder, referred to as the CTG. The proximity query is initially conducted between the CTG and all BV on the tissue surface, before localising the closest point pairs between the instrument and the tissue surface. The stretch factor σ allows modifications to the radius of BV , ensuring that polygons that belong to the same BV prior to tissue deformation still belong to the same BV after deformation. This eliminates the need for BV reconstruction and accelerates the AC evaluation procedure.



(a) Expiration aorta model created in Blender



(b) Inspiration aorta model created in Blender

Figure 5.1: Expiration and inspiration aorta model created in Blender[170]

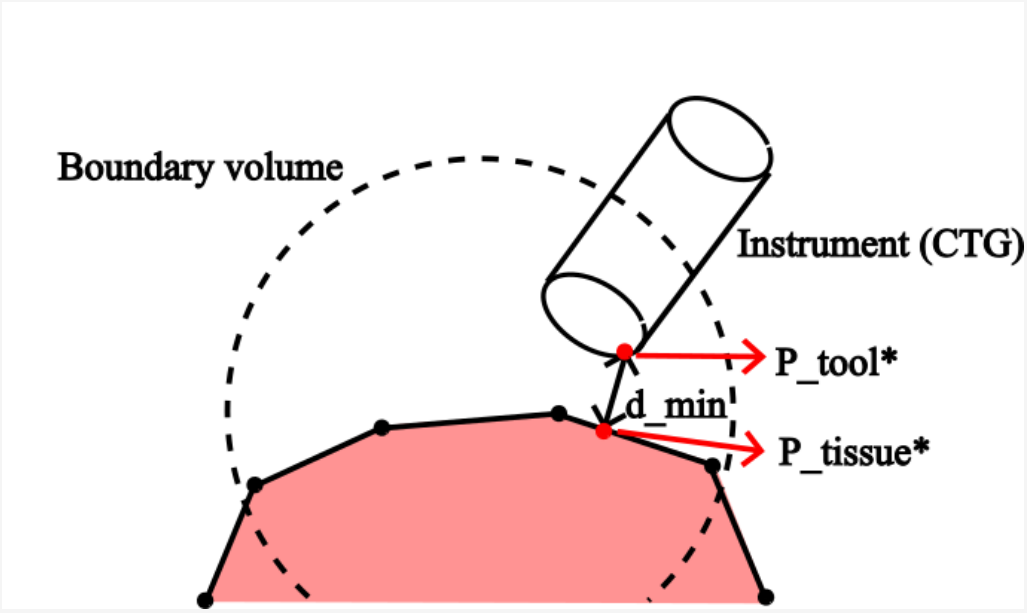


Figure 5.2: Illustration of AC evaluation using DIBS

5.2.3 AC enforcement

5.2.3.1 Energy redirection approach

When a violation of safety regions is detected, an AC force will be generated to inform users of the current situation and guide them to move instruments out of the safety regions. To maintain energy dissipativity of the entire system, the dissipative controller developed in [68] is incorporated in the overall pipeline design. The controller is energy-dissipative because of an energy redirection approach.

The elasto-plastic friction model describes that the total displacement $\mathbf{x}(t)$ consists of recoverable elastic component $\mathbf{z}(t)$ and permanent plastic component $\mathbf{w}(t)$. The friction force generated $\mathbf{f}_f(t)$ in 3D at time instant t is calculated as

$$\mathbf{f}_f(t) = \Sigma_0 \mathbf{z}(t) + \Sigma_1 \dot{\mathbf{z}}(t) + \Sigma_2 \dot{\mathbf{x}}(t) \tag{5.1}$$

where $\Sigma_0, \Sigma_1, \Sigma_2$ are all 3×3 diagonal matrices that store gains along translational DOFs. Based on the algorithm in [68], the energy redirection approach relies on the generation of anisotropic friction forces. $\mathbf{z}(t)$ is calculated based on the projection of elastic displacement candidate $\mathbf{z_c}(t)$ onto a conical set $C(t) \subset \mathbb{R}^3$. A graphical illustration is presented in Figure.5.3.

$$C(t) = \{\mathbf{w} : \mathbf{w} \in \mathbb{R}^3, \Theta(\mathbf{w}, \mathbf{p}(t)) \leq \theta, ||\mathbf{w}|| \leq z_{\text{css}}(t)\} \tag{5.2}$$

where θ is the apex angle of the cone, and $\mathbf{p}(t)$ is the vector that points from the current target position to the tool tip position.

The candidate for elastic displacement vector $\mathbf{z_c}(t)$ is expressed as

$$\mathbf{z_c}(t) = \mathbf{z}(t-1) + \Delta\mathbf{x}(t) \tag{5.3}$$

The actual elastic displacement vector $\mathbf{z}(t)$ is the projection of $\mathbf{z_c}(t)$ onto the conical set $C(t)$. Mathematically, it can be expressed as follows

$$\mathbf{z}(t) = \underset{\mathbf{w}\in C(t)}{\text{argmin}} ||\mathbf{w} - \mathbf{z_c}(t)|| \tag{5.4}$$

$$\mathbf{z}(t) = \begin{cases} \mathbf{z_c}(t) & \Theta(\mathbf{z_c}(t), \mathbf{p}(t)) < \theta \wedge ||\mathbf{z_c}(t)|| \leq \mathsf{z}_{\mathsf{css}}(t) \\ \mathsf{z}_{\mathsf{css}}(t)\hat{\mathbf{z}_c}(t) & \Theta(\mathbf{z_c}(t), \mathbf{p}(t)) < \theta \wedge ||\mathbf{z_c}(t)|| > \mathsf{z}_{\mathsf{css}}(t) \\ \tilde{\mathsf{z}}_{\mathsf{c}}(t)\hat{\mathbf{y}} & \text{otherwise} \end{cases} \tag{5.5}$$

$$\tilde{z_c}(t) = \begin{cases} 0 & \mathbf{z_c}(t) \cdot \hat{\mathbf{y}} \leq 0 \\ \mathbf{z_c}(t) \cdot \hat{\mathbf{y}} & 0 < \mathbf{z_c}(t) \cdot \hat{\mathbf{y}} < z_{css}(t) \\ \mathsf{z}_{\mathsf{css}}(t) & \text{otherwise} \end{cases} \tag{5.6}$$

where $\hat{\mathbf{y}}$ is unit vector that defines the intersection between cone $C(t)$ the plane formed by $\mathbf{z_c}(t)$ and $\mathbf{p}(t)$.

It is also worth mentioning that, based on different AC generation approaches, the expressions for $\mathbf{x}(t)$ and $\mathbf{p}(t)$ change accordingly. In this study, $P_{tip}(t)$ refers to the current tip position of the instrument, and $P_{tgt}(t)$ refers to the current target position on the reference trajectory. $\Delta\mathbf{x}(t)$ and $\mathbf{p}(t)$ are defined as follows

$$\Delta\mathbf{x}(t) = \frac{P_{tgt}(t) - P_{tip}(t)}{||P_{tgt}(t) - P_{tip}(t)||} \tag{5.7}$$

$$\mathbf{p}(t) = \frac{P^*_{tool} - P^*_{tissue}}{\mathsf{d}_{\mathsf{min}}} \tag{5.8}$$

According to Rydén's algorithm [60], the instrument position is denoted as HIP, P_{HIP}, and the proxy point, P_{proxy}, denotes the permissible position of the instrument tip. If there is no violation of the safety regions, P_{proxy} coincides with P_{HIP}. Otherwise, P_{proxy} denotes the position to which P_{HIP} should retract. In this case, the definitions of $\Delta\mathbf{x}(t)$ and $\mathbf{p}(t)$ change as follows

$$\Delta\mathbf{x}(t) = \frac{P_{tgt}(t) - P_{HIP}(t)}{||P_{tgt}(t) - P_{HIP}(t)||} \tag{5.9}$$

$$\mathbf{p}(t) = \frac{P_{HIP} - P_{proxy}}{||P_{HIP} - P_{proxy}||} \tag{5.10}$$

Although the dissipative controller can be applied to all 6-DOFs, this study implements the FRDAC pipeline through the built-in impedance controller of the dVRK, constraining only translational movements. Therefore, the development of the FRDAC pipeline for tele-operative surgery is limited to translational movements, while constraints on rotational components are left for future study.

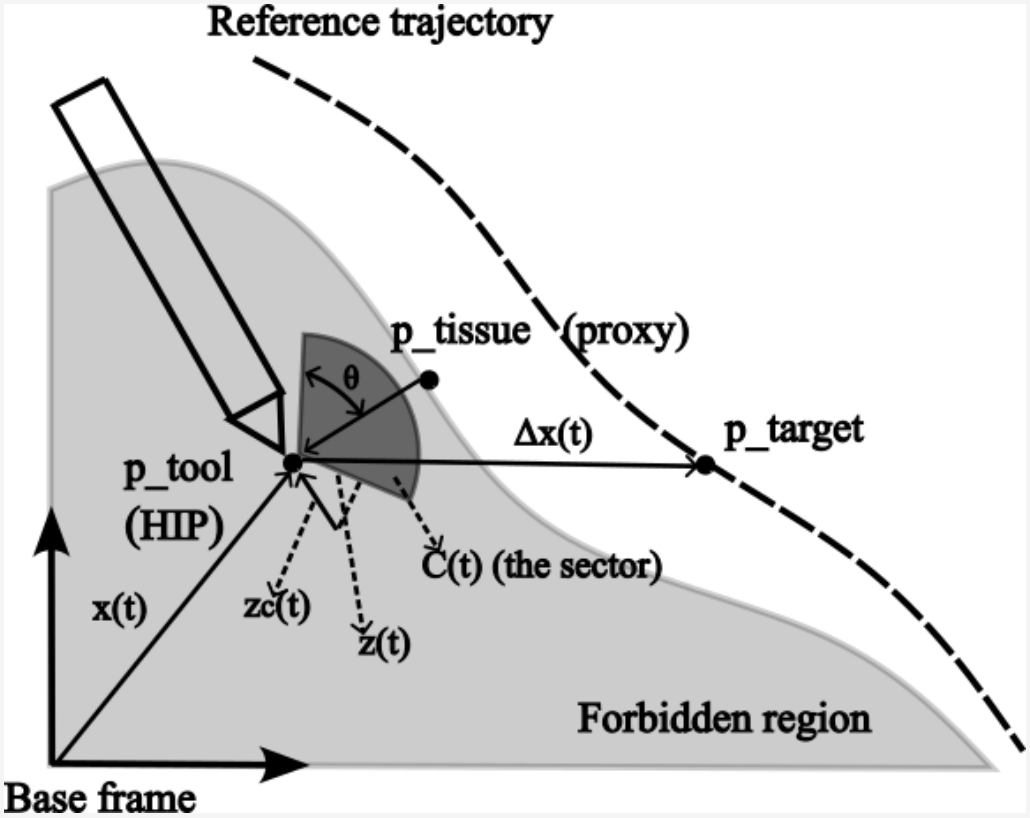


Figure 5.3: Illustration of the dissipative AC controller

5.2.3.2 Mapping between SSMs and PSMs

The first-generation dVRK emulates the commercial da Vinci system in the teleoperation mode. The SSMs consist of 7 DOFs, which are mapped to the joint motions of PSMs. The orientation of the SSMs relative to users' field of view is always synchronised with that of the PSMs relative to the camera frame. In this way, the direction in which the instrument moves in the view of users is always aligned with their hand movements. All the joints on the SSMs and PSMs are equipped with encoders for position reading, and the dVRK system enables itself to send position commands to move robot arms to a desired pose. In the teleoperation mode, the movement of the SSMs is mapped to its paired PSMs with a scaling factor. The mapping between the SSMs and PSMs

is presented in Figure.5.4. Prior to the movement of the SSMs, the system measures the current position and orientation of the SSMs relative to the base frame. After the movement, the orientation and position of the SSMs are measured. The PSMs orientation is then set to match that of the SSMs. Finally, the translational movement of the SSMs is downscaled and sent to the PSMs.

Algorithm Motion mapping between the SSM and PSM

Require: SSM initial position P_{SSM}^{init}, PSM initial position P_{PSM}^{init}

while tele-opeartion **do**

$P_{SSM} \leftarrow P_{SSM}$ ▷ Get SSM position

$\mathbf{T}_{SSM} \leftarrow \mathbf{T}_{SSM}$ ▷ Get SSM orientation

$\mathbf{T}_{PSM} \leftarrow \mathbf{T}_{SSM}$ ▷ Align SSM and PSM orientation

$\mathbf{t}_{SSM} \leftarrow P_{SSM} - P_{SSM}^{init}$ ▷ Find SSM translation

$P_{PSM}^{tgt} \leftarrow scale \cdot \mathbf{t}_{SSM} + P_{PSM}^{init}$ ▷ Set PSM target position

end while

Figure 5.4: Mapping between the SSMs and PSMs in tele-operation mode

Under this mapping mechanism, the moving direction of the PSMs relative to the camera frame is always aligned with the moving direction of the SSMs when P_{SSM}^{init} and P_{PSM}^{init} are not reset. Therefore, in the event of safety region violations, the direction of the AC force $\mathbf{f}_f(t)_{PSM}$ on the PSMs side can be mapped to the SSMs side as $\mathbf{f}_f(t)_{SSM}$, where $\hat{\mathbf{f}}_f(t)_{PSM} = \hat{\mathbf{f}}_f(t)_{MTM}$. On the SSMs side, movements opposite to the direction of $\mathbf{f}_f(t)_{SSM}$ are prohibited via the built-in impedance controller.

5.2.3.3 Impedance controller in the first-generation dVRK

The impedance controller of the dVRK regulates movements on the SSMs side along three translational directions. The implementation of the impedance controller is through the dVRK built-in ROS topic **"cisst_msgs::prmCartesianImpedanceGains"**. The ROS topic controls the impedance gains along the x, y and z directions in Cartesian space. Along each of the x, y and z axes, the impedance gain is enforced separately for both positive and negative directions. When the impedance gain in a given direction is increased, movement along that direction becomes impeded. When an AC force $\mathbf{f}_f(t)_{SSM}$ is generated, impedance gains along the x, y and z directions are increased proportionately according to $\mathbf{f}_f(t)_{SSM}$. In this way, when users attempt to move in the opposite direction of $\mathbf{f}_f(t)_{SSM}$, resistance will be sensed by users, thereby indirectly guiding them to move the instrument out of the forbidden region.

5.3 Experiments

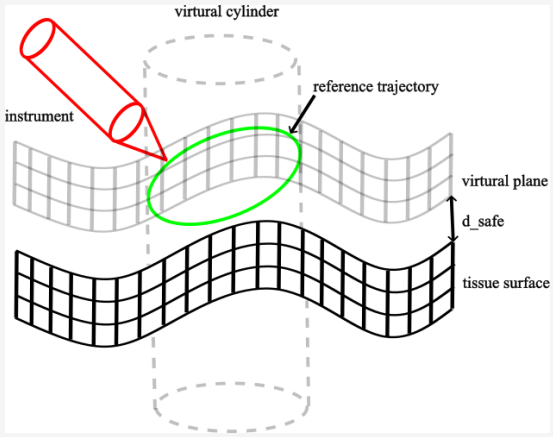
5.3.1 Experiments design

Following from the previous chapter where *in vitro* experiments were conducted in an automated manner under the assumption of a "virtual" surgeon who would move the instrument outside forbidden regions along the direction of the AC force, this chapter focuses on testing the FRDAC pipeline in a user-present scenario. Instead of adopting the hybrid force-position controller to emulate retraction movements by a perfect "virtual" surgeon, in the user study, when a violation of the safety regions is detected, the impedance controller will adjust impedance gains according to the generated AC force. It is then up to the user's discretion to respond to the change of impedance during manipulation. As a pilot user study, only the author, who has previous experience in operating the dVRK, participated as a user. This is because, due to hardware limitations and the immaturity of other essential technical modules, such as 3D reconstruction from stereo images, and online segmentation of forbidden regions *etc.*, the experiment design is still in a rudimentary testing stage.

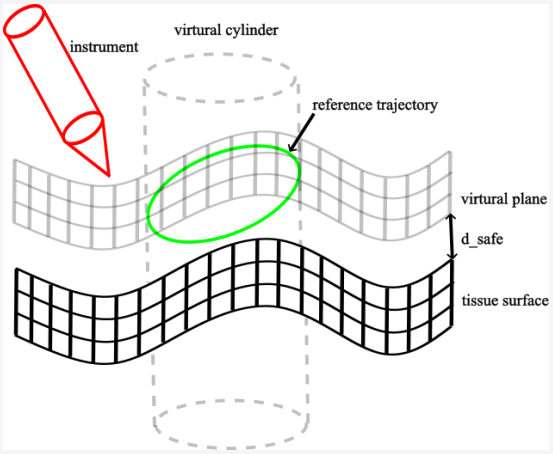
The pilot user study simulates a tissue incision procedure, using an aorta phantom to represent the organ being incised. To simulate the pulsating movements caused by respiratory motions, the aorta phantom is connected to a water pump that regulates the water flow into the phantom, thereby controlling the level of deformation. In addition to the aorta phantom, the experimental setup consists of a RGBD camera, the Acusense 3D (Revopoint 3D Inc®) that captures surface point cloud at the rate of 10 Hz, with a resolution of 0.5 mm at a working distance of 500 mm.

The simulated tissue incision task involves the use of a single instrument (Forceps 40036E, Intuitive Inc®) tele-operated with one hand by the user. The task requires the user to move the instrument along a predefined cutting trajectory without accidentally damaging surrounding tissue area as the organ undergoes dynamic movements. To avoid damaging the silicone aorta phantom, the reference trajectory was set as a circular trajectory that sits above the phantom surface across various anatomical regions. The reference trajectory is updated as the phantom undergoes deformation, and it is assumed that only the tissue surface that is outside the cylindrical area formed by the reference trajectory needs to be protected. When the instrument is detected to be located outside the cylinder and that the minimum distance between the instrument and tissue surface is smaller than a predefined safety distance d_{safe}, the AC controller will be triggered. A graphic illustration is presented in Figure.5.5.

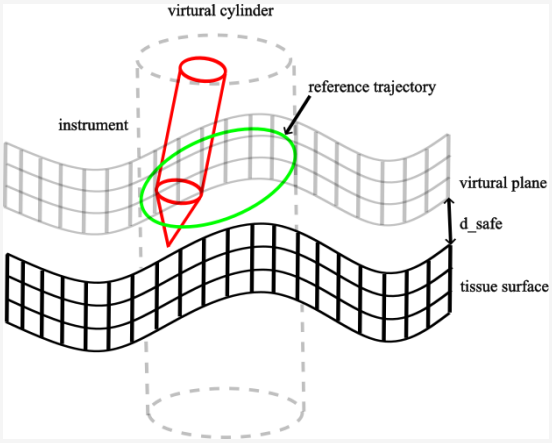
Prior to the experiments, hand-eye calibration was performed between the Acusense camera and PSM1. During trajectory tracking, the reference circular trajectory is continuously updated and overlaid onto the colour image of the current surgical scene. Due to technical limitations, the real-time image captured with the overlaid reference trajectory cannot be streamed to the surgeon side



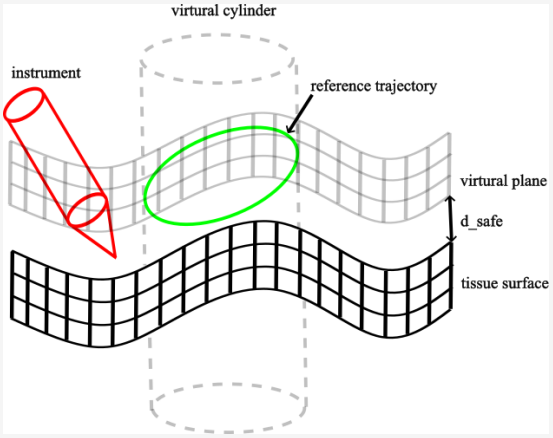
(a) $d_{min} > d_{safe}$, tip is inside the cylinder, FRDAC not in action



(b) $d_{min} > d_{safe}$, tip is outside the cylinder, FRDAC not in action



(c) $d_{min} < d_{safe}$, tip is inside the cylinder. FRDAC not in action



(d) $d_{min} < d_{safe}$, tip is outside the cylinder. FRDAC in action

Figure 5.5: Illustration of when FRDAC is triggered on during trajectory tracking.

console; instead, it is displayed on a monitor next to the user. Altogether, there are 72 points on the reference trajectory, and as the instrument is being held to follow the updated trajectory, both the current instrument tip and the reference target point are back projected on the frame in blue and red, respectively.

To evaluate the effectiveness of the proposed FRDAC pipeline, experiments were conducted in both static and dynamic scenarios using different AC strategies across five repetitive trials. In both static and dynamic scenarios, freehand tracking was conducted as a baseline contrast group. Experiments conducted freehandedly, using the FRDAC approach proposed in this study, and using Rydén's approach are represented as $\boldsymbol{Exp}_{\text{free,k}}$, $\boldsymbol{Exp}_{\text{ours,k}}$, and $\boldsymbol{Exp}_{\text{Rydén,k}}$, respectively, where $k \in \{1, 2, 3, 4, 5\}$ refers to the k^{th} trial. In both static and dynamic scenarios, five $\boldsymbol{Exp}_{\text{free}}$ trials were conducted first, followed by five $\boldsymbol{Exp}_{\text{Rydén}}$ trials, and concluded by five $\boldsymbol{Exp}_{\text{ours}}$ trials.

5.3.2 Experimental setup

The experimental setup is shown in Figure.5.6, consisting of the Acusense camera, the PSM1 onto which the instrument is attached, and the silicone aorta phantom that is connected to a water pump. In this study, the Surgeon Side Manipulator Right (SSMR) is paired with PSM1 for teleoperation. Prior to the tele-operation, hand-eye calibration was performed once between the Acusense camera and the base frame of the PSM1.

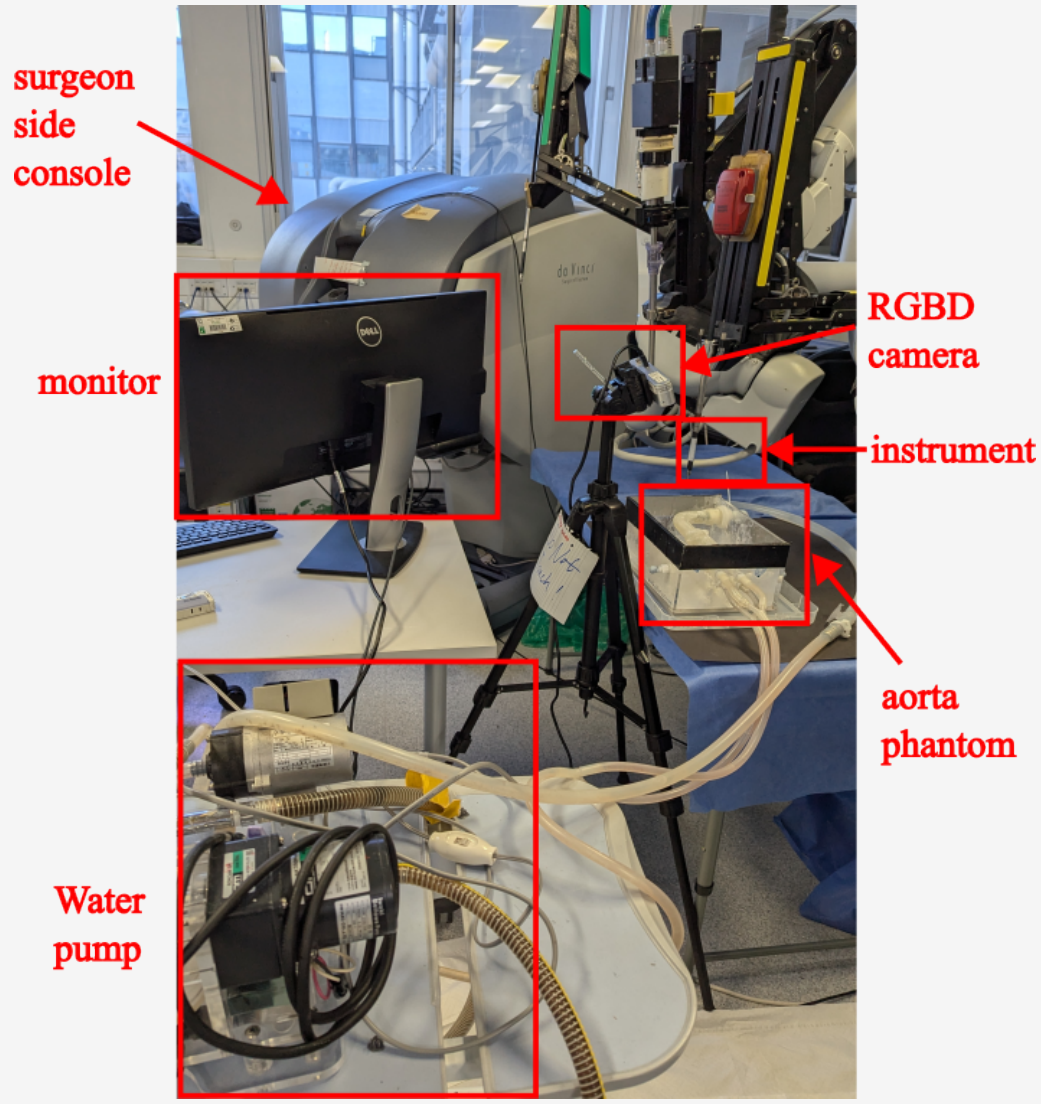


Figure 5.6: Experimental setup in the user-present experiments in Chapter 5.

5.4 Results and discussions

5.4.1 Static trajectory tracking results

The same evaluation criteria used in Chapter 4 are applied in this study. Unlike the static tracking experiments in Chapter 4, where only a single trial was conducted due to the predicted repetitive tracking performance from the automated process, the pilot user involved five trials with different FRDAC approaches to minimise potential bias introduced by human factors.

During each freehand trajectory tracking trial, the average distance between the instrument tip and updated target point on the reference trajectory is defined as $d_{traj} = \frac{1}{N}\sum_{i=1}^{N}||P_i - Q_i||$, where P_i and Q_i denote the actual tool tip position at the i^{th} instance and its corresponding target point on the updated reference trajectory, respectively. The average minimum distance from the phantom surface is defined as e minimum distance returned by the the DIBS query at the i^{th} instance. $d_{phantom} = \frac{1}{N}\sum_{i=1}^{N}\min\langle P_i, Cloud^i_{tissue}\rangle$, where $Cloud^i_{tissue}$ represents the downsampled tissue point cloud at the i^{th} instance. The definition of d_{traj} also applies to all trials in $\boldsymbol{Exp}_{ours}$ and $\boldsymbol{Exp}_{Rydén}$. Although the definition for $d_{phantom}$ applies to $\boldsymbol{Exp}_{Rydén}$, in $d_{phantom} = \frac{1}{N}\sum_{i=1}^{N} d_{min,i}$, where $d_{min,i}$ denotes the minimum distance returned by the the DIBS query at the i^{th} instance.

Static trajectory tracking results are presented in Figure.5.7, where the average $d_{phantom}$ and d_{traj} across all five trials are shown as bars. Figure.5.7 illustrates that in $\boldsymbol{Exp}_{free}$, $\boldsymbol{Exp}_{ours}$ and $\boldsymbol{Exp}_{Rydén}$, $d_{phantom} > d_{safe}$, suggesting that in a user-present static scenario, safety requirements can be maintained even without the assistance of FRDAC. Additionally, both $d_{phantom}$ and d_{traj} in $\boldsymbol{Exp}_{ours}$ are smaller than those in $\boldsymbol{Exp}_{Rydén}$, indicating that the mesh-represented FRDAC approach allows the instrument to maintain a closer distance to the static phantom surface, provided that the distance remains beyond the safety margin. This suggests that the FRDAC approach proposed in this study prioritised tracking accuracy over maintaining a larger safety margin, which aligns with the finding in Chapter 4. It is also noted that with the assistance of either FRDAC approach, $d_{phantom}$ and d_{traj} become smaller compared to when no AC assistance is provided. This demonstrates that the effectiveness of AC in improving tracking task performance whilst maintaining task safety.

5.4.2 Dynamic trajectory tracking results

During dynamic tracking experiments, the level of deformation is controlled by the water pump valve, with "fast" deformation applied, as defined in Chapter 4. Dynamic trajectory tracking results are presented in Figure.5.8.

Compared to the static scenario, the average $d_{phantom}$ in $\boldsymbol{Exp}_{free}$ has dropped significantly from 30.39 mm to 19.26 mm, slightly below d_{safe}. This indicates that, in a dynamic scenario without the assistance of FRDAC, it is difficult for the user to gauge the distance between the instrument and the moving tissue surface based on visual information alone, indirectly jeopardising task safety. On

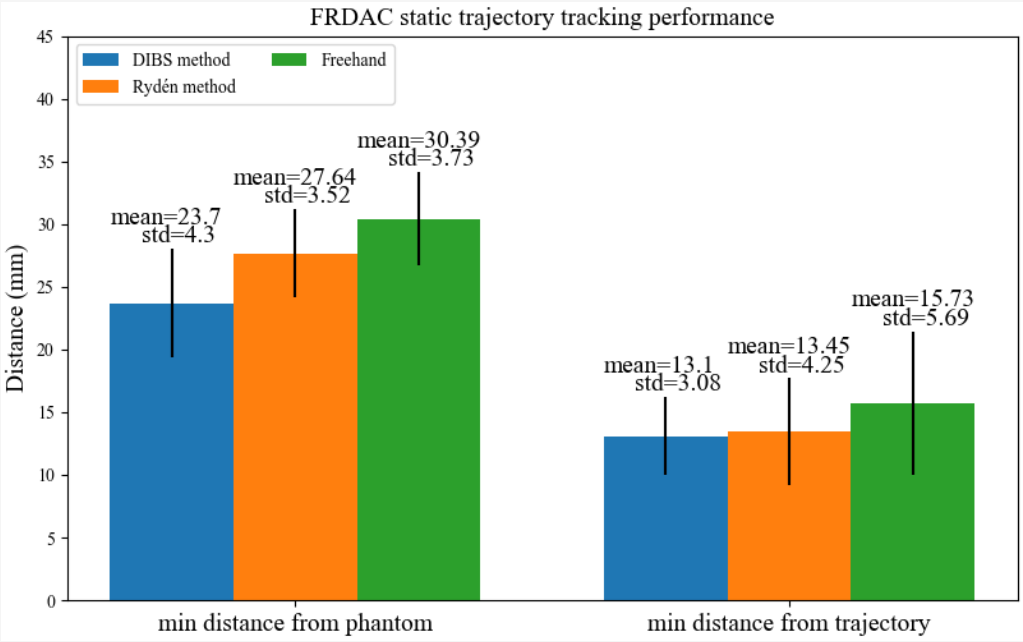


Figure 5.7: Static trajectory tracking results in Chapter 5.

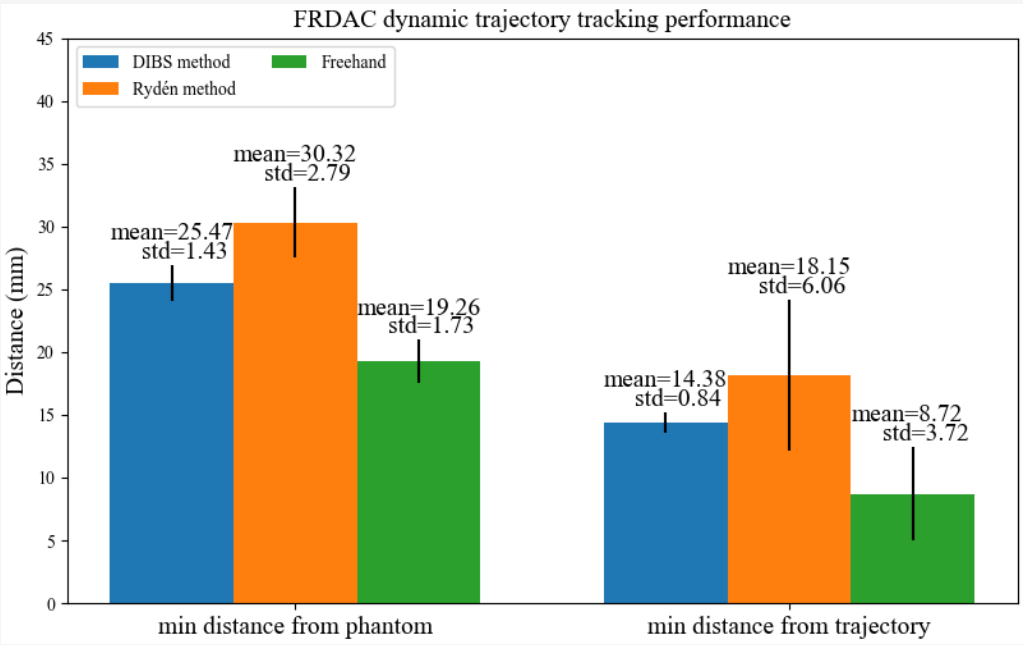


Figure 5.8: Dynamic trajectory tracking results in Chapter 5.

the contrary, $d_{phantom}$ in both $\boldsymbol{Exp}_{ours}$ and $\boldsymbol{Exp}_{Rydén}$ are larger than d_{safe}, suggesting the effectiveness of both FRDAC in a dynamic scenario. Both $d_{phantom}$ and d_{traj} in $\boldsymbol{Exp}_{ours}$ are smaller than those in $\boldsymbol{Exp}_{Rydén}$, confirming the previous finding that the FRDAC approach proposed in this study prioritised tracking accuracy over maintaining a larger safety margin. It is hypothesised that the FRDAC in $\boldsymbol{Exp}_{ours}$ permits a smaller safety margin due to the finer mesh representation and point-to-plane proximity query, making it less susceptible to noisy point clouds that can trigger false alarms for

AC generation. Analysis of Variance (ANOVA) tests were also conducted to compare the average $d_{phantom}$ and d_{traj} in different scenarios with the assistance of different FRDAC approaches, and p values are presented in Table.5.1. It shows that there is no statistical significance among $\boldsymbol{Exp}_{ours}$, $\boldsymbol{Exp}_{Rydén}$, and $\boldsymbol{Exp}_{free}$ during static tracking. Compared to the static tracking results in Chapter 4, it is suspected that, in a static scenario, the human element compensates for discrepancies in the ability to maintain task safety across different AC approaches.

category	relationship	p value for d_{traj}	p value for $d_{phantom}$
Static	(freehand, ours, Rydén)	$p = 0.75$	$p = 0.40$
Dynamic	(freehand, ours, Rydén)	$p = 0.042$	$p << 0.05$

Table 5.1: P value of one-way ANOVA tests for tracking experiments in Chapter 5. $p << 0.05$ represents that $p < 5e - 3$.

Figure.5.9 and 5.10 present the overlay of the reference circular trajectory on the camera frame, at frame 42 and frame 61, respectively. The difference between Figure.5.9b and 5.10bindicates the change in the affine transformation matrix at two time instances. For all experimental trials, 72 target points on the reference trajectory were updated sequentially at each camera frame. Consequently, all experimental trials took the amount of same time to complete. Although in Chapter 4 it was noted that there are times in $\boldsymbol{Exp}_{Rydén}$ when the instrument gets stuck in a certain region due to the interference from noisy point clouds, no such situation was observed in this pilot user study. This suggests that humans can compensate for erroneous AC guidance in a teleoperation scenario, although at the sacrifice of comfort.

5.4.3 Discussion

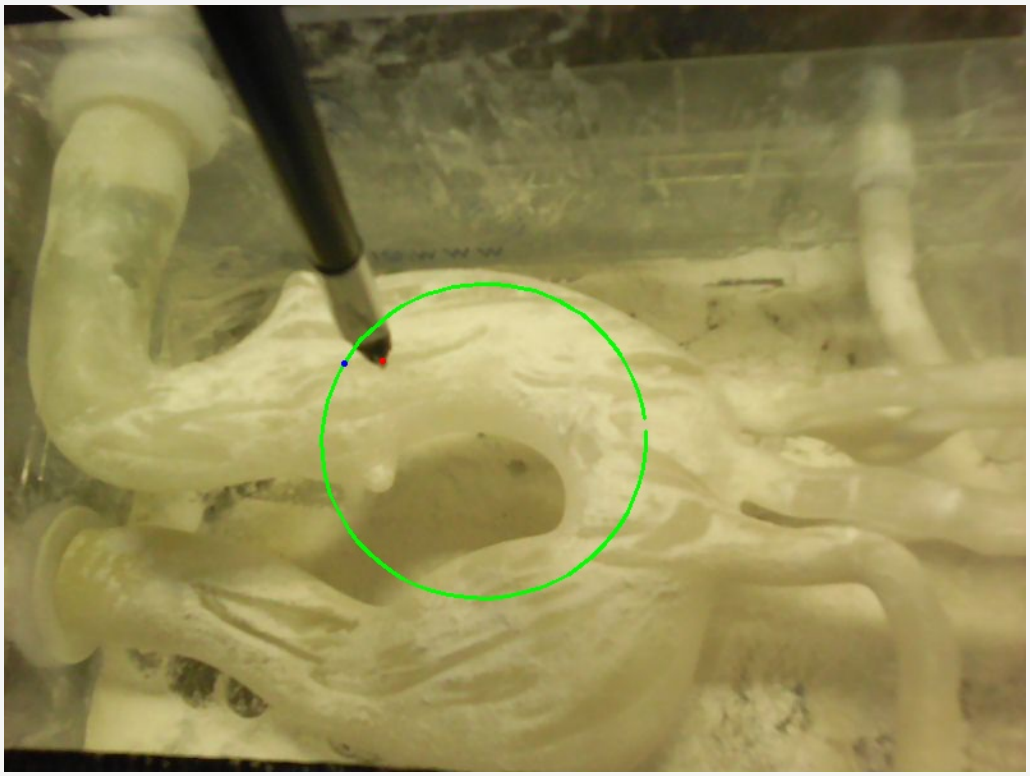
Although the results of the pilot user study mostly align with those of Chapter 4, affirming the effectiveness of the proposed FRDAC pipeline in assisting surgical tasks in a user-present teleoperation scenario, other factors still need to be taken into consideration for the development of a more mature approach that can be seamlessly incorporated into clinical practice.

To facilitate the AC generation process, a RGBD camera was introduced into the experimental setup, directly streaming the point cloud of the dynamic tissue surface. However, in a more clinically realistic scenario, only a pair of stereoscopic endoscopic camera cameras would be available, capturing the same surgical scene from two perspectives. Therefore, the setup requires an additional block for 3D reconstruction from stereo images. The accuracy and speed at which surface points are be generated will have significant impact on the overall performance of the FRDAC pipeline.

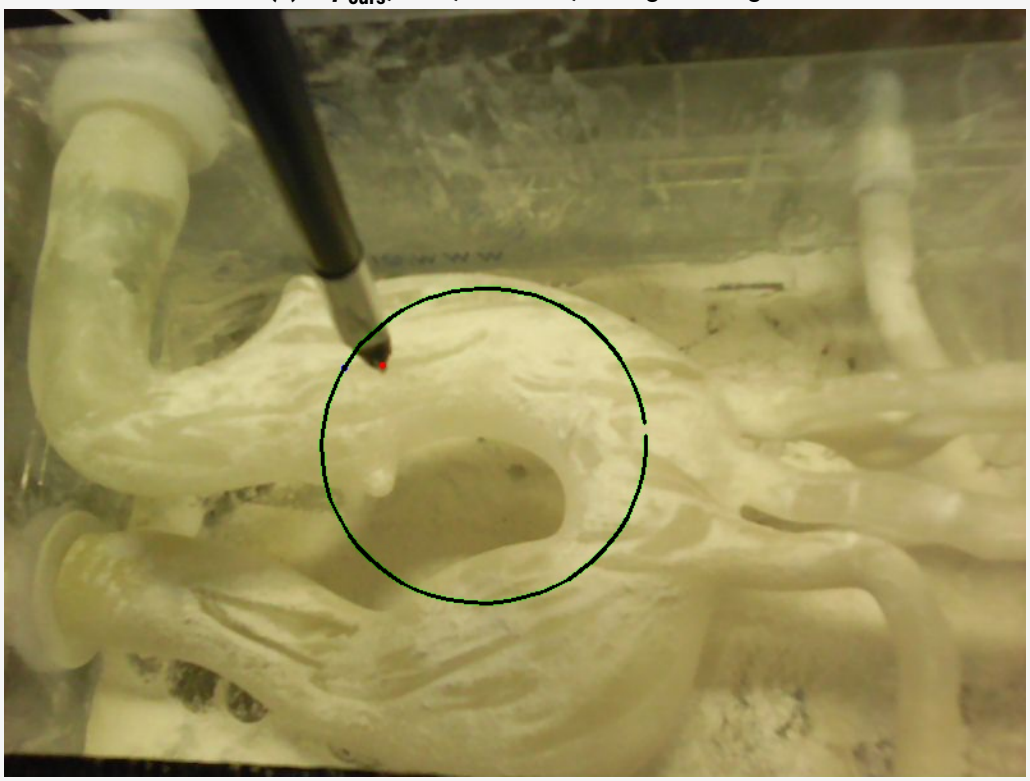
In this pilot user study, only the author, who has previous experience in the dVRK, was involved. To obtain more neutral and general feedback on the assistance provided FRDAC, more users with different levels of expertise in tele-operation should be involved. In addition to accuracy, the level

of comfort that users receive AC guidance should also be considered. The dissipative AC force was enforced through the built-in impedance controller, which can only passively inform users of the desired moving direction. It would be worth investigating how the proposed FRDAC perform on a tele-operative surgical robot setup that enables active force feedback, to examine whether the generated dissipative force could impair system safety.

Both this pilot user study and Chapter 4 conclude that, compared to Rydén's approach, the mesh-represented FRDAC approach proposed in this study favours accuracy over task safety. However, the experiments conducted so far have been limited to an incision procedure on a virtual surface that changes according to the dynamic movements of a phantom. Although a study that allows direct incision on a dynamic tissue surface would provide a more straightforward way to visualise the differences between FRDAC approaches, there are factors that would impact the evaluation metrics. First, the deformation the phantom undergoes resembles respiratory motions, and it is assumed that affine registration is sufficient to simply non-rigid registration. However, instrument tracking in contact with a dynamic tissue surface inevitably results in tool-tissue interaction, which cannot be accounted for by affine registration, thus affecting tracking performance. To compensate for that, non-rigid registration algorithms should be incorporated into the AC generation block. The challenge remains that the computational cost of non-rigid registration algorithms is high, which delays the entire FRDAC pipeline. Second, during surface tracking experiments, obtaining accurate tool tip position is crucial. For a cable-driven robot like the first-generation dVRK, it requires calibration on encoder readings on-the-fly. Therefore, an additional kinematics calibration block should be incorporated to the FRDAC pipeline. Third, there also exists limitations in the experimental design. In both static and dynamic trajectory experiments, repetitive trials were conducted sequentially in the order of $\boldsymbol{Exp}_{\text{free}}$, $\boldsymbol{Exp}_{\text{Rydén}}$, and $\boldsymbol{Exp}_{\text{ours}}$. It is likely that the user may develop better operating skills over extended period of training, which could affect the evaluation of different FRDAC strategies. Therefore, a better approach is to conduct trials in a randomised order. In all experiments, the surgical scene was captured by a fixed camera and then projected onto a monitor for the user to observe, which is equivalent to a monocular setup. However, this introduces more challenges for the user in estimating depth, potentially leading to worse performance in $\boldsymbol{Exp}_{\text{free}}$. Considering that the orientation of the plane on which surgical tasks are performed may also influence the ease of execution without the assistance of AC, future experiments will include surgical tasks that involve changing camera orientations intra-operatively.

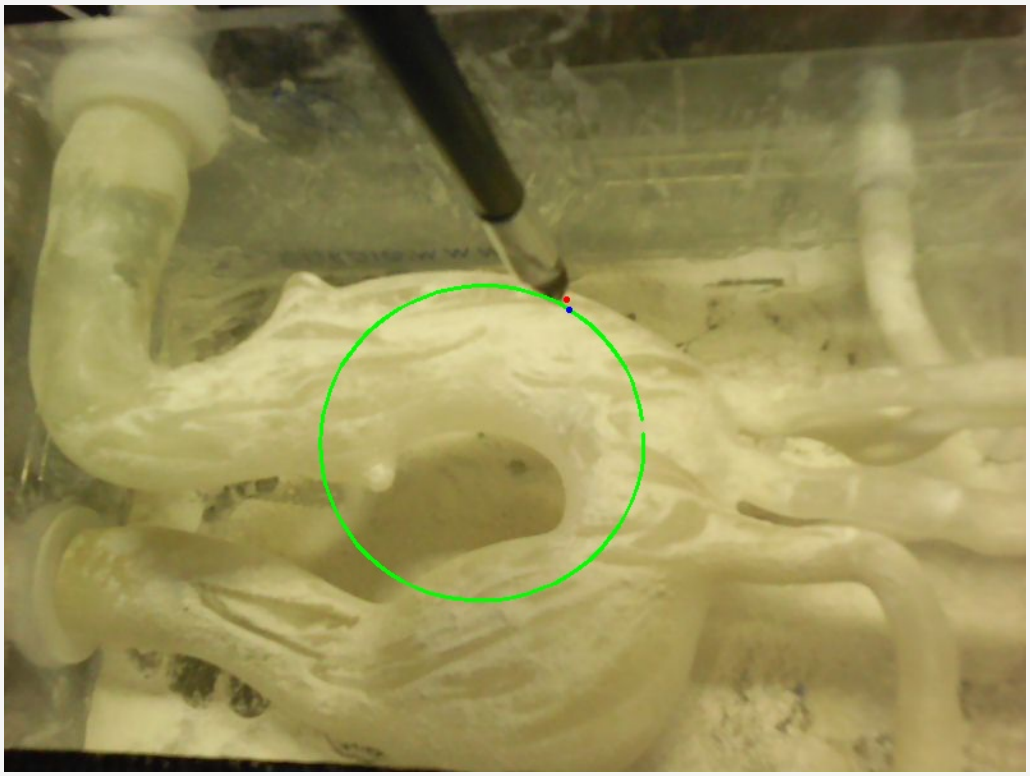


(a) Exp_{ours}, run3, frame 42, during tracking

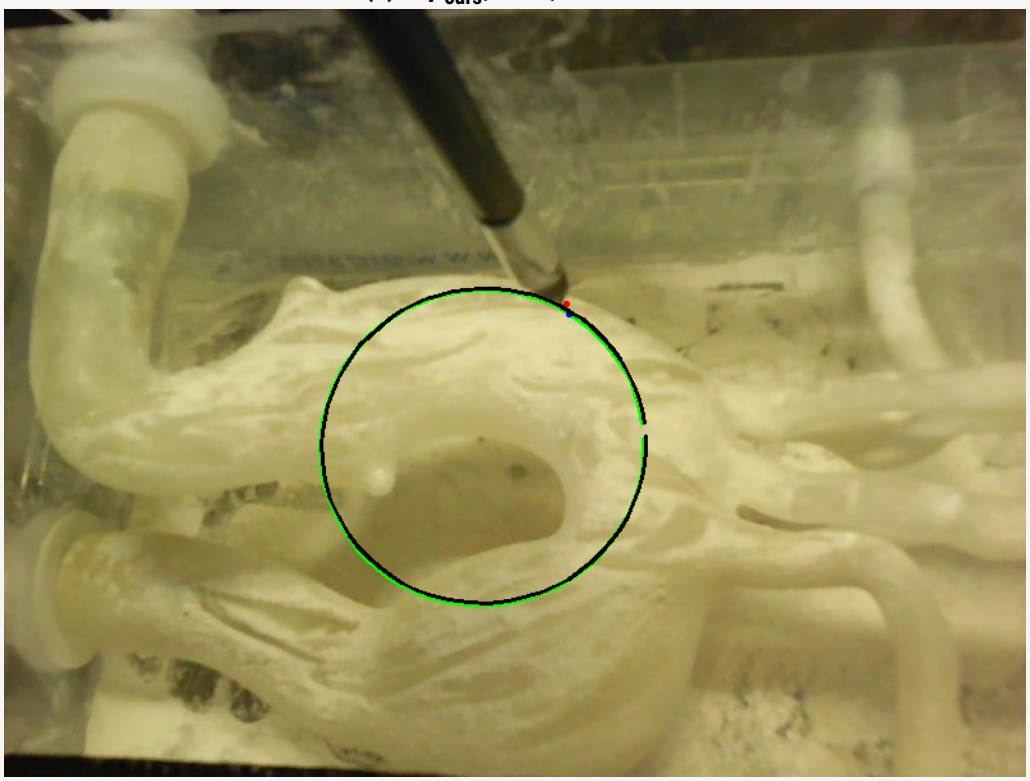


(b) Exp_{ours}, run3, frame 42, post-processed

Figure 5.9: Dynamic reference trajectory overlay, frame 42. The green trajectory represents the current reference trajectory. The blue point red point represent the current target point and current instrument tip position, respectively. The black circle represents the the overlay of the reference trajectory based on the affine transformation matrix obtained at frame 42.



(a) Exp_{ours}, run3, frame 61



(b) Exp_{ours}, run3, frame 61

Figure 5.10: Dynamic reference trajectory overlay, frame 61. The green trajectory represents the current reference trajectory (frame 61). The black circle represents the the overlay of the reference trajectory based on the affine transformation matrix obtained at frame 42.

5.5 Conclusion

In this pilot user study, the mesh-represented FRDAC approach was evaluated in a user-present teleoperation scenario on the first-generation dVRK for the first time. As a pilot use study, only the author, who has previous experience in the dVRK, was involved. *In vitro* experiments were performed, where the user tele-operates an instrument to follow a virtual circular trajectory above a dynamically moving silicone aorta phantom that is connected to a water pump. The predefined trajectory is overlaid on the real-time image, serving as a visual cue for the user. Tracking tests were conducted with different FRDAC approaches, in both static and dynamic scenarios. The tracking results demonstrate the effectiveness of both FRDAC in maintaining a safety distance in a dynamic scenario, compared to when no AC is provided to the user. The results also align with the previous findings in Chapter 4, showing that the mesh-represented FRDAC approach priorities accuracy over a larger safety margin and can be implemented at a speed that supports interactive updates of tissue deformation. Future studies will focus on refining the FRDAC framework and recruiting more users with varying levels of expertise in teleoperation to conduct more extensive experiments, thereby obtaining evaluations of both effectiveness and user comfort, which are further described in the next chapter.

Chapter 6

Conclusion

First, the main conclusions of each chapter of this thesis are reiterated and then related to the objectives established at the onset of this study. Specifically, the introduction elaborates on how the ultimate objective, ***"to develop a bespoke control framework that assists surgeons during tele-operation with reduced mental workload and enhanced task safety"****, supports research activities conducted in all the previous chapters, including literature reviews (Chapter 2), algorithm design (Chapter 3,4), and algorithm validations (Chapter 4,5). Through the course of this research, limitations of this study emerged, which are discussed and analysed in the second section. Potential measures to overcome these limitations are left to future studies, which are presented in the third and final section.*

6.1 Main Conclusions

To address one of the biggest constraints of most commercially available tele-operative surgical robots, the lack of haptic feedback, the overarching goal of this thesis is to develop a bespoke control framework that assists surgeons during tele-operative surgery, reducing their mental workload and enhancing task safety. To achieve the ultimate goal, several research tasks must be undertaken, as outlined in the previous chapters.This chapter aims to summarise the main conclusions and associate them with the ultimate research aim of this thesis. These research tasks, initially introduced in Chapter 1, are listed below.

Research Task 1
Explore relevant literature on the topic of AC applied to tele-operative surgery to recognise the design requirements and identify limitations of current approaches.

Research Task 2
Explore relevant literature on the dVRK to identify technical constraints of the system and essential calibrations to compensate for these constraints when conducting various aspects of research involving the robot.

Research Task 3
Develop a calibration framework to address the end-effector positioning error induced by the cable-driven property of first-generation dVRKs, to provide more accurate inputs for the AC pipeline.

Research Task 4
Establish a bespoke AC pipeline for tele-operative surgery, allowing for factors such as dynamic movements of tissue surfaces and the speed requirement for effective haptic guidance to be met.

Research Task 5
Verify the effectiveness of the established AC pipeline on a realistic experimental setup with user-in-the-loop.

The synthesis of the conclusions presented in the previous chapters suggests that these research tasks have been successfully completed. The contributions are briefly summarised below, followed by more detailed explanations for each chapter.

Chapter 2 - Related Work

A Identification of the significance of haptics for surgeons operating tele-operative surgical robots, which mostly lack haptic feedback, and the proposal of AC as an alternative avenue.

B Identification of key components in the design of AC to accommodate a clinically related scenario, leading to the introduction of FRDAC.

C Selection of the hardware setup, the first-generation dVRK, for the validation of the FRDAC algorithm, along with the identification of technical constraints and essential calibration procedures for the testing platform.

Chapter 3 Conclusions: On-the-fly hand-eye calibration for the da Vinci surgical robot

A Development of an on-the-fly calibration framework that builds on a particle filter, leveraging the cylindrical geometry of surgical instruments.

B Validation of the efficacy of the proposed framework through quantitative and qualitative experiments.

C Comparative studies against other state-of-the-art calibration approaches in the current literature.

Chapter 4 Conclusions: Proof-of-concept study on FRDAC in tele-operative surgery

A The proposal of a pipeline design for a dissipative FRDAC controller that utilises a depth-sensing camera to accommodate dynamic tissue deformation.

B Design of *in vitro* experiments to verify the effectiveness of the proposed FRDAC pipeline in assisting a tele-operative trajectory tracking task implemented by a "virtual surgeon".

C Quantitative analysis of the advantage of the proposed mesh-represented FRDAC over the state-of-the-art, a sphere-represented FRDAC strategy.

Chapter 5 Conclusions: Pilot user study on FRDAC in tele-operative surgery

A *In vitro* experiments where the mesh-represented FRDAC approach was first evaluated in a user-present teleoperation scenario on the first-generation dVRK.

B Quantitative and qualitative analysis to evaluate test performance with the assistance of the proposed FRDAC pipeline, compared to when no AC is provided to the user or other FRDAC approaches are applied.

6.1.1 Chapter 2 Conclusions: Related Work

This chapter introduced the background theory and key concepts that help readers develop a better understanding of the research conducted throughout this thesis. The overarching goal of this thesis was proposed, which is to develop a control framework that assists surgeons in performing tele-operated RMIS, with the aim of reducing their mental workload during complex procedures. Achieving this objective requires both algorithm development and validation. Factors that need to be taken into consideration and gaps that need to filled are identified through the literature review presented in this chapter.

The first section presents an overview of the development of surgical robots from their inception to their current status, with an emphasis on tele-operated surgical robots. Landmark events in the history of surgical robots development are highlighted. Specifically, some of the trending commercially available tele-operated surgical platforms are introduced. The advantages and disadvantages of these platforms, as well as prevalent research aimed to address these disadvantages, are also discussed, which justifies the adoption of AC as the avenue of research in this thesis.

The second section presents an overview of AC including its concept, classifications, and implementation details, aiming to address Objective 1. The current literature on AC is evaluated, with a focus on the implementation of AC on tele-operated surgery. Existing challenges and potential solutions to address these gaps are discussed, forming the basis for the algorithm development.

The final section presents an overview of the first-generation dVRK, the hardware platform upon which the developed algorithm is tested, aiming to address Objective 2. In addition to an introduction of its technical components and operational details, its inherent technical limitations and potential solutions to address these limitations are discussed in depth. The analysis forms the basis for the calibration framework designed to ensure the fidelity of the algorithm validation outcome.

6.1.2 Chapter 3 Conclusions: On-the-fly hand-eye calibration for the da Vinci surgical robot

This chapter addresses one of the main technical constraints of the first-generation dVRK, the positioning inaccuracy at the end effector, caused by multiple time-variant factors including wear and tear, inaccurate forward transmission kinematics, *etc.*, as explained in Chapter 2.

To address the constraint, an on-the-fly hand-eye calibration framework was proposed to improve end-effector positioning accuracy for da Vinci surgical instruments. The entire calibration framework comprises a particle filter for estimating the hand-eye transformation matrix and an individual calibration module for dVRK joint 4 angle readings. The proposed method solely relies on edge information from cylindrical tool shafts, avoiding dependence on feature detection on the end effector, which makes it more robust to challenging surgical scenarios, such as occlusion.

Both quantitative and qualitative studies were conducted to verify the effectiveness of the proposed framework in improving end-effector positioning accuracy. Comparison studies were also conducted between the proposed approach and other calibration approaches. The experimental results validated that an on-the-fly calibration approach that incorporates real-time feedback about the surgical scenario outperforms model-based approaches when there is a limited size of training data.

The proposed on-the-fly hand-eye calibration framework potentially enables obtaining a more accurate surgical instrument end-effector position, contributing to the implementation of FRDAC with high-precision. Hence, Objective 3 is addressed.

6.1.3 Chapter 4 Conclusions: Proof-of-concept study on FRDAC in tele-operative surgery

Having identified technical challenges that need to be overcome before FRAC can benefit tele-operative surgery in a clinical setting, in this chapter, a pipeline design for an energy dissipative FRAC strategy is proposed, which accommodates the dynamic tissue deformation caused by respiratory movements, by utilising a depth sensing camera.

The proposed FRAC strategy adopts a fine mesh representation, with a total number of 122,806 polygons in the case study presented, while running at 43.48Hz. *In vitro* trajectory tracking experiments were designed, which were conducted by a "virtual" surgeon to aid quantitative assessment of the method, including its effectiveness in maintaining task safety, which was confirmed by successfully maintaining a pre-defined safety distance across all trials.

Comparative studies were also conducted to investigate the robustness and time-efficiency of our method against other FRAC methods that rely on simple geometry AC representations. It is demonstrated that the proposed method provides a more robust and effective guidance overall, while maintaining comparable, if not lower, time costs.

Through these experiments, the effectiveness of the proposed AC was verified, and its potential to be of assistance in a real clinical setup was preliminarily demonstrated. Hence, Objective 4 is addressed.

6.1.4 Chapter 5 Conclusions: Pilot user study on FRDAC in tele-operative surgery

Following from the previous chapter, where the proposed mesh-represented FRDAC pipeline was evaluated in an automated manner assuming the presence of a "virtual" surgeon, this chapter focuses on evaluating the effectiveness of the FRDAC in a user-present tele-operation scenario. As a pilot user study, only the author, who has prior experience in the dVRK is involved.

As a pilot user study, only the author, who has prior experience in the dVRK is involved. In the

experiments, a tissue incision task was conducted *in vitro* by the user on a dynamically moving silicone aorta phantom, simulating periodic movements caused by respiration.

The tracking results demonstrated the effectiveness of the proposed FRDAC approach in maintaining a safety distance in a dynamic scenario compared to when no AC was provided to the user. The results also aligned with the previous findings in Chapter 4, showing that the mesh-represented FRDAC approach prioritises accuracy over a larger safety margin and can be implemented at a speed that supports interactive updates of tissue deformation. Furthermore, experimental results confirmed the effectiveness of the proposed FRDAC pipeline in a user-present dynamic scenario, addressing Objective 5.

6.1.5 Main Conclusion

The combined conclusions of all chapters suggest that the proposed FRDAC has the potential for adoption in real tele-surgery scenarios.

The design of the FRDAC pipeline accommodates periodic tissue movements, which are common in surgical applications. To better describe surface features, complex geometric primitives were adopted for representing dynamic tissue surface during AC generation. To facilitate the update of AC on the moving tissue surface, reasonable assumptions were made and justified in simulation. Additionally, the design of the AC controller ensures energy dissipativity, allowing the AC pipeline to be applied to other robotic platforms equipped with active force feedback. Experimental results show that the pipeline operates at 43.48 Hz, which is sufficient to capture periodic tissue movements caused by respiration.

The proof-of-concept study demonstrates that the FRDAC can assist a “virtual surgeon” who acts perfectly on AC guidance in a dynamic scenario. Subsequently, the pilot user study further confirmed the effectiveness of the FRDAC in a user-present scenario. To address potential eventualities during FRDAC implementations on a cable-driven tele-operation surgical platform, such as the first-generation da Vinci robot, the on-the-fly hand-eye calibration algorithm can be adopted to provide more accurate position inputs for AC evaluation.

6.2 Limitations

Throughout this thesis, some limitations have been underlined. These limitations arise from assumptions that were made during algorithm development and a lack of further extensive experiments to validate the FRDAC pipeline in a more clinically relevant scenario. These limitations are briefly summarised below, followed by detailed explanations for each technical chapter.

Chapter 3 - On-the-fly hand-eye calibration for the da Vinci surgical robot

- **A** Reliance on edge features of surgical instruments, which can be hard to obtain in a real clinical scenario.
- **B** Requirement of accurate position of joint 4, which usually relies on a marker, usually not available in a clinical theatre.
- **C** Results from the comparative study with another particle filter framework that relies on key point feature detection did not demonstrate a significant reduction in back-projection errors.
- **D** There is a lack of online experiments demonstrating the effectiveness of the proposed calibration framework in dynamically reducing positioning errors.

Chapter 4 - Proof-of-concept study on FRDAC in tele-operative surgery

- **A** The assumption that the 3D point cloud of tissue surface is readily available.
- **B** The assumption that affine registration is sufficient in handling periodic tissue movements.
- **C** The assumption that FPFH feature correspondences remain unchanged during dynamic tissue deformation.
- **D** The assumption that a "virtual" surgeon that perfectly acts upon AC guidance.

Chapter 5 - Pilot user study on FRDAC in tele-operative surgery

- **A** No volunteer study and a lack of subjective feedback from users with different levels of expertise in tele-operation.
- **B** A lack of stereo image feedback for the user during the trajectory tracking experiments.
- **C** The assumption of a defined forbidden region, which would be difficult to identify in a clinical setup.
- **D** No exploration into the actual incision task involving tissue contact.
- **E** No exploration into expanding the existing FRDAC to all 6 DOFs.

6.2.1 Chapter 3 Limitations: On-the-fly hand-eye calibration for the da Vinci surgical robot

The on-the-fly hand-eye calibration framework builds on the assumption that edge features of cylindrical instruments are readily available, either through marker-based or marker-free segmentation algorithms, such as the SAM. However, obtaining accurate edge features during a real clinical setup is not only challenging but also time-consuming. Moreover, the accuracy of SAM is not qualified for medical applications. The robustness of the proposed calibration framework against spurious edge detection results remains to be further investigated.

The calibration framework includes a module for the individual calibration of joint 4 position based on edge features. This is because the angle of rotation is related to the position of cylinder edges in the image via projection geometry. To obtain an accurate value for joint 4 position, a prerequisite is the initial joint 4 position. In a real clinical setup, there is no direct access to individual joint readings, and it usually requires the assistance of a marker to calculate the initial joint position via computer vision techniques and inverse kinematics. However, due to sterilisation considerations, it is challenging to introduce an external marker into the clinical theatre, thus restricting its application scenario to lab trials only.

Comparative results with another calibration approach that builds upon a particle filter utilising key point features for updating weights indicated that there was no significant reduction in back-projection errors using the calibration framework proposed in this study. Potential reasons include the instability of the edge features detected using SAM and the inaccuracy of the initial hand-eye calibration result. To validate these assumptions, a potential approach is to design an online calibration study with initial hand-eye transformation matrices across different levels of inaccuracy and observe how the calibration framework dynamically corrects the positioning inaccuracies.

6.2.2 Chapter 4 Limitations: Proof-of-concept study on FRDAC in tele-operative surgery

As a proof-of-concept study, the FRDAC developed in this chapter is based on the assumption that the 3D point cloud of the tissue surface is readily available. To validate the FRDAC framework, a depth-sensing camera was incorporated into the experimental setup, providing point cloud at a rate of 10 Hz. However, in an actual tele-operation scenario, only a pair of stereoscopic endoscopic cameras is available. Therefore, there requires an additional module for 3D reconstruction from stereo image pairs, a procedure that is typically computationally expensive. The incorporation of the 3D reconstruction module may affect the level of comfort for users receiving AC guidance due to a time delay.

To speed up the implementation of the FRDAC pipeline, two major assumptions were made. First, it was assumed that during respiratory movements, the periodic deformation that the tissue under-

goes could be simplified as affine transformation. Second, to enhance registration accuracy, FPFH features on the tissue surface were detected and matched prior to conducting affine registration, with the assumption that the feature correspondences would remain unchanged throughout the deformation. Although these assumptions have been verified through simulation experiments, it would be more beneficial to incorporate non-rigid registration into the FRDAC pipeline, as it would allow for a larger range of deformation beyond respiratory movements, for example, in dissection tasks where local deformation occurs due to tool-tissue interaction. Additionally, more robust feature detection and matching algorithms can be adopted to replace the FPFH feature detection module.

AC enforcement in this study was achieved through a hybrid force-position controller, assuming that there exists a "virtual" surgeon that could perfectly act upon the generated AC guidance. However, in reality, users with different levels of expertise in tele-operation may react differently to the same haptic cue. Whether the generated AC poses as a useful guideline or a distracting disturbance remains to be investigated through user studies.

6.2.3 Chapter 5 Limitations: Pilot user study on FRDAC in tele-operative surgery

First and foremost, only the author was involved in the pilot user study as a user who has previous experience in the dVRK. Although the experimental results demonstrated the effectiveness of the FRDAC in maintaining task safety in a user-present dynamic scenario, it is still not convincing enough to prove its ability to assist a wider range of users. Qualitative studies to gauge the level of comfort for users when receiving AC guidance should be conducted.

The experimental designs should be further refined. During the trajectory tracking experiments, the reference trajectory was overlaid and updated on the 2D image of the current scene captured by an RGBD camera. The lack of stereo information increased the mental workload for the user to estimate depth during task operation, potentially leading to worse performance in trajectory tracking without any AC assistance. One way to address this limitation is to include surgical tasks that involve changing camera orientations intra-operatively.. Additionally, to better evaluate different FRDAC strategies, experimental trials should be conducted in a randomised order to account for the possibility that users may develop better operating skills over extended period of training. Moreover, more extensive surgical tasks that involve actual surface contact should be designed to provide a more straightforward evaluation of the proposed FRDAC pipeline. However, that would involve tool-tissue interaction and demand a higher reaction speed in response to tissue deformation.

All the experiments conducted throughout this thesis assume that the forbidden region has already been defined pre-operatively, in the form of a circular region on the tissue surface *per se*. However, the definition and update of forbidden regions are not easy to implement during a real surgery.

Therefore, to advance the adoption of FRDAC pipeline in a clinical theatre, it requires an additional module for real-time identification of forbidden regions, assisted by more advanced computer vision algorithms, for example.

The AC enforcement was achieved through the built-in impedance controller of the first-generation dVRK. Although the energy-redirection approach featured in the dissipative controller is applicable to all 6 DOFs, only translational movements were constrained in this study. This is because the impedance controller only constrains translational movements in the x, y and z directions in Cartesian space. The FRDAC pipeline developed in this study can be effectively transferred to another tele-operative system, potentially equipped with active force feedback. It remains to be investigated whether energy passivity can be maintained when the FRDAC is enforced across all 6 DOFs.

6.3 Future Work

A review of the contributions of all previous chapters shows that the research objectives laid out at the onset of this study have been achieved. However, through the course of research and experiments, limitations emerged, which were discussed in detail in the previous section. To propel further research in the field of AC and provide a guideline for future researchers working on FRDAC, potential directions for future work are discussed in this section.

As an initial step towards the development of an on-the-fly hand-eye calibration framework aimed at addressing encoder reading errors and hand-eye calibration errors simultaneously, the author has identified some technical components that require further refinement. Although the proposed calibration framework has proven effective in improving positioning accuracy for a cable-driven robot, a residual positioning error still exists, exceeding the accuracy requirement for any sub-millimetre-scale treatment. One potential solution to address this issue is to develop an on-the-fly calibration framework for all individual joint angles, likely with increased reliance on accurate feature detection on surgical instruments. Additionally, the robustness of the algorithm against noisy edge detection needs to be investigated. Considering greater technical efforts required in obtaining accurate tool edges compared to key points detection, the necessity of using edge features instead of key points needs to be further justified. In this study, the SAM method was adopted to demonstrate the feasibility of using marker-free approaches to obtaining tool edges from a segmented tool contour. However, the SAM model is not robust enough in clinical scenes to segment instruments. Therefore, with advancements in more accurate segmentation algorithms tailored for medical applications, such as the MedSAM model [176], edge detection accuracy in the proposed calibration framework is expected to improve, leading to a better calibration performance. Future experiments should verify the feasibility of the proposed algorithm in response to different magnitudes of instantaneous changes in the hand-eye calibration matrix. Online demonstrations involving sudden position changes in both the camera and instruments would also provide valuable insights

This study argued that an on-the-fly approach provides more robust calibration performance than an offline calibration approach, given the time-variant nature of the error source. Although edge features were solely used in the particle filter-based calibration framework, it was acknowledged that obtaining accurate edge features is usually challenging in a real clinical setup. To compensate for this technical constraint, more robust features detection and matching algorithms, either through conventional or learning-based approaches, remain to be further investigated and updated in the current framework. Additionally, more extensive experiments should be conducted to evaluate the robustness of the framework against spurious feature detection results and its effectiveness in correcting inaccurate initial hand-eye calibration results on-the-fly.

To accommodate for dynamic tissue movements during AC implementation, different image modalities can be adopted to monitor the real-time surgical scene, such as ultrasound, CT, and point

clouds. In this study, the FRDAC pipeline relies on dynamic AC generation from surface point clouds, which are streamed by a depth-sensing camera. However, it bypasses the essential procedure of 3D reconstruction from stereo images captured by the endoscopic cameras of the dVRK. The accuracy of 3D reconstruction may be affected by the fidelity of the camera parameters, which can change dynamically due to factors such as temperature; therefore, it requires essential dynamic camera calibrations on the dVRK. Additionally, there should be requirements on the speed at which 3D construction is performed, since it may affect the level of comfort for users when receiving AC guidance. To accommodate a larger range of deformation, it is highly recommended to incorporate non-rigid registration modules into the current pipeline, although at the cost of increased computational effort. Therefore, it is left to future studies to develop a customised non-rigid registration algorithm that efficiently describes deformation encountered in a specific surgical procedure.

In order to provide more convincing results to demonstrate the effectiveness of the proposed FRDAC pipeline, a wider user study involving individuals with different levels of expertise in tele-operation is required. Both quantitative and qualitative measures should be taken. With the additional module for non-rigid registration, more extensive experiments involving contact with the tissue surface can be conducted, providing a more straightforward evaluation metric for FRDAC. Given that the definition and update of forbidden regions are challenging, it would be beneficial to incorporate an additional module for real-time segmentation of forbidden regions into the current framework. To verify that the FRDAC is generalisable across different surgical robot platforms, more extensive studies should be conducted where the existing FRDAC is expanded to all 6 DOFs and applied to different robotic systems.

Tele-operation not only enhances surgeons' dexterity in performing surgical tasks in challenging scenarios within the operating theatre but also promises a future where surgeons can work across a long distance, addressing the uneven distribution of medical resources and enabling more effective, cost-efficient training. With the advantages of tele-surgery being more widely acknowledged, an increase in the adoption of tele-operative surgical robots is expected, potentially leading to greater competition in the market. To promote a wider adoption of tele-operative surgical platforms in the future, this thesis proposed a generalisable high-level control framework that assists surgeons in maintaining task safety without relying on external devices in theory. While similar assistance can be provided by tele-operative robots with haptic feedback, the manufacture and maintenance costs would increase sharply. On the contrary, the FRDAC developed in this thesis does not incur additional costs and is customisable for various surgical applications. With advancements in computer vision and deep learning algorithms, it is envisioned that surgeons in the future would benefit from augmented dexterity through the automation of tedious surgical subtasks, shared control, AC, and other innovations. Throughout the process, modules within the proposed FRDAC pipeline may be upgraded for enhanced accuracy, and data inputs can be sourced from various resources. Nevertheless, the pipeline's framework can be of reference value for fu-

ture researchers seeking to refine it. In this sense, the research conducted in this thesis brings the adoption of FRDAC in a real clinical setup a step closer, benefiting surgical implementations in the future.

References

[1] Robinson, T. and Stiegmann, G. "Minimally invasive surgery". In: *Endoscopy* 36.01 (2004), pp. 48–51.

[2] Corcione, F., Esposito, C., Cuccurullo, D., et al. "Advantages and limits of robot-assisted laparoscopic surgery: preliminary experience". In: *Surgical Endoscopy and Other Interventional Techniques* 19 (2005), pp. 117–119.

[3] Gerhardus, D. "Robot-assisted surgery: The future is here." In: *Journal of Healthcare Management* 48.4 (2003).

[4] Kwoh, Y., Hou, J., Jonckheere, E., et al. "A robot with improved absolute positioning accuracy for CT guided stereotactic brain surgery". In: *IEEE Transactions on Biomedical Engineering* 35.2 (1988), pp. 153–160. DOI: 10.1109/10.1354.

[5] Davies, B., Harris, S., Lin, W., et al. "Active compliance in robotic surgery—the use of force control as a dynamic constraint". In: *Proceedings of the Institution of Mechanical Engineers, Part H: Journal of Engineering in Medicine* 211.4 (1997), pp. 285–292.

[6] *https://www.intuitive.com*. 2024.

[7] Marchegiani, F., Siragusa, L., Zadoroznyj, A., et al. "New robotic platforms in general surgery: what's the current clinical scenario?" In: *Medicina* 59.7 (2023), p. 1264.

[8] Smith Jr, J. A. and Herrell, S. D. "Robotic-assisted laparoscopic prostatectomy: do minimally invasive approaches offer significant advantages?" In: *Journal of clinical oncology* 23.32 (2005), pp. 8170–8175.

[9] Freschi, C., Ferrari, V., Melfi, F., et al. "Technical review of the da Vinci surgical telemanipulator". In: *The International Journal of Medical Robotics and Computer Assisted Surgery* 9.4 (2013), pp. 396–406.

[10] Pinzon, D., Byrns, S., and Zheng, B. "Prevailing trends in haptic feedback simulation for minimally invasive surgery". In: *Surgical innovation* 23.4 (2016), pp. 415–421.

[11] Kelly, S. *Intuitive details launch plan for New Da Vinci 5 Robot*. Mar. 2024.

[12] Shrader, T. *How much is a Surgical Robot?* Nov. 2023.

[13] Enayati, N., De Momi, E., and Ferrigno, G. "Haptics in robot-assisted surgery: Challenges and benefits". In: *IEEE reviews in biomedical engineering* 9 (2016), pp. 49–65.

[14] Bowyer, S. A., Davies, B. L., and Baena, F. R. y. "Active constraints/virtual fixtures: A survey". In: *IEEE Transactions on Robotics* 30.1 (2013), pp. 138–157.

[15] Rosenberg, L. B. "The use of virtual fixtures as perceptual overlays to enhance operator performance in remote environments". In: *Air force material command* (1992), pp. 1–42.

[16] Rosenberg, L. B. "Virtual fixtures: Perceptual tools for telerobotic manipulation". In: *Proceedings of IEEE virtual reality annual international symposium*. Ieee. 1993, pp. 76–82.

[17] Davies, B., Jakopec, M., Harris, S. J., et al. "Active-constraint robotics for surgery". In: *Proceedings of the IEEE* 94.9 (2006), pp. 1696–1704.

[18] D'Ettorre, C., Mariani, A., Stilli, A., et al. "Accelerating Surgical Robotics Research: A Review of 10 Years With the da Vinci Research Kit". In: *IEEE Robotics & Automation Magazine* 28.4 (2021), pp. 56–78. DOI: 10.1109/MRA.2021.3101646.

[19] Cui, Z., Cartucho, J., Giannarou, S., et al. “Caveats on the first-generation da Vinci research kit: Latent technical constraints and essential calibrations”. In: *IEEE Robotics & Automation Magazine* (2023).
[20] Davies, B., Hibberd, R., Coptcoat, M., et al. “A surgeon robot prostatectomy—a laboratory evaluation”. In: *Journal of medical engineering & technology* 13.6 (1989), pp. 273–277.
[21] Pransky, J. “ROBODOC-surgical robot success story”. In: *Industrial Robot: An International Journal* 24.3 (1997), pp. 231–233.
[22] Doarn, C. R., Hufford, K., Low, T., et al. “Telesurgery and robotics”. In: *Telemedicine and e-Health* 13.4 (2007), pp. 369–380.
[23] Sackier, J. M. and Wang, Y. “Robotically assisted laparoscopic surgery: from concept to development”. In: *Surgical endoscopy* 8 (1994), pp. 63–66.
[24] Sackier, J. M., Wooters, C., Jacobs, L., et al. “Voice activation of a surgical robotic assistant”. In: *The American Journal of Surgery* 174.4 (1997), pp. 406–409.
[25] Reichenspurner, H., Damiano, R. J., Mack, M., et al. “Use of the voice-controlled and computer-assisted surgical system ZEUS for endoscopic coronary artery bypass grafting”. In: *The Journal of thoracic and cardiovascular surgery* 118.1 (1999), pp. 11–16.
[26] Marescaux, J., Leroy, J., Gagner, M., et al. “Transatlantic robot-assisted telesurgery”. In: *Nature* 413.6854 (2001), pp. 379–380.
[27] Kalan, S., Chauhan, S., Coelho, R. F., et al. “History of robotic surgery”. In: *Journal of Robotic Surgery* 4 (2010), pp. 141–147.
[28] Mendivil, A., Holloway, R. W., and Boggess, J. F. “Emergence of robotic assisted surgery in gynecologic oncology: American perspective”. In: *Gynecologic oncology* 114.2 (2009), S24–S31.
[29] Guy-Bernard, C., Jacques, H., Olivier, G., et al. “Feasibility of robotic laparoscopic surgery: 146 cases”. In: *World journal of surgery* 25 (2001), pp. 1467–1477.
[30] Muaddi, H., El Hafid, M., Choi, W. J., et al. “Clinical outcomes of robotic surgery compared to conventional surgical approaches (laparoscopic or open): a systematic overview of reviews”. In: *Annals of surgery* 273.3 (2021), pp. 467–473.
[31] Ballantyne, G. H. and Moll, F. “The da Vinci telerobotic surgical system: the virtual operative field and telepresence surgery”. In: *Surgical Clinics* 83.6 (2003), pp. 1293–1304.
[32] Hellan, M., Stein, H., and Pigazzi, A. “Totally robotic low anterior resection with total mesorectal excision and splenic flexure mobilization”. In: *Surgical endoscopy* 23 (2009), pp. 447–451.
[33] Ngu, J. C.-Y., Tsang, C. B.-S., and Koh, D. C.-S. “The da Vinci Xi: a review of its capabilities, versatility, and potential role in robotic colorectal surgery”. In: *Robotic Surgery: Research and Reviews* (2017), pp. 77–85.
[34] Mohan, A., Wara, U. U., Shaikh, M. T. A., et al. “Telesurgery and robotics: an improved and efficient era”. In: *Cureus* 13.3 (2021).
[35] Lengyel, B. C., Chinnadurai, P., Corr, S. J., et al. “Robot-assisted vascular surgery: literature review, clinical applications, and future perspectives”. In: *Journal of Robotic Surgery* 18.1 (2024), p. 328.
[36] Thomas, B. C., Slack, M., Hussain, M., et al. “Preclinical evaluation of the versius surgical system, a new robot-assisted surgical device for use in minimal access renal and prostate surgery”. In: *European urology focus* 7.2 (2021), pp. 444–452.
[37] Aresu, G., Dunning, J., Routledge, T., et al. “Preclinical evaluation of Versius, an innovative device for use in robot-assisted thoracic surgery”. In: *European Journal of Cardio-Thoracic Surgery* 62.3 (2022), ezac178.

[38] Morton, J., Hardwick, R. H., Tilney, H. S., et al. "Preclinical evaluation of the versius surgical system, a new robot-assisted surgical device for use in minimal access general and colorectal procedures". In: *Surgical endoscopy* 35 (2021), pp. 2169–2177.
[39] Prata, F., Ragusa, A., Tempesta, C., et al. "State of the art in robotic surgery with Hugo RAS system: feasibility, safety and clinical applications". In: *Journal of personalized medicine* 13.8 (2023), p. 1233.
[40] Bravi, C. A., Balestrazzi, E., De Loof, M., et al. "Robot-assisted radical prostatectomy performed with different robotic platforms: first comparative evidence between Da Vinci and HUGO robot-assisted surgery robots". In: *European Urology Focus* 10.1 (2024), pp. 107–114.
[41] Longmore, S. K., Naik, G., and Gargiulo, G. D. "Laparoscopic robotic surgery: Current perspective and future directions". In: *Robotics* 9.2 (2020), p. 42.
[42] Brownlee, E. M. and Slack, M. "The role of the versius surgical robotic system in the paediatric population". In: *Children* 9.6 (2022), p. 805.
[43] Sarchi, L., Mottaran, A., Bravi, C. A., et al. "Robot-assisted radical prostatectomy feasibility and setting with the Hugo™ robot-assisted surgery system." In: *BJU international* 130.5 (2022).
[44] Winfield, A. F. "Future directions in tele-operated robotics". In: *Telerobotic applications* (2000), pp. 147–163.
[45] Kaul, S., Shah, N. L., and Menon, M. "Learning curve using robotic surgery". In: *Current urology reports* 7.2 (2006), pp. 125–129.
[46] Kitagawa, M., Okamura, A. M., Bethea, B. T., et al. "Analysis of suture manipulation forces for teleoperation with force feedback". In: *Medical Image Computing and Computer-Assisted Intervention—MICCAI 2002: 5th International Conference Tokyo, Japan, September 25–28, 2002 Proceedings, Part I 5*. Springer. 2002, pp. 155–162.
[47] Tran, N., Wu, J. Y., Deguet, A., et al. "A deep learning approach to intrinsic force sensing on the da Vinci surgical robot". In: *2020 Fourth IEEE International Conference on Robotic Computing (IRC)*. IEEE. 2020, pp. 25–32.
[48] Pacchierotti, C., Meli, L., Chinello, F., et al. "Cutaneous haptic feedback to ensure the stability of robotic teleoperation systems". In: *The International Journal of Robotics Research* 34.14 (2015), pp. 1773–1787.
[49] Grammatikopoulou, M., Leibrandt, K., and Yang, G.-Z. "Motor channelling for safe and effective dynamic constraints in Minimally Invasive Surgery". In: *2016 IEEE/RSJ International Conference on Intelligent Robots and Systems (IROS)*. 2016, pp. 4317–4323. DOI: 10.1109/IROS.2016.7759635.
[50] Marinho, M. M., Adorno, B. V., Harada, K., et al. "Dynamic Active Constraints for Surgical Robots Using Vector-Field Inequalities". In: *IEEE Transactions on Robotics* 35.5 (2019), pp. 1166–1185. DOI: 10.1109/TRO.2019.2920078.
[51] Leibrandt, K., Marcus, H. J., Kwok, K.-W., et al. "Implicit active constraints for a compliant surgical manipulator". In: *2014 IEEE International Conference on Robotics and Automation (ICRA)*. 2014, pp. 276–283. DOI: 10.1109/ICRA.2014.6906622.
[52] Wottawa, C. R., Genovese, B., Nowroozi, B. N., et al. "Evaluating tactile feedback in robotic surgery for potential clinical application using an animal model". In: *Surgical endoscopy* 30 (2016), pp. 3198–3209.
[53] Turro, N. and Khatib, O. "Haptically augmented teleoperation". In: *Experimental Robotics VII*. Springer. 2001, pp. 1–10.
[54] Luo, J., Liu, W., Qi, W., et al. "A vision-based virtual fixture with robot learning for teleoperation". In: *Robotics and Autonomous Systems* 164 (2023), p. 104414.

[55] Cai, Y., Choi, P., Hui, C.-W. V., et al. "A Task Space Virtual Fixture Architecture for Teleoperated Surgical System With Slave Joint Limit Constraints". In: *IEEE/ASME Transactions on Mechatronics* 27.1 (2022), pp. 69–80. DOI: 10.1109/TMECH.2021.3058174.

[56] Petersen, J. G. and Baena, F. R. "A dynamic active constraints approach for hands-on robotic surgery". In: *2013 IEEE/RSJ International Conference on Intelligent Robots and Systems*. 2013, pp. 1966–1971. DOI: 10.1109/IROS.2013.6696617.

[57] Ren, J., Patel, R. V., McIsaac, K. A., et al. "Dynamic 3-D Virtual Fixtures for Minimally Invasive Beating Heart Procedures". In: *IEEE Transactions on Medical Imaging* 27.8 (2008), pp. 1061–1070. DOI: 10.1109/TMI.2008.917246.

[58] Padhan, J., Tsekos, N., Al-Ansari, A., et al. "Dynamic Guidance Virtual Fixtures for Guiding Robotic Interventions: Intraoperative MRI-guided Transapical Cardiac Intervention Paradigm". In: *2022 IEEE 22nd International Conference on Bioinformatics and Bioengineering (BIBE)*. IEEE. 2022, pp. 265–270.

[59] Kastritsi, T., Papageorgiou, D., Sarantopoulos, I., et al. "Stability of active constraints enforcement in sensitive regions defined by point-clouds for robotic surgical procedures". In: *2019 18th European Control Conference (ECC)*. IEEE. 2019, pp. 1604–1609.

[60] Ryden, F. and Chizeck, H. J. "Forbidden-region virtual fixtures from streaming point clouds: Remotely touching and protecting a beating heart". In: *2012 IEEE/RSJ International Conference on Intelligent Robots and Systems*. IEEE. 2012, pp. 3308–3313.

[61] Bentley, J. L. "Multidimensional binary search trees used for associative searching". In: *Communications of the ACM* 18.9 (1975), pp. 509–517.

[62] Bowyer, S. A. and Rodriguez y Baena, F. "Deformation invariant bounding spheres for dynamic active constraints in surgery". In: *Proceedings of the Institution of Mechanical Engineers, Part H: Journal of Engineering in Medicine* 228.4 (2014), pp. 350–361.

[63] Clarkson, K. L. "Nearest-neighbor searching and metric space dimensions". In: (2006).

[64] Abbott, J. J. and Okamura, A. M. "Stable forbidden-region virtual fixtures for bilateral telemanipulation". In: (2006).

[65] Ryden, F., Kosari, S. N., and Chizeck, H. J. "Proxy method for fast haptic rendering from time varying point clouds". In: *2011 IEEE/RSJ International Conference on Intelligent Robots and Systems*. IEEE. 2011, pp. 2614–2619.

[66] Kikuuwe, R., Takesue, N., and Fujimoto, H. "A control framework to generate nonenergy-storing virtual fixtures: Use of simulated plasticity". In: *IEEE Transactions on Robotics* 24.4 (2008), pp. 781–793.

[67] Bowyer, S. A. and Baena, F. R. y. "Dynamic frictional constraints for robot assisted surgery". In: *2013 World Haptics Conference (WHC)*. IEEE. 2013, pp. 319–324.

[68] Bowyer, S. A. and Rodriguez y Baena, F. "Dynamic frictional constraints in translation and rotation". In: *2014 IEEE International Conference on Robotics and Automation (ICRA)*. 2014, pp. 2685–2692. DOI: 10.1109/ICRA.2014.6907244.

[69] Bowyer, S. A. and Baena, F. R. y. "Dissipative control for physical human–robot interaction". In: *IEEE Transactions on Robotics* 31.6 (2015), pp. 1281–1293.

[70] Enayati, N., Costa, E. C. A., Ferrigno, G., et al. "A dynamic non-energy-storing guidance constraint with motion redirection for robot-assisted surgery". In: *2016 IEEE/RSJ International Conference on Intelligent Robots and Systems (IROS)*. IEEE. 2016, pp. 4311–4316.

[71] Kastritsi, T., Papageorgiou, D., Sarantopoulos, I., et al. "Guaranteed active constraints enforcement on point cloud-approximated regions for surgical applications". In: *2019 International Conference on Robotics and Automation (ICRA)*. IEEE. 2019, pp. 8346–8352.

[72] Ferraguti, F., Preda, N., Bonfe, M., et al. "Bilateral teleoperation of a dual arms surgical robot with passive virtual fixtures generation". In: *2015 IEEE/RSJ International Conference on Intelligent Robots and Systems (IROS)*. IEEE. 2015, pp. 4223–4228.

[73] Kwok, K.-W., Tsoi, K. H., Vitiello, V., et al. "Dimensionality reduction in controlling articulated snake robot for endoscopy under dynamic active constraints". In: *IEEE Transactions on robotics* 29.1 (2012), pp. 15–31.

[74] Funda, J., Taylor, R. H., Eldridge, B., et al. "Constrained Cartesian motion control for teleoperated surgical robots". In: *IEEE Transactions on Robotics and Automation* 12.3 (1996), pp. 453–465.

[75] Li, M., Ishii, M., and Taylor, R. H. "Spatial motion constraints using virtual fixtures generated by anatomy". In: *IEEE Transactions on Robotics* 23.1 (2007), pp. 4–19.

[76] Gonçalves, V. M., Fraisse, P., Crosnier, A., et al. "Parsimonious kinematic control of highly redundant robots". In: *IEEE Robotics and Automation Letters* 1.1 (2015), pp. 65–72.

[77] Marinho, M. M., Adorno, B. V., Harada, K., et al. "Active constraints using vector field inequalities for surgical robots". In: *2018 IEEE International Conference on Robotics and Automation (ICRA)*. IEEE. 2018, pp. 5364–5371.

[78] Kwok, K.-W., Mylonas, G. P., Sun, L. W., et al. "Dynamic active constraints for hyper-redundant flexible robots". In: *International Conference on Medical Image Computing and Computer-Assisted Intervention*. Springer. 2009, pp. 410–417.

[79] Dagnino, G., Liu, J., Abdelaziz, M. E., et al. "Haptic feedback and dynamic active constraints for robot-assisted endovascular catheterization". In: *2018 IEEE/RSJ International Conference on Intelligent Robots and Systems (IROS)*. IEEE. 2018, pp. 1770–1775.

[80] Selvaggio, M., Notomista, G., Chen, F., et al. "Enhancing bilateral teleoperation using camera-based online virtual fixtures generation". In: *2016 IEEE/RSJ International Conference on Intelligent Robots and Systems (IROS)*. IEEE. 2016, pp. 1483–1488.

[81] Selvaggio, M., Fontanelli, G. A., Ficuciello, F., et al. "Passive virtual fixtures adaptation in minimally invasive robotic surgery". In: *IEEE Robotics and Automation Letters* 3.4 (2018), pp. 3129–3136.

[82] Moccia, R., Iacono, C., Siciliano, B., et al. "Vision-based dynamic virtual fixtures for tools collision avoidance in robotic surgery". In: *IEEE Robotics and Automation Letters* 5.2 (2020), pp. 1650–1655.

[83] Wang, L., Chen, Z., Chalasani, P., et al. "Updating virtual fixtures from exploration data in force-controlled model-based telemanipulation". In: *International Design Engineering Technical Conferences and Computers and Information in Engineering Conference*. Vol. 50152. American Society of Mechanical Engineers. 2016, V05AT07A031.

[84] Bischof, B., Glück, T., Böck, M., et al. "A path/surface following control approach to generate virtual fixtures". In: *IEEE Transactions on Robotics* 34.6 (2018), pp. 1577–1592.

[85] Kazanzides, P., Chen, Z., Deguet, A., et al. "An open-source research kit for the da Vinci® Surgical System". In: *2014 IEEE international conference on robotics and automation (ICRA)*. IEEE. 2014, pp. 6434–6439.

[86] Kwartowitz, D. M., Herrell, S. D., and Galloway, R. L. "Toward image-guided robotic surgery: determining intrinsic accuracy of the da Vinci robot". In: *International Journal of Computer Assisted Radiology and Surgery* 1 (2006), pp. 157–165.

[87] Ferguson, J. M., Cai, L. Y., Reed, A., et al. "Toward image-guided partial nephrectomy with the da Vinci robot: exploring surface acquisition methods for intraoperative re-registration". In: *Medical imaging 2018: Image-guided procedures, robotic interventions, and modeling*. Vol. 10576. SPIE. 2018, pp. 49–59.

[88] Baumkircher, A., Seme, K., Munih, M., et al. "Collaborative Robot Precision Task in Medical Microbiology Laboratory". In: *Sensors* 22.8 (2022), p. 2862.
[89] Seita, D., Krishnan, S., Fox, R., et al. "Fast and Reliable Autonomous Surgical Debridement with Cable-Driven Robots Using a Two-Phase Calibration Procedure". In: *2018 IEEE International Conference on Robotics and Automation (ICRA)*. 2018, pp. 6651–6658. DOI: 10.1109/ICRA.2018.8460583.
[90] Wilcox, A., Kerr, J., Thananjeyan, B., et al. "Learning to Localize, Grasp, and Hand Over Unmodified Surgical Needles". In: *2022 International Conference on Robotics and Automation (ICRA)*. 2022, pp. 9637–9643. DOI: 10.1109/ICRA46639.2022.9812393.
[91] Zhong, F., Wang, Y., Wang, Z., et al. "Dual-Arm Robotic Needle Insertion With Active Tissue Deformation for Autonomous Suturing". In: *IEEE Robotics and Automation Letters* 4.3 (2019), pp. 2669–2676. DOI: 10.1109/LRA.2019.2913082.
[92] Sundaresan, P., Thananjeyan, B., Chiu, J., et al. "Automated Extraction of Surgical Needles from Tissue Phantoms". In: *2019 IEEE 15th International Conference on Automation Science and Engineering (CASE)*. 2019, pp. 170–177. DOI: 10.1109/COASE.2019.8843089.
[93] Hwang, M., Thananjeyan, B., Paradis, S., et al. "Efficiently Calibrating Cable-Driven Surgical Robots With RGBD Fiducial Sensing and Recurrent Neural Networks". In: *IEEE Robotics and Automation Letters* 5.4 (2020), pp. 5937–5944. DOI: 10.1109/LRA.2020.3010746.
[94] Hwang, M., Thananjeyan, B., Seita, D., et al. "Superhuman surgical peg transfer using depth-sensing and deep recurrent neural networks". In: *arXiv preprint arXiv:2012.12844* (2020).
[95] Hwang, M., Seita, D., Thananjeyan, B., et al. "Applying Depth-Sensing to Automated Surgical Manipulation with a da Vinci Robot". In: *2020 International Symposium on Medical Robotics (ISMR)*. 2020, pp. 22–29. DOI: 10.1109/ISMR48331.2020.9312948.
[96] Banach, A., Leibrandt, K., Grammatikopoulou, M., et al. "Active Contraints for Tool-Shaft Collision Avoidance in Minimally Invasive Surgery". In: *2019 International Conference on Robotics and Automation (ICRA)*. 2019, pp. 1556–1562. DOI: 10.1109/ICRA.2019.8794147.
[97] Zhong, F., Wang, Z., Chen, W., et al. "Hand-Eye Calibration of Surgical Instrument for Robotic Surgery Using Interactive Manipulation". In: *IEEE Robotics and Automation Letters* 5.2 (2020), pp. 1540–1547. DOI: 10.1109/LRA.2020.2967685.
[98] Morris, M., Shoham, M., and Nahon, M. "Applications and theoretical issues of cable-driven robots". In: *Proceedings of the Florida Conference on Recent Advances in Robotics, Boca Raton, FL, USA*. 2009, pp. 21–22.
[99] Haghighipanah, M., Miyasaka, M., Li, Y., et al. "Unscented kalman filter and 3d vision to improve cable driven surgical robot joint angle estimation". In: *2016 IEEE international conference on robotics and automation (ICRA)*. IEEE. 2016, pp. 4135–4142.
[100] Miyasaka, M., Matheson, J., Lewis, A., et al. "Measurement of the cable-pulley coulomb and viscous friction for a cable-driven surgical robotic system". In: *2015 IEEE/RSJ international conference on intelligent robots and systems (IROS)*. IEEE. 2015, pp. 804–810.
[101] Haghighipanah, M., Miyasaka, M., Li, Y., et al. "Unscented kalman filter and 3d vision to improve cable driven surgical robot joint angle estimation". In: *2016 IEEE international conference on robotics and automation (ICRA)*. IEEE. 2016, pp. 4135–4142.
[102] Chrysilla, G., Eusman, N., Deguet, A., et al. "A compliance model to improve the accuracy of the da Vinci Research Kit (dVRK)". In: *Acta Polytechnica Hungarica* 16.8 (2019).
[103] Huang, S. "Kinematic Calibration for da Vinci Surgical Robot". PhD thesis. Case Western Reserve University, 2019.
[104] Roth, Z., Mooring, B., and Ravani, B. "An overview of robot calibration". In: *IEEE Journal on Robotics and Automation* 3.5 (1987), pp. 377–385.

[105] Fattori, G., Lomax, A. J., Weber, D. C., et al. "Technical assessment of the NDI Polaris Vega optical tracking system". In: *Radiation oncology* 16.1 (2021), pp. 1–4.
[106] Richter, F., Lu, J., Orosco, R. K., et al. "Robotic Tool Tracking Under Partially Visible Kinematic Chain: A Unified Approach". In: *IEEE Transactions on Robotics* 38.3 (2022), pp. 1653–1670. DOI: 10.1109/TRO.2021.3111441.
[107] Ye, M., Zhang, L., Giannarou, S., et al. "Real-time 3d tracking of articulated tools for robotic surgery". In: *International conference on medical image computing and computer-assisted intervention*. Springer. 2016, pp. 386–394.
[108] Richter, F., Zhang, Y., Zhi, Y., et al. "Augmented reality predictive displays to help mitigate the effects of delayed telesurgery". In: *2019 International Conference on Robotics and Automation (ICRA)*. IEEE. 2019, pp. 444–450.
[109] Fontanelli, G. A., Ficuciello, F., Villani, L., et al. "Modelling and identification of the da Vinci Research Kit robotic arms". In: *2017 IEEE/RSJ International Conference on Intelligent Robots and Systems (IROS)*. 2017, pp. 1464–1469. DOI: 10.1109/IROS.2017.8205948.
[110] Yilmaz, N., Wu, J. Y., Kazanzides, P., et al. "Neural network based inverse dynamics identification and external force estimation on the da Vinci Research Kit". In: *2020 IEEE International Conference on Robotics and Automation (ICRA)*. IEEE. 2020, pp. 1387–1393.
[111] Wang, Y., Gondokaryono, R., Munawar, A., et al. "A convex optimization-based dynamic model identification package for the da Vinci Research Kit". In: *IEEE Robotics and Automation Letters* 4.4 (2019), pp. 3657–3664.
[112] Novoseltseva, A. "Force Feedback for the Patient Side Manipulator of the daVinci Research Kit". PhD thesis. Master's Thesis, Worcester Polytechnic Institute, 2018.
[113] Pachtrachai, K., Vasconcelos, F., Chadebecq, F., et al. "Adjoint transformation algorithm for hand–eye calibration with applications in robotic assisted surgery". In: *Annals of biomedical engineering* 46.10 (2018), pp. 1606–1620.
[114] Pachtrachai, K., Allan, M., Pawar, V., et al. "Hand-eye calibration for robotic assisted minimally invasive surgery without a calibration object". In: *2016 IEEE/RSJ International Conference on Intelligent Robots and Systems (IROS)*. 2016, pp. 2485–2491. DOI: 10.1109/IROS.2016.7759387.
[115] Horaud, R. and Dornaika, F. "Hand-eye calibration". In: *The international journal of robotics research* 14.3 (1995), pp. 195–210.
[116] Jiang, J., Luo, X., Luo, Q., et al. "An overview of hand-eye calibration". In: *The International Journal of Advanced Manufacturing Technology* (2021), pp. 1–21.
[117] Daniilidis, K. "Hand-eye calibration using dual quaternions". In: *The International Journal of Robotics Research* 18.3 (1999), pp. 286–298.
[118] Tsai, R. Y., Lenz, R. K., et al. "A new technique for fully autonomous and efficient 3 d robotics hand/eye calibration". In: *IEEE Transactions on robotics and automation* 5.3 (1989), pp. 345–358.
[119] Wang, Z., Liu, Z., Ma, Q., et al. "Vision-based calibration of dual RCM-based robot arms in human-robot collaborative minimally invasive surgery". In: *IEEE Robotics and Automation Letters* 3.2 (2017), pp. 672–679.
[120] Shiu, Y. C. and Ahmad, S. "Calibration of wrist-mounted robotic sensors by solving homogeneous transform equations of the form AX= XB". In: (1987).
[121] Zhuang, H., Roth, Z. S., and Sudhakar, R. "Simultaneous robot/world and tool/flange calibration by solving homogeneous transformation equations of the form AX= YB". In: *IEEE Transactions on Robotics and Automation* 10.4 (1994), pp. 549–554.

[122] Fischler, M. A. and Bolles, R. C. "Random sample consensus: a paradigm for model fitting with applications to image analysis and automated cartography". In: *Communications of the ACM* 24.6 (1981), pp. 381–395.
[123] Roberti, A., Piccinelli, N., Meli, D., et al. "Improving rigid 3-d calibration for robotic surgery". In: *IEEE Transactions on Medical Robotics and Bionics* 2.4 (2020), pp. 569–573.
[124] Özgüner, O., Shkurti, T., Huang, S., et al. "Camera-Robot Calibration for the Da Vinci Robotic Surgery System". In: *IEEE Transactions on Automation Science and Engineering* 17.4 (2020), pp. 2154–2161. DOI: 10.1109/TASE.2020.2986503.
[125] Wang, C., Cartucho, J., S. Elson, D., et al. "Towards Autonomous Control of Surgical Instruments using Adaptive-Fusion Tracking and Robot Self-Calibration". In: *2022 IEEE/RSJ International Conference on Intelligent Robots and Systems (IROS)*. 2022.
[126] Cartucho, J., Wang, C., Huang, B., et al. "An enhanced marker pattern that achieves improved accuracy in surgical tool tracking". In: *Computer Methods in Biomechanics and Biomedical Engineering: Imaging & Visualization* 10.4 (2022), pp. 400–408.
[127] Zhang, Z., Zhang, L., and Yang, G.-Z. "A computationally efficient method for hand–eye calibration". In: *International journal of computer assisted radiology and surgery* 12.10 (2017), pp. 1775–1787.
[128] Tsai, R. Y., Lenz, R. K., et al. "A new technique for fully autonomous and efficient 3 d robotics hand/eye calibration". In: *IEEE Transactions on robotics and automation* 5.3 (1989), pp. 345–358.
[129] Turner, J. D. and Junkins, J. L. "Optimal large-angle single-axis rotational maneuvers of flexible spacecraft". In: *Journal of Guidance and Control* 3.6 (1980), pp. 578–585.
[130] Shiu, Y. C. and Ahmad, S. "Calibration of wrist-mounted robotic sensors by solving homogeneous transform equations of the form AX= XB". In: (1987).
[131] Wang, C.-C. "Extrinsic calibration of a vision sensor mounted on a robot". In: *ieee Transactions on Robotics and Automation* 8.2 (1992), pp. 161–175.
[132] Park, F. C. and Martin, B. J. "Robot sensor calibration: solving AX= XB on the Euclidean group". In: *IEEE Transactions on Robotics and Automation* 10.5 (1994), pp. 717–721.
[133] Horaud, R. and Dornaika, F. "Hand-eye calibration". In: *The international journal of robotics research* 14.3 (1995), pp. 195–210.
[134] Daniilidis, K. "Hand-eye calibration using dual quaternions". In: *The International Journal of Robotics Research* 18.3 (1999), pp. 286–298.
[135] De Ma, S. "A self-calibration technique for active vision systems". In: *IEEE Transactions on Robotics and Automation* 12.1 (1996), pp. 114–120.
[136] Andreff, N., Horaud, R., and Espiau, B. "On-line hand-eye calibration". In: *Second International Conference on 3-D Digital Imaging and Modeling (Cat. No. PR00062)*. IEEE. 1999, pp. 430–436.
[137] Heller, J., Havlena, M., and Pajdla, T. "Globally optimal hand-eye calibration using branch-and-bound". In: *IEEE Transactions on Pattern Analysis and Machine Intelligence* 38.5 (2015), pp. 1027–1033.
[138] Zhao, Z. "Hand-eye calibration using convex optimization". In: *2011 IEEE International Conference on Robotics and Automation*. IEEE. 2011, pp. 2947–2952.
[139] Shah, M. "Solving the robot-world/hand-eye calibration problem using the Kronecker product". In: *Journal of Mechanisms and Robotics* 5.3 (2013), p. 031007.
[140] Zhuang, H., Roth, Z. S., and Sudhakar, R. "Simultaneous robot/world and tool/flange calibration by solving homogeneous transformation equations of the form AX= YB". In: *IEEE Transactions on Robotics and Automation* 10.4 (1994), pp. 549–554.

[141] Hirsh, R. L., DeSouza, G. N., and Kak, A. C. "An iterative approach to the hand-eye and base-world calibration problem". In: *Proceedings 2001 ICRA. IEEE International Conference on Robotics and Automation (Cat. No. 01CH37164)*. Vol. 3. IEEE. 2001, pp. 2171–2176.

[142] Dornaika, F. and Horaud, R. "Simultaneous robot-world and hand-eye calibration". In: *IEEE transactions on Robotics and Automation* 14.4 (1998), pp. 617–622.

[143] Strobl, K. H. and Hirzinger, G. "Optimal hand-eye calibration". In: *2006 IEEE/RSJ international conference on intelligent robots and systems*. IEEE. 2006, pp. 4647–4653.

[144] Zhao, Z. "Simultaneous robot-world and hand-eye calibration by the alternative linear programming". In: *Pattern Recognition Letters* 127 (2019), pp. 174–180.

[145] Li, A., Wang, L., and Wu, D. "Simultaneous robot-world and hand-eye calibration using dual-quaternions and Kronecker product". In: *Int. J. Phys. Sci* 5.10 (2010), pp. 1530–1536.

[146] Allan, M., Ourselin, S., Hawkes, D. J., et al. "3-D pose estimation of articulated instruments in robotic minimally invasive surgery". In: *IEEE transactions on medical imaging* 37.5 (2018), pp. 1204–1213.

[147] Hao, R., Özgüner, O., and Çavuşoğlu, M. C. "Vision-Based Surgical Tool Pose Estimation for the da Vinci® Robotic Surgical System". In: *2018 IEEE/RSJ International Conference on Intelligent Robots and Systems (IROS)*. 2018, pp. 1298–1305. DOI: 10.1109/IROS.2018.8594471.

[148] Lu, J., Richter, F., and Yip, M. C. "Pose estimation for robot manipulators via keypoint optimization and sim-to-real transfer". In: *IEEE Robotics and Automation Letters* 7.2 (2022), pp. 4622–4629.

[149] Baek, Y. M., Tanaka, S., Harada, K., et al. "Robust visual tracking of robotic forceps under a microscope using kinematic data fusion". In: *IEEE/ASME Transactions on Mechatronics* 19.1 (2012), pp. 278–288.

[150] Thrun, S. "Particle Filters in Robotics." In: *UAI*. Vol. 2. Citeseer. 2002, pp. 511–518.

[151] Doignon, C. and Mathelin, M. de. "A Degenerate Conic-Based Method for a Direct Fitting and 3-D Pose of Cylinders with a Single Perspective View". In: *Proceedings 2007 IEEE International Conference on Robotics and Automation*. 2007, pp. 4220–4225. DOI: 10.1109/ROBOT.2007.364128.

[152] Lu, B., Li, B., Dou, Q., et al. "A Unified Monocular Camera-Based and Pattern-Free Hand-to-Eye Calibration Algorithm for Surgical Robots With RCM Constraints". In: *IEEE/ASME Transactions on Mechatronics* 27.6 (2022), pp. 5124–5135. DOI: 10.1109/TMECH.2022.3166522.

[153] Becke, M. and Schlegl, T. "Least squares pose estimation of cylinder axes from multiple views using contour line features". In: *IECON 2015 - 41st Annual Conference of the IEEE Industrial Electronics Society*. 2015, pp. 001855–001861. DOI: 10.1109/IECON.2015.7392371.

[154] Canny, J. "A Computational Approach to Edge Detection". In: *IEEE Transactions on Pattern Analysis and Machine Intelligence* PAMI-8.6 (1986), pp. 679–698. DOI: 10.1109/TPAMI.1986.4767851.

[155] Moré, J. J. "The Levenberg-Marquardt algorithm: implementation and theory". In: *Numerical analysis: proceedings of the biennial Conference held at Dundee, June 28–July 1, 1977*. Springer. 2006, pp. 105–116.

[156] Hartley, R. and Zisserman, A. *Multiple view geometry in computer vision*. Cambridge university press, 2003.

[157] Wilson, J. T., Tsao, T.-C., Hubschman, J.-P., et al. "Evaluating remote centers of motion for minimally invasive surgical robots by computer vision". In: *2010 IEEE/ASME International Conference on Advanced Intelligent Mechatronics*. 2010, pp. 1413–1418. DOI: 10.1109/AIM.2010.5695924.

[158] Kazanzides, P., Chen, Z., Deguet, A., et al. "An Open-Source Research Kit for the da Vinci Surgical System". In: *IEEE Intl. Conf. on Robotics and Auto. (ICRA)*. Hong Kong, China, June 1, 2014, pp. 6434–6439.
[159] Bradski, G., Kaehler, A., et al. "OpenCV". In: *Dr. Dobb's journal of software tools* 3.2 (2000).
[160] Duda, R. O. and Hart, P. E. "Use of the Hough transformation to detect lines and curves in pictures". In: *Communications of the ACM* 15.1 (1972), pp. 11–15.
[161] Kirillov, A., Mintun, E., Ravi, N., et al. "Segment anything". In: *arXiv preprint arXiv:2304.02643* (2023).
[162] Zhuang, Y. and Canny, J. "Haptic interaction with global deformations". In: *Proceedings 2000 ICRA. Millennium Conference. IEEE International Conference on Robotics and Automation. Symposia Proceedings (Cat. No.00CH37065)*. Vol. 3. 2000, 2428–2433 vol.3. DOI: 10.1109/ROBOT.2000.846391.
[163] Kosari, S. N., Rydén, F., Lendvay, T. S., et al. "Forbidden region virtual fixtures from streaming point clouds". In: *Advanced Robotics* 28.22 (2014), pp. 1507–1518. DOI: 10.1080/01691864.2014.962613.
[164] Yamamoto, T., Abolhassani, N., Jung, S., et al. "Augmented reality and haptic interfaces for robot-assisted surgery". In: *The International Journal of Medical Robotics and Computer Assisted Surgery* 8.1 (2012), pp. 45–56.
[165] Myronenko, A. and Song, X. "Point set registration: Coherent point drift". In: *IEEE transactions on pattern analysis and machine intelligence* 32.12 (2010), pp. 2262–2275.
[166] Hirose, O. "A Bayesian formulation of coherent point drift". In: *IEEE transactions on pattern analysis and machine intelligence* 43.7 (2020), pp. 2269–2286.
[167] Hirose, O. "Acceleration of non-rigid point set registration with downsampling and Gaussian process regression". In: *IEEE Transactions on Pattern Analysis and Machine Intelligence* 43.8 (2020), pp. 2858–2865.
[168] Yang, H., Shi, J., and Carlone, L. "TEASER: Fast and Certifiable Point Cloud Registration". In: *IEEE Trans. Robotics* (2020).
[169] Rusu, R. B., Blodow, N., and Beetz, M. "Fast point feature histograms (FPFH) for 3D registration". In: *2009 IEEE international conference on robotics and automation*. IEEE. 2009, pp. 3212–3217.
[170] Community, B. O. *Blender - a 3D modelling and rendering package*. Blender Foundation. Stichting Blender Foundation, Amsterdam, 2018.
[171] Sailer, A. M., Wagemans, B. A., Das, M., et al. "Quantification of respiratory movement of the aorta and side branches". In: *Journal of Endovascular Therapy* 22.6 (2015), pp. 905–911.
[172] Raibert, M. H. and Craig, J. J. "Hybrid position/force control of manipulators". In: (1981).
[173] Zhou, Q.-Y., Park, J., and Koltun, V. "Open3D: A Modern Library for 3D Data Processing". In: *arXiv:1801.09847* (2018).
[174] Enayati, N., Ferrigno, G., and De Momi, E. "Performance metrics for guidance active constraints in surgical robotics". In: *The International Journal of Medical Robotics and Computer Assisted Surgery* 14.1 (2018), e1873.
[175] Huang, K., Chitrakar, D., Rydén, F., et al. "Evaluation of haptic guidance virtual fixtures and 3D visualization methods in telemanipulation—a user study". In: *Intelligent Service Robotics* 12.4 (2019), pp. 289–301.
[176] Ma, J., He, Y., Li, F., et al. "Segment anything in medical images". In: *Nature Communications* 15.1 (2024), p. 654.

Appendices

A Questionnaire study among dVRK users

The questionnaire consists of three sections, corresponding to kinematic/dynamics data (data from the PSMs, ECM, and SSMs), imaging data (images captured by the dVRK's endoscope), and system data (e.g., signals from the foot pedals for teleoperation), respectively. For each section, users first need to answer a yes-or-no question to determine if they have used the type of data before. If not, they could skip to the next section; otherwise, they are instructed to point out the sources of error in that data type which they reckon may have affected their research results. Users are prompted to identify the sources of error from a list of selected options that were gathered from literature review and consultation with leading researchers. In addition, the participants are also available to put in other potential sources of error by themselves. A total of 35 responses have been collected from 20 different institutions, summarized as follows:

A.1 Kinematics and dynamics data

Approximately 95% of the participants have experience in dealing with kinematics and dynamics data. The most commonly identified problems are "inaccurate forward-kinematics" (66%) and "inaccurate hand-eye calibration" (66%), followed by issues with the surgical instruments (56%), and "inaccurate potentiometer calibration" (50%), as shown in Figure A.1.

A.2 Imaging data

Approximately 70% of the participants have experience in dealing with imaging data streamed from the endoscope of the dVRK. The most commonly identified problem with imaging data is "inaccurate camera calibration" (83%), followed by "low pixel resolution" (65%), as shown in Figure A.1.

In addition to the sources of error listed from the selection box, 20% of the participants have reflected that there is a significant difference between the left and right image, mainly perceived as colour mismatch. Also, 13% of the participants have pointed out the presence of noise in the images.

A.3 System state data

Approximately 30% of the participants have experience in dealing with system state data. No significant sources of error have been identified here.

A.4 Questionnaire Analysis

It is also discovered that a significant percentage of dVRK users are either not aware of the necessity for certain calibrations, or not familiar with the methods for certain calibrations. Specifically, 40% of the users are not aware that the camera intrinsic parameters are not constant; 20% are not aware of the methods for kinematics calibration, and 30% are not aware of potentiometer calibration. In addition, 25% of the users reported that they bypassed hand-eye calibration in their research, which can be explained by the fact that some institutes mainly use the dVRKs for the purpose of training or conducting user studies, where the human element makes redundant the hand-eye calibration.

After discussions with the participants, it is gathered that 63% of the dVRK users are dissatisfied with the current standard definition Standard-Definition (SD) cameras on the first generation dVRK. It is suggested from our analysis that the incorporation of cameras with high-definition High-Definition (HD) and a faster frame rate into the dVRK system would be preferable, such that the image data would be better synchronized with the kinematics data, thereby contributing towards better system functionality and usability.

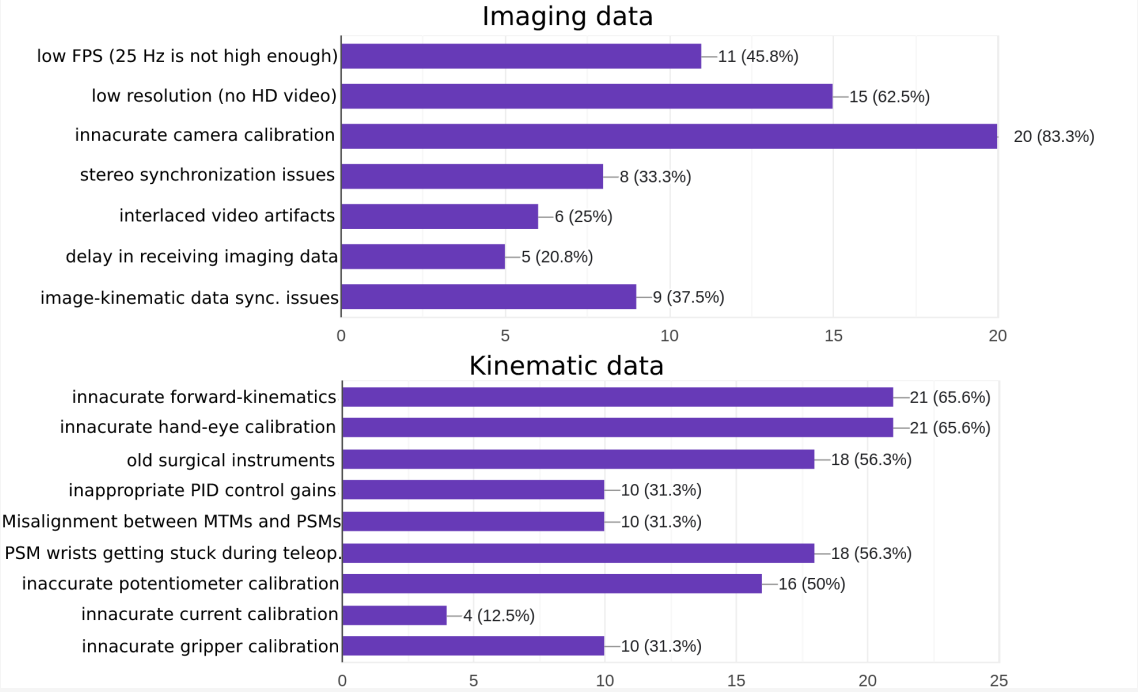


Figure A.1: Questionnaire study among dVRK users.

B Figure Licenses

This section of the appendix lists the copyright licenses for reused images across this thesis. Specifically, the following licenses are listed in order:

1. Figure 2.1 on page 31
2. Figure 2.2 on page 32
3. Figure 2.4 on page 34
4. Figure 2.6 on page 41, Figure 2.7 on page 42
5. Figure 3.7 on page 76

Marketplace

Order Number: 1560058
Order Date: 26 Dec 2024

Payment Information

Zejian Cui
zejian.cui19@imperial.ac.uk
Payment method: Invoice

Billing Address:
Mr. Zejian Cui
Friendship House
London, SE1 0AD
United Kingdom

+44 7419921105
zejian.cui19@imperial.ac.uk

Customer Location:
Mr. Zejian Cui
Friendship House
London, SE1 0AD
United Kingdom

Order Details

1. Gynecologic oncology

Billing Status: Open

Article: Emergence of robotic assisted surgery in gynecologic oncology: American perspective.

Order License ID	1560058-1	**Type of Use**	Republish in a thesis/dissertation
Order detail status	Completed	**Publisher**	ACADEMIC PRESS
ISSN	1095-6859	**Portion**	Image/photo/illustration

0.00 USD
Republication Permission

LICENSED CONTENT

Publication Title	Gynecologic oncology	**Publication Type**	e-Journal
Article Title	Emergence of robotic assisted surgery in gynecologic oncology: American perspective.	**Start Page**	S24
		End Page	S31
		Issue	2 Suppl
Author / Editor	Society of Gynecologic Oncologists.	**Volume**	114
		URL	http://www.sciencedirect.com/science/journal/00908258
Date	01/01/1972		
Language	English		
Country	United States of America		
Rightsholder	Elsevier Science & Technology Journals		

REQUEST DETAILS

Portion Type	Image/photo/illustration	**Distribution**	Worldwide
Number of Images / Photos / Illustrations	1	**Translation**	Original language of publication
Format (select all that apply)	Electronic	**Copies for the Disabled?**	No
		Minor Editing Privileges?	No
Who Will Republish the Content?	Academic institution	**Incidental Promotional Use?**	No
		Currency	USD
Duration of Use	Life of current edition		
Lifetime Unit Quantity	Up to 499		
Rights Requested	Main product		

NEW WORK DETAILS

Title	Mr	**Institution Name**	Imperial College London
Instructor Name	Zejian Cui	**Expected Presentation Date**	2025-04-30

ADDITIONAL DETAILS

The Requesting Person / Organization to Appear on the License	Zejian Cui

REQUESTED CONTENT DETAILS

Title, Description or Numeric Reference of the Portion(s)	zeus robot	**Title of the Article / Chapter the Portion Is From**	Emergence of robotic assisted surgery in gynecologic oncology: American perspective.
Editor of Portion(s)	Mendivil, Alberto; Holloway, Robert W.; Boggess, John F.	**Author of Portion(s)**	Mendivil, Alberto; Holloway, Robert W.; Boggess, John F.
Volume / Edition	114		
Page or Page Range of Portion	S24-S31	**Issue, if Republishing an Article From a Serial**	2 Suppl
		Publication Date of Portion	2009-08-01

Elsevier Science & Technology Journals Terms and Conditions

Elsevier publishes Open Access articles in both its Open Access journals and via its Open Access articles option in subscription journals, for which an author selects a user license permitting certain types of reuse without permission. Before proceeding please check if the article is Open Access on http://www.sciencedirect.com and refer to the user license for the individual article. Any reuse not included in the user license terms will require permission. You must always fully and appropriately credit the author and source. If any part of the material to be used (for example, figures) has appeared in the Elsevier publication for which you are seeking permission, with credit or acknowledgement to another source it is the responsibility of the user to ensure their reuse complies with the terms and conditions determined by the rights holder. Please contact permissions@elsevier.com with any queries.

Total Items: 1

Subtotal: 0.00 USD

Order Total: 0.00 USD

Marketplace Permissions General Terms and Conditions

The following terms and conditions ("General Terms"), together with any applicable Publisher Terms and Conditions, govern User's use of Works pursuant to the Licenses granted by Copyright Clearance Center, Inc. ("CCC") on behalf of the applicable Rightsholders of such Works through CCC's applicable Marketplace transactional licensing services (each, a "Service").

1) **Definitions.** For purposes of these General Terms, the following definitions apply:

"License" is the licensed use the User obtains via the Marketplace platform in a particular licensing transaction, as set forth in the Order Confirmation.

"Order Confirmation" is the confirmation CCC provides to the User at the conclusion of each Marketplace transaction. "Order Confirmation Terms" are additional terms set forth on specific Order Confirmations not set forth in the General Terms that can include terms applicable to a particular CCC transactional licensing service and/or any Rightsholder-specific terms.

"Rightsholder(s)" are the holders of copyright rights in the Works for which a User obtains licenses via the Marketplace platform, which are displayed on specific Order Confirmations.

"Terms" means the terms and conditions set forth in these General Terms and any additional Order Confirmation Terms collectively.

"User" or "you" is the person or entity making the use granted under the relevant License. Where the person accepting the Terms on behalf of a User is a freelancer or other third party who the User authorized to accept the General Terms on the User's behalf, such person shall be deemed jointly a User for purposes of such Terms.

"Work(s)" are the copyright protected works described in relevant Order Confirmations.

2) **Description of Service.** CCC's Marketplace enables Users to obtain Licenses to use one or more Works in accordance with all relevant Terms. CCC grants Licenses as an agent on behalf of the copyright rightsholder identified in the relevant Order Confirmation.

3) **Applicability of Terms.** The Terms govern User's use of Works in connection with the relevant License. In the event of any conflict between General Terms and Order Confirmation Terms, the latter shall govern. User acknowledges that Rightsholders have complete discretion whether to grant any permission, and whether to place any limitations on any grant, and that CCC has no right to supersede or to modify any such discretionary act by a Rightsholder.

4) **Representations; Acceptance.** By using the Service, User represents and warrants that User has been duly authorized by the User to accept, and hereby does accept, all Terms.

5) **Scope of License; Limitations and Obligations.** All Works and all rights therein, including copyright rights, remain the sole and exclusive property of the Rightsholder. The License provides only those rights expressly set forth in the terms and conveys no other rights in any Works

6) **General Payment Terms.** User may pay at time of checkout by credit card or choose to be invoiced. If the User chooses to be invoiced, the User shall: (i) remit payments in the manner identified on specific invoices, (ii) unless otherwise specifically stated in an

Order Confirmation or separate written agreement, Users shall remit payments upon receipt of the relevant invoice from CCC, either by delivery or notification of availability of the invoice via the Marketplace platform, and (iii) if the User does not pay the invoice within 30 days of receipt, the User may incur a service charge of 1.5% per month or the maximum rate allowed by applicable law, whichever is less. While User may exercise the rights in the License immediately upon receiving the Order Confirmation, the License is automatically revoked and is null and void, as if it had never been issued, if CCC does not receive complete payment on a timely basis.

7) **General Limits on Use.** Unless otherwise provided in the Order Confirmation, any grant of rights to User (i) involves only the rights set forth in the Terms and does not include subsequent or additional uses, (ii) is non-exclusive and non-transferable, and (iii) is subject to any and all limitations and restrictions (such as, but not limited to, limitations on duration of use or circulation) included in the Terms. Upon completion of the licensed use as set forth in the Order Confirmation, User shall either secure a new permission for further use of the Work(s) or immediately cease any new use of the Work(s) and shall render inaccessible (such as by deleting or by removing or severing links or other locators) any further copies of the Work. User may only make alterations to the Work if and as expressly set forth in the Order Confirmation. No Work may be used in any way that is unlawful, including without limitation if such use would violate applicable sanctions laws or regulations, would be defamatory, violate the rights of third parties (including such third parties' rights of copyright, privacy, publicity, or other tangible or intangible property), or is otherwise illegal, sexually explicit, or obscene. In addition, User may not conjoin a Work with any other material that may result in damage to the reputation of the Rightsholder. Any unlawful use will render any licenses hereunder null and void. User agrees to inform CCC if it becomes aware of any infringement of any rights in a Work and to cooperate with any reasonable request of CCC or the Rightsholder in connection therewith.

8) **Third Party Materials.** In the event that the material for which a License is sought includes third party materials (such as photographs, illustrations, graphs, inserts and similar materials) that are identified in such material as having been used by permission (or a similar indicator), User is responsible for identifying, and seeking separate licenses (under this Service, if available, or otherwise) for any of such third party materials; without a separate license, User may not use such third party materials via the License.

9) **Copyright Notice.** Use of proper copyright notice for a Work is required as a condition of any License granted under the Service. Unless otherwise provided in the Order Confirmation, a proper copyright notice will read substantially as follows: "Used with permission of [Rightsholder's name], from [Work's title, author, volume, edition number and year of copyright]; permission conveyed through Copyright Clearance Center, Inc." Such notice must be provided in a reasonably legible font size and must be placed either on a cover page or in another location that any person, upon gaining access to the material which is the subject of a permission, shall see, or in the case of republication Licenses, immediately adjacent to the Work as used (for example, as part of a by-line or footnote) or in the place where substantially all other credits or notices for the new work containing the republished Work are located. Failure to include the required notice results in loss to the Rightsholder and CCC, and the User shall be liable to pay liquidated damages for each such failure equal to twice the use fee specified in the Order Confirmation, in addition to the use fee itself and any other fees and charges specified.

10) **Indemnity.** User hereby indemnifies and agrees to defend the Rightsholder and CCC, and their respective employees and directors, against all claims, liability, damages, costs, and expenses, including legal fees and expenses, arising out of any use of a Work beyond the scope of the rights granted herein and in the Order Confirmation, or any use of a Work which has been altered in any unauthorized way by User, including claims of defamation or infringement of rights of copyright, publicity, privacy, or other tangible or intangible property.

11) **Limitation of Liability.** UNDER NO CIRCUMSTANCES WILL CCC OR THE RIGHTSHOLDER BE LIABLE FOR ANY DIRECT, INDIRECT, CONSEQUENTIAL, OR INCIDENTAL DAMAGES (INCLUDING WITHOUT LIMITATION DAMAGES FOR LOSS OF BUSINESS PROFITS OR INFORMATION, OR FOR BUSINESS INTERRUPTION) ARISING OUT OF THE USE OR INABILITY TO USE A WORK, EVEN IF ONE OR BOTH OF THEM HAS BEEN ADVISED OF THE POSSIBILITY OF SUCH DAMAGES. In any event, the total liability of the Rightsholder and CCC (including their respective employees and directors) shall not exceed the total amount actually paid by User for the relevant License. User assumes full liability for the actions and omissions of its principals, employees, agents, affiliates, successors, and assigns.

12) **Limited Warranties.** THE WORK(S) AND RIGHT(S) ARE PROVIDED "AS IS." CCC HAS THE RIGHT TO GRANT TO USER THE RIGHTS GRANTED IN THE ORDER CONFIRMATION DOCUMENT. CCC AND THE RIGHTSHOLDER DISCLAIM ALL OTHER WARRANTIES RELATING TO THE WORK(S) AND RIGHT(S), EITHER EXPRESS OR IMPLIED, INCLUDING WITHOUT LIMITATION IMPLIED WARRANTIES OF MERCHANTABILITY OR FITNESS FOR A PARTICULAR PURPOSE. ADDITIONAL RIGHTS MAY BE REQUIRED TO USE ILLUSTRATIONS, GRAPHS, PHOTOGRAPHS, ABSTRACTS, INSERTS, OR OTHER PORTIONS OF THE WORK (AS OPPOSED TO THE ENTIRE WORK) IN A MANNER CONTEMPLATED BY USER; USER UNDERSTANDS AND AGREES THAT NEITHER CCC NOR THE RIGHTSHOLDER MAY HAVE SUCH ADDITIONAL RIGHTS TO GRANT.

13) **Effect of Breach.** Any failure by User to pay any amount when due, or any use by User of a Work beyond the scope of the License set forth in the Order Confirmation and/or the Terms, shall be a material breach of such License. Any breach not cured within 10 days of written notice thereof shall result in immediate termination of such License without further notice. Any unauthorized (but licensable) use of a Work that is terminated immediately upon notice thereof may be liquidated by payment of the Rightsholder's ordinary license price therefor; any unauthorized (and unlicensable) use that is not terminated immediately for any reason (including, for example, because materials containing the Work cannot reasonably be recalled) will be subject to all remedies available at law or in equity, but in no event to a payment of less than three times the Rightsholder's ordinary license price for the most closely analogous licensable use plus Rightsholder's and/or CCC's costs and expenses incurred in collecting such payment.

14) **Additional Terms for Specific Products and Services.** If a User is making one of the uses described in this Section 14, the additional terms and conditions apply:

a) ***Print Uses of Academic Course Content and Materials (photocopies for academic coursepacks or classroom handouts).*** For photocopies for academic coursepacks or classroom handouts the following additional terms apply:

i) The copies and anthologies created under this License may be made and assembled by faculty members individually or at their request by on-campus bookstores or copy centers, or by off-campus copy shops and other similar entities.

ii) No License granted shall in any way: (i) include any right by User to create a substantively non-identical copy of the Work or to edit or in any other way modify the Work (except by means of deleting material immediately preceding or following the entire portion of the Work copied) (ii) permit "publishing ventures" where any particular anthology would be systematically marketed at multiple institutions.

iii) Subject to any Publisher Terms (and notwithstanding any apparent contradiction in the Order Confirmation arising from data provided by User), any use authorized under the academic pay-per-use service is limited as follows:

A) any License granted shall apply to only one class (bearing a unique identifier as assigned by the institution, and thereby including all sections or other subparts of the class) at one institution;

B) use is limited to not more than 25% of the text of a book or of the items in a published collection of essays, poems or articles;

C) use is limited to no more than the greater of (a) 25% of the text of an issue of a journal or other periodical or (b) two articles from such an issue;

D) no User may sell or distribute any particular anthology, whether photocopied or electronic, at more than one institution of learning;

E) in the case of a photocopy permission, no materials may be entered into electronic memory by User except in order to produce an identical copy of a Work before or during the academic term (or analogous period) as to which any particular permission is granted. In the event that User shall choose to retain materials that are the subject of a photocopy permission in electronic memory for purposes of producing identical copies more than one day after such retention (but still within the scope of any permission granted), User must notify CCC of such fact in the applicable permission request and such retention shall constitute one copy actually sold for purposes of calculating permission fees due; and

F) any permission granted shall expire at the end of the class. No permission granted shall in any way include any right by User to create a substantively non-identical copy of the Work or to edit or in any other way modify the Work (except by means of deleting material immediately preceding or following the entire portion of the Work copied).

iv) Books and Records; Right to Audit. As to each permission granted under the academic pay-per-use Service, User shall maintain for at least four full calendar years books and records sufficient for CCC to determine the numbers of copies made by User under such permission. CCC and any representatives it may designate shall have the right to audit such books and records at any time during User's ordinary business hours, upon two days' prior notice. If any such audit shall determine that User shall have underpaid for, or underreported, any photocopies sold or by three percent (3%) or more, then User shall bear all the costs of any such audit; otherwise, CCC shall bear the costs of any such audit. Any amount determined by such audit to have been underpaid by User shall immediately be paid to CCC by User, together with interest thereon at the rate of 10% per annum from the date such amount was originally due. The provisions of this paragraph shall survive the termination of this License for any reason.

b) ***Digital Pay-Per-Uses of Academic Course Content and Materials (e-coursepacks, electronic reserves, learning management systems, academic institution intranets).*** For uses in e-coursepacks, posts in electronic reserves, posts in learning management systems, or posts on academic institution intranets, the following additional terms apply:

i) The pay-per-uses subject to this Section 14(b) include:

A) **Posting e-reserves, course management systems, e-coursepacks for text-based content,** which grants authorizations to import requested material in electronic format, and allows electronic access to this material to members of a designated college or university class, under the direction of an instructor designated by the college or university, accessible only under appropriate electronic controls (e.g., password);

B) **Posting e-reserves, course management systems, e-coursepacks for material consisting of photographs or other still images not embedded in text,** which grants not only the authorizations described in Section 14(b)(i)(A) above, but also the following authorization: to include the requested material in course materials for use consistent with Section 14(b)(i)(A) above, including any necessary resizing, reformatting or modification of the resolution of such requested material (provided that such modification does not alter the underlying editorial content or meaning of the requested material, and provided that the resulting modified content is used solely within the scope of, and in a manner consistent with, the particular authorization described in the Order Confirmation and the Terms), but not including any other form of manipulation, alteration or editing of the requested material;

C) **Posting e-reserves, course management systems, e-coursepacks or other academic distribution for audiovisual content,** which grants not only the authorizations described in Section 14(b)(i)(A) above, but also the following authorizations: (i) to include the requested material in course materials for use consistent with Section 14(b)(i)(A) above; (ii) to display and perform the requested material to such members of such class in the physical classroom or remotely by means of streaming media or other video formats; and (iii) to "clip" or reformat the requested material for purposes of time or content management or ease of delivery, provided that such "clipping" or reformatting does not alter the underlying editorial content or meaning of the requested material and that the resulting material is used solely within the scope of, and in a manner consistent with, the particular authorization described in the Order Confirmation and the Terms.

Unless expressly set forth in the relevant Order Conformation, the License does not authorize any other form of manipulation, alteration or editing of the requested material.

ii) Unless expressly set forth in the relevant Order Confirmation, no License granted shall in any way: (i) include any right by User to create a substantively non-identical copy of the Work or to edit or in any other way modify the Work (except by means of deleting material immediately preceding or following the entire portion of the Work copied or, in the case of Works subject to Sections 14(b)(1)(B) or (C) above, as described in such Sections) (ii) permit "publishing ventures" where any particular course materials would be systematically marketed at multiple institutions.

iii) Subject to any further limitations determined in the Rightsholder Terms (and notwithstanding any apparent contradiction in the Order Confirmation arising from data provided by User), any use authorized under the electronic course content pay-per-use service is limited as follows:

A) any License granted shall apply to only one class (bearing a unique identifier as assigned by the institution, and thereby including all sections or other subparts of the class) at one institution;

B) use is limited to not more than 25% of the text of a book or of the items in a published collection of essays, poems or articles;

C) use is limited to not more than the greater of (a) 25% of the text of an issue of a journal or other periodical or (b) two articles from such an issue;

D) no User may sell or distribute any particular materials, whether photocopied or electronic, at more than one institution of learning;

E) electronic access to material which is the subject of an electronic-use permission must be limited by means of electronic password, student identification or other control permitting access solely to students and instructors in the class;

F) User must ensure (through use of an electronic cover page or other appropriate means) that any person, upon gaining electronic access to the material, which is the subject of a permission, shall see:

- a proper copyright notice, identifying the Rightsholder in whose name CCC has granted permission,
- a statement to the effect that such copy was made pursuant to permission,
- a statement identifying the class to which the material applies and notifying the reader that the material has been made available electronically solely for use in the class, and
- a statement to the effect that the material may not be further distributed to any person outside the class, whether by copying or by transmission and whether electronically or in paper form, and User must also ensure that such cover page or other means will print out in the event that the person accessing the material chooses to print out the material or any part thereof.

G) any permission granted shall expire at the end of the class and, absent some other form of authorization, User is thereupon required to delete the applicable material from any electronic storage or to block electronic access to the applicable material.

iv) Uses of separate portions of a Work, even if they are to be included in the same course material or the same university or college class, require separate permissions under the electronic course content pay-per-use Service. Unless otherwise provided in the Order Confirmation, any grant of rights to User is limited to use completed no later than the end of the academic term (or analogous period) as to which any particular permission is granted.

v) Books and Records; Right to Audit. As to each permission granted under the electronic course content Service, User shall maintain for at least four full calendar years books and records sufficient for CCC to determine the numbers of copies made by User under such permission. CCC and any representatives it may designate shall have the right to audit such books and records at any time during User's ordinary business hours, upon two days' prior notice. If any such audit shall determine that User shall have underpaid for, or underreported, any electronic copies used by three percent (3%) or more, then User shall bear all the costs of any such audit; otherwise, CCC shall bear the costs of any such audit. Any amount determined by such audit to have been underpaid by User shall immediately be paid to CCC by User, together with interest thereon at the rate of 10% per annum from the date such amount was originally due. The provisions of this paragraph shall survive the termination of this license for any reason.

c) ***Pay-Per-Use Permissions for Certain Reproductions (Academic photocopies for library reserves and interlibrary loan reporting) (Non-academic internal/external business uses and commercial document delivery).*** The License expressly excludes the uses listed in Section (c)(i)-(v) below (which must be subject to separate license from the applicable Rightsholder) for: academic photocopies for library reserves and interlibrary loan reporting; and non-academic internal/external business uses and commercial document delivery.

i) electronic storage of any reproduction (whether in plain-text, PDF, or any other format) other than on a transitory basis;

ii) the input of Works or reproductions thereof into any computerized database;

iii) reproduction of an entire Work (cover-to-cover copying) except where the Work is a single article;

iv) reproduction for resale to anyone other than a specific customer of User;

v) republication in any different form. Please obtain authorizations for these uses through other CCC services or directly from the rightsholder.

Any license granted is further limited as set forth in any restrictions included in the Order Confirmation and/or in these Terms.

d) ***Electronic Reproductions in Online Environments (Non-Academic-email, intranet, internet and extranet).*** For "electronic reproductions", which generally includes e-mail use (including instant messaging or other electronic transmission to a defined group of recipients) or posting on an intranet, extranet or Intranet site (including any display or performance incidental thereto), the following additional terms apply:

i) Unless otherwise set forth in the Order Confirmation, the License is limited to use completed within 30 days for any use on the Internet, 60 days for any use on an intranet or extranet and one year for any other use, all as measured from the "republication date" as identified in the Order Confirmation, if any, and otherwise from the date of the Order Confirmation.

ii) User may not make or permit any alterations to the Work, unless expressly set forth in the Order Confirmation (after request by User and approval by Rightsholder); provided, however, that a Work consisting of photographs or other still images not embedded in text may, if necessary, be resized, reformatted or have its resolution modified without additional express permission, and a Work consisting of audiovisual content may, if necessary, be "clipped" or reformatted for purposes of time or content management or ease of delivery (provided that any such resizing, reformatting, resolution modification or "clipping" does not alter the underlying editorial content or meaning of the Work used, and that the resulting material is used solely within the scope of, and in a manner consistent with, the particular License described in the Order Confirmation and the Terms.

15) **Miscellaneous.**

a) User acknowledges that CCC may, from time to time, make changes or additions to the Service or to the Terms, and that Rightsholder may make changes or additions to the Rightsholder Terms. Such updated Terms will replace the prior terms and conditions in the order workflow and shall be effective as to any subsequent Licenses but shall not apply to Licenses already granted and paid for under a prior set of terms.

b) Use of User-related information collected through the Service is governed by CCC's privacy policy, available online at www.copyright.com/about/privacy-policy/.

c) The License is personal to User. Therefore, User may not assign or transfer to any other person (whether a natural person or an organization of any kind) the License or any rights granted thereunder; provided, however, that, where applicable, User may assign such License in its entirety on written notice to CCC in the event of a transfer of all or substantially all of User's rights in any new material which includes the Work(s) licensed under this Service.

d) No amendment or waiver of any Terms is binding unless set forth in writing and signed by the appropriate parties, including, where applicable, the Rightsholder. The Rightsholder and CCC hereby object to any terms contained in any writing prepared by or on behalf of the User or its principals, employees, agents or affiliates and purporting to govern or otherwise relate to the License described in the Order Confirmation, which terms are in any way inconsistent with any Terms set forth in the Order Confirmation, and/or in CCC's standard operating procedures, whether such writing is prepared prior to, simultaneously with or subsequent to the Order Confirmation, and whether such writing appears on a copy of the Order Confirmation or in a separate instrument.

e) The License described in the Order Confirmation shall be governed by and construed under the law of the State of New York, USA, without regard to the principles thereof of conflicts of law. Any case, controversy, suit, action, or proceeding arising out of, in connection with, or related to such License shall be brought, at CCC's sole discretion, in any federal or state court located in the County of New York, State of New York, USA, or in any federal or state court whose geographical jurisdiction covers the location of the Rightsholder set forth in the Order Confirmation. The parties expressly submit to the personal jurisdiction and venue of each such federal or state court.

Last updated October 2022

Marketplace

Order Number: 1560051
Order Date: 26 Dec 2024

Payment Information

Zejian Cui
zejian.cui19@imperial.ac.uk
Payment method: Invoice

Billing Address:
Mr. Zejian Cui
Friendship House
London, SE1 0AD
United Kingdom

+44 7419921105
zejian.cui19@imperial.ac.uk

Customer Location:
Mr. Zejian Cui
Friendship House
London, SE1 0AD
United Kingdom

Order Details

1. Journal of robotic surgery

Billing Status: Open

Article: Robot-assisted vascular surgery: literature review, clinical applications, and future perspectives

Order License ID	1560051-1	**Type of Use**	Republish in a thesis/dissertation
Order detail status	Completed	**Publisher**	Springer-Verlag London Ltd
ISSN	1863-2491	**Portion**	Image/photo/illustration

0.00 USD
Republication Permission

LICENSED CONTENT

Publication Title	Journal of robotic surgery	**Rightsholder**	Springer Nature BV
Article Title	Robot-assisted vascular surgery: literature review, clinical applications, and future perspectives	**Publication Type**	e-Journal
		Start Page	328
		Issue	1
Date	01/01/2007	**Volume**	18
Language	English		
Country	United Kingdom of Great Britain and Northern Ireland		

REQUEST DETAILS

Portion Type	Image/photo/illustration	**Distribution**	Worldwide
Number of Images / Photos / Illustrations	1	**Translation**	Original language of publication
Format (select all that apply)	Electronic	**Copies for the Disabled?**	No
		Minor Editing Privileges?	No
Who Will Republish the Content?	Academic institution	**Incidental Promotional Use?**	No
		Currency	USD
Duration of Use	Life of current and all future editions		
Lifetime Unit Quantity	Up to 499		
Rights Requested	Main product		

NEW WORK DETAILS

Title	Mr	**Institution Name**	Imperial College London
Instructor Name	Zejian Cui	**Expected Presentation Date**	2025-04-30

ADDITIONAL DETAILS

The Requesting Person / Organization to Appear on the License	Zejian Cui

REQUESTED CONTENT DETAILS

Title, Description or Numeric Reference of the Portion(s)	illustration of the da vinci robot evolution	**Title of the Article / Chapter the Portion Is From**	Robot-assisted vascular surgery: literature review, clinical applications, and future perspectives
Editor of Portion(s)	Lengyel, Balazs C.; Chinnadurai, Ponraj; Corr, Stuart J.; Lumsden, Alan B.; Bavare, Charudatta S.	**Author of Portion(s)**	Lengyel, Balazs C.; Chinnadurai, Ponraj; Corr, Stuart J.; Lumsden, Alan B.; Bavare, Charudatta S.
Volume / Edition	18		
Page or Page Range of Portion	328	**Publication Date of Portion**	2024-12-01

Total Items: 1

Subtotal: 0.00 USD

Order Total: 0.00 USD

Marketplace Permissions General Terms and Conditions

The following terms and conditions ("General Terms"), together with any applicable Publisher Terms and Conditions, govern User's use of Works pursuant to the Licenses granted by Copyright Clearance Center, Inc. ("CCC") on behalf of the applicable Rightsholders of such Works through CCC's applicable Marketplace transactional licensing services (each, a "Service").

1) **Definitions.** For purposes of these General Terms, the following definitions apply:

"License" is the licensed use the User obtains via the Marketplace platform in a particular licensing transaction, as set forth in the Order Confirmation.

"Order Confirmation" is the confirmation CCC provides to the User at the conclusion of each Marketplace transaction. "Order Confirmation Terms" are additional terms set forth on specific Order Confirmations not set forth in the General Terms that can include terms applicable to a particular CCC transactional licensing service and/or any Rightsholder-specific terms.

"Rightsholder(s)" are the holders of copyright rights in the Works for which a User obtains licenses via the Marketplace platform, which are displayed on specific Order Confirmations.

"Terms" means the terms and conditions set forth in these General Terms and any additional Order Confirmation Terms collectively.

"User" or "you" is the person or entity making the use granted under the relevant License. Where the person accepting the Terms on behalf of a User is a freelancer or other third party who the User authorized to accept the General Terms on the User's behalf, such person shall be deemed jointly a User for purposes of such Terms.

"Work(s)" are the copyright protected works described in relevant Order Confirmations.

2) **Description of Service.** CCC's Marketplace enables Users to obtain Licenses to use one or more Works in accordance with all relevant Terms. CCC grants Licenses as an agent on behalf of the copyright rightsholder identified in the relevant Order Confirmation.

3) **Applicability of Terms.** The Terms govern User's use of Works in connection with the relevant License. In the event of any conflict between General Terms and Order Confirmation Terms, the latter shall govern. User acknowledges that Rightsholders have complete discretion whether to grant any permission, and whether to place any limitations on any grant, and that CCC has no right to supersede or to modify any such discretionary act by a Rightsholder.

4) **Representations; Acceptance.** By using the Service, User represents and warrants that User has been duly authorized by the User to accept, and hereby does accept, all Terms.

5) **Scope of License; Limitations and Obligations.** All Works and all rights therein, including copyright rights, remain the sole and exclusive property of the Rightsholder. The License provides only those rights expressly set forth in the terms and conveys no other rights in any Works

6) **General Payment Terms.** User may pay at time of checkout by credit card or choose to be invoiced. If the User chooses to be invoiced, the User shall: (i) remit payments in the manner identified on specific invoices, (ii) unless otherwise specifically stated in an Order Confirmation or separate written agreement, Users shall remit payments upon receipt of the relevant invoice from CCC, either by delivery or notification of availability of the invoice via the Marketplace platform, and (iii) if the User does not pay the invoice within 30 days of receipt, the User may incur a service charge of 1.5% per month or the maximum rate allowed by applicable law, whichever is less. While User may exercise the rights in the License immediately upon receiving the Order Confirmation, the License is automatically revoked and is null and void, as if it had never been issued, if CCC does not receive complete payment on a timely basis.

7) **General Limits on Use.** Unless otherwise provided in the Order Confirmation, any grant of rights to User (i) involves only the rights set forth in the Terms and does not include subsequent or additional uses, (ii) is non-exclusive and non-transferable, and (iii) is subject to any and all limitations and restrictions (such as, but not limited to, limitations on duration of use or circulation) included in the Terms. Upon completion of the licensed use as set forth in the Order Confirmation, User shall either secure a new permission for

further use of the Work(s) or immediately cease any new use of the Work(s) and shall render inaccessible (such as by deleting or by removing or severing links or other locators) any further copies of the Work. User may only make alterations to the Work if and as expressly set forth in the Order Confirmation. No Work may be used in any way that is unlawful, including without limitation if such use would violate applicable sanctions laws or regulations, would be defamatory, violate the rights of third parties (including such third parties' rights of copyright, privacy, publicity, or other tangible or intangible property), or is otherwise illegal, sexually explicit, or obscene. In addition, User may not conjoin a Work with any other material that may result in damage to the reputation of the Rightsholder. Any unlawful use will render any licenses hereunder null and void. User agrees to inform CCC if it becomes aware of any infringement of any rights in a Work and to cooperate with any reasonable request of CCC or the Rightsholder in connection therewith.

8) **Third Party Materials.** In the event that the material for which a License is sought includes third party materials (such as photographs, illustrations, graphs, inserts and similar materials) that are identified in such material as having been used by permission (or a similar indicator), User is responsible for identifying, and seeking separate licenses (under this Service, if available, or otherwise) for any of such third party materials; without a separate license, User may not use such third party materials via the License.

9) **Copyright Notice.** Use of proper copyright notice for a Work is required as a condition of any License granted under the Service. Unless otherwise provided in the Order Confirmation, a proper copyright notice will read substantially as follows: "Used with permission of [Rightsholder's name], from [Work's title, author, volume, edition number and year of copyright]; permission conveyed through Copyright Clearance Center, Inc." Such notice must be provided in a reasonably legible font size and must be placed either on a cover page or in another location that any person, upon gaining access to the material which is the subject of a permission, shall see, or in the case of republication Licenses, immediately adjacent to the Work as used (for example, as part of a by-line or footnote) or in the place where substantially all other credits or notices for the new work containing the republished Work are located. Failure to include the required notice results in loss to the Rightsholder and CCC, and the User shall be liable to pay liquidated damages for each such failure equal to twice the use fee specified in the Order Confirmation, in addition to the use fee itself and any other fees and charges specified.

10) **Indemnity.** User hereby indemnifies and agrees to defend the Rightsholder and CCC, and their respective employees and directors, against all claims, liability, damages, costs, and expenses, including legal fees and expenses, arising out of any use of a Work beyond the scope of the rights granted herein and in the Order Confirmation, or any use of a Work which has been altered in any unauthorized way by User, including claims of defamation or infringement of rights of copyright, publicity, privacy, or other tangible or intangible property.

11) **Limitation of Liability.** UNDER NO CIRCUMSTANCES WILL CCC OR THE RIGHTSHOLDER BE LIABLE FOR ANY DIRECT, INDIRECT, CONSEQUENTIAL, OR INCIDENTAL DAMAGES (INCLUDING WITHOUT LIMITATION DAMAGES FOR LOSS OF BUSINESS PROFITS OR INFORMATION, OR FOR BUSINESS INTERRUPTION) ARISING OUT OF THE USE OR INABILITY TO USE A WORK, EVEN IF ONE OR BOTH OF THEM HAS BEEN ADVISED OF THE POSSIBILITY OF SUCH DAMAGES. In any event, the total liability of the Rightsholder and CCC (including their respective employees and directors) shall not exceed the total amount actually paid by User for the relevant License. User assumes full liability for the actions and omissions of its principals, employees, agents, affiliates, successors, and assigns.

12) **Limited Warranties.** THE WORK(S) AND RIGHT(S) ARE PROVIDED "AS IS." CCC HAS THE RIGHT TO GRANT TO USER THE RIGHTS GRANTED IN THE ORDER CONFIRMATION DOCUMENT. CCC AND THE RIGHTSHOLDER DISCLAIM ALL OTHER WARRANTIES RELATING TO THE WORK(S) AND RIGHT(S), EITHER EXPRESS OR IMPLIED, INCLUDING WITHOUT LIMITATION IMPLIED WARRANTIES OF MERCHANTABILITY OR FITNESS FOR A PARTICULAR PURPOSE. ADDITIONAL RIGHTS MAY BE REQUIRED TO USE ILLUSTRATIONS, GRAPHS, PHOTOGRAPHS, ABSTRACTS, INSERTS, OR OTHER PORTIONS OF THE WORK (AS OPPOSED TO THE ENTIRE WORK) IN A MANNER CONTEMPLATED BY USER; USER UNDERSTANDS AND AGREES THAT NEITHER CCC NOR THE RIGHTSHOLDER MAY HAVE SUCH ADDITIONAL RIGHTS TO GRANT.

13) **Effect of Breach.** Any failure by User to pay any amount when due, or any use by User of a Work beyond the scope of the License set forth in the Order Confirmation and/or the Terms, shall be a material breach of such License. Any breach not cured within 10 days of written notice thereof shall result in immediate termination of such License without further notice. Any unauthorized (but licensable) use of a Work that is terminated immediately upon notice thereof may be liquidated by payment of the Rightsholder's ordinary license price therefor; any unauthorized (and unlicensable) use that is not terminated immediately for any reason (including, for example, because materials containing the Work cannot reasonably be recalled) will be subject to all remedies available at law or in equity, but in no event to a payment of less than three times the Rightsholder's ordinary license price for the most closely analogous licensable use plus Rightsholder's and/or CCC's costs and expenses incurred in collecting such payment.

14) **Additional Terms for Specific Products and Services.** If a User is making one of the uses described in this Section 14, the additional terms and conditions apply:

a) ***Print Uses of Academic Course Content and Materials (photocopies for academic coursepacks or classroom handouts).*** For photocopies for academic coursepacks or classroom handouts the following additional terms apply:

i) The copies and anthologies created under this License may be made and assembled by faculty members individually or at their request by on-campus bookstores or copy centers, or by off-campus copy shops and other similar entities.

ii) No License granted shall in any way: (i) include any right by User to create a substantively non-identical copy of the Work or to edit or in any other way modify the Work (except by means of deleting material immediately preceding or following the entire portion of the Work copied) (ii) permit "publishing ventures" where any particular anthology would be systematically marketed at multiple institutions.

iii) Subject to any Publisher Terms (and notwithstanding any apparent contradiction in the Order Confirmation arising from data provided by User), any use authorized under the academic pay-per-use service is limited as follows:

A) any License granted shall apply to only one class (bearing a unique identifier as assigned by the institution, and thereby including all sections or other subparts of the class) at one institution;

B) use is limited to not more than 25% of the text of a book or of the items in a published collection of essays, poems or articles;

C) use is limited to no more than the greater of (a) 25% of the text of an issue of a journal or other periodical or (b) two articles from such an issue;

D) no User may sell or distribute any particular anthology, whether photocopied or electronic, at more than one institution of learning;

E) in the case of a photocopy permission, no materials may be entered into electronic memory by User except in order to produce an identical copy of a Work before or during the academic term (or analogous period) as to which any particular permission is granted. In the event that User shall choose to retain materials that are the subject of a photocopy permission in electronic memory for purposes of producing identical copies more than one day after such retention (but still within the scope of any permission granted), User must notify CCC of such fact in the applicable permission request and such retention shall constitute one copy actually sold for purposes of calculating permission fees due; and

F) any permission granted shall expire at the end of the class. No permission granted shall in any way include any right by User to create a substantively non-identical copy of the Work or to edit or in any other way modify the Work (except by means of deleting material immediately preceding or following the entire portion of the Work copied).

iv) Books and Records; Right to Audit. As to each permission granted under the academic pay-per-use Service, User shall maintain for at least four full calendar years books and records sufficient for CCC to determine the numbers of copies made by User under such permission. CCC and any representatives it may designate shall have the right to audit such books and records at any time during User's ordinary business hours, upon two days' prior notice. If any such audit shall determine that User shall have underpaid for, or underreported, any photocopies sold or by three percent (3%) or more, then User shall bear all the costs of any such audit; otherwise, CCC shall bear the costs of any such audit. Any amount determined by such audit to have been underpaid by User shall immediately be paid to CCC by User, together with interest thereon at the rate of 10% per annum from the date such amount was originally due. The provisions of this paragraph shall survive the termination of this License for any reason.

b) ***Digital Pay-Per-Uses of Academic Course Content and Materials (e-coursepacks, electronic reserves, learning management systems, academic institution intranets).*** For uses in e-coursepacks, posts in electronic reserves, posts in learning management systems, or posts on academic institution intranets, the following additional terms apply:

i) The pay-per-uses subject to this Section 14(b) include:

A) **Posting e-reserves, course management systems, e-coursepacks for text-based content,** which grants authorizations to import requested material in electronic format, and allows electronic access to this material to members of a designated college or university class, under the direction of an instructor designated by the college or university, accessible only under appropriate electronic controls (e.g., password);

B) **Posting e-reserves, course management systems, e-coursepacks for material consisting of photographs or other still images not embedded in text,** which grants not only the authorizations described in Section 14(b)(i)(A) above, but also the following authorization: to include the requested material in course materials for use consistent with Section 14(b)(i)(A) above, including any necessary resizing, reformatting or modification of the resolution of such requested material (provided that such modification does not alter the underlying editorial content or meaning of the requested material, and provided that the resulting modified content is used solely within the scope of, and in a manner consistent with, the particular authorization described in the Order Confirmation and the Terms), but not including any other form of manipulation, alteration or editing of the requested material;

C) **Posting e-reserves, course management systems, e-coursepacks or other academic distribution for audiovisual content,** which grants not only the authorizations described in Section 14(b)(i)(A) above, but also the following authorizations: (i) to include the requested material in course materials for use consistent with Section 14(b)(i)(A) above; (ii) to display and perform the requested material to such members of such class in the physical classroom or remotely by means of streaming media or other video formats; and (iii) to "clip" or reformat the requested material for purposes of time or content management or ease of delivery, provided that such "clipping" or reformatting does not alter the underlying editorial content or meaning of the requested material and that the resulting material is used solely within the scope of, and in a manner consistent with, the particular authorization described in the Order Confirmation and the Terms. Unless expressly set forth in the relevant Order Conformation, the License does not authorize any other form of manipulation, alteration or editing of the requested material.

ii) Unless expressly set forth in the relevant Order Confirmation, no License granted shall in any way: (i) include any right by User to create a substantively non-identical copy of the Work or to edit or in any other way modify the Work (except by means of deleting material immediately preceding or following the entire portion of the Work copied or, in the case of Works subject to Sections 14(b)(1)(B) or (C) above, as described in such Sections) (ii) permit "publishing ventures" where any particular course materials would be systematically marketed at multiple institutions.

iii) Subject to any further limitations determined in the Rightsholder Terms (and notwithstanding any apparent contradiction in the Order Confirmation arising from data provided by User), any use authorized under the electronic course content pay-per-

use service is limited as follows:

A) any License granted shall apply to only one class (bearing a unique identifier as assigned by the institution, and thereby including all sections or other subparts of the class) at one institution;

B) use is limited to not more than 25% of the text of a book or of the items in a published collection of essays, poems or articles;

C) use is limited to not more than the greater of (a) 25% of the text of an issue of a journal or other periodical or (b) two articles from such an issue;

D) no User may sell or distribute any particular materials, whether photocopied or electronic, at more than one institution of learning;

E) electronic access to material which is the subject of an electronic-use permission must be limited by means of electronic password, student identification or other control permitting access solely to students and instructors in the class;

F) User must ensure (through use of an electronic cover page or other appropriate means) that any person, upon gaining electronic access to the material, which is the subject of a permission, shall see:

- a proper copyright notice, identifying the Rightsholder in whose name CCC has granted permission,
- a statement to the effect that such copy was made pursuant to permission,
- a statement identifying the class to which the material applies and notifying the reader that the material has been made available electronically solely for use in the class, and
- a statement to the effect that the material may not be further distributed to any person outside the class, whether by copying or by transmission and whether electronically or in paper form, and User must also ensure that such cover page or other means will print out in the event that the person accessing the material chooses to print out the material or any part thereof.

G) any permission granted shall expire at the end of the class and, absent some other form of authorization, User is thereupon required to delete the applicable material from any electronic storage or to block electronic access to the applicable material.

iv) Uses of separate portions of a Work, even if they are to be included in the same course material or the same university or college class, require separate permissions under the electronic course content pay-per-use Service. Unless otherwise provided in the Order Confirmation, any grant of rights to User is limited to use completed no later than the end of the academic term (or analogous period) as to which any particular permission is granted.

v) Books and Records; Right to Audit. As to each permission granted under the electronic course content Service, User shall maintain for at least four full calendar years books and records sufficient for CCC to determine the numbers of copies made by User under such permission. CCC and any representatives it may designate shall have the right to audit such books and records at any time during User's ordinary business hours, upon two days' prior notice. If any such audit shall determine that User shall have underpaid for, or underreported, any electronic copies used by three percent (3%) or more, then User shall bear all the costs of any such audit; otherwise, CCC shall bear the costs of any such audit. Any amount determined by such audit to have been underpaid by User shall immediately be paid to CCC by User, together with interest thereon at the rate of 10% per annum from the date such amount was originally due. The provisions of this paragraph shall survive the termination of this license for any reason.

c) ***Pay-Per-Use Permissions for Certain Reproductions (Academic photocopies for library reserves and interlibrary loan reporting) (Non-academic internal/external business uses and commercial document delivery).*** The License expressly excludes the uses listed in Section (c)(i)-(v) below (which must be subject to separate license from the applicable Rightsholder) for: academic photocopies for library reserves and interlibrary loan reporting; and non-academic internal/external business uses and commercial document delivery.

i) electronic storage of any reproduction (whether in plain-text, PDF, or any other format) other than on a transitory basis;

ii) the input of Works or reproductions thereof into any computerized database;

iii) reproduction of an entire Work (cover-to-cover copying) except where the Work is a single article;

iv) reproduction for resale to anyone other than a specific customer of User;

v) republication in any different form. Please obtain authorizations for these uses through other CCC services or directly from the rightsholder.

Any license granted is further limited as set forth in any restrictions included in the Order Confirmation and/or in these Terms.

d) ***Electronic Reproductions in Online Environments (Non-Academic-email, intranet, internet and extranet).*** For "electronic reproductions", which generally includes e-mail use (including instant messaging or other electronic transmission to a defined group of recipients) or posting on an intranet, extranet or Intranet site (including any display or performance incidental thereto), the following additional terms apply:

i) Unless otherwise set forth in the Order Confirmation, the License is limited to use completed within 30 days for any use on the Internet, 60 days for any use on an intranet or extranet and one year for any other use, all as measured from the "republication date" as identified in the Order Confirmation, if any, and otherwise from the date of the Order Confirmation.

ii) User may not make or permit any alterations to the Work, unless expressly set forth in the Order Confirmation (after request by User and approval by Rightsholder); provided, however, that a Work consisting of photographs or other still images not embedded in text may, if necessary, be resized, reformatted or have its resolution modified without additional express permission, and a Work consisting of audiovisual content may, if necessary, be "clipped" or reformatted for purposes of time or content management or ease of delivery (provided that any such resizing, reformatting, resolution modification or "clipping" does not alter the underlying editorial content or meaning of the Work used, and that the resulting material is used solely within the scope of, and in a manner consistent with, the particular License described in the Order Confirmation and the Terms.

15) **Miscellaneous.**

a) User acknowledges that CCC may, from time to time, make changes or additions to the Service or to the Terms, and that Rightsholder may make changes or additions to the Rightsholder Terms. Such updated Terms will replace the prior terms and conditions in the order workflow and shall be effective as to any subsequent Licenses but shall not apply to Licenses already granted and paid for under a prior set of terms.

b) Use of User-related information collected through the Service is governed by CCC's privacy policy, available online at www.copyright.com/about/privacy-policy/.

c) The License is personal to User. Therefore, User may not assign or transfer to any other person (whether a natural person or an organization of any kind) the License or any rights granted thereunder; provided, however, that, where applicable, User may assign such License in its entirety on written notice to CCC in the event of a transfer of all or substantially all of User's rights in any new material which includes the Work(s) licensed under this Service.

d) No amendment or waiver of any Terms is binding unless set forth in writing and signed by the appropriate parties, including, where applicable, the Rightsholder. The Rightsholder and CCC hereby object to any terms contained in any writing prepared by or on behalf of the User or its principals, employees, agents or affiliates and purporting to govern or otherwise relate to the License described in the Order Confirmation, which terms are in any way inconsistent with any Terms set forth in the Order Confirmation, and/or in CCC's standard operating procedures, whether such writing is prepared prior to, simultaneously with or subsequent to the Order Confirmation, and whether such writing appears on a copy of the Order Confirmation or in a separate instrument.

e) The License described in the Order Confirmation shall be governed by and construed under the law of the State of New York, USA, without regard to the principles thereof of conflicts of law. Any case, controversy, suit, action, or proceeding arising out of, in connection with, or related to such License shall be brought, at CCC's sole discretion, in any federal or state court located in the County of New York, State of New York, USA, or in any federal or state court whose geographical jurisdiction covers the location of the Rightsholder set forth in the Order Confirmation. The parties expressly submit to the personal jurisdiction and venue of each such federal or state court.

Last updated October 2022

Marketplace

Order Confirmation

Thank you, your order has been placed. An email confirmation has been sent to you. Your order license details and printable licenses will be available within 24 hours. Please access Manage Account for final order details.

This is not an invoice. Please go to manage account to access your order history and invoices.

CUSTOMER INFORMATION

Payment by invoice: You can cancel your order until the invoice is generated by contacting customer service.

Billing Address

Mr. Zejian Cui
Friendship House
London, SE1 0AD
United Kingdom

+44 7419921105
zejian.cui19@imperial.ac.uk

Customer Location

Mr. Zejian Cui
Friendship House
London, SE1 0AD
United Kingdom

PO Number (optional)

N/A

Payment options

Invoice

PENDING ORDER CONFIRMATION

Confirmation Number: Pending

Order Date: 26-Dec-2024

1. BJU international

0.00 USD

Article: Robot-assisted radical prostatectomy feasibility and setting with the Hugo™ robot-assisted surgery system

Order License ID	Pending	**Publisher**	BLACKWELL PUBLISHING
ISSN	1464-410X		
Type of Use	Republish in a thesis/dissertation	**Portion**	Image/photo/illustration

LICENSED CONTENT

Publication Title	BJU international	**Publication Type**	e-Journal
Article Title	Robot-assisted radical prostatectomy feasibility and setting with the Hugo™ robot-assisted surgery system	**Start Page**	671
		End Page	675
		Issue	5
Author / Editor	British Association of Urological Surgeons., European Society of Paediatric Urology., International Society of Urology.	**Volume**	130
		URL	http://onlinelibrary.wiley.com/journal/10.1111/(ISSN)1464-410X
Date	01/01/1999		
Language	English		
Country	United Kingdom of Great Britain and Northern Ireland		
Rightsholder	John Wiley & Sons - Books		

REQUEST DETAILS

Portion Type	Image/photo/illustration	**Distribution**	Worldwide
Number of Images / Photos / Illustrations	1	**Translation**	Original language of publication
Format (select all that apply)	Electronic	**Copies for the Disabled?**	No
Who Will Republish the Content?	Academic institution	**Minor Editing Privileges?**	No
		Incidental Promotional Use?	No
Duration of Use	Life of current and all future editions	**Currency**	USD
Lifetime Unit Quantity	Up to 499		
Rights Requested	Main product		

NEW WORK DETAILS

Title	Mr	**Institution Name**	Imperial College London
Instructor Name	Zejian Cui	**Expected Presentation Date**	2025-04-30

ADDITIONAL DETAILS

The Requesting Person / Organization to Appear on the License	Zejian Cui

REQUESTED CONTENT DETAILS

Title, Description or Numeric Reference of the Portion(s)	Hugo robot picture	**Title of the Article / Chapter the Portion Is From**	Robot-assisted radical prostatectomy feasibility and setting with the Hugo™ robot-assisted surgery system
Editor of Portion(s)	Sarchi, Luca; Mottaran, Angelo; Bravi, Carlo Andrea; Paciotti, Marco; Farinha, Rui; Piazza, Pietro; Puliatti, Stefano; De Groote, Ruben; De Naeyer, Geert; Gallagher, Anthony; Breda, Alberto; Mottrie, Alexandre	**Author of Portion(s)**	Sarchi, Luca; Mottaran, Angelo; Bravi, Carlo Andrea; Paciotti, Marco; Farinha, Rui; Piazza, Pietro; Puliatti, Stefano; De Groote, Ruben; De Naeyer, Geert; Gallagher, Anthony; Breda, Alberto; Mottrie, Alexandre
Volume / Edition	130		
Page or Page Range of Portion	671-675	**Publication Date of Portion**	2022-11-01

RIGHTSHOLDER TERMS AND CONDITIONS

No right, license or interest to any trademark, trade name, service mark or other branding ("Marks") of WILEY or its licensors is granted hereunder, and you agree that you shall not assert any such right, license or interest with respect thereto. You may not alter, remove or suppress in any manner any copyright, trademark or other notices displayed by the Wiley material. This Agreement will be void if the Type of Use, Format, Circulation, or Requestor Type was misrepresented during the licensing process. In no instance may the total amount of Wiley Materials used in any Main Product, Compilation or Collective work comprise more than 5% (if figures/tables) or 15% (if full articles/chapters) of the (entirety of the) Main Product, Compilation or Collective Work. Some titles may be available under an Open Access license. It is the Licensors' responsibility to identify the type of Open Access license on which the requested material was published, and comply fully with the terms of that license for the type of use specified Further details can be found on Wiley Online Library http://olabout.wiley.com/WileyCDA/Section/id-410895.html.

Total Items: 1

Total Due: 0.00 USD

Accepted: Marketplace Permissions General Terms and Conditions and any applicable Publisher Terms and Conditions

Marketplace

Order Number: 1560053
Order Date: 26 Dec 2024

Payment Information

Zejian Cui
zejian.cui19@imperial.ac.uk
Payment method: Invoice

Billing Address:
Mr. Zejian Cui
Friendship House
London, SE1 0AD
United Kingdom

+44 7419921105
zejian.cui19@imperial.ac.uk

Customer Location:
Mr. Zejian Cui
Friendship House
London, SE1 0AD
United Kingdom

Order Details

1. IEEE transactions on robotics : a publication of the IEEE Robotics and Automation Society

Billing Status: Open

Article: Active Constraints/Virtual Fixtures: A Survey

Order License ID	1560053-1	**Type of Use**	Republish in a thesis/dissertation
Order detail status	Completed		
ISSN	1552-3098	**Publisher**	IEEE
		Portion	Chart/graph/table/figure

0.00 USD
Republication Permission

LICENSED CONTENT

Publication Title	IEEE transactions on robotics : a publication of the IEEE Robotics and Automation Society	**Rightsholder**	The Institute of Electrical and Electronics Engineers, Incorporated (IEEE)
Article Title	Active Constraints/Virtual Fixtures: A Survey	**Publication Type**	Journal
Author / Editor	Institute of Electrical and Electronics Engineers., IEEE Robotics and Automation Society.	**Start Page**	138
		End Page	157
		Issue	1
		Volume	30
Date	01/01/2004		
Language	English		
Country	United States of America		

REQUEST DETAILS

Portion Type	Chart/graph/table/figure	**Distribution**	Worldwide
Number of Charts / Graphs / Tables / Figures Requested	2	**Translation**	Original language of publication
Format (select all that apply)	Electronic	**Copies for the Disabled?**	No
		Minor Editing Privileges?	No
Who Will Republish the Content?	Academic institution	**Incidental Promotional Use?**	No
		Currency	USD
Duration of Use	Life of current and all future editions		
Lifetime Unit Quantity	Up to 499		
Rights Requested	Main product		

NEW WORK DETAILS

Title	Mr	**Institution Name**	Imperial College London

Instructor Name	Zejian Cui	**Expected Presentation Date**	2025-04-30

ADDITIONAL DETAILS

The Requesting Person / Organization to Appear on the License	Zejian Cui

REQUESTED CONTENT DETAILS

Title, Description or Numeric Reference of the Portion(s)	potential field & proxy	**Title of the Article / Chapter the Portion Is From**	Active Constraints/Virtual Fixtures: A Survey
		Author of Portion(s)	Bowyer, Stuart A.; Davies, Brian L.; Rodriguez y Baena, Ferdinando
Editor of Portion(s)	Bowyer, Stuart A.; Davies, Brian L.; Rodriguez y Baena, Ferdinando	**Issue, if Republishing an Article From a Serial**	1
Volume / Edition	30		
Page or Page Range of Portion	138-157	**Publication Date of Portion**	2014-02-01

The Institute of Electrical and Electronics Engineers, Incorporated (IEEE) Terms and Conditions

IEEE allows for reuse of content in a thesis or dissertation for $0 and no license is required. IEEE does not have the right to license republication of Images and Photos. Please contact the author of the IEEE content to request the rights for the needed images and photos. IEEE allows reuse of an Excerpt when licensing permission for reuse of a Page. If you wish to license more than 10 figures, please contact IEEE directly at: pubs-permissions@ieee.org. IEEE will provide a discounted cost for bulk figure purchases. If you are an Author or a Member of IEEE, and are affiliated with or requesting on behalf of a non-commercial or non-profit organization, please use RightsLink to request republication permissions at: https://ieeexplore.ieee.org/. IEEE offers special pricing for Authors and Members of IEEE in RightsLink that is not available on copyright.com

Total Items: 1

Subtotal: 0.00 USD

Order Total: 0.00 USD

Marketplace Permissions General Terms and Conditions

The following terms and conditions ("General Terms"), together with any applicable Publisher Terms and Conditions, govern User's use of Works pursuant to the Licenses granted by Copyright Clearance Center, Inc. ("CCC") on behalf of the applicable Rightsholders of such Works through CCC's applicable Marketplace transactional licensing services (each, a "Service").

1) **Definitions.** For purposes of these General Terms, the following definitions apply:

"License" is the licensed use the User obtains via the Marketplace platform in a particular licensing transaction, as set forth in the Order Confirmation.

"Order Confirmation" is the confirmation CCC provides to the User at the conclusion of each Marketplace transaction. "Order Confirmation Terms" are additional terms set forth on specific Order Confirmations not set forth in the General Terms that can include terms applicable to a particular CCC transactional licensing service and/or any Rightsholder-specific terms.

"Rightsholder(s)" are the holders of copyright rights in the Works for which a User obtains licenses via the Marketplace platform, which are displayed on specific Order Confirmations.

"Terms" means the terms and conditions set forth in these General Terms and any additional Order Confirmation Terms collectively.

"User" or "you" is the person or entity making the use granted under the relevant License. Where the person accepting the Terms on behalf of a User is a freelancer or other third party who the User authorized to accept the General Terms on the User's behalf, such person shall be deemed jointly a User for purposes of such Terms.

"Work(s)" are the copyright protected works described in relevant Order Confirmations.

2) **Description of Service.** CCC's Marketplace enables Users to obtain Licenses to use one or more Works in accordance with all relevant Terms. CCC grants Licenses as an agent on behalf of the copyright rightsholder identified in the relevant Order Confirmation.

3) **Applicability of Terms.** The Terms govern User's use of Works in connection with the relevant License. In the event of any conflict between General Terms and Order Confirmation Terms, the latter shall govern. User acknowledges that Rightsholders have complete discretion whether to grant any permission, and whether to place any limitations on any grant, and that CCC has no right to supersede or to modify any such discretionary act by a Rightsholder.

4) **Representations; Acceptance.** By using the Service, User represents and warrants that User has been duly authorized by the User to accept, and hereby does accept, all Terms.

5) **Scope of License; Limitations and Obligations.** All Works and all rights therein, including copyright rights, remain the sole and exclusive property of the Rightsholder. The License provides only those rights expressly set forth in the terms and conveys no other rights in any Works

6) **General Payment Terms.** User may pay at time of checkout by credit card or choose to be invoiced. If the User chooses to be invoiced, the User shall: (i) remit payments in the manner identified on specific invoices, (ii) unless otherwise specifically stated in an Order Confirmation or separate written agreement, Users shall remit payments upon receipt of the relevant invoice from CCC, either by delivery or notification of availability of the invoice via the Marketplace platform, and (iii) if the User does not pay the invoice within 30 days of receipt, the User may incur a service charge of 1.5% per month or the maximum rate allowed by applicable law, whichever is less. While User may exercise the rights in the License immediately upon receiving the Order Confirmation, the License is automatically revoked and is null and void, as if it had never been issued, if CCC does not receive complete payment on a timely basis.

7) **General Limits on Use.** Unless otherwise provided in the Order Confirmation, any grant of rights to User (i) involves only the rights set forth in the Terms and does not include subsequent or additional uses, (ii) is non-exclusive and non-transferable, and (iii) is subject to any and all limitations and restrictions (such as, but not limited to, limitations on duration of use or circulation) included in the Terms. Upon completion of the licensed use as set forth in the Order Confirmation, User shall either secure a new permission for further use of the Work(s) or immediately cease any new use of the Work(s) and shall render inaccessible (such as by deleting or by removing or severing links or other locators) any further copies of the Work. User may only make alterations to the Work if and as expressly set forth in the Order Confirmation. No Work may be used in any way that is unlawful, including without limitation if such use would violate applicable sanctions laws or regulations, would be defamatory, violate the rights of third parties (including such third parties' rights of copyright, privacy, publicity, or other tangible or intangible property), or is otherwise illegal, sexually explicit, or obscene. In addition, User may not conjoin a Work with any other material that may result in damage to the reputation of the Rightsholder. Any unlawful use will render any licenses hereunder null and void. User agrees to inform CCC if it becomes aware of any infringement of any rights in a Work and to cooperate with any reasonable request of CCC or the Rightsholder in connection therewith.

8) **Third Party Materials.** In the event that the material for which a License is sought includes third party materials (such as photographs, illustrations, graphs, inserts and similar materials) that are identified in such material as having been used by permission (or a similar indicator), User is responsible for identifying, and seeking separate licenses (under this Service, if available, or otherwise) for any of such third party materials; without a separate license, User may not use such third party materials via the License.

9) **Copyright Notice.** Use of proper copyright notice for a Work is required as a condition of any License granted under the Service. Unless otherwise provided in the Order Confirmation, a proper copyright notice will read substantially as follows: "Used with permission of [Rightsholder's name], from [Work's title, author, volume, edition number and year of copyright]; permission conveyed through Copyright Clearance Center, Inc." Such notice must be provided in a reasonably legible font size and must be placed either on a cover page or in another location that any person, upon gaining access to the material which is the subject of a permission, shall see, or in the case of republication Licenses, immediately adjacent to the Work as used (for example, as part of a by-line or footnote) or in the place where substantially all other credits or notices for the new work containing the republished Work are located. Failure to include the required notice results in loss to the Rightsholder and CCC, and the User shall be liable to pay liquidated damages for each such failure equal to twice the use fee specified in the Order Confirmation, in addition to the use fee itself and any other fees and charges specified.

10) **Indemnity.** User hereby indemnifies and agrees to defend the Rightsholder and CCC, and their respective employees and directors, against all claims, liability, damages, costs, and expenses, including legal fees and expenses, arising out of any use of a Work beyond the scope of the rights granted herein and in the Order Confirmation, or any use of a Work which has been altered in any unauthorized way by User, including claims of defamation or infringement of rights of copyright, publicity, privacy, or other tangible or intangible property.

11) **Limitation of Liability.** UNDER NO CIRCUMSTANCES WILL CCC OR THE RIGHTSHOLDER BE LIABLE FOR ANY DIRECT, INDIRECT, CONSEQUENTIAL, OR INCIDENTAL DAMAGES (INCLUDING WITHOUT LIMITATION DAMAGES FOR LOSS OF BUSINESS PROFITS OR INFORMATION, OR FOR BUSINESS INTERRUPTION) ARISING OUT OF THE USE OR INABILITY TO USE A WORK, EVEN IF ONE OR BOTH OF THEM HAS BEEN ADVISED OF THE POSSIBILITY OF SUCH DAMAGES. In any event, the total liability of the Rightsholder and CCC (including their respective employees and directors) shall not exceed the total amount actually paid by User for the relevant License. User assumes full liability for the actions and omissions of its principals, employees, agents, affiliates, successors, and assigns.

12) **Limited Warranties.** THE WORK(S) AND RIGHT(S) ARE PROVIDED "AS IS." CCC HAS THE RIGHT TO GRANT TO USER THE RIGHTS GRANTED IN THE ORDER CONFIRMATION DOCUMENT. CCC AND THE RIGHTSHOLDER DISCLAIM ALL OTHER WARRANTIES RELATING TO THE WORK(S) AND RIGHT(S), EITHER EXPRESS OR IMPLIED, INCLUDING WITHOUT LIMITATION IMPLIED WARRANTIES OF MERCHANTABILITY OR FITNESS FOR A PARTICULAR PURPOSE. ADDITIONAL RIGHTS MAY BE REQUIRED TO USE ILLUSTRATIONS, GRAPHS, PHOTOGRAPHS, ABSTRACTS, INSERTS, OR OTHER PORTIONS OF THE WORK (AS OPPOSED TO THE ENTIRE WORK) IN A MANNER CONTEMPLATED BY USER; USER UNDERSTANDS AND AGREES THAT NEITHER CCC NOR THE RIGHTSHOLDER MAY HAVE SUCH ADDITIONAL RIGHTS TO GRANT.

13) **Effect of Breach.** Any failure by User to pay any amount when due, or any use by User of a Work beyond the scope of the License set forth in the Order Confirmation and/or the Terms, shall be a material breach of such License. Any breach not cured within 10 days of written notice thereof shall result in immediate termination of such License without further notice. Any unauthorized (but licensable) use of a Work that is terminated immediately upon notice thereof may be liquidated by payment of the Rightsholder's ordinary license price therefor; any unauthorized (and unlicensable) use that is not terminated immediately for any reason (including, for example, because materials containing the Work cannot reasonably be recalled) will be subject to all remedies available at law or in equity, but in no event to a payment of less than three times the Rightsholder's ordinary license price for the most closely analogous licensable use plus Rightsholder's and/or CCC's costs and expenses incurred in collecting such payment.

14) **Additional Terms for Specific Products and Services.** If a User is making one of the uses described in this Section 14, the additional terms and conditions apply:

a) ***Print Uses of Academic Course Content and Materials (photocopies for academic coursepacks or classroom handouts).*** For photocopies for academic coursepacks or classroom handouts the following additional terms apply:

i) The copies and anthologies created under this License may be made and assembled by faculty members individually or at their request by on-campus bookstores or copy centers, or by off-campus copy shops and other similar entities.

ii) No License granted shall in any way: (i) include any right by User to create a substantively non-identical copy of the Work or to edit or in any other way modify the Work (except by means of deleting material immediately preceding or following the entire portion of the Work copied) (ii) permit "publishing ventures" where any particular anthology would be systematically marketed at multiple institutions.

iii) Subject to any Publisher Terms (and notwithstanding any apparent contradiction in the Order Confirmation arising from data provided by User), any use authorized under the academic pay-per-use service is limited as follows:

A) any License granted shall apply to only one class (bearing a unique identifier as assigned by the institution, and thereby including all sections or other subparts of the class) at one institution;

B) use is limited to not more than 25% of the text of a book or of the items in a published collection of essays, poems or articles;

C) use is limited to no more than the greater of (a) 25% of the text of an issue of a journal or other periodical or (b) two articles from such an issue;

D) no User may sell or distribute any particular anthology, whether photocopied or electronic, at more than one institution of learning;

E) in the case of a photocopy permission, no materials may be entered into electronic memory by User except in order to produce an identical copy of a Work before or during the academic term (or analogous period) as to which any particular permission is granted. In the event that User shall choose to retain materials that are the subject of a photocopy permission in electronic memory for purposes of producing identical copies more than one day after such retention (but still within the scope of any permission granted), User must notify CCC of such fact in the applicable permission request and such retention shall constitute one copy actually sold for purposes of calculating permission fees due; and

F) any permission granted shall expire at the end of the class. No permission granted shall in any way include any right by User to create a substantively non-identical copy of the Work or to edit or in any other way modify the Work (except by means of deleting material immediately preceding or following the entire portion of the Work copied).

iv) Books and Records; Right to Audit. As to each permission granted under the academic pay-per-use Service, User shall maintain for at least four full calendar years books and records sufficient for CCC to determine the numbers of copies made by User under such permission. CCC and any representatives it may designate shall have the right to audit such books and records at any time during User's ordinary business hours, upon two days' prior notice. If any such audit shall determine that User shall have underpaid for, or underreported, any photocopies sold or by three percent (3%) or more, then User shall bear all the costs of any such audit; otherwise, CCC shall bear the costs of any such audit. Any amount determined by such audit to have been underpaid by User shall immediately be paid to CCC by User, together with interest thereon at the rate of 10% per annum from the date such amount was originally due. The provisions of this paragraph shall survive the termination of this License for any reason.

b) ***Digital Pay-Per-Uses of Academic Course Content and Materials (e-coursepacks, electronic reserves, learning management systems, academic institution intranets).*** For uses in e-coursepacks, posts in electronic reserves, posts in learning management systems, or posts on academic institution intranets, the following additional terms apply:

i) The pay-per-uses subject to this Section 14(b) include:

A) **Posting e-reserves, course management systems, e-coursepacks for text-based content,** which grants authorizations to import requested material in electronic format, and allows electronic access to this material to members of a designated college or university class, under the direction of an instructor designated by the college or university, accessible only under appropriate electronic controls (e.g., password);

B) **Posting e-reserves, course management systems, e-coursepacks for material consisting of photographs or other still images not embedded in text,** which grants not only the authorizations described in Section 14(b)(i)(A) above, but also the following authorization: to include the requested material in course materials for use consistent with Section 14(b)(i)(A) above, including any necessary resizing, reformatting or modification of the resolution of such requested material (provided that such modification does not alter the underlying editorial content or meaning of the requested material, and provided that the resulting modified content is used solely within the scope of, and in a manner consistent with, the particular authorization described in the Order Confirmation and the Terms), but not including any other form of manipulation, alteration or editing of the requested material;

C) **Posting e-reserves, course management systems, e-coursepacks or other academic distribution for audiovisual content,** which grants not only the authorizations described in Section 14(b)(i)(A) above, but also the following authorizations: (i) to include the requested material in course materials for use consistent with Section 14(b)(i)(A) above; (ii) to display and perform the requested material to such members of such class in the physical classroom or remotely by

means of streaming media or other video formats; and (iii) to "clip" or reformat the requested material for purposes of time or content management or ease of delivery, provided that such "clipping" or reformatting does not alter the underlying editorial content or meaning of the requested material and that the resulting material is used solely within the scope of, and in a manner consistent with, the particular authorization described in the Order Confirmation and the Terms. Unless expressly set forth in the relevant Order Conformation, the License does not authorize any other form of manipulation, alteration or editing of the requested material.

ii) Unless expressly set forth in the relevant Order Confirmation, no License granted shall in any way: (i) include any right by User to create a substantively non-identical copy of the Work or to edit or in any other way modify the Work (except by means of deleting material immediately preceding or following the entire portion of the Work copied or, in the case of Works subject to Sections 14(b)(1)(B) or (C) above, as described in such Sections) (ii) permit "publishing ventures" where any particular course materials would be systematically marketed at multiple institutions.

iii) Subject to any further limitations determined in the Rightsholder Terms (and notwithstanding any apparent contradiction in the Order Confirmation arising from data provided by User), any use authorized under the electronic course content pay-per-use service is limited as follows:

A) any License granted shall apply to only one class (bearing a unique identifier as assigned by the institution, and thereby including all sections or other subparts of the class) at one institution;

B) use is limited to not more than 25% of the text of a book or of the items in a published collection of essays, poems or articles;

C) use is limited to not more than the greater of (a) 25% of the text of an issue of a journal or other periodical or (b) two articles from such an issue;

D) no User may sell or distribute any particular materials, whether photocopied or electronic, at more than one institution of learning;

E) electronic access to material which is the subject of an electronic-use permission must be limited by means of electronic password, student identification or other control permitting access solely to students and instructors in the class;

F) User must ensure (through use of an electronic cover page or other appropriate means) that any person, upon gaining electronic access to the material, which is the subject of a permission, shall see:

- a proper copyright notice, identifying the Rightsholder in whose name CCC has granted permission,
- a statement to the effect that such copy was made pursuant to permission,
- a statement identifying the class to which the material applies and notifying the reader that the material has been made available electronically solely for use in the class, and
- a statement to the effect that the material may not be further distributed to any person outside the class, whether by copying or by transmission and whether electronically or in paper form, and User must also ensure that such cover page or other means will print out in the event that the person accessing the material chooses to print out the material or any part thereof.

G) any permission granted shall expire at the end of the class and, absent some other form of authorization, User is thereupon required to delete the applicable material from any electronic storage or to block electronic access to the applicable material.

iv) Uses of separate portions of a Work, even if they are to be included in the same course material or the same university or college class, require separate permissions under the electronic course content pay-per-use Service. Unless otherwise provided in the Order Confirmation, any grant of rights to User is limited to use completed no later than the end of the academic term (or analogous period) as to which any particular permission is granted.

v) Books and Records; Right to Audit. As to each permission granted under the electronic course content Service, User shall maintain for at least four full calendar years books and records sufficient for CCC to determine the numbers of copies made by User under such permission. CCC and any representatives it may designate shall have the right to audit such books and records at any time during User's ordinary business hours, upon two days' prior notice. If any such audit shall determine that User shall have underpaid for, or underreported, any electronic copies used by three percent (3%) or more, then User shall bear all the costs of any such audit; otherwise, CCC shall bear the costs of any such audit. Any amount determined by such audit to have been underpaid by User shall immediately be paid to CCC by User, together with interest thereon at the rate of 10% per annum from the date such amount was originally due. The provisions of this paragraph shall survive the termination of this license for any reason.

c) ***Pay-Per-Use Permissions for Certain Reproductions (Academic photocopies for library reserves and interlibrary loan reporting) (Non-academic internal/external business uses and commercial document delivery).*** The License expressly excludes the uses listed in Section (c)(i)-(v) below (which must be subject to separate license from the applicable Rightsholder) for: academic photocopies for library reserves and interlibrary loan reporting; and non-academic internal/external business uses and commercial document delivery.

i) electronic storage of any reproduction (whether in plain-text, PDF, or any other format) other than on a transitory basis;

ii) the input of Works or reproductions thereof into any computerized database;

iii) reproduction of an entire Work (cover-to-cover copying) except where the Work is a single article;

iv) reproduction for resale to anyone other than a specific customer of User;

v) republication in any different form. Please obtain authorizations for these uses through other CCC services or directly from the rightsholder.

Any license granted is further limited as set forth in any restrictions included in the Order Confirmation and/or in these Terms.

d) ***Electronic Reproductions in Online Environments (Non-Academic-email, intranet, internet and extranet).*** For "electronic reproductions", which generally includes e-mail use (including instant messaging or other electronic transmission to a defined group of recipients) or posting on an intranet, extranet or Intranet site (including any display or performance incidental thereto), the following additional terms apply:

i) Unless otherwise set forth in the Order Confirmation, the License is limited to use completed within 30 days for any use on the Internet, 60 days for any use on an intranet or extranet and one year for any other use, all as measured from the "republication date" as identified in the Order Confirmation, if any, and otherwise from the date of the Order Confirmation.

ii) User may not make or permit any alterations to the Work, unless expressly set forth in the Order Confirmation (after request by User and approval by Rightsholder); provided, however, that a Work consisting of photographs or other still images not embedded in text may, if necessary, be resized, reformatted or have its resolution modified without additional express permission, and a Work consisting of audiovisual content may, if necessary, be "clipped" or reformatted for purposes of time or content management or ease of delivery (provided that any such resizing, reformatting, resolution modification or "clipping" does not alter the underlying editorial content or meaning of the Work used, and that the resulting material is used solely within the scope of, and in a manner consistent with, the particular License described in the Order Confirmation and the Terms.

15) **Miscellaneous.**

a) User acknowledges that CCC may, from time to time, make changes or additions to the Service or to the Terms, and that Rightsholder may make changes or additions to the Rightsholder Terms. Such updated Terms will replace the prior terms and conditions in the order workflow and shall be effective as to any subsequent Licenses but shall not apply to Licenses already granted and paid for under a prior set of terms.

b) Use of User-related information collected through the Service is governed by CCC's privacy policy, available online at www.copyright.com/about/privacy-policy/.

c) The License is personal to User. Therefore, User may not assign or transfer to any other person (whether a natural person or an organization of any kind) the License or any rights granted thereunder; provided, however, that, where applicable, User may assign such License in its entirety on written notice to CCC in the event of a transfer of all or substantially all of User's rights in any new material which includes the Work(s) licensed under this Service.

d) No amendment or waiver of any Terms is binding unless set forth in writing and signed by the appropriate parties, including, where applicable, the Rightsholder. The Rightsholder and CCC hereby object to any terms contained in any writing prepared by or on behalf of the User or its principals, employees, agents or affiliates and purporting to govern or otherwise relate to the License described in the Order Confirmation, which terms are in any way inconsistent with any Terms set forth in the Order Confirmation, and/or in CCC's standard operating procedures, whether such writing is prepared prior to, simultaneously with or subsequent to the Order Confirmation, and whether such writing appears on a copy of the Order Confirmation or in a separate instrument.

e) The License described in the Order Confirmation shall be governed by and construed under the law of the State of New York, USA, without regard to the principles thereof of conflicts of law. Any case, controversy, suit, action, or proceeding arising out of, in connection with, or related to such License shall be brought, at CCC's sole discretion, in any federal or state court located in the County of New York, State of New York, USA, or in any federal or state court whose geographical jurisdiction covers the location of the Rightsholder set forth in the Order Confirmation. The parties expressly submit to the personal jurisdiction and venue of each such federal or state court.

Last updated October 2022

Marketplace

Order Number: 1569904
Order Date: 23 Jan 2025

Payment Information

Zejian Cui
zejian.cui19@imperial.ac.uk
Payment method: Invoice

Billing Address:
Mr. Zejian Cui
Flat 7, Adelphi Court
London, W4 4QF
United Kingdom

+44 7419921105
zejian.cui19@imperial.ac.uk

Customer Location:
Mr. Zejian Cui
Flat 7, Adelphi Court
London, W4 4QF
United Kingdom

Order Details

1. IEEE robotics and automation letters

Billing Status: Open

Article: Efficiently Calibrating Cable-Driven Surgical Robots with RGBD Fiducial Sensing and Recurrent Neural Networks

Order License ID	1569904-1	**Type of Use**	Republish in a thesis/dissertation
Order detail status	Completed		
ISSN	2377-3766	**Portion**	Chart/graph/table/figure

0.00 GBP
Republication Permission

LICENSED CONTENT

Publication Title	IEEE robotics and automation letters	**Publication Type**	Journal
Article Title	Efficiently Calibrating Cable-Driven Surgical Robots with RGBD Fiducial Sensing and Recurrent Neural Networks	**Start Page**	5937
		End Page	5944
		Issue	4
		Volume	5
Date	01/01/2016		
Language	English		
Country	United States of America		
Rightsholder	The Institute of Electrical and Electronics Engineers, Incorporated (IEEE)		

REQUEST DETAILS

Portion Type	Chart/graph/table/figure	**Distribution**	U.K. and Commonwealth (excluding Canada)
Number of Charts / Graphs / Tables / Figures Requested	1	**Translation**	Original language of publication
Format (select all that apply)	Electronic	**Copies for the Disabled?**	No
Who Will Republish the Content?	Academic institution	**Minor Editing Privileges?**	No
		Incidental Promotional Use?	No
Duration of Use	Life of current and all future editions	**Currency**	GBP
Lifetime Unit Quantity	Up to 999		
Rights Requested	Main product		

NEW WORK DETAILS

Title	Mr	**Institution Name**	Imperial College London
Instructor Name	Zejian Cui	**Expected Presentation Date**	2025-08-01

ADDITIONAL DETAILS

The Requesting Person / Organization to Appear on the License	Zejian Cui

REQUESTED CONTENT DETAILS

Title, Description or Numeric Reference of the Portion(s)	da Vinci coordinate system	**Title of the Article / Chapter the Portion Is From**	Efficiently Calibrating Cable-Driven Surgical Robots with RGBD Fiducial Sensing and Recurrent Neural Networks
Editor of Portion(s)	Hwang, Minho; Thananjeyan, Brijen; Paradis, Samuel; Seita, Daniel; Ichnowski, Jeffrey; Fer, Danyal; Low, Thomas; Goldberg, Ken	**Author of Portion(s)**	Hwang, Minho; Thananjeyan, Brijen; Paradis, Samuel; Seita, Daniel; Ichnowski, Jeffrey; Fer, Danyal; Low, Thomas; Goldberg, Ken
Volume / Edition	5		
Page or Page Range of Portion	5937-5944	**Issue, if Republishing an Article From a Serial**	4
		Publication Date of Portion	2020-10-01

The Institute of Electrical and Electronics Engineers, Incorporated (IEEE) Terms and Conditions

IEEE allows for reuse of content in a thesis or dissertation for $0 and no license is required. IEEE does not have the right to license republication of Images and Photos. Please contact the author of the IEEE content to request the rights for the needed images and photos. IEEE allows reuse of an Excerpt when licensing permission for reuse of a Page. If you wish to license more than 10 figures, please contact IEEE directly at: pubs-permissions@ieee.org. IEEE will provide a discounted cost for bulk figure purchases. If you are an Author or a Member of IEEE, and are affiliated with or requesting on behalf of a non-commercial or non-profit organization, please use RightsLink to request republication permissions at: https://ieeexplore.ieee.org/. IEEE offers special pricing for Authors and Members of IEEE in RightsLink that is not available on copyright.com

Total Items: 1

Subtotal: 0.00 GBP

Order Total: 0.00 GBP

Marketplace Permissions General Terms and Conditions

The following terms and conditions ("General Terms"), together with any applicable Publisher Terms and Conditions, govern User's use of Works pursuant to the Licenses granted by Copyright Clearance Center, Inc. ("CCC") on behalf of the applicable Rightsholders of such Works through CCC's applicable Marketplace transactional licensing services (each, a "Service").

1) **Definitions.** For purposes of these General Terms, the following definitions apply:

"License" is the licensed use the User obtains via the Marketplace platform in a particular licensing transaction, as set forth in the Order Confirmation.

"Order Confirmation" is the confirmation CCC provides to the User at the conclusion of each Marketplace transaction. "Order Confirmation Terms" are additional terms set forth on specific Order Confirmations not set forth in the General Terms that can include terms applicable to a particular CCC transactional licensing service and/or any Rightsholder-specific terms.

"Rightsholder(s)" are the holders of copyright rights in the Works for which a User obtains licenses via the Marketplace platform, which are displayed on specific Order Confirmations.

"Terms" means the terms and conditions set forth in these General Terms and any additional Order Confirmation Terms collectively.

"User" or "you" is the person or entity making the use granted under the relevant License. Where the person accepting the Terms on behalf of a User is a freelancer or other third party who the User authorized to accept the General Terms on the User's behalf, such person shall be deemed jointly a User for purposes of such Terms.

"Work(s)" are the copyright protected works described in relevant Order Confirmations.

2) **Description of Service.** CCC's Marketplace enables Users to obtain Licenses to use one or more Works in accordance with all relevant Terms. CCC grants Licenses as an agent on behalf of the copyright rightsholder identified in the relevant Order Confirmation.

3) **Applicability of Terms.** The Terms govern User's use of Works in connection with the relevant License. In the event of any conflict between General Terms and Order Confirmation Terms, the latter shall govern. User acknowledges that Rightsholders have complete discretion whether to grant any permission, and whether to place any limitations on any grant, and that CCC has no right to supersede or to modify any such discretionary act by a Rightsholder.

4) **Representations; Acceptance.** By using the Service, User represents and warrants that User has been duly authorized by the User to accept, and hereby does accept, all Terms.

5) **Scope of License; Limitations and Obligations.** All Works and all rights therein, including copyright rights, remain the sole and exclusive property of the Rightsholder. The License provides only those rights expressly set forth in the terms and conveys no other rights in any Works

6) **General Payment Terms.** User may pay at time of checkout by credit card or choose to be invoiced. If the User chooses to be invoiced, the User shall: (i) remit payments in the manner identified on specific invoices, (ii) unless otherwise specifically stated in an Order Confirmation or separate written agreement, Users shall remit payments upon receipt of the relevant invoice from CCC, either by delivery or notification of availability of the invoice via the Marketplace platform, and (iii) if the User does not pay the invoice within 30 days of receipt, the User may incur a service charge of 1.5% per month or the maximum rate allowed by applicable law, whichever is less. While User may exercise the rights in the License immediately upon receiving the Order Confirmation, the License is automatically revoked and is null and void, as if it had never been issued, if CCC does not receive complete payment on a timely basis.

7) **General Limits on Use.** Unless otherwise provided in the Order Confirmation, any grant of rights to User (i) involves only the rights set forth in the Terms and does not include subsequent or additional uses, (ii) is non-exclusive and non-transferable, and (iii) is subject to any and all limitations and restrictions (such as, but not limited to, limitations on duration of use or circulation) included in the Terms. Upon completion of the licensed use as set forth in the Order Confirmation, User shall either secure a new permission for further use of the Work(s) or immediately cease any new use of the Work(s) and shall render inaccessible (such as by deleting or by removing or severing links or other locators) any further copies of the Work. User may only make alterations to the Work if and as expressly set forth in the Order Confirmation. No Work may be used in any way that is unlawful, including without limitation if such use would violate applicable sanctions laws or regulations, would be defamatory, violate the rights of third parties (including such third parties' rights of copyright, privacy, publicity, or other tangible or intangible property), or is otherwise illegal, sexually explicit, or obscene. In addition, User may not conjoin a Work with any other material that may result in damage to the reputation of the Rightsholder. Any unlawful use will render any licenses hereunder null and void. User agrees to inform CCC if it becomes aware of any infringement of any rights in a Work and to cooperate with any reasonable request of CCC or the Rightsholder in connection therewith.

8) **Third Party Materials.** In the event that the material for which a License is sought includes third party materials (such as photographs, illustrations, graphs, inserts and similar materials) that are identified in such material as having been used by permission (or a similar indicator), User is responsible for identifying, and seeking separate licenses (under this Service, if available, or otherwise) for any of such third party materials; without a separate license, User may not use such third party materials via the License.

9) **Copyright Notice.** Use of proper copyright notice for a Work is required as a condition of any License granted under the Service. Unless otherwise provided in the Order Confirmation, a proper copyright notice will read substantially as follows: "Used with permission of [Rightsholder's name], from [Work's title, author, volume, edition number and year of copyright]; permission conveyed through Copyright Clearance Center, Inc." Such notice must be provided in a reasonably legible font size and must be placed either on a cover page or in another location that any person, upon gaining access to the material which is the subject of a permission, shall see, or in the case of republication Licenses, immediately adjacent to the Work as used (for example, as part of a by-line or footnote) or in the place where substantially all other credits or notices for the new work containing the republished Work are located. Failure to include the required notice results in loss to the Rightsholder and CCC, and the User shall be liable to pay liquidated damages for each such failure equal to twice the use fee specified in the Order Confirmation, in addition to the use fee itself and any other fees and charges specified.

10) **Indemnity.** User hereby indemnifies and agrees to defend the Rightsholder and CCC, and their respective employees and directors, against all claims, liability, damages, costs, and expenses, including legal fees and expenses, arising out of any use of a Work beyond the scope of the rights granted herein and in the Order Confirmation, or any use of a Work which has been altered in any unauthorized way by User, including claims of defamation or infringement of rights of copyright, publicity, privacy, or other tangible or intangible property.

11) **Limitation of Liability.** UNDER NO CIRCUMSTANCES WILL CCC OR THE RIGHTSHOLDER BE LIABLE FOR ANY DIRECT, INDIRECT, CONSEQUENTIAL, OR INCIDENTAL DAMAGES (INCLUDING WITHOUT LIMITATION DAMAGES FOR LOSS OF BUSINESS PROFITS OR INFORMATION, OR FOR BUSINESS INTERRUPTION) ARISING OUT OF THE USE OR INABILITY TO USE A WORK, EVEN IF ONE OR BOTH OF THEM HAS BEEN ADVISED OF THE POSSIBILITY OF SUCH DAMAGES. In any event, the total liability of the Rightsholder and CCC (including their respective employees and directors) shall not exceed the total amount actually paid by User for the relevant License. User assumes full liability for the actions and omissions of its principals, employees, agents, affiliates, successors, and assigns.

12) **Limited Warranties.** THE WORK(S) AND RIGHT(S) ARE PROVIDED "AS IS." CCC HAS THE RIGHT TO GRANT TO USER THE RIGHTS GRANTED IN THE ORDER CONFIRMATION DOCUMENT. CCC AND THE RIGHTSHOLDER DISCLAIM ALL OTHER WARRANTIES RELATING TO THE WORK(S) AND RIGHT(S), EITHER EXPRESS OR IMPLIED, INCLUDING WITHOUT LIMITATION IMPLIED WARRANTIES OF MERCHANTABILITY OR FITNESS FOR A PARTICULAR PURPOSE. ADDITIONAL RIGHTS MAY BE REQUIRED TO USE ILLUSTRATIONS, GRAPHS, PHOTOGRAPHS, ABSTRACTS, INSERTS, OR OTHER PORTIONS OF THE WORK (AS OPPOSED TO THE ENTIRE WORK) IN A MANNER CONTEMPLATED BY USER; USER UNDERSTANDS AND AGREES THAT NEITHER CCC NOR THE RIGHTSHOLDER MAY HAVE SUCH ADDITIONAL RIGHTS TO GRANT.

13) **Effect of Breach.** Any failure by User to pay any amount when due, or any use by User of a Work beyond the scope of the License set forth in the Order Confirmation and/or the Terms, shall be a material breach of such License. Any breach not cured within 10 days of written notice thereof shall result in immediate termination of such License without further notice. Any unauthorized (but licensable) use of a Work that is terminated immediately upon notice thereof may be liquidated by payment of the Rightsholder's ordinary license price therefor; any unauthorized (and unlicensable) use that is not terminated immediately for any reason (including, for example, because materials containing the Work cannot reasonably be recalled) will be subject to all remedies available at law or in equity, but in no event to a payment of less than three times the Rightsholder's ordinary license price for the most closely analogous licensable use plus Rightsholder's and/or CCC's costs and expenses incurred in collecting such payment.

14) **Additional Terms for Specific Products and Services.** If a User is making one of the uses described in this Section 14, the additional terms and conditions apply:

a) ***Print Uses of Academic Course Content and Materials (photocopies for academic coursepacks or classroom handouts).*** For photocopies for academic coursepacks or classroom handouts the following additional terms apply:

i) The copies and anthologies created under this License may be made and assembled by faculty members individually or at their request by on-campus bookstores or copy centers, or by off-campus copy shops and other similar entities.

ii) No License granted shall in any way: (i) include any right by User to create a substantively non-identical copy of the Work or to edit or in any other way modify the Work (except by means of deleting material immediately preceding or following the entire portion of the Work copied) (ii) permit "publishing ventures" where any particular anthology would be systematically marketed at multiple institutions.

iii) Subject to any Publisher Terms (and notwithstanding any apparent contradiction in the Order Confirmation arising from data provided by User), any use authorized under the academic pay-per-use service is limited as follows:

A) any License granted shall apply to only one class (bearing a unique identifier as assigned by the institution, and thereby including all sections or other subparts of the class) at one institution;

B) use is limited to not more than 25% of the text of a book or of the items in a published collection of essays, poems or articles;

C) use is limited to no more than the greater of (a) 25% of the text of an issue of a journal or other periodical or (b) two articles from such an issue;

D) no User may sell or distribute any particular anthology, whether photocopied or electronic, at more than one institution of learning;

E) in the case of a photocopy permission, no materials may be entered into electronic memory by User except in order to produce an identical copy of a Work before or during the academic term (or analogous period) as to which any particular permission is granted. In the event that User shall choose to retain materials that are the subject of a photocopy permission in electronic memory for purposes of producing identical copies more than one day after such retention (but still within the scope of any permission granted), User must notify CCC of such fact in the applicable permission request and such retention shall constitute one copy actually sold for purposes of calculating permission fees due; and

F) any permission granted shall expire at the end of the class. No permission granted shall in any way include any right by User to create a substantively non-identical copy of the Work or to edit or in any other way modify the Work (except by means of deleting material immediately preceding or following the entire portion of the Work copied).

iv) Books and Records; Right to Audit. As to each permission granted under the academic pay-per-use Service, User shall maintain for at least four full calendar years books and records sufficient for CCC to determine the numbers of copies made by User under such permission. CCC and any representatives it may designate shall have the right to audit such books and records at any time during User's ordinary business hours, upon two days' prior notice. If any such audit shall determine that User shall have underpaid for, or underreported, any photocopies sold or by three percent (3%) or more, then User shall bear all the costs of any such audit; otherwise, CCC shall bear the costs of any such audit. Any amount determined by such audit to have been underpaid by User shall immediately be paid to CCC by User, together with interest thereon at the rate of 10% per annum from the date such amount was originally due. The provisions of this paragraph shall survive the termination of this License for any reason.

b) ***Digital Pay-Per-Uses of Academic Course Content and Materials (e-coursepacks, electronic reserves, learning management systems, academic institution intranets).*** For uses in e-coursepacks, posts in electronic reserves, posts in learning management systems, or posts on academic institution intranets, the following additional terms apply:

i) The pay-per-uses subject to this Section 14(b) include:

A) **Posting e-reserves, course management systems, e-coursepacks for text-based content,** which grants authorizations to import requested material in electronic format, and allows electronic access to this material to members of a designated college or university class, under the direction of an instructor designated by the college or university, accessible only under appropriate electronic controls (e.g., password);

B) **Posting e-reserves, course management systems, e-coursepacks for material consisting of photographs or other still images not embedded in text,** which grants not only the authorizations described in Section 14(b)(i)(A) above, but also the following authorization: to include the requested material in course materials for use consistent with Section 14(b)(i)(A) above, including any necessary resizing, reformatting or modification of the resolution of such requested material (provided that such modification does not alter the underlying editorial content or meaning of the requested material, and provided that the resulting modified content is used solely within the scope of, and in a manner consistent with, the particular authorization described in the Order Confirmation and the Terms), but not including any other form of manipulation, alteration or editing of the requested material;

C) **Posting e-reserves, course management systems, e-coursepacks or other academic distribution for audiovisual content,** which grants not only the authorizations described in Section 14(b)(i)(A) above, but also the following authorizations: (i) to include the requested material in course materials for use consistent with Section 14(b)(i)(A) above; (ii) to display and perform the requested material to such members of such class in the physical classroom or remotely by

means of streaming media or other video formats; and (iii) to "clip" or reformat the requested material for purposes of time or content management or ease of delivery, provided that such "clipping" or reformatting does not alter the underlying editorial content or meaning of the requested material and that the resulting material is used solely within the scope of, and in a manner consistent with, the particular authorization described in the Order Confirmation and the Terms. Unless expressly set forth in the relevant Order Conformation, the License does not authorize any other form of manipulation, alteration or editing of the requested material.

ii) Unless expressly set forth in the relevant Order Confirmation, no License granted shall in any way: (i) include any right by User to create a substantively non-identical copy of the Work or to edit or in any other way modify the Work (except by means of deleting material immediately preceding or following the entire portion of the Work copied or, in the case of Works subject to Sections 14(b)(1)(B) or (C) above, as described in such Sections) (ii) permit "publishing ventures" where any particular course materials would be systematically marketed at multiple institutions.

iii) Subject to any further limitations determined in the Rightsholder Terms (and notwithstanding any apparent contradiction in the Order Confirmation arising from data provided by User), any use authorized under the electronic course content pay-per-use service is limited as follows:

A) any License granted shall apply to only one class (bearing a unique identifier as assigned by the institution, and thereby including all sections or other subparts of the class) at one institution;

B) use is limited to not more than 25% of the text of a book or of the items in a published collection of essays, poems or articles;

C) use is limited to not more than the greater of (a) 25% of the text of an issue of a journal or other periodical or (b) two articles from such an issue;

D) no User may sell or distribute any particular materials, whether photocopied or electronic, at more than one institution of learning;

E) electronic access to material which is the subject of an electronic-use permission must be limited by means of electronic password, student identification or other control permitting access solely to students and instructors in the class;

F) User must ensure (through use of an electronic cover page or other appropriate means) that any person, upon gaining electronic access to the material, which is the subject of a permission, shall see:

- a proper copyright notice, identifying the Rightsholder in whose name CCC has granted permission,
- a statement to the effect that such copy was made pursuant to permission,
- a statement identifying the class to which the material applies and notifying the reader that the material has been made available electronically solely for use in the class, and
- a statement to the effect that the material may not be further distributed to any person outside the class, whether by copying or by transmission and whether electronically or in paper form, and User must also ensure that such cover page or other means will print out in the event that the person accessing the material chooses to print out the material or any part thereof.

G) any permission granted shall expire at the end of the class and, absent some other form of authorization, User is thereupon required to delete the applicable material from any electronic storage or to block electronic access to the applicable material.

iv) Uses of separate portions of a Work, even if they are to be included in the same course material or the same university or college class, require separate permissions under the electronic course content pay-per-use Service. Unless otherwise provided in the Order Confirmation, any grant of rights to User is limited to use completed no later than the end of the academic term (or analogous period) as to which any particular permission is granted.

v) Books and Records; Right to Audit. As to each permission granted under the electronic course content Service, User shall maintain for at least four full calendar years books and records sufficient for CCC to determine the numbers of copies made by User under such permission. CCC and any representatives it may designate shall have the right to audit such books and records at any time during User's ordinary business hours, upon two days' prior notice. If any such audit shall determine that User shall have underpaid for, or underreported, any electronic copies used by three percent (3%) or more, then User shall bear all the costs of any such audit; otherwise, CCC shall bear the costs of any such audit. Any amount determined by such audit to have been underpaid by User shall immediately be paid to CCC by User, together with interest thereon at the rate of 10% per annum from the date such amount was originally due. The provisions of this paragraph shall survive the termination of this license for any reason.

c) ***Pay-Per-Use Permissions for Certain Reproductions (Academic photocopies for library reserves and interlibrary loan reporting) (Non-academic internal/external business uses and commercial document delivery).*** The License expressly excludes the uses listed in Section (c)(i)-(v) below (which must be subject to separate license from the applicable Rightsholder) for: academic photocopies for library reserves and interlibrary loan reporting; and non-academic internal/external business uses and commercial document delivery.

i) electronic storage of any reproduction (whether in plain-text, PDF, or any other format) other than on a transitory basis;

ii) the input of Works or reproductions thereof into any computerized database;

iii) reproduction of an entire Work (cover-to-cover copying) except where the Work is a single article;

iv) reproduction for resale to anyone other than a specific customer of User;

v) republication in any different form. Please obtain authorizations for these uses through other CCC services or directly from the rightsholder.

Any license granted is further limited as set forth in any restrictions included in the Order Confirmation and/or in these Terms.

d) ***Electronic Reproductions in Online Environments (Non-Academic-email, intranet, internet and extranet).*** For "electronic reproductions", which generally includes e-mail use (including instant messaging or other electronic transmission to a defined group of recipients) or posting on an intranet, extranet or Intranet site (including any display or performance incidental thereto), the following additional terms apply:

i) Unless otherwise set forth in the Order Confirmation, the License is limited to use completed within 30 days for any use on the Internet, 60 days for any use on an intranet or extranet and one year for any other use, all as measured from the "republication date" as identified in the Order Confirmation, if any, and otherwise from the date of the Order Confirmation.

ii) User may not make or permit any alterations to the Work, unless expressly set forth in the Order Confirmation (after request by User and approval by Rightsholder); provided, however, that a Work consisting of photographs or other still images not embedded in text may, if necessary, be resized, reformatted or have its resolution modified without additional express permission, and a Work consisting of audiovisual content may, if necessary, be "clipped" or reformatted for purposes of time or content management or ease of delivery (provided that any such resizing, reformatting, resolution modification or "clipping" does not alter the underlying editorial content or meaning of the Work used, and that the resulting material is used solely within the scope of, and in a manner consistent with, the particular License described in the Order Confirmation and the Terms.

15) **Miscellaneous.**

a) User acknowledges that CCC may, from time to time, make changes or additions to the Service or to the Terms, and that Rightsholder may make changes or additions to the Rightsholder Terms. Such updated Terms will replace the prior terms and conditions in the order workflow and shall be effective as to any subsequent Licenses but shall not apply to Licenses already granted and paid for under a prior set of terms.

b) Use of User-related information collected through the Service is governed by CCC's privacy policy, available online at www.copyright.com/about/privacy-policy/.

c) The License is personal to User. Therefore, User may not assign or transfer to any other person (whether a natural person or an organization of any kind) the License or any rights granted thereunder; provided, however, that, where applicable, User may assign such License in its entirety on written notice to CCC in the event of a transfer of all or substantially all of User's rights in any new material which includes the Work(s) licensed under this Service.

d) No amendment or waiver of any Terms is binding unless set forth in writing and signed by the appropriate parties, including, where applicable, the Rightsholder. The Rightsholder and CCC hereby object to any terms contained in any writing prepared by or on behalf of the User or its principals, employees, agents or affiliates and purporting to govern or otherwise relate to the License described in the Order Confirmation, which terms are in any way inconsistent with any Terms set forth in the Order Confirmation, and/or in CCC's standard operating procedures, whether such writing is prepared prior to, simultaneously with or subsequent to the Order Confirmation, and whether such writing appears on a copy of the Order Confirmation or in a separate instrument.

e) The License described in the Order Confirmation shall be governed by and construed under the law of the State of New York, USA, without regard to the principles thereof of conflicts of law. Any case, controversy, suit, action, or proceeding arising out of, in connection with, or related to such License shall be brought, at CCC's sole discretion, in any federal or state court located in the County of New York, State of New York, USA, or in any federal or state court whose geographical jurisdiction covers the location of the Rightsholder set forth in the Order Confirmation. The parties expressly submit to the personal jurisdiction and venue of each such federal or state court.

Last updated October 2022